Published in final edited form as:
Chem Rev. 2014 April 9; 114(7): 3963–4038. doi:10.1021/cr400443z.

The Mononuclear Molybdenum Enzymes§

Russ Hille[*,†], **James Hall**[†], and **Partha Basu**[*,‡]

[†]Department of Biochemistry, University of California, Riverside, Riverside, California 92521, United States

[‡]Department of Chemistry and Biochemistry, Duquesne University, Pittsburgh, Pennsylvania 15282, United States

1. INTRODUCTION AND SCOPE

Molybdenum is the only second-row transition metal required by most living organisms, and is nearly universally distributed in biology. Enzymes containing molybdenum in their active sites have long been recognized,[1] and at present over 50 molybdenum-containing enzymes have been purified and biochemically characterized; a great many more gene products have been annotated as putative molybdenum-containing proteins on the basis of genomic and bioinformatic analysis.[2] In certain cases, our understanding of the relationship between enzyme structure and function is such that we can speak with confidence as to the detailed nature of the reaction mechanism and, with the availability of high-resolution X-ray crystal structures, the specific means by which transition states are stabilized and reaction rate is accelerated within the friendly confines of the active site. At the same time, our understanding of the biosynthesis of the organic cofactor that accompanies molybdenum (variously called molybdopterin or pyranopterin), the manner in which molybdenum is incorporated into it, and then further modified as necessary prior to insertion into apoprotein has also (in at least some cases) become increasingly well understood.

It is now well-established that all molybdenum-containing enzymes other than nitrogenase (in which molybdenum is incorporated into a [$MoFe_7S_9$] cluster of the active site) fall into three large and mutually exclusive families, as exemplified by the enzymes xanthine oxidase, sulfite oxidase, and DMSO reductase; these enzymes represent the focus of the present account.[3] The structures of the three canonical molybdenum centers in their oxidized Mo(VI) states are shown in Figure 1, along with that for the pyranopterin cofactor. The active sites of members of the xanthine oxidase family have an $LMo^{VI}OS$-(OH) structure with a square-pyramidal coordination geometry. The apical ligand is a Mo=O ligand, and the equatorial plane has two sulfurs from the enedithiolate side chain of the pyranopterin cofactor, a catalytically labile Mo–OH group, and most frequently a Mo=S. Nonfunctional forms of these enzymes exist in which the equatorial Mo=S is replaced with a second

§**DEDICATION**
This account is dedicated to John H. Enemark, in recognition of his 50 years of scholarship, mentorship, and friendship.

[*]**Corresponding Authors:**russ.hille@ucr.edu, basu@duq.edu.

The authors declare no competing financial interest.

Mo=O; in at least one member of the family the Mo=S is replaced by a Mo=Se, and in others it is replaced by a more complex –S–Cu–S–Cys to give a binuclear center. Members of the sulfite oxidase family have a related $LMo^{VI}O_2$(S–Cys) active site, again square-pyramidal with an apical Mo=O and a bidentate enedithiolate Ligand (L) in the equatorial plane but with a second equatorial Mo=O (rather than Mo–OH) and a cysteine ligand contributed by the protein (rather than a Mo=S) completing the molybdenum coordination sphere. The final family is the most diverse structurally, although all members possess two (rather than just one) equiv of the pyranopterin cofactor and have an $L_2Mo^{VI}Y(X)$ trigonal prismatic coordination geometry. DMSO reductase itself has a catalytically labile Mo=O as Y and a serinate ligand as X completing the metal coordination sphere of oxidized enzyme. Other family members have cysteine (the bacterial Nap periplasmic nitrate reductases), selenocysteine (formate dehydrogenase H), –OH (arsenite oxidase), or aspartate (the NarGHI dissimilatory nitrate reductases) in place of the serine. Some enzymes have S or even Se in place of the Mo=O group. Members of the DMSO reductase family exhibit a general structural homology to members of the aldehyde:ferredoxin oxidoreductase family of tungsten-containing enzymes;[4] indeed, the first pyranopterin-containing enzyme to be crystallographically characterized was the tungsten-containing aldehyde:ferredoxin oxidoreductase from *Pyrococcus furiosus*,[5] a fact accounting for why many workers in the field prefer “pyranopterin” (or, perhaps waggishly, “tungstopterin”) to “molybdopterin”. The term pyranopterin will generally be used in the present account.

What follows is first a summary of our understanding of the biosynthesis of the pyranopterin cofactor, then a discussion of members of each family of molybdenum enzymes in turn. An emphasis has been placed on the relationship of structure to function for the many proteins involved in the biology of molybdenum for which X-ray crystal structures exist, and with the large and growing number of molybdenum-containing enzymes identified by genomics and proteomics analysis, the focus here is on those systems that are best understood from a biochemical standpoint. More recent results are emphasized, and the reader is referred to other reviews for more comprehensive coverage of the literature prior to 1995.[3,6] The reader is also referred to other recently appearing reviews in the general area for the perspectives of other workers in the field, particularly with regard to genomic, proteomic, and/or metallomic analyses of systems, which due to space limitations are not considered in detail here.[2c,7]

2. THE MOLYBDENUM COFACTOR

2.1. Biosynthesis of the Basic Form of the Molybdenum Cofactor

Biosynthesis of the most basic form of the molybdenum center involves three steps: (1) cyclization of GTP to form a cyclopyranoperin monophosphate (cPMP) intermediate; (2) sulfuration of cPMP to give the now mature pyranopterin (often abbreviated MPT for historical reasons); and (3) coordination of molybdate to the enedithiolate thus generated.[7d,e] The first step in the process, conversion of GTP to cPMP (referred to in the earlier literature as “Precursor Z”), is catalyzed in *E. coli* by the enzymes MoaA and MoaC; their cognates are Cnx2 and Cnx3 in *A. thaliana*, and MOCS1A and MOCS1B in humans. MoaA is a member of the large radical-SAM family of enzymes,[8] and the X-ray crystal structure for the enzyme from several sources has been reported.[9] MoaA *Staphylococcus aureus* is typical,

being a 2 × 41 kDa homodimer with each subunit possessing a canonical [4Fe-4S] cluster in its amino-terminal domain, and a second in its C-terminal domain (Figure 2). Both iron–sulfur clusters are coordinated by only three cysteine residues. The final ligand position in the N-terminal cluster is occupied by the aminoacyl end of *S*-adenosylmethionine (SAM, bound in a bidentate fashion),[9] while that of the C-terminal cluster coordinates the exocyclic amino group of GTP.[10] The cognate MOCS1A in humans is similarly constituted.[11]

It had originally been thought that the reaction mechanism of MoaA was similar to that of GTP cyclohydrolase I,[12] but recent work has demonstrated that this is not the case. The reaction instead is radical-based, beginning with the MoaA-catalyzed abstraction of the 3′ hydrogen atom by 5′-deoxyAd·, generated by reductive cleavage of SAM at the N-terminal [4Fe-4S] cluster.[13] Radical migration reaction affords (8*S*)-3′,8-*cyclo*-7,8-dihydroguanosine 5′-triphosphate (3′,8-cH_2GTP, see Figure 3), which has been isolated, characterized by NMR and mass spectrometry, and shown to be converted to cPMP by MoaC with high specificity.[14] The subsequent conversion of 3′,8-cH_2GTP to cPMP has been proposed to occur by hydrolytic ring-opening of the erstwhile imidazole subnucleus of substrate, followed by formation of the pyran and cyclophosphate rings of cPMP,[14] as shown in Figure 3 (although alternative mechanisms have also been proposed[13]).

MoaC from a number of organisms, including *E. coli*[15] and *Thermus thermophilus*,[16] has also been crystallographically characterized, and a comparison of the structures indicates that the basic catalytic unit is an α_2 dimer (although higherorder structures can be seen; the *E. coli* enzyme, for example, aggregates as an $(\alpha_2)_3$ trimer of dimers). As seen in the *T. thermophilus* enzyme complexed with GTP (Figure 4), the monomers within the dimer are arranged head-to-tail, with the core of each active site consisting of a four-helix bundle flanked by a pair of four-stranded β-sheets, one from each subunit, that form a contiguous sheet. The GTP binding sites are found at each end of the oblong dimer, with each subunit contributing interactions with the substrate analogue in both active sites (Figure 4, right). The guanine ring itself lies on the surface of the protein against a pair of alanine residues that terminate one of the central α-helices, while the triphosphate tail extends into the protein. A molecule of citrate from the crystallization mother liquor is bound adjacent to the GTP, and interacts with a number of residues that are highly conserved among MoaC's from different organisms. It has been suggested that the ring-opened ribose carbons of the actual substrate for MoaC bind in this portion of the active site.[16] An efficient total synthesis of cPMP has recently been reported that yields material that can be enzymatically converted to mature cofactor capable of reconstituting apo sulfite oxidase.[17]

The second step in the biosynthetic pathway involves sulfuration of cPMP to form the mature pyranopterin (molybdopterin) cofactor with its *cis*-dithiolene functionality. The MPT synthase catalyzing the reaction from both *E. coli*[18] and *Staphylococcus aureus*[19] has been examined crystallographically. The bacterial enzymes are $(\alpha\beta)_2$ heterotetramers consisting of two equivalents each of the MoaD and MoaE gene products (the corresponding enzymes in *A. thaliana* are Cnx7 and Cnx6, and in humans MOCS2B and MOCS2A). While the structure of the substrate cPMP in free solution has been shown by NMR to possess a *gem* diol rather than a keto group on the pyran ring,[20] it is the keto form that is observed crystallographically in the active site of MoaE.[19] As shown in Figure 5, amino acid residues

from both MoaE subunits interact with the cPMP bound in each active site. The C-terminal tail of MoaD, ending with a characteristic Gly-Gly motif, is sulfurated to form a thiocarboxylate that extends into the active site of MoaE (see further below).[21] Consistent with prior biochemical evidence,[22] it is evident from the crystal structure that the sulfuration process must proceed sequentially, with two successive equivalents of sulfur-charged MoaD binding to each active site of the $(MoaE)_2$ core in the course of turnover. The reaction proceeds as shown in Figure 6,[19,22,23] with attack of the thiocarboxylate from two successive equivalents of sulfurated MoaD on the pyran ring of cPMP, first at C2′ and then C1′, followed by dehydration to afford the dithiolene of the mature cofactor. Mutational studies with *S. aureus* ModE have identified Lys 116 and 123 (Lys 119 and 126 in the *E. coli* enzyme) as being important for sulfuration at C2′ and C1′, respectively,[22] most likely by stabilizing hydroxide for hydrolysis of the thioester intermediate.[19] The possibility that a single cPMP could be sulfurated at first one active site of the $(MoaD{\cdot}MoaE)_2$ heterotetramer and subsequently transferred to the second active site for completion of the sulfuration process has been considered,[21b] but the $MoaD_2$ core of the heterotetramer is closely packed, and absent an obvious channel in the crystal structure this would require dissociation of the singly sulfurated intermediate into free solution, which seems unlikely.

In *E. coli*, sulfuration of MoaD is catalyzed by MoeB (Cnx5 in *A. thaliana* and MOCS3 in humans). The reaction involves initial formation of a MoaD·MoeB complex, followed by the Mg^{2+}·ATP-dependent adenylylation of the MoaD C-terminus. It is this acyl adenylate form of MoaD, still in complex with MoeB, that reacts with the sulfur atom donor, which in *E. coli* has been shown to be the cysteine desulfurase IscS[24] (the human cognate sulfurating the MoaD homologue MOCS2B is NFS1[25]). IscS and its homologues (including NifS, which is involved in assembly of the metal clusters of nitrogenase[26]) are pyridoxal phosphate-dependent cysteine desulfurases that transfer the sulfur from substrate cysteine to an active site cysteine residue of the enzyme (Cys 328 in the case of the *E. coli* IscS[27]) to form a persulfide, releasing the remainder of the substrate cysteine as alanine. As illustrated in Figure 7, the IscS Cys 328 persulfide is believed to attack the adenylylated MoaD C-terminus, releasing AMP and creating a transient perthiocarboxylate linkage between IscS and MoaD. This is then reductively cleaved in a reaction that likely involves Cys 187 of MoeB on the basis of homology to the ubiquitin system,[28] resulting in disulfide bond formation between MoeB and IscS (which must subsequently be reductively cleaved to regenerate the system). The now sulfurated thiocarboxylate of MoaD then dissociates from MoeB and binds to MoaE to initiate another round of cofactor sulfuration. The overall process for MoaD sulfuration is summarized in Figure 7. It is to be noted that the eukaryotic sulfurases Cnx5 and MOCS3 are considerably larger than the bacterial MoeB, and possess a C-terminal rhodanese-like domain as well as the N-terminal domain with homology to MoeB; it is this C-terminal domain, with a highly conserved cysteine (Cys 412 in MOCS3), that is the proximal sulfur donor to the adenylylated MOCS2A, in these eukaryotic systems.[29] Recently, a rhodanese-like protein, YnjE, has been identified in *E. coli* that appears to facilitate sulfur transfer from IscS specifically to MoaD (as opposed to any of the other physiological partners for IscS in *E. coli*) and appears to represent a bacterial cognate to the rhodanese domains of the eukaryotic Cnx5 and MOCS3 proteins.[30]

Crystal structures for the $(\alpha\beta)_2$ MoaD/MoeB complex from *E. coli* in the free form, the ATP complex, and with adenylylated MoaD have all been reported.[28a] In the complex possessing adenylylated MoaD, one αβ unit of which is shown in Figure 8, the C-terminus of MoaD extends deeply into the active site of MoeB, with the acyl adenylate interacting with several specific amino acid residues of the active site. Unfortunately, residues 182–188 of MoeB (including Cys 187 that is thought to be involved in sulfur transfer from IscS (see Figure 7)) are not resolved in any of the structures. It is evident, however, that this loop passes above the C-terminus of MoaD in the perspective shown in Figure 8, right. This loop appears to protect the acyl adenylate from solvent, but as suggested by its disordered electron density is likely able to move so as to allow IscS access to the adenylylated C-terminus of bound MoaD.

As indicated above, the crystal structure of IscS is also known.[27] As shown in Figure 9, the homodimeric protein has an active site defined by the position of pyridoxal phosphate, bound as a Schiff base to Lys 206. Unfortunately, in a situation analogous to the case with Cys 187 of MoeB, the Cys 328 of IscS that is involved in sulfur transfer to MoaD is located in an unresolved loop in the crystal structure of IscS. It is clear from the positions of the resolved residues that delimit the unresolved loop (Ala 326 and Leu 333), however, that this loop is generally well-positioned so as to accept the sulfur from cysteine in the course of the reaction with PLP and then swivel to the surface of the protein to present the Cys 328 persulfide to the adenylylated C-terminus of MoaD within the MoaD:MoeB complex.[27] It has been noted that MoaD and MoeB are very similar in their overall structures to ThiS and ThiF, respectively, that are involved in formation of the thiazole ring of thiamin.[18a,28a] Similarly, MoaD also closely resembles ubiquitin, and MoeB bears a similar relationship to a 351-aa. segment (residues 400–750) of the ubiquitin-activating enzyme E_1. Given the functional as well as structural similarities between the pyranopterin and ubiquitin systems, with MoaD and ubiquitin both activated by adenylylation of a conserved GG-containing C-terminus, and the presumed ancient origins of the pyranopterin biosynthetic pathway,[31] it has been suggested that the MoaDE system represents the evolutionary progenitor to the ubiquitin system.[18a] Interestingly, MOCS3 (the human homologue to MoaD) has recently been shown to sulfurate another ubiquitin-like protein in yeast, URM1, that is involved in sulfuration of tRNA's, further underscoring the similarities of these systems.[32]

The final step in the biosynthesis of the basic form of the molybdenum cofactor is the insertion of the metal itself. By contrast to the biology of most first-row transition metals, which are typically present in the cell as cations, that of molybdenum involves the anionic (and highly water-soluble) molybdate ion. Molybdate enters the cell via a specific transporter system, in the case of *E. coli* ModABC, a member of the ATP-binding cassette (ABC) superfamily of membrane transporters.[33] The ModABC system from the archaeon *Archeoglobus fulgidus* was in fact the first member of this important family of transporters to be structurally characterized in the full range of conformational states that are involved in the active uptake of the target molecule or ion.[34] As shown in Figure 10, the system consists of a periplasmic binding protein (ModA; blue), a dimeric transmembrane component (ModB; gray), and a cytoplasmic ATPase subunit (ModC, also dimeric; red). ATP hydrolysis in the ModC subunits drives a conformational change in the membrane-spanning

$ModB_2$ dimer that alternately opens it to the periplasm and cytoplasm, thus effecting ion transport. Once in the cell, molybdate is stored bound to small (~7 kDa) binding proteins, the best characterized of which are the molbindins from *Clostridium pasteurianum*[35] and *Sporomusa ovata*[36] (see further below). In *E. coli*, molybdate is next added to the pyranopterin cofactor by the gene products MogA and MoeA (corresponding to the bifunctional Cnx1 in *A. thaliana*[37] and, amazingly, two domains of the neurotransmitter-scaffolding protein gephyrin in humans[38]). The process is more complicated than might have been expected, involving adenylylation of the pyranopterin phosphate prior to insertion of the metal.[39] The adenylylation step is catalyzed by MogA, and crystal structures for a number of homologues are now known, including the trimeric MogA *E. coli* enzyme[40] as well as the cognate *A. thaliana* Cnx1-G domain and gephyrin-G domain from both rat[41] and human;[42] all structures are very similar (rmsd ~1.0 Å). The overall trimeric structure, as represented by the human gephyrin G domain, is shown in Figure 11, as is a close-up of the *A. thaliana* Cnx1-G domain in complex with the adenylylated pyranopterin cofactor, where it can be seen that the cofactor binds at the surface of the protein with the enedithiolate exposed to solvent.[42a] It has been noted that the region surrounding the MPT-AMP binding pocket is more highly conserved than the remainder of the protein surface,[40] suggesting that it may be involved in interactions with physiological partners (see below). Interestingly, in the crystal structure of the Cnx1-G·MPT-AMP complex, a Cu(I) ion is found coordinated to the enedithiolate in the crystal structure (Figure 11, center). Such binding may be adventitious, however, as (at least in the *E. coli* system) a number of other metals are also able to bind the pyranopterin enedithiolate.[43] Furthermore, copper has been shown (again in *E. coli*) not to be required for maturation of the molybdenum cofactor.[44] It has also been shown in both prokaryotic and eukaryotic systems that, while MogA (or Cnx1-G) is required for molybdate insertion at physiological concentrations of the metal (1–10 μM), at nonphysiologically high concentrations of molybdate MoeA alone is able to catalyze metal incorporation in the absence of MogA and adenylylation of the pyranoperin.[43,45–47]

Finally (under physiological concentrations of molybdate), MogA presents the now adenylylated cofactor to MoeA, which catalyzes the actual insertion of molybdate (including displacement of copper, if present) to give the most basic form of the complete cofactor, which is most likely formulated as $LMo^{VI}O_2(OH)$ (or, perhaps less likely, as *fac* $LMo^{VI}O_3$). The reaction involves the molybdate-dependent hydrolysis of the adenylylated pyranopterin cofactor, releasing AMP, and a specific mechanism has been proposed whereby insertion occurs via an adenylylmolybdate intermediate (bearing in mind the well-known chemical similarities between molybdate and phosphate, this putative intermediate would be equivalent to ADP).[39b] The crystal structure of *E. coli* MoeA has been determined,[48] as has that for the cognate E domains of *A. thaliana* Cnx1 and human gephyrin in complex with the β-loop of the glycine receptor (with which it interacts physiologically).[49] Both proteins are dimers, with the overall architecture shown in Figure 12 (for the *A. thaliana* Cnx1-E domain). Each extended subunit consists of four discrete domains, of which Domain III is found to have significant structural homology to MogA. On the basis of this homology to MogA, a putative active site for Cnx1-E and gephyrin-E has been identified (Figure 12, asterisks). Structures for full-length Cnx1 or gephyrin are not available, but a model for gephyrin has been constructed on the basis of the assumption that its G domain forms stable

trimers (see Figure 11), with the G domain of each subunit occupying a position relative to that subunit's E domain that is comparable to that of the G-like domain of one subunit in the crystal structure of the dimeric gephyrin-E to the other subunit within the dimer.[50] Roughly speaking, a monomer of gephyrin would resemble the structure shown in Figure 12 with the gray and yellow E domain and green G domain; this then trimerizes about the G domain as shown in Figure 11. Such a model juxtaposes the active sites of G and E domains of adjacent subunits within the trimer, with subdomain I from one subunit constituting a flap that protects from solvent and presumably facilitating substrate/product channeling between the two active sites.[50] The model also provides a ready explanation as to why the linker between the E and G domains in gephyrin is so much larger than in Cnx1:[42b] with the G domain N-terminal to the E domain in gephyrin but C-terminal in Cnx1, a longer linker is required in the former case to allow the G domain to assume the position shown in Figure 12. It remains for future work to establish the validity of this model for the structure of full-length Cnx1 and gephyrin, the importance of which is underscored by the recent demonstration that in in vitro studies, intact gephyrin exhibits a 300-fold greater activity in cofactor biosynthesis than the isolated components.[50]

2.2. Gene Regulation of Molybdenum Cofactor Biosynthesis

In *E. coli*, most of the genes that encode the enzymes responsible for molybdenum cofactor biosynthesis are found in the *moaABCDE* gene cluster,[51] which is under tight transcriptional control.[52] Expression requires the presence of molybdate, which binds the dimeric ModE transcription element to up-regulate transcription of the structural genes for molybdenum-containing enzymes[53] as well as the *moaABCDE* operon,[52–54] and down-regulates the *modABCD* operon for the molybdate transporter.[54c,55] ModE is an α_2 dimer, encoded by an independently transcribed gene immediately upstream of the polycistronic *modABCD* operon.[56] Each subunit of ModE has an N-terminal DNA-binding domain with a classic helix-turn-helix motif, and a C-terminal domain that binds molybdate (Figure 13). Molybdate binding induces a conformational change in ModE that enables it to bind to a rather highly conserved DNA regulatory element in both eubacteria and archaea (having the consensus sequence TATATAxxxGxxxTATATA in *E. coli*). The molybdenum-binding C-termini of ModE together possess two molybdate binding sites, each of which involves residues from both subunits. The C-terminal domain of ModE represents a tandem duplication of the molybdate-binding motif seen in the molbindin (Mop) molybdate storage proteins.[54d,56,57] Ser 126, Arg 128, and Lys 183 from one subunit and the backbone amide of Ala 184 from the other are involved in binding the anion in each binding site. Since most bacterial molybdenum enzymes are involved in anaerobic respiration (on, e.g., nitrate, formate or DMSO), the *moaABCDE* operon in *E. coli* is also regulated by the transcription factor FNR (for fumarate nitrate regulator), which is involved in regulating gene expression in the transition from aerobic to anaerobic growth in bacteria.[58] FNR is a member of the Crp/FNR family of transcription factors[59] that under anaerobic conditions is a homodimer with subunits possessing an N-terminal O_2-sensing domain and a C-terminal DNA-binding domain. The two N-terminal domains coordinate a unique [4Fe-4S] iron–sulfur cluster at their interface, and in the reduced [4Fe-4S] form, FNR up-regulates the *moaABCDE* operon. Upon exposure to O_2 and oxidation, however, the iron–sulfur cluster of FNR converts to a

pair of [2Fe-2S] clusters leading to dissociation of the dimer, loss of DNA binding,[60] and down-regulation of *moaABCDE*.

The *moaABCDE* operon is also subject to feedback inhibition at the level of translation by a riboswitch, a relatively newly identified genetic regulatory element that allows mRNA to selectively bind a given metabolite.[61] The molybdenum cofactor riboswitch is broadly distributed in both eubacteria and archaea, and found upstream of the *moaA* gene in the untranslated region of the mRNA.[52,62] It recognizes and binds the full molybdated cofactor when it accumulates in the cell;[63] this binding presumably results in a conformational change in the riboswitch that shuts down translation of the mRNA. The secondary structure of the molybdenum cofactor riboswitch includes five extended base-pairing regions as well as a classic tetraloop/tetraloop receptor motif that dictates the overall tertiary structure of the riboswitch.[63] A pattern of selected mobility and exposure to solvent along its base sequence is a further indication of a well-defined tertiary structure. The specificity of the molybdenum cofactor riboswitch is such that it binds the molybdenum-containing form of the cofactor, but not the tungsten-containing form (genes encoding tungsten-containing enzymes possess their own, distinct riboswitch that lacks one of the base-pair regions but is otherwise very similar to the molybdenum cofactor riboswitch).[63] In *E. coli*, the *mobA*, *modABC*, *MoeAB*, and *mogA* loci also possess the molybdenum cofactor riboswitch, and presumably are similarly downregulated upon binding of the cofactor. The mRNA encoding DMSO reductase, formate dehydrogenase, TMAO reductase, nitrate reductase, and aldehyde oxidase (but not, apparently, those for xanthine dehydrogenase) also have the riboswitch,[63] and expression in these cases is presumably upregulated upon cofactor binding. In all of these genes, the cofactor-binding portion of the riboswitch (the so-called aptamer) is highly conserved, while the portion involved in regulation of gene expression in response to cofactor binding (the expression platform) is less so. In the case of the *moaABCDE* operon, the expression platform overlaps with the ribosome binding site of the mRNA, providing a ready structural basis for downregulation of expression upon binding of the cofactor.[63]

2.3. Intracellular Trafficking of the Molybdenum Cofactor

As indicated above, the structure of the basic molybdenum cofactor formed to this stage is $LMo^{VI}O_2(OH)$ (or *fac* $LMo^{VI}O_3$), with a square-pyramidal coordination geometry. It is well-known that the cofactor is extremely sensitive to air-oxidation,[64] and there is accumulating evidence that, at least in eukaryotes, the newly synthesized cofactor does not exist in free solution in the cell but is maintained bound to a storage protein to protect it from oxidation. The best characterized such storage protein is from *Chlamydomonas reinhardtii*, which has been shown to bind the molybdenum cofactor tightly and prevent its oxidation,[65] and also is capable of transferring the bound cofactor directly to apo nitrate reductase from *Neurospora crassa*.[66] *A. thaliana* encodes nine such proteins that similarly bind the molybdenum cofactor with micromolar affinities,[67] and are thought to be tissue-specific; these are very similar to that of the *C. reinhardtii* protein.[68] The structure of the tetrameric carrier protein from *C. reinhardtii* is shown in Figure 14, with the likely cofactor binding site identified through site-directed mutagenesis studies thought to include Met 60 and Pro 69.

An additional aspect of cofactor trafficking in eukaryotes is that biosynthesis of the pyranopterin is compartmentalized, with formation of cPMP taking place in the mitochondrial matrix and the remaining steps in the cytosol.[29a,69] In *Arabidopsis*, transport of cPMP out of the mitochondrion occurs in an ATP-dependent manner via ATM3, another member of the ABC transporter family.[70] In humans, the cytosolic sulfuration of cPMP by MOCS2B and MOCS2A has recently been shown to involve the (also cytoplasmically localized) cysteine desulfurase NFS1.[71] Once synthesized in the cytosol, trafficking of the basic cofactor to members of the sulfite oxidase family appears to involve direct transfer from the carrier proteins discussed above, as in both *Chlamydomonas*[72] and *Arabidopsis*[67] these have been shown capable of transferring bound cofactor directly to *apo* nitrate reductase. It is to be noted, however, that *apo* sulfite oxidase is also capable of spontaneously taking up the cofactor in vitro.[45a] Furthermore, direct transfer of the molybdenum cofactor from Cnx1-E to *apo* sulfite oxidase has also been demonstrated, although Cnx1-E does not appear to function actively to insert the cofactor but merely as a reservoir for it.[39b] On the other hand, trafficking to members of the xanthine oxidase family involves the direct participation of the sulfurase that inserts the equatorial Mo=S of these enzymes into the molybdenum coordination sphere, and is thus a more complex process (see section 2.4).

In prokaryotes, trafficking of the cofactor to specific enzymes occurs principally via additional modification of the basic molybdenum cofactor by extension as a dinucleotide of guanine, cytosine, adenine, or inosine in a manner that is species-specific.[73] In *E. coli*, YedY (see section 4.4) is the only protein known to use the basic form of the cofactor as generated by MogA and MoeA.[74] Members of the DMSO reductase family utilize MGD (for molybdopterin guanine dinucleotide), while members of the xanthine oxidase family (the xanthine dehydrogenases XdhABC and XdhD and periplasmic aldehyde oxidoreductase PaoABC) utilize the cytosine dinucleotide, MCD.[75] The enzymes that catalyze formation of the MGD and MCD dinucleotides are MobA[76] and MocA,[77] respectively, and both proteins have been shown to require the full molybdenum-containing cofactor for extension to the dinucleotide.[78] The structure of *E. coli* MobA is known, both with and without GTP bound.[79] The enzyme is an $(\alpha_2)_4$ octomer, with the monomer structure shown in Figure 15. There is significant sequence homology (including 22% sequence identity) between MobA and MocA, and it is likely that the latter has a very similar structure to the former. For both proteins, the N-terminal and C-terminal domains (residues 1–100, and 101–192, respectively) have been shown to be functional cassettes, with the N-terminal domain responsible for binding the correct nucleotide triphosphate and the C-terminal domain for recognizing apoproteins requiring that specific dinucleotide, MGD or MCD.[80] Those residues important in imparting specificity for GTP versus CTP in the N-terminal domain have been identified, and map to the pocket in which the base binds in the complex of MobA with GTP (Figure 15, lower right in red). There is evidence to suggest that in *E. coli*, MogA, MoeA, MobA, and MobB form a supramolecular complex in the cell.[81]

In *E. coli*, those enzymes utilizing the MCD dinucleotide from of the pyranopterin all require the insertion of a Mo=S group into the metal coordination sphere, and MocA presumably passes MCD onto the sulfurase responsible for incorporation of this Mo=S

group prior to insertion of the sulfurated cofactor into apoprotein (see section 2.4). Those proteins utilizing MGD all have a bisMGD active site (Figure 1), and necessarily require two equivalents of MGD to form the mature molybdenum center. The process by which bis(MGD) is formed is not well understood at present, although it is known that MobA, MPT, and Mg·GTP are sufficient in an in vitro system to reconstitute the apo DMSO reductase from *R. sphaeroides* (one of the simplest enzymes of this family).[82] (A second gene product of the *mob* operon, MobB, enhances the efficiency of bis(MGD) incorporation under certain conditions, but is not required either in vivo or in vitro to effect reconstitution.[76b,83]) Although the substrate binding groove of the MobA monomer is unable to accommodate two equivalents of MGD (Figure 15, right), it is possible that the dinucleotide forms across subunits of the octamer (possibly with the involvement of MobB[83b]); very recently, it has been shown that MobA acts on the bispyranopterin form of the cofactor with two equivalents of the pyranopterin coordinated to the molybdenum.[84]

In vivo, insertion of the cofactor into apoprotein may be facilitated by chaperone proteins that are associated with most (but not all) bis(MGD)-utilizing enzymes, particularly those that are destined for export to the periplasm. In *E. coli*, these chaperones include: NarJ, NarW, and NapD for the NarGHI, NarZWY and NapA nitrate reductases (respectively), FdnJ for the FdnGHI formate dehydrogenase, DmsD for the DmsABC DMSO reductase, and TorD for the TorA trimethylamine-*N*-oxide reductase. These proteins stabilize the apoprotein, facilitate cofactor insertion[7a,85] and target the fully folded holoenzyme for export to the periplasm by the Tat system,[86] thus preventing export of apoprotein prior to insertion of the molybdenum cofactor (and assembly of additional subunits in some cases, see below). These chaperones interact with apoprotein in two places: the N-terminal twin-arginine leader sequence that targets periplasmic proteins for export and an as yet undefined region of the core of the protein.[87] The crystal structures are known for these chaperones from *E. coli* and other organisms,[88] and those for the DmsD from *E. coli*[88b] and TorD from *Shewanella massilia*[88c] are shown in Figure 16. DmsD is a monomer, with N- and C-terminal domains indicated in gray and blue, respectively. Interestingly, the dimeric TorD has undergone domain-swapping such that each half of the dimer consists of N-and C-termini from different subunits. Helix 5 of TorD (Figure 16, red asterisks) has been shown to be essential in the interaction with the core of the TorA TMAO reductase,[87b] and presumably the cognate regions of other chaperones do as well. Again, however, at least in the case of the *R. sphaeroides* DMSO reductase, MobA alone is sufficient to ensure insertion of the bispyranopterin molybdenum cofactor in vitro.

As indicated above, members of the xanthine oxidase family require the insertion of a Mo=S group into the molybdenum coordination sphere for activity,[89] and the process by which this occurs has become increasingly well-understood. Interestingly, while the biosynthetic pathway for pyranopterin itself is highly conserved between prokaryotes and eukaryotes, the present evidence indicates that the sulfurases from the two kingdoms are not closely related and do not complement one another in vivo. In prokaryotes, the process is best understood for the xanthine dehydrogenase system of *R. capsulatus*. The first two genes of the *xdhABC* operon encode the structural genes for the organism's xanthine dehydrogenase (the Fe/S- and FAD-containing XdhA, and the Mo-containing XdhB),[90] while the *xdhC* gene encodes a

specific sulfurase that has been shown to accept the basic molybdenum cofactor from MoeB[78] and catalyze replacement of the equatorial Mo=O group of the cofactor with sulfur that is provided by a specific PLP-dependent cysteine desulfurase (NifS4).[91] Many organisms possess multiple *xdhC*-like genes, which are usually (but not always) integrated into operons encoding members of the xanthine oxidase family of enzymes. A phylogenetic analysis of these genes, which typically exhibit only relatively weak sequence identity (rarely greater than 25%), has been presented in which the XdhC homologues for enzymes that utilize the mononucleotide form of the cofactor are segregated from those utilizing MCD.[92]

Sulfuration of the molybdenum cofactor has similarities to the sulfuration of cPMP discussed above. The cysteine desulfurase involved, NifS, catalyzes the formation of a persulfide on one of its cysteine residues,[26] and this then sulfurates the XdhC-bound molybdenum cofactor. The crystal structure of the persulfide form of NifS has been reported,[93] and as shown in Figure 17 is found to consist of three domains arranged in a flattened triangle. The persulfide of Cys 364 is found on the surface of the protein near the active site PLP (forming a Schiff base with Lys 226), which sits at the interface of the three domains. The cofactor sulfuration reaction most likely involves an SN_2-like ligand exchange reaction from an $LMo^{VI}O_2(OH)$ to an $LMo^{VI}OS(OH)$ structure that results in inversion of the stereochemistry of the molybdenum center (as elaborated upon further in section 4.2.1, the molybdenum centers of the nonsulfurated sulfite oxidase and the sulfurated xanthine oxidoreductase have opposite stereochemistry). Also, it is important to recognize that release of the terminal persulfide sulfur from a putative CysS–S–Mo intermediate requires attack by a nucleophile. A conserved cysteine has been identified in XdhC enzymes (Cys 82 in the *E. coli* XdhC) that may be involved in the formation of a transient interprotein disulfide analogous to that seen with the MoeB:MoaD system discussed above (see Figure 7).

The crystal structures for XdhC homologues from both *Mycobacterium smegmatis* (PDB 2WE7) and *Bacillus halodurans* (PDB 3ON5) have been deposited in the Protein Data Bank (although neither structure has been published in the scientific literature). The *B. halodurans* structure is the more complete and, as shown in Figure 18, each subunit of the 2 × 40 kDa homodimer consists of two well-organized N and C-terminal domains, the latter of which has a classic nucleotide-binding Rossmann fold. The dimer is organized head-to-tail, with a putative cofactor binding site located in a large depression on the surface of the protein at the dimer interface (and which involves the N-terminal domain of one subunit and the C-terminal domain of the other). The highly conserved Cys 92 (in the N-terminal domain, homologous to Cys 82 of the *R. capsulatus* XdhC) that is likely involved in the sulfuration process lies at the edge of this depression. If this is indeed the cofactor binding site, the persulfide of NifS would have ready access to the cofactor. On the basis of the proteomics analysis of Neumann and Leimkühler,[92] it appears likely that the *B. halodurans* XdhC homologue binds one or another dinucleotide form of the molybdenum cofactor rather than the mononucleotide form.

Molybdenum cofactor sulfurases have been identified from a number of eukaryotes,[94] including humans.[95] Considerable biochemical information is available for the ABA3 sulfurase from *A. thaliana*, which in the in vitro assays is able to sulfurate the desulfo form

of aldehyde oxidase.[94c] The protein is a 2 × 92 kDa homodimer, with each subunit consisting of an N-terminal pyridoxal-phosphate-binding domain homologous to the bacterial cysteine desulfurases SufS, NifS, and IscS discussed above. However, although the C-terminal portion of ABA3 is functionally equivalent to the bacterial XdhC, there is negligible sequence identity between the two,[94c] and the two are not able to complement one another in vivo. The role of the sulfurases in cofactor insertion is discussed further below. The cognate to ABA3 in humans is HMCS, and the family appears to be well-conserved in eukaryotes.[96]

2.4. Cofactor Insertion into Apoenzyme

Cofactor insertion in the case of members of the sulfite oxidase family appears to be straightforward, as the cofactor is not particularly deeply buried in the holoenzyme. As illustrated by the structure of the *A. thaliana* sulfite oxidase[97] (Figure 19), it is evident from an examination of the overall protein fold (common to all family members) that the two helices indicated in yellow and blue, possibly along with the N-terminal subdomain in green, could easily move apart transiently in a largely folded apoprotein to accommodate the cofactor; thermal energy alone might be sufficient to induce the necessary conformational changes. Indeed, as indicated above, the cofactor has been shown to bind spontaneously to apo sulfite oxidase in vitro,[39b,45a] although the (most likely passive) involvement of carrier proteins may occur in the case of *apo* nitrate reductase.[72,67] Very recently, it has been demonstrated that in vitro cofactor insertion into apo nitrate reductase from *Neurospora crassa* also occurs spontaneously.[98] Under physiological conditions, however, it cannot be excluded that the Cnx1 (and its orthologues in other organisms) that catalyzes the final molybdenum insertion step into the cofactor may be involved in a specific protein–protein interaction with apoenzymes in the course of cofactor insertion.

The insertion process is necessarily more complex for members of the DMSO reductase family, as the bis pyranopterin form of the cofactor is not simply more deeply buried but also significantly more complicated (particularly when present as the dinucleotide). As discussed above, cofactor insertion involves MobA and usually (but not always) a chaperone; again MobA acts on the bispyranopterin version of the cofactor. The available data suggest that the chaperone stabilizes a distinct apoprotein configuration that enables cofactor insertion.[85b] Members of the DMSO reductase family share a common core protein fold for the molybdenum-binding portion of the protein. As shown in Figure 19 for the *S. massilia* TMAOR reductase,[99] the protein's Domain IV (in blue), which consists of the contiguous stretch from Lys 630 to the C-terminal Ile 798, constitutes a cap on the back side of protein opposite the wide funnel that provides substrate access to the active site molybdenum center. This domain is a highly conserved structural feature of this family. Removal of this cap exposes the entirety of the bis(MGD) cofactor, with the two pyranopterins oriented on top and the molybdenum beneath. Domain IV makes extensive contacts with the pyranopterins and diphosphates of the two equivalents of MGD, but a simple hinge motion swinging the domain to the left as shown in Figure 19 (toward Domains II and III in yellow and green) would expose the cofactor binding site. Absent the cofactor, such a motion might be easily facilitated by binding of TorD and could conceivably occur spontaneously at room temperature. Hopefully, structures of apo forms of

this family of enzyme in complex with their chaperones will be forthcoming in the near future.

Insertion of the molybdenum center into enzymes of the xanthine oxidase family constitutes the greatest challenge. The molybdenum center is not simply deeply buried, but the two protein domains that line the narrow, 15 Å-long solvent access channel to the active site are laced together by multiple passes of the polypeptide chain, and there is no readily identifiable domain motion that might provide better access to the active site of apoenzyme. In both prokaryotic and eukaryotic systems, however, it has become increasingly clear that the enzymes responsible for sulfuration of the cofactor destined for members of the xanthine oxidase family of enzymes participate directly in its insertion once the sulfur has been incorporated. In *R. capsulatus*, for example, the XdhC gene product has been shown to be directly involved in inserting the cofactor, once sulfurated, into the apo form of xanthine dehydrogenase.[78,91a,c,100] XdhC binds only to the apo form of xanthine dehydrogenase,[91c] and only after the pair of [2Fe-2S] clusters and FAD of xanthine dehydrogenase have been incorporated and its subunits assembled into an $(\alpha\beta)_2$ heterotetramer,[100b] indicating that the apoprotein has complete (or nearly complete) structural integrity at the point at which the molybdenum center is incorporated, but exists in a distinct configuration from the holoenzyme. Among eukaryotes, the ABA3 sulfurase of *Arabidopsis thaliana* has also been identified as being involved in cofactor insertion.[94c,101]

Recently, two of us (Hall and Hille) have identified a very highly conserved structural motif in members of the xanthine oxidase family (residues 1011–1136 in the bovine enzyme, residues 463–603 in the XdhB subunit of the *R. capsulatus* enzyme) that may be important in recruiting the XdhC insertion machinery.[102] The identified region is a highly conserved structural feature of members of the xanthine oxidase family, although there are structural details and sequence variations that differ from organism to organism, which could account for the general failure of bacterial systems to efficiently incorporate cofactor into heterologously expressed eukaryotic members of the xanthine oxidase family. Among the implications of the model proposed is that the molybdenum center is inserted “molybdenum first” from the side of the protein opposite the substrate access channel to the active site, followed by the pyranopterin and finally its phosphorylated side chain. In the CO dehydrogenase from *Oligotropha carboxidovorans*,[103] another member of the molybdenum hydroxylase family that possesses the cytosine dinucleotide form of the pyranopterin cofactor, the cytosine portion of the cofactor extends toward the protein surface sandwiched between the (now collapsed) walls of the putative cofactor access channel identified.

As indicated above, two homologues of the *R. capsulatus* XdhC have been crystallographically characterized, from *B. halodurans* and *M. smegmatis* (PDB 3ON5 and 2WE7, respectively, both of which are unpublished), which allows a model for the insertion process to be developed. Figure 20 shows a model of the *B. halodurans* XdhC homologue in complex with the *R. capsulatus* xanthine dehydrogenase, and it can be seen that there is an excellent overall fit in the identified region of the xanthine dehydrogenase that may be involved in interacting with XdhC (in red in Figure 20). In this model, the putative cofactor binding sites in the XdhC homologue (see Figure 18) lie on the surface of the homologue facing the dehydrogenase, but more or less on the opposite side of the cofactor binding site

from the substrate access channel. As has been pointed out previously,[102] it appears that a significant conformational change, likely involving the two regions in red in Figure 20, is required to allow access to the cofactor binding site. In comparing the amino acid sequences of bacterial and vertebrate members of the xanthine oxidase family of enzymes, it is evident that each subunit of the former invariably possesses two 19–20 aa inserts, and in the model these interact intimately with the docked XdhC homologue. One of these lies at the end of the region shown in red in Figure 20 (indicated in yellow). The majority of the second bacterial insert is not resolved in any of the several crystal structures that have been reported, but its general position on the surface of the protein is readily discerned (in yellow, Figure 20, arrows) and is seen to lie immediately on either side of the docked XdhC homologue, near its subunit interface. It has previously been suggested that these inserts play an important role in recruiting XdhC for cofactor insertion into the bacterial enzymes, and their absence in eukaryotic enzymes may account for why the latter typically have very low levels of cofactor incorporation when expressed from recombinant bacterial systems.[102]

3. THE XANTHINE OXIDASE FAMILY

3.1. Overview

Members of the xanthine oxidase family of molybdenum-containing enzymes usually catalyze the oxidative hydroxylation of a carbon center of their substrates (most often an aromatic heterocycle or an aldehyde). Bovine xanthine oxidase is the prototypical member and is one of the longest-studied enzymes, having been first purified to homogeneity in 1924.[104] The enzyme as typically isolated from cow's milk is an oxidase, but the physiologically relevant form expressed in most vertebrate tissues is a dehydrogenase that utilizes NAD^+ rather than O_2 as oxidizing substrate. The mammalian dehydrogenase is reversibly converted to the oxidase by oxidation of thiols to disulfides, or irreversibly converted by mild proteolysis. Because the oxidase and dehydrogenase forms are products of the same gene, the enzyme is perhaps best referred to generically as xanthine oxidoreductase. By contrast to the mammalian enzyme, that from other sources (including avian, insect, and bacterial) exists as a stable dehydrogenase. The molybdenum-containing xanthine oxidoreductases are extremely broadly distributed in biology, and only a few organisms oxidize xanthine by alternative means. *Aspergillus nidulans* and certain yeasts utilize an Fe^{2+}/α-ketoglutarate hydroxylase to convert xanthine to uric acid,[105] and a third xanthine-oxidizing system has recently been identified in *Klebsiella* species.[106] In addition to the xanthine-metabolizing molybdenum enzymes, most organisms also encode one or more aldehyde oxidases that are very similar in reactivity and cofactor constitution to their xanthine-oxidizing counterparts, but which are obligatory oxidases unable to utilize NAD^+ as oxidizing substrate.

All members of the xanthine oxidase family have redox-active centers in addition to the molybdenum center (at which xanthine is oxidatively hydroxylated to uric acid): minimally a pair of spinach-ferredoxin-like [2Fe-2S] clusters, and usually FAD as well. O_2 and NAD^+ react at the FAD site rather than the molybdenum center, and as a result intramolecular electron transfer between molybdenum and FAD via the intervening iron–sulfur centers is an obligatory aspect of turnover. The otherwise closely related aldehyde:ferredoxin

oxidoreductase from organisms such as *Desulfovibrio gigas* lack FAD (see section 3.3.1), and the 4-hydroxybenzoyl-CoA reductase from *Thaura aromatica* (see section 3.4.4) has an additional redox-active center, a [4Fe-4S] cluster. In all cases, the redox-active centers are found in discretely folded domains or autonomous subunits, with the eukaryotic enzymes being organized as α_2 dimers, and the bacterial enzymes typically as $(\alpha\beta)_2$ or $(\alpha\beta\gamma)_2$ oligomers. The variation in overall subunit organization notwithstanding, the homologous regions of these enzymes exhibit a very high degree of structural similarity to one another. The complex overall structure of the eukaryotic enzymes appears to have been built up from simpler elements over the course of evolution, from the original $(\alpha\beta\gamma)_2$ form through the $(\alpha\beta)_2$ intermediate to the $(\alpha)_2$ form seen in eukaryotes. Having said this, the order of the genes in bacterial operons does not always reflect order of the cognate domains in the eukaryotic proteins. The two [2Fe-2S]-containing domains are invariably N-terminal to the central FAD domain in the protein, followed by the C-terminal molybdenum-binding portion of the protein, but in, for example, the operon encoding the $(\alpha\beta\gamma)_2$ CO dehydrogenase from *Oligotropha carboxidovorans*, the genes are arranged in the order FAD–Fe/S–Mo (*coxMSL*, respectively).[107]

3.2. Xanthine Oxidoreductase

3.2.1. Introduction to Structure—The X-ray crystal structures of xanthine oxidoreductase from bovine milk, in both dehydrogenase and oxidase forms,[108] followed the earlier report of the structure of the aldehyde:ferredoxin oxidor-eductase from *Desulfovibrio gigas* (that lacked FAD).[109] The structure of the bovine xanthine dehydrogenase, as elucidated by Pai, Nishino, and co-workers,[108] is shown in Figure 21, with the domains containing each of the redox-active centers color-coded. Each monomer consists of five domains, from the N-terminus: two domains each with a [2Fe-2S] ferredoxin-like cluster, a first with principally β-sheet secondary structure and resembling the fold seen in spinach ferredoxin, and a second fold that is principally α-helical; a third domain that possesses FAD (this domain is absent in the *D. gigas* enzyme); and two large, C-terminal domains that together bind the active site molybdenum center at their interface. The subunit contacts in the dimer are limited and entirely within the molybdenum-binding portion of the protein (as discussed above in regard to the possible manner in which the molybdenum cofactor is inserted). The molybdenum centers themselves are some 52 Å apart, and the electron-transfer pathways of the two monomers are well-insulated from one another. The polypeptide strand makes a single pass in going from one domain to the next within each monomer, meaning that not only are the domains themselves autonomous structural elements of the polypeptide but that each domain is encoded by a contiguous stretch of the structural gene for the protein (consistent with the gene duplication/fusion process by which the protein presumably arose). The disposition of the redox-active centers within each protomer defines an approximately linear pathway for electron transfer from the molybdenum center (site of the reductive half-reaction) to the FAD (site of the oxidative half-reaction), with the two iron–sulfur centers intervening.

The two iron–sulfur centers of xanthine oxidase have long been distinguishable on the basis of their EPR signals.[110] That designated Fe/S I signal has $g_{1,2,3}$ = 2.022, 1.932, 1.894, with unexceptional linewidths and relaxation properties for a [2Fe-2S] cluster, while Fe/S II has

$g_{1,2,3}$ = 2.110, 1.991, 1.902 and unusually broad linewidths and relaxation properties such that it is observed only below 25 K.[111] Site-directed mutagenesis studies with rat xanthine oxidoreductase have allowed assignment of the two iron–sulfur clusters,[112] with Fe/S I being the cluster in the unusual α-helical domain that is proximal to the molybdenum center and Fe/S II that in the more commonly seen ferredoxin-like domain. This assignment is consistent with the known coupling of Fe/S I to the molybdenum center,[113] because this is the [2Fe-2S] cluster that is proximal to the molybdenum in the crystal structure. The pathway for electron transfer within the enzyme is thus Mo → Fe/S I → Fe/S II → FAD. It is interesting to note that the distal amino group of the pyranopterin cofactor is within hydrogen-bonding distance to one of the cysteine residues (Cys 150 in the bovine enzyme) coordinating the nearer Fe/S I.

The structure of the molybdenum center is shown in Figure 1, although it is to be noted that the Mo=S rather than Mo=O was initially considered to occupy the apical position of the molybdenum coordination sphere of the *D. gigas* aldehyde oxidoreductase.[114] Subsequent spectroscopic work with the bovine enzyme[115] and crystallography with CO dehydrogenase[103,116] and quinoline 2-oxidoreductase,[117] as well as that of bovine xanthine oxidase complexed with the slow substrate FYX-051,[118] has clearly demonstrated that it is the Mo=O that is apical, and it is now generally recognized that this is the case in all enzymes of the xanthine oxidase family. Also, the catalytically labile equatorial oxygen ligand is now understood to be a hydroxide ligand rather than water,[119] a point that has mechanistic implications (see below). Figure 22 shows the active site of bovine xanthine dehydrogenase, including several amino acid residues that have been shown to be catalytically important (see below). Phe 914 and Phe 1009 (in the bovine enzyme numbering) sit at the end of a 14.5 Å long substrate access channel and constrain substrate, once bound, to a plane approximately parallel to the apical Mo=O group of the molybdenum center. The equatorial Mo–OH projects directly toward the substrate binding site. Four other active site residues are universally conserved in prokaryotic as well as eukaryotic xanthine oxidoreductases and dehydrogenases: Glu 802, Gln 767, Glu 1261, and Arg 880. These residues, along with the molybdenum center itself, define the structural environment in which catalysis takes place; the roles of these residues in catalysis are discussed further below.

3.2.2. Reaction Mechanism—The overall reaction mechanism of xanthine oxidoreductase is now generally understood to occur as shown in Figure 23[3,120] with proton abstraction of the equatorial Mo–OH by the active site Glu 1261, followed by nucleophilic attack on the carbon to be hydroxylated. The equatorial ligand must be hydroxide rather than water, as only the deprotonated Mo–O^- is sufficiently nucleophilic to undertake the reaction. Concomitant hydride transfer to the Mo=S group gives an initial $LMo^{IV}O(SH)(OR)$ intermediate. This then breaks down by displacement of product from the molybdenum coordination sphere by hydroxide from solvent, with electron transfer from the molybdenum to the other redox-active centers of the enzyme and deprotonation of the Mo–SH to return to the Mo=S of oxidized enzyme. The sequence in which the later events occur depends on the reaction conditions and the substrate utilized; when electron transfer out of the molybdenum center precedes displacement of product, an $LMo^{V}OS(OR)$ species eliciting an EPR signal

termed “very rapid” (on the basis of the kinetics of its appearance in the course of the reaction of enzyme with xanthine) is formed. Under most conditions, however, product dissociation precedes electron transfer out of the molybdenum center, and the “very rapid” species is by-passed. The evidence in support of this mechanism includes the following:

- Water is the ultimate source of the oxygen atom incorporated into the hydroxyl group of product in the course of the reaction,[121] but a catalytically labile oxygen site on the enzyme exists that is the proximal hydroxyl donor (regenerated from solvent at the completion of each catalytic cycle).[122] This catalytically labile oxygen has been shown to be the equatorial Mo–OH of the molybdenum coordination sphere,[120,123] consistent with the protein crystal structure showing the Mo–OH pointing toward the substrate binding site.[108]
- The kinetic parameters k_{cat}/K_m and k_{red}/K_D, which track the reaction of free enzyme with free substrate through the first irreversible step of the reaction, both exhibit a bell-shaped pH dependence,[124] consistent with base catalysis on neutral substrate (pK_a 7.4[125]). The lower pK_a of 6.6 has subsequently been attributed to the active site Glu 1261 observed crystallographically.[126] The absence of the ionization with the higher pK_a in the pH profile of k_{cat} or k_{red} rules out it arising from any functional group on the enzyme.[124]
- The reactivity of enzyme toward a homologous series of quinazoline derivatives is consistent with a mechanism involving nucleophilic attack on substrate.[127]
- The Mo–SH proton of the reduced center, while solvent-exchangeable, is initially derived from the C-8 position of xanthine that becomes hydroxylated,[128] consistent with reduction of the molybdenum center via hydride transfer to the Mo=S sulfur.
- With the slow substrate 2-hydroxy-6-methylpurine,[129] the reaction proceeds through a reduced Mo(IV) species with product complexed to the molybdenum, which subsequently oxidized by one electron to a Mo(V) species giving rise to the “very rapid” EPR signal.[130]
- Although it had been suggested that the Mo^V species might be formed directly by direct one-electron oxidation of substrate,[131] the lack of correlation between reduction potential and reaction rate in a homologous series of substituted purines indicates that this is not the case.[132]
- The structure of the “very rapid” species has been examined by ESEEM,[133] ENDOR,[134,135] and finally crystallographically;[136] while the ENDOR data were initially interpreted as favoring a direct Mo–C bond in the signal-giving species,[134] it is now clear that the signal-giving species is best formulated as $LMo^VOS(OR)$, with OR being product coordinated in a simple end-on fashion to the molybdenum via the catalytically introduced hydroxyl group, as is observed crystallographically.[135,136]

Not shown in Figure 23 are any of the species giving rise to the “rapid” family of EPR signals that appear on approximately the same time scale as the decay of the “very rapid” signal[137,137b,138] and were long thought to arise from an intermediate lying downstream

from the "very rapid" species in the catalytic sequence. It has been shown that this signal possesses bound substrate rather than product, however, and can be formed very rapidly and noncatalytically simply by binding substrate to enzyme that has been partially prereduced by titration with sodium dithionite and possesses a molybdenum center in the Mo(V) state.[139] Although a deadend intermediate from a kinetic standpoint (the molybdenum center cannot react with substrate until fully reoxidized to the Mo(VI) state), the "rapid" species in fact represents a paramagnetic analogue to the Michaelis complex of the enzyme.

Values for the microscopic rate constants for formation and decay of the key $LMo^{IV}O(SH)(OR)$ intermediate of the reductive half-reaction as a function of temperature have been obtained, and these have been used to obtain the entropy and enthalpy of activation for each step.[140] Formation of the first intermediate has a large negative entropy of activation (−70 cal mol^{-1} deg^{-1}) indicative of a highly ordered transition state, as might be expected on the basis of the likely concerted nucleophilic attack/hydride transfer chemistry involved. Interestingly, this results in a reversal of the relative rate constants for formation and decay of this intermediate over the temperature range 15–50 °C: at lower temperatures, breakdown of the $LMo^{IV}O(SH)(OR)$ intermediate by product dissociation becomes rate-limiting. Indeed, isotope labeling experiments with both the bovine and the chicken enzymes have shown that at lower temperatures product dissociation is predominantly rate-limiting in the reductive half-reaction, and the first (chemical) step of the reaction (leading to the $LMo^{IV}O(SH)(OR)$ intermediate) is faster by a factor of approximately 75.[141]

The reaction mechanism of xanthine oxidase has also been examined computationally by a number of groups, with the results generally supporting the reaction mechanism shown in Figure 23. Voityuk et al.[142] examined the reaction of an $LMo^{VI}OS(OH)$ active site model (with L = butene-2,3-dithiolate) with formamide (a known substrate for the enzyme that gives rise to the "very rapid" EPR signal[143]) and found evidence for a reaction involving nucleophilic attack on the substrate carbon and $sp^2 \rightarrow sp^3$ rehybridization in the course of the reaction. This pathway was found to lie to considerably lower in energy than one involving insertion of the C–H bond of substrate across the Mo=S group to give an intermediate with a direct Mo–C bond, as had been previously suggested.[144] Subsequent computational work with formamide as substrate substantiated the need for the equatorial Mo=S of the molybdenum coordination sphere for catalytic activity: substitution of this sulfur with oxygen raised the activation barrier for hydride transfer substantially (12–17 kcal/mol),[145] more than sufficient to account for the loss of catalytic activity observed experimentally when the sulfur is lost.[89c] Interestingly, substitution of tellurium for sulfur lowered the transition state energy by 3 kcal/mol, suggesting that a tellurium- or selenium-substituted form of the enzyme might exhibit even more activity than the native form. The high covalency of the Mo=S (or, presumably to an even greater degree, Mo=Se) has been shown to be due principally to the π rather than σ interaction between the in-plane ligand p orbital and the redox-active d_{xy} of the molybdenum.[146] This covalency has the effect of substantially delocalizing the formally unoccupied Mo d_{xy} orbital of the oxidized enzyme onto the sulfido group, thereby increasing its electrophilicity relative to an oxo group and enhancing its reactivity as a hydride acceptor. Interestingly, as discussed further below, one member of the xanthine oxidase family, nicotinate dehydrogenase from the anaerobic soil

bacterium *Eubacterium barkerii*, has recently been shown to possess selenium naturally, and the substitution of Se for S in the molybdenum coordination sphere to contribute an additional 3 kcal/mol in transition state stabilization.[145b]

An explicit analysis as to whether nucleophilic attack and hydride transfer are concomitant, or whether the reaction leading to the $LMo^{IV}O(SH)(OR)$ species passes through a discrete sp^3-hybridized intermediate,[147] using both formamide and acetaldehyde among other substrates, has indicated that the concerted mechanism is more energetically favorable, by some 6 kcal/mol, and this seems to be the case even when xanthine rather than formamide is used as substrate in the calculations.[148] Consistent with a reaction mechanism initiated by base-catalyzed abstraction of the Mo–OH, it has been shown that initiating the reaction with the ionized rather than protonated model results in a lower activation barrier (A. Ibdah and R. Hille, unpublished). It has been also proposed that Glu 1261, having abstracted the proton from the Mo–OH, subsequently protonates substrate at N9, and this (rather than substrate tautomerization) contributed further to transition state stabilization. Such a role for Glu 1261 had been suggested previously,[149] but unfortunately Arg 880 of the active site was not explicitly included in the calculations, seriously biasing the results in favor of substrate protonation (as opposed to stabilizing the negative charge accumulating on substrate in the course of nucleophilic attack by charge compensation with the arginine, see below).

A QM/MM approach has also been applied to the reaction mechanism, with the chemical transformations in the active site dealt with quantum mechanically and active residues not directly involved in bond making and breaking treated using less computationally intensive molecular mechanics.[150] Importantly, a large number of combinations of tautomeric forms for xanthine as substrate, ionization states of active site residues, and alternate substrate orientations were explicitly considered, and in all cases the lowest-energy reaction coordinate was found to involve base-assisted nucleophilic attack, as expected.[150a] Referring to Figure 22, with both Glu 1261 and Glu 802 (the former ionized and the latter protonated), the LMoOS-(OH) form of the molybdenum center, and xanthine, pathways starting with substrate oriented in each of the two possible orientations between the two phenylalanine residues were specifically considered. It was concluded that xanthine preferentially bound in the orientation seen crystallographically in the complex of xanthine with the catalytically inactive desulfo form of the enzyme, with its C_6=O oriented toward Arg 880 (see below),[151] but that the reaction proceeded with lower overall activation barrier from the inverted orientation, with the C_2=O oriented toward Arg 880. After the initial nucleophilic attack, the QM/MM results indicated that the reaction progressed through a complicated series of substrate tautomerization and proton transfers to and from the heterocycle in going to completion. Unfortunately, in comparing the barrier heights for the reaction pathways, the authors did not consider the free energy required to populate the less stable but more reactive substrate orientation, and this should necessarily be counted as part of the thermodynamic cost of attaining the transition state. In addition, the calculations began with a protonated Glu 802 (requiring that its pK_a lie well above 8.0), which could have biased the relative activation barriers for the two orientations. It remains for future studies incorporating Arg 880 explicitly in DFT and QM/MM calculations such as these to clarify the relative roles of substrate protonation and tautomerization in contributing to

transition state stabilization. A more detailed discussion of this and other computational studies to the reaction mechanism of xanthine oxidase and related enzymes has been presented elsewhere.[7f]

More recently, a valence bond description of the hydride transfer aspect of the first step of the reaction has been developed.[152] The upshot of the study is that both Mo=S π → C–H σ* and C–H σ → Mo=S π* donation contribute to activation of the C–H bond for heterolytic cleavage, along with O_{eq} lp → C2H σ* and S lp → C–H σ* interactions. It has also been concluded that an O_{eq} lp → Mo + C charge-transfer interaction plays an important role in transition state stabilization, and that the electronic delocalization accruing from charge transfer reduces electronic repulsion along the reaction coordinate, thereby contributing to transition state stabilization. Although the calculated extent of transition state stabilization, ~89.5 kcal/mol, was very large, the results at a qualitative level nevertheless illustrate the specific orbital interactions that facilitate effective hydride transfer from substrate to the molybdenum center.

3.2.3. The Structural Basis of Catalytic Power—In the absence of a suitable recombinant expression system for substantive amounts of the functional eukaryotic xanthine oxidoreductase, the roles of several highly conserved active site residues have been examined by site-directed mutagenesis studies of the *R. capsulatus* xanthine dehydrogenase, which bears strong structural homology to the bovine enzyme and has a virtually identical active site.[153] Residues important in catalysis include Glu 730 (equivalent to Glu 1261 in the bovine enzyme), Glu 232 (Glu 802), Gln 197 (Gln 767), and Arg 310 (Arg 880); refer to Figure 22. The substrate binding site is further comprised of Phe 344 and 459 (Phe 914 and 1009 in the bovine enzyme), which again constrain substrate to a plane approximately parallel to the apical Mo=O bond.

Mutation of Glu 730 in the *R. capsulatus* enzyme to Ala reduces the limiting rate constant for reduction by xanthine by at least 7 orders of magnitude, from 67 s^{-1} to no greater than 0.00005 s^{-1},[154] corresponding to at least 10 kcal/mol of compromised transition state stabilization with the mutant. Mutation of Glu 232 to Ala results in a more modest 12-fold decrease in k_{red} in reductive half-reaction studies, as well as a 12-fold increase in K_d.[154] The equivalent E803 V mutant of the *E. coli*-expressed human xanthine oxidoreductase exhibits a comparable reduction in the steady-state k_{cat} and increase in K_m[149] (although insufficient material was available for more detailed studies of the eukaryotic enzyme). Assuming there is no change in rate-limiting step (but see below), these results indicate that approximately one-half of the ~3 kcal/mol in free energy associated with the interaction of Glu 232 with substrate is used to stabilize the transition state and accelerate reaction rate, with the remainder contributing to substrate affinity. On the basis of the calculated relative stabilities of several tautomers of free xanthine and the purine ring in the $LMo^{IV}O(SH)(OR)$ intermediate, it has been suggested that Glu 232/802 accelerates reaction rate specifically by facilitating a tautomerization of the heterocycle in the course of nucleophilic attack that involves proton transfer from N_3 to N_9 of the purine ring, thereby compensating for the negative charge accumulating on the imidazole subnucleus of the purine in the course of the reaction[155] (see Figure 24). Mutation of another active site residue, Gln 197, to Ala results in only a 7-fold decrease in k_{red}, with the same 34 μM K_d as wild-type enzyme.[154] This

residue does not interact with substrate but instead hydrogen bonds to the apical Mo=O of the molybdenum center at a distance of 3.1 Å, and its mutation appears to alter the intrinsic reactivity of the molybdenum center.

Mutation of Arg 310 to the approximately isosteric Met results in a decrease in the limiting rate constant k_{red} reduction of enzyme by xanthine by a factor of approximately 10^4, to 0.002 s^{-1};[156] consistent with this, an R881M mutant of the human enzyme has no detectable activity in steady-state assays[149] (although again more detailed analysis was not possible due to availability of material). Arg 310/881 is some 8 Å from the Mo–OH oxygen and the locus of the hydroxylation chemistry, and it might have been expected that the principal effect of the mutation would be compromised affinity for substrate. Instead, it is evident from the pronounced effect on k_{red} that the interaction of the arginine with substrate contributes significantly to the catalytic power of the enzyme, stabilizing the transition state by approximately 5.5 kcal/mol. Although less active toward xanthine, however, the R881M mutant had considerably more reactivity toward benzaldehyde as substrate, with both a 2-fold lower K_m and a 3-fold higher k_{cat} as compared to wild-type enzyme.[154] Arg 310/881 is not conserved in the otherwise closely related vertebrate aldehyde oxidases (see section 2.3), where a methionine is usually found instead, and it is evident that this residue contributes to the substrate specificity that distinguishes the two subfamilies of enzyme. How the arginine found in the xanthine-utilizing enzymes contributes specifically to transition state stabilization is suggested by a comparison of the reactivity of enzyme with a homologous series of purine substrates, all hydroxylated at the C-8 position, with the wild-type enzyme and R310M mutant. The substrates fall into two groups: a first consisting of good substrates that react rapidly with wild-type enzyme and which are significantly affected by the R310M mutation, and a second consisting of poor substrates for the wild-type enzyme but which are only minimally affected by the mutation.[156] The results have been interpreted as reflecting the existence of two alternate substrate orientations in the active site, a more catalytically productive one with C_6=O (or C_6=S) of substrate positioned adjacent to Arg 310 to stabilize the negative charge accumulating on the heterocycle in the course of nucleophilic attack, and a second with the purine oriented “upside down” between the two phenylalanine residues, with C_6=O pointing away from Arg 310 so that it is unable to make such a stabilizing interaction. Poor substrates are proposed to bind to wild-type enzyme in this less catalytically productive orientation such that they cannot make use of Arg 310 (or Glu 232 for that matter), but are therefore not affected by the R310M mutation. The implication is that a major factor distinguishing good substrates from poor ones is their orientation in the active site (but see below).

The discussion above with regard to Arg 310/880 illustrates the extent to which substrate orientation is likely to be important in understanding the catalytic roles of different active site residues. With xanthine oriented as shown in Figure 24, Glu 232/802 can facilitate tautomerization as proposed. If substrate instead binds in the opposite orientation, then Glu 802 must stabilize the transition state in some other, unspecified way. Similarly, in the case of Arg 880, if it interacts with the C_2=O rather than C_6=O, it cannot be involved in stabilization of negative charge at the latter position of substrate. Several crystal structures have now been reported for the bovine enzyme in complex with various substrates bound in

the active site that are in fact consistent with the hypothesis that good substrates bind with their C_6=O oriented toward the arginine, and poor ones in the opposite orientation. As shown in Figure 25, 2-hydroxy-6-methylpurine (a poor substrate) is bound with its C_2=O oriented toward Arg 880. By contrast, the complex of enzyme that has been inactivated by reaction of cyanide (thus removing the catalytically essential Mo=S group[89c]) with xanthine (a good substrate) has substrate oriented with its C_6=O oriented toward the arginine in both the bovine[157] and the *R. capsulatus*[158] enzymes; lumazine (the pterin homologue to xanthine and another good substrate) assumes an equivalent orientation.[157] It is to be emphasized that at the resolutions reported, 2.2–2.6 Å for the bovine enzyme, it is generally straightforward to assign substrate orientation.[159] Indeed, the principal issue is not the resolution of the crystal structure but rather the inherent degree of asymmetry in the electron density attributable to the bound substrate. The degree of asymmetry evident in the electron density attributable to bound xanthine as illustrated in Figure 25 (right) is clearly sufficient to define a single preferred orientation for xanthine.

Complicating the issue of substrate orientation, the 1.1 Å resolution structure of a D428A mutant of rat xanthine dehydrogenase in complex with uric acid, but in an apo form lacking the molybdenum center altogether, has been reported.[160] The uric acid is found with its C_2=O oriented toward Arg 803 (in the rat protein), rather than its C_6=O as would have been expected on the basis of the above. Direct comparison between uric acid and xanthine binding is complicated by, however, the fact that while xanthine is neutral at neutral pH, uric acid is ionized to the urate monoanion. The overall position of urate relative to the polypeptide (particularly with regard to the two phenylalanine residues) is virtually identical to that seen previously in the complex of reduced enzyme with the inhibitor alloxanthine.[158] Alloxanthine directly coordinates the molybdenum via its N2 ring nitrogen (a position equivalent to the C-8 of purines), displacing the equatorial Mo–OH. In both structures, the heterocycle sits some 1.5–2.0 Å deeper into the active site than can substrate when the Mo–OH group is present. The relative positions of the heterocycles for which crystal structures exist are shown in Figure 26, and the key question is the orientation that substrate prefers in the shallower, catalytically relevant position. A second crystal structure has recently been reported of urate complexed with enzyme that had been prereduced by Ti(III)·citrate. In this structure, there is finite electron density intervening between the heterocycle and molybdenum, indicating that urate has displaced the equatorial Mo–OH ligand of the molybdenum coordination sphere.[160] Again, the heterocycle is oriented with its C_2=O rather than C_6=O carbonyl oriented toward the arginine (and again, deeper into the active site), although the fact that urate exists as the monoanion at neutral pH raises questions as to its suitability as a surrogate for the neutral xanthine. Regardless of its orientation, however, it is interesting that the C-8 carbon of bound urate appears to be sp^3 rather than sp^2-hybridized, implying that the structure is that of a species formed subsequent to nucleophilic attack and formation of the C–O bond of product, but prior to hydride transfer. The stability of this species suggests that nucleophilic attack and hydride transfer occur sequentially rather than concomitantly in leading to the $LMo^{IV}O(SH)(OR)$ intermediate, although the strongly reducing conditions used to generate the sample may have resulted in a species not directly relevant to the catalytic sequence. The upshot is that the question of substrate orientation thus remains unresolved. Were catalysis to proceed with substrate oriented with its C_2=O

oriented toward Arg 880, the several active site residues must play different roles in substrate binding and rate acceleration. Specifically, Glu 802 cannot be involved in protonating the imidazole subnucleus of the heterocycle, and it has been suggested instead that Glu 1261 does so after abstracting the Mo–OH proton.[149] Glu 802 is instead proposed to be protonated and hydrogen bonding to the proximal C-6 carbonyl group of substrate. This alternate interpretation is supported by the QM/MM work described above[150] (although as indicated above, questions remain as to proper gauging of the relative activation barriers for the two substrate orientations, as well as the proper ionization state of Glu 802 and the presence of Arg 880 in the calculations).

Regardless of the issue of substrate orientation in the active site, it is important to recognize that the effect of the mutations discussed above in all likelihood underestimates the intrinsic effect on catalysis, because with wild-type enzyme the rate-limiting step in the reductive half-reaction is product release rather than the chemical step of the reaction (i.e., formation of the $LMo^{IV}O(SH)(OR)$ intermediate): in the case of the bovine and chicken enzymes, it has been shown that the chemical step of the reaction is some 75-fold faster than product release.[141] Assuming that the chemical step has become rate-limiting in the E730A, R310M, and E232A mutants described above, the actual effect of a given mutation on the kinetics of enzyme reduction is larger by approximately another two orders of magnitude (and ~2.8 kcal/mol in transition state stabilization). The precise extent to which product release is rate-limiting in the *R. capsulatus* enzyme has not been determined experimentally.

Xanthine oxidase not only hydroxylates xanthine at C-8 to give uric acid but also hypoxanthine at C-2 to give xanthine, and crystal structures of bovine xanthine oxidase in complex with hypoxanthine (at 1.8 Å resolution) and the chemotherapeutic agent 6-mercaptopurine (at 2.6 Å resolution) have been reported.[161] For both hypoxanthine and 6-mercaptopurine, two different orientations are observed in the two active sites of the crystallographic asymmetric unit (in each case containing one protein dimer). One orientation is appropriate for hydroxylation at C-2 of substrate, leading to xanthine or 6-thioxanthine as product, respectively; the other has C-8 oriented toward the active site molybdenum center, as if to give 6,8-dihydroxypurine or 6-thio-8-hydroxypurine. It has been shown that hypoxanthine is in fact hydroxylated quantitatively at C-2, indicating that the crystallographically observed orientation that would lead to hydroxylation at C-8 is not catalytically productive.[161] A MOPAC analysis of hypoxanthine shows that that the C-2 position is indeed substantially more electron-deficient than C-8, indicating that it is intrinsically more susceptible to nucleophilic attack. The observed enzyme preference for hydroxylation of hypoxanthine at C-2 over C-8 thus appears to involve a combination of substrate orientation effects and differences in the intrinsic reactivity of the two sites. This work has also shown that the preferred tautomer of hypoxanthine with N-9 of the imidazole subnucleus is (modestly) more stable than that with N-7 protonated. This being the case, Glu 802 is again positioned so as to facilitate tautomerization and negative charge stabilization in the course of nucleophilic attack on hypoxanthine, this time from N-9 to N-3 (the reverse sense as proposed in the hydroxylation of xanthine at C-8, but reasonable because hydroxylation is occurring on the pyrimidine rather than imidazole subnucleus of substrate). Also, Arg 880 is positioned to stabilize negative charge accumulation on the C_6=O oxygen

as nucleophilic attack progresses. A comparison of the effects of mutation of Glu 803 and Arg 881 of human xanthine oxidoreductase with xanthine and hypoxanthine as substrate indicates that Arg 881 plays the more important role with xanthine as substrate, but Glu 803 has the greater role catalytically with hypoxanthine as substrate.[149]

In addition to EPR signals such as "rapid" and "very rapid" that are known to be relevant to the catalytic sequence, a number of Mo(V) EPR signals are observed with enzyme that has been inactivated in one way or another. These include the following: "slow" (arising from the nonfunctional desulfo enzyme that has lost its catalytically essential Mo=S group[137]); "formaldehyde inhibited" and "glycol inhibited" (arising from enzyme that has been treated with formaldehyde[162] or ethylene glycol,[163] respectively); "desulfo inhibited" (seen when desulfo enzyme is treated with ethylene glycol[164]); "alloxanthine inhibited" (due to functional enzyme that has been treated with the inhibitor alloxanthine[165]); and "arsenite inhibited" (a family of signals arising from either functional or desulfo enzyme that has been treated with arsenite[166]). The formaldehyde-inhibited signal has been examined by ENDOR spectroscopy,[134,144] it being concluded on the basis of the strong (43 MHz) and isotropic coupling to ^{13}C when labeled formaldehyde is used that the signal-giving species possessed a direct Mo–C bond. The ENDOR of this species has since been revisited, it being concluded that it does not in fact have a direct Mo–C bond but instead has formaldehyde inserted across the equatorial MoOS unit to give a four-membered ring with carbon inserted across the oxygen and sulfur.[167] The unusually strong ^{13}C coupling is due to a strong transannular effect, in which the geometry of the Mo–O–C–S ring places the carbon directly in line with a lobe of the singly occupied Mo d_{xy} orbital, a phenomenon for which there is chemical precedent.[168] With regard to the arsenite-inhibited enzyme, a combined crystallographic and EPR study of the desulfo form of the *D. gigas* aldehyde:ferredoxin oxidoreductase has concluded that arsenite coordinated to the molybdenum in a monodentate fashion and elicits one specific from of arsenite-inhibited EPR signal that apparently arises from binding of inhibitor to desulfo enzyme.[169] On the other hand, a crystallographic study of the functional xanthine oxidase in complex with arsenite clearly shows arsenite spanning the MoOS unit to give a diamond-shaped structure reminiscent of that seen with the formaldehyde-inhibited enzyme, accounting for the very strong[75] As coupling ($I = 3/2$) seen in the EPR signals.[166] The structure is also consistent with previous XAS studies of arsenite-inhibited enzyme, which yielded a Mo–As distance of 3.0 Å and unequivocally demonstrated sulfur in the first coordination shell of arsenic.[170]

3.2.4. Intramolecular Electron Transfer and the Oxidative Half-Reaction—It has long been recognized that intramolecular electron transfer is an integral aspect of turnover of all members of the xanthine oxidase family of enzymes, and that in the course of equilibrium reductive titrations, reducing equivalents distribute themselves according to the relative reduction potentials of the enzyme's redox-active centers on a time scale that is fast as compared to catalysis (with $k_{cat} = 18\ s^{-1}$ at pH 8.5).[171] The explicit rate constants for electron transfer within the bovine enzyme have been examined by both pH-jump[172] and pulse radiolysis[173] methods. In the first type of experiment, advantage is taken of the greater pH dependence of the FAD and molybdenum reduction potentials relative to those of the iron–sulfur clusters to perturb the distribution of reducing equivalents within partially

reduced enzyme. By mixing partially reduced enzyme in dilute buffer at one pH with more concentration buffer at another (under strictly anaerobic conditions), reequilibration of reducing equivalents between Fe/S I and FAD ranges from 155 s^{-1} at pH 6 to 330 s^{-1} at pH 9.[172a] The observed solvent kinetic isotope effect on the observed equilibration is 6.9, and the linear dependence of the observed rate constant on mole fraction of D_2O indicates that the effect involves a single proton.[172b] Knowing the relative reduction potentials of the centers involved (from which the K_{eq}, the ratio of the microscopic forward and reverse rate constants, can be determined) and the observed rate constant for equilibration of reducing equivalents (representing the sum of the forward and reverse rate constants), the forward and reverse rate constants for the equilibrium can be calculated explicitly in both H_2O and D_2O, it being found that the isotope effect is much larger for the $FADH^{\bullet} \rightarrow$ Fe/S I_{ox} electron transfer event than the reverse process. This has led to the conclusion that the N_5–H proton of the neutral flavin semiquinone is in motion as the system traverses the electron-transfer transition state, meaning that proton and electron transfer are coupled. This has been attributed to the destabilization of the $FAD^{\bullet-}$ anionic semiquinone by the protein environment, which makes discrete deprotonation of the neutral semiquinone prior to electron transfer thermodynamically unfavorable.[172b] The relatively slow electron transfer between flavin and Fe/S I accounts for only about one-half of the expected spectral change for the pH jump experiment, and in subsequent pulse radiolysis studies, electron transfer between the molybdenum center and Fe/S I (after the former was extremely rapidly reduced with radiolytically generated radical of methylnicotinamide) has been observed with k_{et} = 8500 s^{-1}.[173a] Subsequent electron transfer from the iron–sulfur centers on to the flavin occurs at 125 s^{-1}, in good agreement with the pH jump work. The observation of Mo $\rightarrow$ Fe/S $\rightarrow$ FAD electron transfer in the protein has subsequently been substantiated with the X-ray crystal structure of the protein, which shows the two iron–sulfur centers intervening between the molybdenum center and FAD. It is noteworthy that the coupled electron/proton transfer involving the iron–sulfur centers and FAD seen with xanthine oxidase contrasts with that exhibited by other flavin- and iron/sulfur-containing systems such as trimethylamine dehydrogenase (which contains a [4Fe-4S] iron–sulfur cluster and a covalently linked FMN[174]). In this protein, clear evidence is seen for discrete prototropic and redox equilibria of the form $FMNH_2/[4Fe\text{-}4S]_{ox} \rightleftharpoons FMNH^{-}/[4Fe\text{-}4S]_{ox} \rightleftharpoons FMNH^{\bullet}/[4Fe\text{-}4S]_{red} \rightleftharpoons FMN^{\bullet-}/[4Fe\text{-}4S]_{red}$.[175] The different behavior of trimethylamine dehydrogenase and xanthine oxidase has been attributed to the fact that the former enzyme does not thermodynamically destabilize the anionic form of the flavin, allowing deprotonation to precede electron transfer out of the flavin.[173b]

Upon reduction of the FAD of xanthine oxidoreductase, reducing equivalents are finally passed on to O_2 or NAD^+ (depending on the enzyme form) to complete the catalytic sequence. As in all members of the xanthine oxidase family, the reductive and oxidative halves of the catalytic cycle are physically separated. For the dehydrogenase forms, reduction of NAD^+ is thought to occur via a straightforward hydride transfer, but the reaction with O_2 is more complicated.[176] Reaction of the fully reduced bovine oxidase with O_2 occurs in four sequential steps, with the six-electron reduced enzyme first oxidized to the four-electron reduced form, and the four-electron reduced to the two-electron reduced form; both steps involve the quantitative reduction of O_2 to H_2O_2. Once the two-electron reduced

form is generated, the remaining two reducing equivalents are lost individually, forming (again quantitatively) two equivalents of superoxide, $O_2^{\bullet-}$. The relative reduction potentials of the redox-active centers are such that in the two-electron reduced enzyme the distribution of reducing equivalents at pH 8.5 gives approximately 50% $FADH_2$ and the remaining 50% with the two iron–sulfur clusters reduced instead (there is little molybdenum reduction in the two-electron reduced enzyme),[171] and the question is why the $FADH_2$ in two-electron reduced enzyme reacts with O_2 to form $O_2^{\bullet-}$, while that in four- and six-electron reduced enzyme forms H_2O_2. In the reaction with six- or four-electron reduced enzyme, H_2O_2 is thought to involve three discrete steps: (1) an initial one-electron transfer to form a nascent $FADH^{\bullet}\cdots O_2^{\bullet-}$ complex; (2) regeneration of $FADH_2$ by rapid electron transfer from the iron–sulfur centers to form a $FADH_2\cdots O_2^{\bullet-}$ complex; and (3) a second (rapid) one-electron transfer to form $FADH^{\bullet}\cdots H_2O_2$. In the absence of extra reducing equivalents in the two-electron reduced enzyme, the initially formed $FADH^{\bullet}\cdots O_2^{\bullet-}$ complex cannot be rereduced by to $FADH_2$, and the reaction of $FADH^{\bullet}$ is sufficiently slow that superoxide escapes. The one-electron reduced enzyme thus generated must form $O_2^{\bullet-}$, and this reaction is very slow (with a bimolecular rate constant of $1.0 \times 10^4\ M^{-1}\ s^{-1}$).[176,177] As discussed further below, the formation of both H_2O_2 and $O_2^{\bullet-}$ by the oxidase from of the enzyme has pathophysiological consequences in mammals, including humans.

3.2.5. Biomedical Considerations—Human disease states associated with genetic dysfunction in the expression of functional xanthine oxidoreductase are termed xanthinurias, and are characterized by low blood levels of uric acid and elevated levels of xanthine. There are three types of deficiency: Type I, due to a genetic defect in the structural gene for the enzyme, resulting in loss of activity; Type II, due to a genetic defect in the sulfurase required by both xanthine oxidoreductase and aldehyde oxidase and resulting in a loss of both activities; and Type III, with a triple deficiency of xanthine oxidoreductase and aldehyde oxidase as well as sulfite oxidase due to defect in biosynthesis of pyranopterin cofactor.[7d] Remarkably, for individuals in this last category in whom the genetic lesion lies in the MOCS1A or B genes involved in biosynthesis of the cPMP that is precursor to the mature pyranopterin, a successful therapy has been developed involving administration of cPMP.[178]

In organisms other than mammals, xanthine oxidoreductase exists solely as a dehydrogenase. In mammals, however, while the enzyme exists normally as a dehydrogenase, it can be post-translationally converted into an oxidase either irreversibly by proteolysis or reversibly by oxidation of cysteine residues.[179] Either modification results in a reorientation of a loop (Gln 423–Lys 433) in the FAD domain),[108] as shown in Figure 27. In the oxidase configuration, this loop is positioned so as to prevent NAD^+ binding, abolishing dehydrogenase activity. The sites of proteolysis and formation of disulfide bonds that accompany the irreversible and reversible XDH to XO transition, respectively, have been identified.[180] In the bovine enzyme, proteolysis occurs to the C-terminal side of Lys 551 and Lys 569 in the linker between the flavin- and molybdenum-binding domains; the residues involved in disulfide bond formation are Cys 535 (also in the linker region) and Cys 992 (in the molybdenum-binding domain). Given the copious production of superoxide and hydrogen peroxide (and possibly, indirectly, the hydroxyl radical through Fenton-like

chemistry) by the oxidase form of xanthine oxidoreductase, this so-called “D-to-O” conversion has been implicated in the oxidative stress associated ischemia-reperfusion injury that occurs in heart attack and stroke.[181] The argument is complicated, however, by the fact that the dehydrogenase form itself reacts readily with O_2, generating even more superoxide as a fraction of catalytic throughput than does the oxidase form (although in the presence of NAD^+ the reaction with O_2 is reduced).[182] In mammals, xanthine oxidoreductase plays an important role in milk secretion as knockout mice, which are otherwise healthy, have seriously deficient lactation.[183] It is not known whether this is related in some way to the mammal-specific D-to-O conversion, but it seems unlikely that the ability of the mammalian enzymes to interconvert is simply an (unfortunate) evolutionary coincidence.

Xanthine oxidoreductase has also been shown to reduce nitrite to NO, a reaction that is possibly very significant from a physiological standpoint.[184] The reaction takes place at the molybdenum center of the enzyme, and while multiple turnovers occur under steady-state conditions, the enzyme is ultimately inactivated by the accumulating NO due to loss of the catalytically essential Mo=S group.[185] The reaction with nitrite is an intrinsic property of the molybdenum center and is independent of the reducing substrate used as xanthine, NADH and 2,3-dihydroxybenzaldehyde are all able to support nitrite reduction to NO. Under pathologically hypoxic conditions xanthine oxidoreductase is estimated to generate as much NO as nitric oxide synthase.[185c] The enzyme can also reduce nitrate to nitrite, and with the subsequent reduction of nitrite this reaction also generates physiologically relevant concentrations of NO.[186] Isotope tracer experiments have shown that NO generated by xanthine oxidoreductase accumulates in both normoxic and hypoxic cardiac tissue.[187] The interested reader is referred to recent reviews covering the possible physiological role of NO and $O_2^{\bullet-}$ generated by xanthine oxidoreductase.[188]

The final biomedical aspect of xanthine oxidoreductase is that the enzyme is the target of drugs for treatment of hyperuricemia.[189] Inhibition of the enzyme does not generally cause severe side effects, although it does lead to an increase in IMP synthesis via the hypoxanthine phosphoribosyl transferase-catalyzed salvage pathway, resulting in feedback inhibition of phosphoribosylprophosphate (PRPP) synthetase and glutamine PRPP amidotransferase by IMP.[190] Also, because many anticancer drugs are purine analogues that are readily metabolized by xanthine oxidoreductase, potentiating their efficacy by inhibiting the enzyme is highly desirable. The development of an effective tandem drug therapy involving treatment with the xanthine oxidoreductase inhibitor allopurinol in conjunction with the antitumor drug 6-mercaptopurine, thereby lowering the doses required of the latter, led to the Nobel Prize in Physiology or Medicine for Gertrude Elion and George Hitchings in 1988. Several potent inhibitors of xanthine oxidoreductase have been developed, and these can be classified as mechanism-based, structure-based, and hybrid inhibitors. Allopurinol is the classic xanthine oxidoreductase inhibitor and an example of a mechanism-based inhibitor.[191] It is oxidized by xanthine oxidoreductase to alloxanthine (4,6-di-OH-pyrazolo-[4,4-*d*]pyrimidine), which binds tightly to the reduced form of the molybdenum cofactor (see Figure 26).[191b] Febuxostat (2-[3-cyano-4-isobutoxyphenyl]-4-methyl-5-thiazolecarboxylic acid)[192] and Pyranostat (1-[3-cyano-4-(2,2-dimethylpropoxy)-

phenyl]-1*H*-pyrazole-4-carboxylic acid)[193] are structure-based inhibitors that are sterically tailored to bind in the substrate binding site (and extending back into the solvent access channel). FYX-051 (4-[5-pyridin-4-yl-1*H*-[1,2,4]triazol-3-yl]-pyridine-2-carbonitrile) is a hybrid-type inhibitor, a slow substrate that coordinates the active site molybdenum center like alloxanthine, but that also interacts extensively with the substrate access channel.[194] Interestingly, FYX-051 does not inhibit the *R. capsulatus* xanthine dehydrogenase,[195] due to the differently shaped solvent access channels in the bacterial and mammalian enzymes. The type of steric complementarity that went into the design of FYX-051 thus presents an attractive strategy for the development of drugs that are species-specific in their action.

3.3. Aldehyde Oxidases

The xanthine-utilizing enzymes described above are very similar in eukaryotes and prokaryotes, and the eukaryotic aldehyde oxidases are very similar to these in cofactor constitution; the aldehyde-utilizing enzymes from bacteria, however, are distinct in at least two regards. First, the prokaryotic enzymes often have a dinucleotide form of the pyranopterin cofactor (typically that of cytosine) in their molybdenum centers. Second, and more importantly, the prokaryotic enzymes often lack an FAD-containing domain/subunit altogether and use ferredoxin rather than NAD^+ or O_2 as oxidizing substrate. For these reasons, we consider the pro- and eukaryotic aldehyde oxidases separately here.

3.3.1. The Bacterial Aldehyde:Ferredoxin Oxidoreductases—The aldehyde:ferredoxin oxidoreductase from *Desulfovibrio gigas* was the first member of the molybdenum hydroxylase family to be characterized crystallographically; it was for this enzyme that the overall coordination geometry of the molybdenum center was established to be square pyramidal[109] and the highly conserved active site glutamate proposed to act as an active site base, facilitating nucleophilic attack of the equatorial Mo–OH on the substrate carbonyl.[126] Additional work was required, however, to establish that the catalytically essential Mo=S group occupied an equatorial rather than apical position[115,117] and that the equatorial oxygen was a Mo–OH rather than Mo–OH_2 as originally proposed. Somewhat surprisingly, based on steady-state assays and the inhibition patterns seen with classic inhibitors of this family of enzymes (e.g., cyanide and ethylene glycol),[196] it has since been suggested that the *D. gigas* enzyme is active in the absence of the Mo=S group that in other enzymes of this family is known to be catalytically essential.[119] Aldehydes are in fact generally more susceptible to nucleophilic attack than heterocycles such as xanthine, but the ability of bovine xanthine oxidase to oxidize aldehydes is strictly dependent on the Mo=S being present, raising concerns regarding the conclusion that the desulfo form of the *D. gigas* enzyme is active. If the desulfo *D. gigas* enzyme is indeed functional, then it is not possible to make generalizations about the reaction mechanism of members of the xanthine oxidase family of enzymes based on its characteristics. The crystal structure of the desulfo *D. gigas* enzyme in complex with the classic inhibitor arsenite has recently been reported, for example, with the inhibitor found coordinated to the molybdenum at the equatorial position normally occupied by the catalytically labile Mo–OH. By contrast, in the above-mentioned structure of the (sulfurated) bovine xanthine oxidase in complex with arsenite,[197] the inhibitor is seen bound to the reduced enzyme in a distinctly different bidentate fashion, with two bridging ligands in the equatorial plane of the molybdenum, one oxygen and the

other sulfur. Interestingly, in the complex with oxidized bovine enzyme, the arsenic itself had a coordination geometry suggesting that it had become oxidized to arsenate (presumably in the X-ray beam).

While [4Fe-4S] iron–sulfur clusters are valence-delocalized, the [2Fe-2S] clusters found in members of the xanthine oxidase family are valence-localized, meaning that one of the two irons specifically becomes ferrous when the diferric oxidized cluster is reduced by one electron. In an elegant study of the *D. gigas* aldehyde oxidoreductase, the redox-active irons have been unambiguously assigned to specific irons in the crystal structure.[198] As indicated in Figure 28, the redox-active iron in Fe/S I (that is proximal to the molybdenum center) is coordinated by Cys 100 and Cys 139, while that in Fe/S II is coordinated by Cys 40 and Cys 45. Given the extremely high homology of the iron–sulfur binding portion of the *D. gigas* and eukaryotic enzymes, it is likely that the corresponding irons are redox-active in the latter enzymes.

In addition to a xanthine dehydrogenase encoded by the *xdhABC* operon and a second closely related product of the *xdhD* gene,[75a,90] the *E. coli* genome possesses the *yagTSRQ* operon that encodes a periplasmically localized aldehyde:ferredoxin oxidoreductase.[75c] The enzyme has a pair of [2Fe-2S] clusters in YagT, FAD in YagS, and a molybdenum center in YagR; YagQ (which is homologous to the XdhC sulfurase from *R. capsulatus* discussed above) is specific for sulfuration of the cytosine dinucleotide (MCD) form of the molybdenum cofactor that is found in both YagTSR and XdhABC (MCD being synthesized by the MobA analogue MocA in E. *coli*).[199] YagTSR is unusual among members of the xanthine oxidase family of enzymes in that: (1) it is an αβγ trimer rather than the more typical $(\alpha\beta\gamma)_2$ hexamer; (2) while it possesses the FAD domain/subunit seen in the eukaryotic forms of the enzyme, it utilizes ferredoxin as oxidizing substrate; and (3) it is periplasmically localized.[75c] YagTSR is able to oxidize a variety of aldehydes, but is particularly effective with aromatic aldehydes (such as cinnamaldehyde, vanillin, and benzaldehyde, all exhibiting $k_{cat}/K_m \approx 10^6\ M^{-1}\ s^{-1}$), and it has been suggested that the enzyme plays a role in detoxifying such compounds when present in the organism's environment.[75c] As a periplasmic aldehyde oxidase, the enzyme has been designated PaoABC,[7e] and has recently been used to develop a biosensor for aromatic aldehydes.[200]

3.3.2. The Eukaryotic Aldehyde Oxidases—Mammalian aldehyde oxidases hydroxylate and inactivate a variety of drugs, including many aromatic heterocycles, but the physiological substrate(s) remain unknown. Experimentally, the aldehyde oxidases differ from the xanthine oxidoreductases in being sensitive to menadione and able to oxidize *N*-methylnicotinamide.[201] Mammalian aldehyde oxidases have been suggested to play a role in retinoic acid biosynthesis,[202] but in humans individuals with a genetic lesion in the molybdenum cofactor sulfurase that is required by both xanthine oxidase and aldehyde oxidase have relatively minor clinical symptoms and no evident developmental abnormalities,[95,203] indicating that systemic biosynthesis of retinoic acid (a major signaling molecule in vertebrate limb development) is not impaired. On the other hand, a mouse knockout for one of the organism's four aldehyde-oxidizing genes has been described in which retinoid metabolism in specific tissues is specifically disrupted (and retinoid-dependent genes generally underexpressed), suggesting that the enzyme may be involved in

the local biosynthesis and biodistribution of retinoic acid in the affected tissues.[204] Interestingly, it has been shown that in humans aldehyde oxidase interacts with and modulates the activity of the ABCA-1 transporter involved in lipid uptake in the liver, suggesting some as yet undefined role for the enzyme in lipid metabolism.[205]

Historically, aldehyde oxidase has been isolated from mammalian liver (most commonly rabbit and rat) and apart from its substrate specificity is found to generally closely resemble the better-studied bovine xanthine oxidoreductase in its physicochemical properties, including the requirement for a catalytically essential Mo=S group in the molybdenum coordination sphere.[182d,201,206] It has long been recognized that the molybdenum centers of the two enzymes are fundamentally the same, with aldehyde oxidase eliciting the same family of “rapid”, “slow”, and “inhibited” EPR signals seen with xanthine oxidase. Notably, however, aldehyde oxidase has not been shown to manifest a “very rapid” type of EPR signal, and preferentially manifests the “rapid Type 2” signal (with coupling to two equivalent protons) rather than the “rapid Type 1” (with coupling to two inequivalent protons) more commonly seen with wild-type enzyme.[182d,206g,h,207] Genes encoding aldehyde oxidases from cow,[208] human,[209] rat,[210] and mouse[211] have all been cloned and shown to share similar intron/exon structures, a reflection of their close evolutionary relationship. In humans, in addition to the single *Aox1* gene,[209] there are two pseudogenes that are not expressed and represent vestigial remnants of two of the three additional isoforms seen in mouse.[182] A major distinction between the four mouse Aox isozymes is tissue distribution rather than substrate specificity;[212] AOX1 is predominant in liver, for example, while the AOH2 homologue is prevalent in the Harderian gland (an exocrine gland located in the orbit of the eye). The sequence alignment for the aldehyde- and xanthine-utilizing enzymes from human, cow, rat, and mouse is shown in Figure 29, where it can be seen that while the two groups of enzymes are generally very similar, there are specific regions (notably in the FAD-binding domain and in the substrate-binding regions of the molybdenum domains) where the aldehyde oxidases as a group diverge from the xanthine oxidoreductases (see below).

Most recently, the recombinantly expressed mouse AOX1 has been characterized biochemically, and the roles of several amino acid residues in the active site examined by site-directed mutagenesis.[213] Consistent with the results discussed above with the *R. capsulatus* xanthine dehydrogenase, mutation of Glu 1265 (equivalent to Glu 730 in the bacterial enzyme) to glutamine results in loss of activity in steady-state assays with a range of aldehyde substrates. Mutation of Val 806 to Glu and Met 884 to Arg in mouse AOX1 (the residues found in the xanthine-utilizing enzymes) also abolishes steady-state activity but does not impart xanthine oxidase activity; this contrasts with results seen with the *R. capsulatus* and human xanthine dehydrogenase, where R881M and E803V mutations reverse specificity toward xanthine and aldehydes.[149,214]

The crystal structure of the mouse AOX3 aldehyde oxidase (mAOX3) has recently been reported.[215] As expected, the overall fold of the protein generally closely resembles that of previously characterized members of this family. Surprisingly, while mAOX3 (like all eukaryotic aldehyde oxidases) is an obligatory oxidase that cannot use NAD^+ as oxidizing substrate, its FAD-binding configuration resembles the dehydrogenase rather than oxidase

configuration for the bovine enzyme shown in Figure 27. Although the sequence of this loop in mAOX3 (^{430}QAPRQQNAFAT^{440}) is considerably less polar than that in the bovine xanthine oxidoreductase (^{423}QASRREDDIAK^{433}), it is likely that the lack of reactivity of mAOX3 toward NAD^+ is instead due to the absence of a critical FFP(T)G(S)YR sequence in its residues 396–402 elsewhere in the flavin-binding domain that is known to be important in interacting with NAD^+[216] (unfortunately, these residues lie in an unresolved loop of the mAOX3 structure).

The conserved phenylalanine residues that define the substrate binding site adjacent to the molybdenum center and the catalytic glutamate occupy essentially identical positions in the mouse AOX3 as seen in the bovine enzyme (Figure 30). Residues that are not conserved (indicated by asterisks in Figure 29, and shown structurally in Figure 30) include Glu 802/Ala 807, Arg 880/Tyr 885 (a methionine in most other aldehyde oxidases), His 884/ Lys889, and Leu 1014/Tyr 1019. Interestingly, the side chain of Lys 889 of mAOX3 (homologous to His 884 of the bovine enzyme) occupies a position similar to that of Arg 880 in the bovine enzyme, but molecular dynamics calculations have suggested that, given its different position in the polypeptide chain, it moves upon substrate binding to interact with Glu 1266 (the active site base). Lys 889 also lies near the solvent access channel of mAOX3, which is considerably wider and more negatively charged than in the xanthine oxidoreductase.

In humans, aldehyde oxidase oxidizes a spectrum of aromatic heterocycles in addition to aldehydes, and many of these are therapeutically important. A recent computational study has successfully accounted for the experimentally observed regioselectivity of substrate hydroxylation for a number of aromatic heterocycles.[217] Also, human aldehyde oxidase has recently been cloned and heterologously expressed in *E. coli*, and while expression levels were modest it proved possible to obtain sufficient functional protein to undertake steady-state kinetic studies.[218] Enzyme activity on a series of substituted quinazoline substrates analogous to that used previously with xanthine oxidase[127] yielded the same general trend in reactivity (with the notable exception of the nitro derivative, which was found not to be an effective substrate for aldehyde oxidase).[218]

The ability of aldehyde oxidase from rat liver to generate both superoxide ion[219] and nitric oxide[220] has also been examined. The enzyme is a copious generator of $O_2^{\bullet-}$ during turnover with 4-(dimethylamino)cinnamaldehyde as substrate, comparable to that of the oxidase form of xanthine oxidoreductase.[219a] NADH is also an effective reducing substrate for aldehyde oxidase, and in turnover with NADH over 65% of the total electron flux through the enzyme forms $O_2^{\bullet-}$. It thus seems that from the standpoint of the (patho)physiological generation of superoxide, the aldehyde oxidases may be as important as xanthine oxidoreductase (see section 3.2.5). Like xanthine oxidoreductase, aldehyde oxidase in the tissues has also been shown to generate NO in the presence of nitrite.[220a] It has been estimated that at physiological concentrations of enzyme and nitrite, aldehyde oxidase is capable of generating as much as 6 nM NO per second in liver, indicating a possibly important role in the generation of this physiologically potent species.

In the context of the overall folds of the aldehyde-oxidizing enzymes from *D. gigas* and mouse, it is interesting to consider how, over the course of evolution, the FAD-binding domain has become inserted into the polypeptide trace of the bacterial enzyme in creating the eukaryotic form of the enzyme. Although portions of the two linker regions that connect first the C-terminus of the second iron–sulfur domain to the N-terminus of FAD domain and second the C-terminus of the FAD domain to the N-terminus of the molybdenum binding portion of the protein are not fully resolved in the structure of the murine (or bovine) enzyme, it is nevertheless clear that the first of these linkers passes in front of the iron–sulfur domains as shown in Figure 31, and, after tracing out the entirety of the FAD domain, the second loops behind the iron–sulfur domains (completing a fifth strand of β sheet in the second of the two molybdenum domains along the way) before leading into the amino terminus of the molybdenum-binding portion of the protein. On the other hand, in the *D. gigas* enzyme, the single 20-aa linker that connects the C-terminus of the second iron–sulfur domain with the N-terminus of the first molybdenum domain spans some 25 Å on the same face of the protein. From a comparison of the two structures, it is possible to establish that the apparent point at which the FAD domain seen in the eukaryotic enzymes is inserted in the bacterial sequence is approximately in the middle of the single prokaryotic linker, as indicated by the asterisk in Figure 31. The point of insertion lies on the opposite side of the two Fe/S domains from the bulk of the FAD domain, and it is for this reason that while the domains are laid out Fe/S II–Fe/S I–FAD–Mo in the primary sequence, their physical disposition in the protein structure is FAD–Fe/S II–Fe/S I–Mo. The FAD domain of the eukaryotic enzymes is positioned by a number of interactions with the Fe/S and Mo domains, including a β turn that protrudes from the first Fe/S domain and is considerably elongated as compared to the β turn seen in the bacterial enzyme (Figure 31, in teal).

Higher plants also encode multiple aldehyde oxidases,[212a] including the enzymes responsible for catalyzing the final steps in the biosynthesis of the plant hormones abscissic acid and indole-3-acetic acid (both reactions involve the oxidative hydroxylation of the respective aldehyde to the carboxylic acid). *Pisum sativum* has three genes encoding aldehyde oxidases, *Psaox1*–3, the last encoding a stress-specific abscissic aldehyde oxidase.[221] *A. thaliana* has four aldehyde oxidase genes, AAO1–4,[222] with AOX1 having a preference for indole-3-acetaldehyde,[223] while AOX3 prefers abscissic aldehyde.[222a,224] The *A. thaliana* AAO1 and AAO3 enzymes have recently been heterologously expressed in *Pichia pastoris*, and their basic biochemical and enzymatic properties characterized.[224b] Both isozymes have the characteristic UV/visible absorption spectra of all members of the xanthine oxidase family, with a broad absorption maximum at ~450 nm and a shoulder at 550 nm, and are inhibited by cyanide by removal of the catalytically essential Mo=S ligand. Like the mammalian enzymes discussed above,[210,219,225] both *A. thaliana* isozymes generate $O_2^{\bullet-}$ as well H_2O_2, which has been implicated in the enzyme's physiological role, possibly as a defense against infection.[224b]

The reaction mechanism for aldehyde oxidases, regardless of origin, is believed to involve the same base-assisted proton abstraction from the equatorial Mo–OH group to initiate catalysis as seen with the xanthine-utilizing enzymes.[126] Nucleophilic attack on the carbonyl carbon of substrate ensues with concomitant hydride transfer to the Mo=S group, through a

tetrahedral transition state[218] in which the C–O bond of product is largely formed and the C–H bond of substrate largely broken (albeit to a somewhat lesser degree). Although the reaction is thought to proceed through the same type of $LMo^{iv}O(SH)(OR)$ intermediate as seen with xanthine oxidase, no EPR signal equivalent to the "very rapid" EPR signal seen with xanthine oxidase has been seen with aldehyde oxidase.[182d]

3.4. Noncanonical Members of the Xanthine Oxidase Family

A great many enzymes of the xanthine oxidase family have been biochemically characterized to greater or lesser degree. While most of these are likely to be very similar to those already described, several are known to have one or more significantly atypical characteristics. What follows is a consideration of several members of this family of enzyme, each of which having been characterized crystallographically, that are noncanonical in terms of the structure of the molybdenum center, the nature of the reaction catalyzed, the type of redox-active centers that are found, or some combination of these.

3.4.1. CO Dehydrogenase—Carboxydotrophic bacteria (e.g., *Oligotropha carboxidovorans*) are aerobes able to grow with CO as sole source of both carbon and energy.[226] A molybdenum-containing CO dehydrogenase catalyzes the critical first step in this process, the oxidation of CO to CO_2,[227] with the reducing equivalents thus obtained ultimately being passed on ultimately to a CO-insensitive terminal oxidase.[228] A portion of the CO_2 thus generated is subsequently fixed nonphotosynthetically via the reductive pentose phosphate pathway.[227] Aerobes such as *O. carboxidovorans* are responsible for a tremendous amount of bioremediation, accounting for the annual clearance of ~2×10^8 metric tons of CO from the environment.[229] The Mo-containing CO dehydrogenase from *O. carboxidovorans* and related organisms is distinct from the highly O_2-sensitive Ni/Fe-containing CO dehydrogenase from obligate anaerobes such as *Clostridum thermoaceticum* or *Methanosarcina barkerii.*[230]

The *O. carboxidovorans* CO dehydrogenase is encoded by the megaplasmid-localized *coxBCMSLDEFGHIK* gene cluster,[107,231] which has the overall organization shown in Figure 32. In addition to the *cosMSL* structural genes encoding the $(\alpha\beta\gamma)_2$ enzyme, the operon includes two genes, *coxF* and *coxI*, that are predicted to encode proteins homologous to XdhC discussed above (at least one of which is presumably involved in insertion of the molybdenum and pyranopterin portion of the binuclear center). Another, *coxD*, encodes a membrane-integral AAA+ ATPase that is involved in the incorporation of the μ-sulfido and copper into the maturing binuclear center.[232] Four other genes encode proteins (CoxB, CoxC, CoxH, and CoxK) that are predicted to possess one (CoxB) to as many as nine (CoxK) transmembrane helices, and one or more of these are likely to be involved in anchoring CO dehydrogenase to its physiological position on the inner side of the cytoplasmic membrane.[228,233] CoxD and CoxK are additionally predicted to bind nucleotides, but it is not known whether these might be ATP/GTP sites or sites for the pyranopterin cofactor.

CO dehydrogenases from both *O. carboxidovorans*[103] and *Hydrogenophaga pseudoflava*[234] have been crystallographically characterized and are found to be virtually identical. The

discussion here focuses on the better-studied *O. carboxidovorans* enzyme. The enzyme has a small subunit (CoxS; 18 kDa) with two [2Fe-2S] iron–sulfur clusters, a medium subunit (CoxM; 30 kDa) that possesses FAD, and a large subunit (CoxL; 89 kDa) that has the active site molybdenum center. Each subunit has considerable sequence homology and virtually identical structure to the corresponding parts of bovine xanthine oxidoreductase. (Note that the order of the *coxMSL* genes (FAD–Fe/S–Mo) in the operon differs from the Fe/S–FAD–Mo order seen in the primary sequence of the eukaryotic enzymes.) Significantly, the active site of CO dehydrogenase is not a mononuclear molybdenum center but rather a binuclear Mo/Cu center having the structure shown in Figure 33.[116,235] The molybdenum has the square-pyramidal coordination geometry seen in other members of this enzyme family, with an apical Mo=O and an equatorial plane consisting of two sulfurs from the pyranopterin cofactor (present as the dinucleotide of cytosine). The remainder of the equatorial plane, however, consists of a μ-sulfido bridge to the Cu(I) in place of the Mo=S found in other members of this family, and a second Mo=O[236] rather than the catalytically labile Mo–OH. The Cu(I) ion possesses a second thiolate ligand contributed by Cys 388, and is also coordinated by a water ligand at a distance of 2.40 Å. The Mo–μS–Cu bond angle is 113°, and the μS–Cu–S(Cys) bond angle is 156°.

CO dehydrogenase is reduced by CO under pseudo firstorder conditions a with k_{red} = 51 s^{-1} at 25 °C.[236] The rate constant is independent of [CO], reflecting a K_d smaller than the ~30 μM lower limit of [CO] that is experimentally accessible. k_{red} is also independent of pH, indicating that there is no acid–base catalysis involved in the reaction going forward from the E_{ox}·CO complex. Interestingly, however, Glu 763 (equivalent to the active site base Glu 1261 in the bovine xanthine oxidoreductase) is conserved in CO dehydrogenase. In the course of reaction with CO, an EPR signal clearly attributable to the Mo/Cu binuclear center accumulates, with $g_{1,2,3}$ = 2.0010, 1.9604, 1.9549 and extremely large hyperfine coupling to the naturally abundant^{63,65}Cu nuclei (I = 3/2), with $A_{1,2,3}$ = 117, 164, and 132 MHz.[236] This EPR signal does not exhibit proton hyperfine and is not changed on preparation of the sample in D_2O, but lines do broaden slightly when ^{13}CO is used as substrate.[236] The signal-giving species appears to represent an enzyme·substrate complex with CO coordinated to the copper of the partially reduced binuclear center. As such, the species represents a paramagnetic analogue of the Michaelis complex, with CO activated for nucleophilic attack on binding to the copper. This interpretation is consistent with computational studies of the enzyme indicating that the reaction progresses from an initial Mo(VI)/Cu(I)·CO complex.[237]

A very high-resolution (1.1 Å) structure of CO dehydrogenase in complex with the inhibitor *n*-butylisonitrile has been reported,[116] in which the bridging sulfur bond to the copper is clearly seen to have been cleaved and the inhibitor inserted between the Mo and Cu. A mechanism has been proposed in which CO similarly inserts itself between the bridging sulfur and copper of the binuclear center in the course of the reaction to yield a bridging thiocarbamate and the reduced molybdenum, as shown in Figure 34, top. The thiocarbamate is then proposed to be hydrolyzed by solvent, with regeneration of the sulfur bridge. An alternate mechanism, based on the structure of the paramagnetic species described above, involves nucleophilic attack by the equatorial Mo=O on an initial Cu· CO complex, followed by formation of CO_2 and formal reduction of the binuclear cluster (Figure 34, bottom); a

variation on this mechanism involves solvent water/hydroxide as nucleophile. In either case, the final step of this alternate mechanism involves reducing equivalents nominally entering the (predominantly Mo-based) redox-active orbital via the copper. A model for the binuclear active site of CO dehydrogenase that possesses many of the salient structural features of the enzyme's active site has recently been shown to exhibit EPR characteristics very similar to those of the enzyme, most particularly the extremely strong Cu superhyperfine.[238] Analysis of this model indicates that the redox-active (singly occupied) molecular orbital has 44% Mo d_{xy} character, with 25% S p character and 21% Cu d_{z2}/d_{xy} character (along with an undefined amount of Cu s character). The copper and bridging sulfur thus act to extend the redox-active orbital spatially a considerable distance from the molybdenum, making it possible for the molybdenum to become reduced in the final step of the reaction as depicted in Figure 34, bottom. The binuclear cluster thus appears to be constructed so as to (1) create a substrate binding site adjacent to the molybdenum that activates CO for nucleophilic attack, and (2) at the same time extend the redoxactive Mo d_{xy} orbital such that it can accept an electron pair in the course of the reaction at the more remote site.

The bridging sulfur of CO dehydrogenase can be removed by reaction with cyanide, which results in loss of the copper as well. A reconstitution protocol has been developed that utilizes Cu(I)·thiourea as the source of copper,[239] and when the silver salt is used instead, activity is partially recovered.[240] The enzyme thus reactivated is reduced by CO under pseudo firstorder conditions with a rate constant of 8.1 s^{-1} (as compared to 51 s^{-1} for the as-isolated enzyme[236]). Significantly, the EPR signal seen upon partial reduction of the enzyme by CO shows the doublets expected for substitution of Ag for Cu ($I = 1/2$ for the naturally occurring^{103,105}Ag), with $g_{1,2,3} = 2.043, 1.9595, 1.9540$ (very similar to the values seen with the as-isolated enzyme) and $A_{1,2,3} = 82.0, 78.9, 81.9$ MHz. The EPR signals of native and silver-substituted CO dehydrogenase are shown in Figure 35.

The principal EPR signal exhibited by the binuclear cluster of substrate-reduced CO dehydrogenase has very recently been examined by ENDOR spectroscopy, using ^{13}CO.[241] The key observation is that the ^{13}C hyperfine coupling is essentially entirely isotropic, with $a_{iso} = 17.3$ MHz. A computational analysis of all likely signal-giving species indicates that the isotropic coupling is inconsistent with any structure in which there is a direct Mo–C bond or one with only a single atom intervening between the molybdenum and carbon. The conclusion is that the signal arises from a Mo^{V}/Cu^{I} species having CO bound at the copper of the binuclear center, a species that amounts to a paramagnetic analogue of the Mo^{VI}/Cu^{I}·CO Michaelis complex in the lower mechanism of Figure 34 as discussed above.

The reaction of CO dehydrogenase with H_2 has also been investigated.[242] The enzyme is reduced by H_2 at a pH-independent rate constant of 5.3 s^{-1} (as compared to 51 s^{-1} with CO), and in the course of the reaction an EPR signal is observed arising from the binuclear center that exhibits strong coupling to two approximately equivalent protons with $A_{1,2,3} = 80, 20,$ and 130 MHz. Both $g_{1,2,3}$ (2.0127, 1.9676, 1.9594) and $A_{1,2,3}(^{63,65}Cu) = 170, 200, 170$) are also significantly different from the parameters manifested by the CO-reduced enzyme, and are also distinct from the signal seen with dithionite-reduced enzyme (which also, however, exhibits proton hyperfine coupling). The signal-giving species seen with H_2-reduced enzyme is attributed to an η^2 complex of H_2 bound side-on at the copper (for which chemical

precedents exist[243]), analogous to the CO complex inferred from the ENDOR work described above. The bound H_2 is expected to be polarized by interaction with the copper,[244] and the reaction has been proposed to proceed by deprotonation to a copper hydride, which subsequently deprotonates to populate the delocalized redox-active orbital of the binuclear cluster.[242]

It has recently been shown that several quinone species are able to effectively oxidize reduced CO dehydrogenase, and that, consistent with the enzyme being membrane-associated, the physiological oxidant for CO dehydrogenase is most likely ubiquinone.[245] The reoxidation reaction has also been shown to occur at the FAD site, as expected. Quinones are unusual physiological oxidants for this family of enzymes, and an examination of the overall fold of the FAD-containing domain of CO dehydrogenase indicates that it resembles the dehydrogenase rather than the oxidase form of the bovine xanthine oxidoreductase, particularly with regard to the position of the mobile loop referred to above that is involved in the D-to-O conversion (Figure 27). A closer examination of the environment of the FAD of CO dehydrogenase, however, indicates that there are significant differences in the environment of the FAD in CO dehydrogenase and xanthine dehydrogenase (Figure 36). A Lys-Asp pair near the pyrimidine subnucleus of the flavin is preserved, for example, but the positions of the Ile and aromatic residues are reversed, with the Ile on the *re* side and Tyr (a Phe in the bovine enzyme) on the *si* side of the isoalloxazine ring.

3.4.2. Nicotinate Dehydrogenase—The anaerobic soil bacterium *E. barkeri* is able to ferment nicotinate to propionate, acetate, carbon dioxide, and ammonia utilizing a pathway that is initiated by the hydroxylation of nicotinate to 6-hydroxynicotinate. This reaction is catalyzed by a molybdenum- and selenium-dependent nicotinate dehydrogenase.[246] Several molybdenum-containing enzymes are known to contain selenium,[247] and a recent genomics analysis has shown that selenium and molybdenum utilization are highly correlated in biology.[7n] Selenium is most commonly found as selenocysteine (e.g., in the molybdenum-containing formate dehydrogenase H from *E. coli*, a member of the DMSO reductase family of enzymes, where it coordinates the active site molybdenum, at least in the oxidized state of the enzyme;[248] see section 5.4.1) or in an acid-labile form (in members of the xanthine oxidase family of molybdenum enzymes, e.g., nicotinate dehydrogenase from *E. barkeri*[246a] and the xanthine oxidoreductases from *Clostridium purinolyticum*,[249] *C. acidiurici*,[250] and *E. barkeri*[251] and the purine hydroxylase from *C. purinolyticum*[249]). In each of these cases, the selenium is essential for activity. The *E. barkeri* nicotinate dehydrogenase that utilizes $NADP^+$ as oxidizing substrate is encoded by the *ndhFSLM* gene cluster, a part of a larger 23.3 kb gene cluster dedicated to the fermentation of nicotinate.[252] The enzyme has an unusual $(\alpha\beta\gamma\delta)_2$ composition, with its NdhS subunit (23 kDa) containing two [2Fe-2S] clusters and NdhF subunit (33 kDa) one FAD molecule; atypically for the xanthine oxidase family of enzymes, the molybdenum-binding portion of nicotinate dehydrogenase is split into two separate subunits, NdhL (50 kDa) and NdhM (37 kDa).[252,253] The crystal structure of nicotinate dehydrogenase shows that the selenium is present in the active site as a terminal Mo=Se ligand and that it occupies the same equatorial position in the molybdenum coordination sphere as the terminal sulfido ligand in other molybdenum hydroxylases.[145b]

The role of selenium in catalysis has been assessed by density functional calculations, which indicate that the transition state for the critical hydride transfer from substrate to the molybdenum center (in a manner that closely follows the reaction mechanism of xanthine oxidase; see Figure 23) is stabilized by an additional 3 kcal/mol with selenium rather than sulfur in the molybdenum coordination sphere.[145b] This being the case, incorporation of selenium into the active site thus accounts for some two orders of magnitude of additional rate acceleration of the chemical step of the reaction.

3.4.3. Quinoline 2-Oxidoreductase—When grown on quinoline as sole carbon and energy source, *Pseudomonas putida* 86 expresses a molybdenum-containing quinoline 2-oxidoreductase that catalyzes the oxidative 2-hydroxylation of quinoline as the first step in its catabolism.[254] The hydroxylated product subsequently spontaneously tautomerizes to 2-oxo-1,2-dihydroquinoline prior to further degradation.[255] Quinoline 2-oxidoreductase is an $(\alpha\beta\gamma)_2$ hexamer with small, medium, and large subunits possessing its pair of [2Fe-2S] centers, FAD, and a molybdenum center.[117] The overall organization closely resembles that of CO dehydrogenase discussed above, including the presence of the pyranpterin cofactor as the dinucleotide of cytosine and the organization of the three structural genes in the order *qorMSL* in the operon encoding the polypeptides. Still, the active site is a mononuclear molybdenum center rather than a binuclear Mo/Cu center as seen in CO dehydrogenase. Quinoline 2-oxidoreductase exhibits UV/visible and EPR characteristics very similar to those of bovine xanthine oxidase, with an absorption maximum at 450 nm and a broad shoulder at 550 nm due to the iron–sulfur and FAD centers of the enzyme (with extensive bleaching substantially upon reduction of the enzyme) and a “rapid Type 1” Mo(V) EPR signal with coupling to two inequivalent protons.[254] Its molybdenum center closely resembles that of xanthine oxidase described above with an $LMo^{VI}OS(OH)$ coordination sphere, and it was in fact the first enzyme in which the catalytically labile Mo=S was correctly assigned crystallographically to be in the equatorial rather than apical position in the molybdenum coordination sphere.[117] As shown in Figure 37, the active site residues Glu 743 and Gln 224 occupy positions equivalent to Glu 1261 and Gln 787 in the bovine enzyme discussed above, but the position equivalent to Glu 802 in the bovine enzyme is Ala 259 in quinoline 2-oxidoreductase, and that to Arg 880 is Val 339. As with the *R. capsulatus* xanthine dehydrogenase, mutation of Glu 743 to valine dramatically reduces catalytic activity, reflecting the importance of the residue in catalysis.[117] The sides of the substrate binding site of quinoline 2-oxidoreductase are constrained by loops of polypeptide rather than the Phe residues seen in the bovine xanthine oxidase, and the substrate binding site of quinoline 2-oxidoreductase is capped by Trp 331 (this position is occupied by a much smaller Leu 872 than the structure of the bovine enzyme).

3.4.4. 4-Hydroxybenzoyl-CoA Reductase—4-Hydroxybenzoyl-CoA reductase from *Thauera aromatica*[256] is a critical enzyme in the metabolism of phenolic compounds in this and related obligate anaerobes, which lack the O_2-utilizing mono-and dioxygenases used by aerobes to cleave the aromatic ring. The enzyme catalyzes the reductive dehydroxylation of substrate to benzoyl-CoA, a key metabolic intermediate, which is then reductively dearomatized by benzoyl-CoA reductase prior to subsequent degradation. The reaction catalyzed by 4-hydroxybenzoyl-CoA reductase is in principle the reverse of that catalyzed

by xanthine oxidoreductase, with the reducing equivalents required for the reaction provided by a 2x[4Fe-4S] bacterial ferredoxin.[257] Like many of the bacterial molybdenum hydroxylases discussed above, the archaeal 4-hydroxybenzoyl-CoA reductase is an $(\alpha\beta\gamma)_2$ hexamer, with separate molybdenum-, FAD-, and 2x[2Fe-2S]-containing subunits, and an overall protein fold that closely resembles that of other members of this enzyme family.[258] Again, the pyranopterin cofactor of the molybdenum center is present as the dinucleotide of cytosine. As shown in Figure 38, however, 4-hydroxybenzoyl-CoA reductase is unique in that it has an additional [4Fe-4S] cluster resident in a 41-amino acid insert in the FAD subunit; the [4Fe-4S] cluster is the presumed point of entry of reducing equivalents from ferredoxin.[258] The reduction potentials of the several redox-active centers of 4-hydroxybenzoyl-CoA reductase have been determined,[259] with unusually low potentials seen for the FAD ($\Delta E_{FAD/FADH\cdot} = -250$ mV, $\Delta E_{FADH\cdot/FADH2} = -470$ mV) and molybdenum center ($\Delta E_{Mo}{}^{VI/V} = -380$ mV, $\Delta E_{Mo}{}^{V/IV} = -500$ mV), and substantially higher reduction potentials for the two [2Fe-2S] centers (−205 and −255 mV for Fe/S I and II, respectively); the [4Fe-4S] cluster also possesses a low potential (−465 mV). Electron flow is in the reverse direction of that seen in other members of this family, but is thermodynamically favorable overall given the extremely low reduction potential of the donor ferredoxin. The [4Fe-4S] cluster of benzoyl-CoA reductase is unusually far from the isoalloxazine ring of the FAD, 16.5 Å, but this is compensated for by an unusually high peptide packing density in the intervening region and an essentially direct covalent link from Cys 122 (coordinating one of the iron atoms of the cluster) through Arg 121 to Phe 233, which π-stacks onto the *si* face of the isoalloxazine ring.[258] Because of these structural considerations, electron transfer to the FAD is likely to be sufficiently fast so as to not be rate-limiting to turnover.

Given that the xanthine oxidase reaction involves obligatory two-electron chemistry,[132] and that the enzyme is known to catalyze the dehydroxylation of uric acid to xanthine under strongly reducing conditions,[260] the possibility cannot be excluded that the 4-hydroxybenzoyl-CoA dehydrogenase reaction in fact runs simply in the reverse of the hydroxylation pathway for xanthine oxidase, with hydride transfer from an equatorial Mo-SH to C-4 of molybdenum-coordinated substrate, followed directly by dehydroxylation and rearomatization. It has been proposed, however, that the enzyme operates via a radical-based Birch-like mechanism,[259] in which a first reducing equivalent is added to molybdenum-coordinated substrate, followed by protonation at C-4 of substrate and addition of a second reducing equivalent, which leads to dehydroxylation and rearomatization. It remains for future work to distinguish between these mechanistic possibilities.

4. THE SULFITE OXIDASE FAMILY

4.1. Overview

The second major family of molybdenum-containing enzymes consists of sulfite oxidases and dehydrogenases from both eukaryotes and prokaryotes, and the assimilatory nitrate reductases from eukaryotes (the dissimilatory bacterial enzymes being members of the third family of molybdenum enzymes, see section 5.4). These enzymes are thought to be true oxygen atom transferases, with either an $LMo^{VI}O_2(S–Cys)$ as oxygen atom donor or $LMo^{IV}O(OH)(S–Cys)$ as acceptor in the active site. In addition to the well-studied

vertebrate sulfite oxidases and eukaryotic nitrate reductases, newer members of this family include plant sulfite oxidase and the bacterial sulfite dehydrogenases, as well as members of a broadly distributed group of proteins identified using genomics and related approaches, including YedY from *Escherichia coli*, and a number of enzymes from bacteria (YcbX, YiiM, CysJ) or mammals (mARC) that often have the ability to dehydroxylate hydroxyamines and related compounds.[261] As discussed further below, the family also contains a large number of proteins homologous to the C-terminal domain of the ABA3 molybdenum cofactor sulfurases that are now understood to coordinate the molybdenum center with a cysteine residue.

As indicated in Figure 1, members of the sulfite oxidase family have an $LMo^{IV}O_2$(S–Cys) coordination sphere, with a cysteine ligand contributed by the polypeptide. Although the molybdenum centers of both the xanthine oxidase and the sulfite oxidase families possess a square-pyramidal coordination geometry with an apical Mo=O as well as three sulfurs and an oxygen in the equatorial plane, Schwarz and Mendel[262] have pointed out that the orientation of the molybdenum coordination sphere with respect to the pyranopterin cofactor is opposite in the two families: with the pyranopterin group oriented to the left of the metal as shown in Figure 39, the apical Mo=O points up for all members of the xanthine oxidase family, and down for all members of the sulfite oxidase family. Further, Rothery et al. have noted that the conformation of the pyranopterin in members of the xanthine oxidase family is considerably more twisted than that in members of the sulfite oxidase family (Figure 39, far right); the xanthine oxidase configuration appears to be that of a tetrahydropterin, while the sulfite oxidase configuration is that of a dihydropterin.[263] It has been further noted that the tetrahydro form specifically appears to be involved in mediating electron transfer into or out of the molybdenum center from/to nearby redox-active centers in both the xanthine oxidase and the DMSO reductase families (see section 5). Indeed, an analysis of the MCD of the paramagnetic “very rapid” species seen with xanthine oxidase has led to the conclusion that electron egress from the molybdenum center to the nearer Fe/S I of the enzyme principally involves σ rather than π interactions between the molybdenum and pyranopterin,[115] consistent with the latter being in the tetrahydro oxidation state. It is to be emphasized that the configuration of the pyranopterin appears to be dictated by steric and hydrogen-bonding interactions with the polypeptide, which is fixed in the case of each enzyme. It is thus unlikely that the pyranopterin itself is formally redox-active in any given enzyme. A similar conclusion has been drawn from a consideration of the inherent chemistry of metallopterin models.[7h,264]

4.2. Sulfite-Oxidizing Enzymes

4.2.1. Vertebrate Sulfite Oxidase—The best understood enzyme of this family is the eponymous sulfite oxidase from chicken, whose crystal structure has been determined as shown in Figure 40. The enzyme from this and other vertebrates (including humans) is an α_2 dimer with each subunit consisting of a small N-terminal cytochrome *b* domain connected via a 12-to 15-aa tether (only part of which is clearly resolved in the crystal structure) to the main body of the subunit, which consists of molybdenum-binding and dimerization domains.[265] Like members of the xanthine oxidase family, the redox-active centers of one subunit are well-separated from those of the other, some 38 Å at closest approach

(molybdenum-to-molybdenum). Also like xanthine oxidase, the reductive and oxidative halves of the catalytic sequence are physically separated, sulfite being reduced at the molybdenum center and the reducing equivalents thus obtained passed on to the heme via intramolecular electron transfer prior to transfer on to its physiological oxidant, cytochrome *c*. Like cytochrome *c*, the vertebrate sulfite oxidase is localized in the intermembrane space of the mitochondrion. Both an N-terminal targeting sequence and correct incorporation of the molybdenum cofactor are required for correct subcellular localization; incorporation of the molybdenum center is also required for subsequent heme incorporation and dimerization.[266]

In the crystal structure, the two heme domains are not oriented the same way relative to their respective molybdenum domains, and each is in any case >30 Å from the molybdenum center of its own subunit (a distance confirmed in solution studies of the enzyme using pulsed EPE[267]); it is thus evident that substantial movement of the heme domain is necessary to bring the two redox-active centers into close enough proximity for the electron transfer that is integral to catalysis (see below). The molybdenum center of the chicken sulfite oxidase has the square structure shown in Figure 1, but the equatorial Mo–O distance is 2.22 Å, reflecting reduction of the protein in the X-ray beam, with protonation of the equatorial oxygen to give a Mo–OH.[265] X-ray absorption spectroscopic (XAS) studies have clearly shown that the oxidized enzyme possesses two Mo=O groups at a distance of 1.71 Å.[268] As shown in Figure 40, a cluster of highly conserved residues consisting of Arg 138, Arg 190, Trp 204, Tyr 322, and Arg 450 surrounds a bound product sulfate molecule in the reported structure of the chicken enzyme,[265] and the substrate binding site is thus clearly defined. The sulfate lies near the equatorial oxygen of the molybdenum coordination sphere, consistent with a mechanism involving direct oxygen atom transfer (see below). More recent crystallographic studies of the recombinant chicken enzyme in the absence of substrate have shown that Arg 450 swings away from the binding site in the absence of bound sulfate.[269] In the absence of sulfate, chloride occupies the binding site, interacting with Arg 190 and Trp 204. As discussed further below, this appears to represent a “blocked” form of the enzyme in which substrate/product is sterically obstructed from entering/departing the binding site.

Sulfite oxidase has been proposed to function in a fashion similar to that of MoO_2 model compounds whose oxygen atom transfer chemistry has been extensively studied,[270] with the enzyme alternating between dioxo Mo(VI) and monooxo Mo(IV) species.[271] Hall and co-workers have used a density functional approach to examine the mechanism of oxygen atom transfer of $LMo^{VI}O_2$ clusters of the type found in the active site of sulfite oxidase.[272] They find that a key aspect of the reaction of the oxidized cluster with an oxygen atom acceptor is the interaction between a lone pair of the oxygen atom acceptor (a phosphine was used in the computational work) and a π* orbital of one of the two Mo=O groups (the equatorial Mo=O in the enzymes, which as mentioned above is oriented directly toward the substrate binding pocket in the protein structure). P–O bond formation results in transfer of an electron pair involved in the π interaction between molybdenum and the oxygen atom under attack to a molybdenum d orbital, leading to formal two-electron reduction of the molybdenum. The two Mo=O groups of the oxidized complex compete for π ligation with the same set of molybdenum d orbitals, and the loss of the second Mo=O group in the course

of this reaction allows the remaining Mo=O to interact more strongly with the (now reduced) molybdenum. This interaction involves one σ and two π interactions in a formal triple bond, which recoups some of the enthalpic cost of cleaving a strong metal–oxo bond and labilizes the oxo group in what has been referred to as the "spectator oxo" effect.[273]

On the basis of the reactivity of the enzyme with the dimethylsulfite,[271a] a substrate analogue in which the oxyanion groups of substrate have been blocked by methylation, thus leaving only the lone pair to participate in the reaction, the enzyme has been proposed to function similarly.[271b] k_{red} (the limiting rate constant for enzyme reduction at high [substrate], reflecting the breakdown of the E_{ox}·S complex) is largely unchanged as compared to sulfite (170 s^{-1} for dimethylsulfite, as compared to 194 s^{-1} for sulfite), while the K_d increases over 300-fold upon methylation (to 11 mM from 33 μM). With control experiments undertaken to ensure that enzyme reduction was not due to slow hydrolysis of dimethylsulfite to sulfite in aqueous solution, it can be concluded that (1) the oxyanion groups are not involved in accelerating the rate of breakdown of the E_{ox}·S complex (by, for example, directly coordinating to the molybdenum); and (2) the oxyanion groups of sulfite contribute some 3 kcal/mol toward substrate binding, but are not the only forces that contribute to enzyme affinity for substrate (because k_{obs} exhibits a hyperbolic dependence on [dimethylsulfite]). A reaction mechanism predicated on oxygen atom transfer has subsequently been supported by a computational study of the enzyme's molybdenum center in which the reactivity of the equatorial oxygen of the molybdenum coordination sphere specifically is found to be activated for oxygen atom transfer.[274] A direct oxygen atom transfer mechanism is now generally accepted, although it is to be noted that there is as yet no direct experimental demonstration of oxygen atom transfer from enzyme to substrate.

The fundamental differences in reactivity of the catalytically labile oxygens of xanthine oxidase (the equatorial Mo–OH) and sulfite oxidase (the equatorial Mo=O occupying the equivalent position in the molybdenum coordination sphere) deserve further comment. In the case of sulfite oxidase, while the reaction involves nucleophilic attack on an inherently very electronegative oxygen, that oxygen is doubly bound to a six-valent electron sink in the Mo(VI), and there is abundant experimental as well as computational work clearly indicating that the reaction of a MoO_2 unit with a nucleophilic oxo acceptor is facile. In the case of xanthine oxidase, deprotonation of the equatorial Mo–OH generates a nucleophilic rather than electrophilic oxygen that proceeds to attack the substrate carbon to be hydroxylated. The difference in reactivity appears to be a reflection of the intrinsic reactivity of the metal center. Specifically, the highly covalent Mo=S that is adjacent to the Mo–OH in the equatorial plane provides a low-barrier hydride acceptor in the course of the nucleophilic attack that leads to the reduction of the molybdenum center. Thus, in the case of sulfite oxidase the chemistry occurs in a plane containing the two oxo groups that is perpendicular to the equatorial plane of the molybdenum coordination sphere, while in the case of xanthine oxidase the chemistry occurs in the equatorial plane. The key aspect that dictates the plane in which the chemistry occurs is the presence of a thiolate or sulfido ligand adjacent to the catalytically labile oxygen, and the availability of an equatorial in-plane S π bond that can accept the departing hydride from substrate.[275]

A comparison of the pH dependence of both the reductive and the oxidative half-reactions of the catalytic cycle for chicken sulfite oxidase indicates that under most conditions the reductive half-reaction (i.e., the reaction of anaerobic, oxidized enzyme with sulfite) is predominantly rate-limiting, but that particularly at low pH the oxidative half-reaction (the reaction of reduced enzyme with cytochrome c) becomes partially so.[276] k_{red} (again, the limiting rate constant reduction at high [sulfite] and tracking the breakdown of the E·S complex) is essentially pH-independent at 200 s^{-1}, while k_{red}/K_d (the second-order rate constant for reaction of free substrate with free enzyme in the low [sulfite] regime) exhibits a sigmoidal pH dependence with a pK_a of 9.3, reflecting the ionization of a functional group that must be protonated for the reaction to proceed. Subsequently, the steady-state and rapid-reaction kinetic behavior of human sulfite oxidase, both wild-type enzyme and a Y343F mutant, has subsequently been examined (Tyr 343 in the human enzyme corresponding to Tyr 322 in the chicken enzyme),[277] with both the holoenzyme and the molybdenum fragment alone being examined. At low ionic strength, the pH dependence of both k_{cat} and k_{cat}/K_m for the wild-type holoenzyme enzyme is bell-shaped and closely mimics the behavior seen with the chicken enzyme. The profiles for the Y343F mutant are also bell-shaped and shifted by ~1 pH from wild-type enzyme (to higher pH in the case of k_{cat} and to lower in the case of k_{cat}/K_m), and the maximum observed value was reduced by a factor of 3–5 with respect to wild-type enzyme. The implication is that ionization of Tyr 343 cannot be responsible for the observed pH dependence of wild-type enzyme. The pH profile for k_{red} from rapid reaction studies is independent of pH at ~80 s^{-1} for the wild-type holoenzyme, but with the mutant is modestly base-catalyzed, increasing from 5 s^{-1} at low pH to a maximum value above 60 s^{-1} above pH 9.5 with an apparent pK_a >10. With the molybdenum fragments alone, there is only a modest effect of the mutation on k_{red} (both ~2000 s^{-1} at pH 7), but K_d increases by approximately an order of magnitude in the mutant (from 186 μM to 1.6 mM). The substantially faster rate constants seen with the fragment as compared to the holoenzyme have been attributed to extremely rapid formation of a Mo^{IV}·sulfate species, which elicits the spectral change at the molybdenum center being followed experimentally, with subsequent electron transfer onto the heme (in the case of holoenzyme) being rate-limited by sulfate release.[277] Interestingly, neither the wild-type molybdenum fragment nor its Y343F mutant exhibited the sensitivity to excess substrate inhibition that is seen with either full-length form. Overall, Tyr 343 is thus seen to contribute approximately 1.5 kcal/mol to both substrate binding and also to stabilization of the transition state for product dissociation in the course of the reaction.

A C207S mutant of recombinant sulfite oxidase from rat has also been examined, in which the cysteine coordinating the molybdenum has been replaced by a serine.[278] The mutant exhibits a perturbed UV–visible absorption spectrum and a 2000-fold reduction in specific activity. An XAS analysis has shown that the oxidized molybdenum center of the mutant protein has an $LMo^{VI}O_3$ core, and that Ser 207 does not coordinate the metal in the mutant protein.[268b] It subsequently has been shown that reduction of the C207S mutant yields a center with a single Mo=O group, with the serine now presumably coordinated to the metal to give a $LMo^{IV}O(OH)$-(O–Ser) species.[279] The Mo–OSer bond appears to persist in the Mo(V) valence state at pH 6.0, which exhibits an EPR signal with $g_{1,2,3}$ of 1.9789, 1.9654, 1.9545, significantly shifted from the values seen with the low-pH signal of wild-type

enzyme ($g_{1,2,3}$ = 2.0037, 1.9720, 1.9658[279]). Proton coupling is evident in the EPR signal of the C207S mutant, but is much weaker than seen with wild-type enzyme.[280] More recently, Cys 185 of the chicken enzyme (equivalent to Cys 207 of the mammalian enzyme) has been mutated to both Ser and Ala, and the variants were examined by X-ray crystallography and XAS.[281] Both the lack of reactivity toward sulfite and the $LMo^{VI}O_3$ core of oxidized enzyme are confirmed. Interestingly, in the C185S mutant (but not the C185A mutant), most of a 31-residue loop (residues 310–340, including Tyr 332) is disordered in the X-ray crystal structure, indicating that the mutation induces a conformational rearrangement in the vicinity of the active site.

Very recently, a variant of the molybdenum-binding domain of human sulfite oxidase has been reported in which the Cys 207 that coordinates the molybdenum has been replaced by selenocysteine, this being accomplished by mutating all four cysteines other than Cys 207 to serine and expressing the domain under sulfur-free conditions with selenocysteine added to minimal medium; exchange at the molybdenum center was confirmed by XAS.[282] The C207U variant exhibited a 1.5-fold greater k_{cat}/K_m than the wild-type domain, and the pH optimum was shifted to ~7 from the value of 8.5 for wildtype enzyme. Interestingly, the Mo(V) EPR exhibited by the variant at low pH had $g_{1,2,3}$ = 2.022, 1.975, 1.964, as compared to 2.003, 1.972, 1.966 for the wild-type domain. The significant shift in g_1 is consistent with its known sensitivity to changes in the equatorial plane of the molybdenum center, and the increase in g_1 is expected in light of the greater covalency of the Mo–Se relative to Mo–S bond. The signal also exhibited the expected ^1H hyperfine coupling of ~26 MHz. The difference in EPR between Cys- and Sec-containing domains was essentially abolished in the high-pH signal, presumably due to the decreased covalency of the Mo–Se bond at the higher pH.

A clinically identified R160Q variant of human sulfite oxidase has also been recombinantly expressed and characterized.[283] The mutation results in a decrease in steady-state k_{cat} from 16 to 2.4 s^{-1}, and a significant increase in K_m from 17 μM to 1.7 mM; the overall effect on k_{cat}/K_m is very significant, 3 orders of magnitude. While K_m is not a proper thermodynamic parameter (it is necessarily a function of microscopic rate constants from multiple steps of the catalytic sequence[284]), it is evident that substrate affinity is seriously compromised in the R180Q mutant, consistent with the known position of Arg 160 in the substrate binding site. Surprisingly, in the crystal structure of the R138Q mutant of the chicken enzyme (equivalent to the R160Q variant of the human protein identified clinically), Arg 450 faces into the substrate binding cavity, even in the absence of sulfate. The predominant effect of the mutation thus may not actually be on the reductive half-reaction of the catalytic cycle but rather (through the effect on the position of Arg 450) on the rate constant for electron transfer from the molybdenum center to the heme, prior to electron transfer on to cytochrome c (see below). It is worth noting that the corresponding Arg 55 in the closely related sulfite dehydrogenase from *Starkeya novella* has also been mutated to Met with results comparable to those seen with the chicken enzyme: the effect on the limiting rate constant for enzyme reduction at high [sulfite] is modest, but K_d increases 3 orders of magnitude.[285]

Intramolecular electron transfer within the chicken and human sulfite oxidases has been extensively studied by Enemark and co-workers. Under most conditions, rate constants for electron equilibration between the molybdenum and heme in the one-electron reduced state of the wild-type chicken enzyme are on the order of 2000 s^{-1}, although at high pH and in the presence of anions such as sulfate the observed rate constant falls to as low as 35 s^{-1}.[286] Given the known reduction potentials for the Mo(VI/V) and heme (III/II) couples, the microscopic rate constants for the forward and reverse processes can be deconvoluted, with the rate constant for Mo → Fe electron transfer found to be essentially pH-independent at 700 s^{-1}, while that for Fe → Mo electron transfer is seen to decrease approximately monotonically from 600 s^{-1} at pH 8.5 to 140 s^{-1} at pH 7.[286] Qualitatively consistent with the notion that extensive heme domain motion is required for intramolecular electron transfer, increasing solvent viscosity from 1.0 to 2.0 cP reduces the rate constant for intramolecular electron equilibration by a factor of 2.[287] Electron transfer is also compromised upon reducing the length of the 14-aa tether connecting the heme- and molybdenum-containing portions of human sulfite oxidase: removal of five residues reduces the rate constant for electron equilibration from ~450 s^{-1} at pH 7.0 to 6 s^{-1}, with more modest deletions resulting in intermediate effects.[288]

The effect of several point mutations on intramolecular electron transfer has also been investigated, for the most part restricted to studies with the human enzyme. Mutation of Tyr 343 to Phe, discussed above with regard to the effect on catalysis, reduces the observed rate constant for electron equilibration between the molybdenum and heme in one-electron reduced enzyme by approximately an order of magnitude.[289] Electron equilibration within the R160Q mutant is even more dramatically affected, being reduced by a factor of almost 1000 from that seen in wild-type enzyme, from 411 to 0.64 s^{-1}, making electron transfer entirely rate-limiting for catalysis in the mutant.[290] An R160K mutation exhibits only a 4-fold reduction in the rate constant for electron equilibration, underscoring the importance of a positive charge at position 160 for effective electron transfer (presumably by helping to orient the heme domain relative to the molybdenum domain in the electron-transfer configuration).[290] Other mutations identified on the basis of clinical manifestations of individuals with variants of sulfite oxidase are G473D and A208D, both of which decrease the rate constant for electron equilibration within one-electron reduced enzyme by a factor in excess of 1000, again making intramolecular electron transfer rate-limiting to catalysis.[291] That a G473A mutant exhibits only modestly slower electron transfer than wild-type again underscores the importance of local charge in influencing electron transfer rates (although it is unclear whether in this case the reduced k_{cat} is due to an electrostatically compromised interaction with the heme domain, as thought to be the case with the Arg 160 mutants, or to the fact that the G473D mutant is simply conformationally compromised, as reflected in its altered UV circular dichroism).

Sulfite oxidase has also been examined by protein film voltammetry. In the presence of 1 mM sulfite, chicken sulfite oxidase that has been immobilized on a pyrolytic graphite edge electrode exhibits a catalytic wave at +90 mV (vs SHE).[292] The shape of the waveform indicates a one-electron process, and it has been concluded that the behavior reflects the catalytically limiting intramolecular transfer of reducing equivalents from the molybdenum

center to the heme within the enzyme rather than the obligatory two-electron chemistry of oxygen atom transfer. On the basis of the amplitude of the catalytic wave, only ~5% of the immobilized enzyme appears to be engaged in turnover, presumably reflecting the small portion of the immobilized enzyme in a configuration where the molybdenum and heme are close enough for intramolecular electron transfer to occur. More recently, sulfite oxidase and cytochrome *c* have been coimmobilized in molecular layers onto a specially treated electrode.[293] Addition of sulfite results in a catalytic wave that can be observed even at very rapid scan rates, indicating that the enzyme, once reduced by sulfite, efficiently passes electrons on to cytochrome *c* then on to the electrode. The catalytic current is dependent on sulfite concentration below 2 mM, with an effective K_m of approximately 310 μM. In this study, unfortunately, no estimate was provided as to the fraction of immobilized enzyme molecules that were catalytically active.

The molybdenum center of chicken sulfite oxidase has been extensively studied by EPR, with three basic forms of Mo(V) signal observed. These are designated “low-pH”, “high-pH”, and “phosphate-inhibited”, based on the conditions under which they are generated.[279] The “low-pH” signal exhibits strong hyperfine coupling to a single solvent-exchangeable proton that is absent in the “high pH” signal. It has been demonstrated using ENDOR, however, that a solvent-exchangeable and strongly but very anisotropically coupled proton is in fact present in the “high-pH” species of chicken sulfite oxidase, probably a Mo–OH/D group as assigned in the “low-pH” signal.[294] The difference in the extent of coupling as a function of pH is ascribed to differences in orientation of the bent Mo–O–H moiety, with the proton situated in a lobe of the singly occupied d_{xy} orbital at low pH, and rotated out of it at high pH. Proton coupling in the high-pH signal exhibits a rather broad range of values (i.e., dispersion), suggesting a (limited) distribution of configurations in the signal-giving species. In the low-pH species, on the other hand, the dispersion in coupling is not as pronounced, and the proton appears to be more conformationally constrained (possibly due to a hydrogen-bonding interaction between the Mo–OH and the cysteine sulfur coordinating to the molybdenum[294b]). Pulsed ENDOR and EPR studies of the low-pH signal have identified coupling due to the nonexchangeable C_α proton of the Mo-liganded Cys 185/207 in both chicken and human sulfite oxidases, at a distance of 2.8 Å.[295] This distance increases to 3.3 Å in the high-pH signal, attributed to a change in the torsional angle of the liganded cysteine itself relative to the molybdenum ligand field.

Both the low- and the high-pH EPR signals of sulfite oxidase show strong coupling to a solvent-exchangeable oxygen when the sample is prepared in ^{17}O-labeled water,[296] although the nature of the coupling is distinct in each case. Initially ascribed to a terminal Mo=O group, subsequent resonance Raman work[297] has suggested that this coupling arises from the equatorial Mo–OH rather than apical Mo=O in the signal-giving Mo(V) species. More recently, pulsed EPR spectroscopy has provided evidence for a second, more weakly coupled (but still solvent-exchangeable) oxygen in the high-pH form of sulfite oxidase.[298] This more weakly coupled oxygen has been assigned to the apical Mo=O of the molybdenum center on the basis of its hyperfine and quadrupolar coupling (6.4 and 1.5 MHz, respectively) with those of model complexes.[123,299] The axial Mo=O of high-pH sulfite oxidase exchanges much more slowly with solvent than does the equatorial Mo–OH,

and after several hours of incubation in 60% $H_2{}^{17}O$, only ~10% of the Mo(V) centers have exchanged.[300] The slow rate of exchange accounts for the earlier resonance Raman result that only a single Mo=O in the molybdenum center was solvent-exchangeable on the time scale of that experiment.[297] Pulsed EPR studies of the R160Q mutant of human sulfite oxidase in $H_2{}^{17}O$ at low pH have also provided evidence for a second, weakly coupled and solvent exchangeable oxygen that was originally assigned to the apical Mo=O of the molybdenum center,[301] but more recently has been reinterpreted as the oxygen of bound sulfite (or sulfate).[302] The implication is that the apical Mo=O group is not solvent exchangeable at low pH, again consistent with the resonance Raman work.

Chloride is a well-established inhibitor of the vertebrate sulfite oxidases, and is known to influence the pH-dependent interconversion of the low-pH and high-pH forms of the Mo(V) state, favoring the low pH form.[303] Although analysis of ^{35}Cl versus ^{37}Cl coupling in the low pH EPR signal was initially interpreted as evidence for direct coordination of chloride to molybdenum at the vacant ligand position *trans* to the apical Mo=O group,[304] a subsequent examination of the quadrupole interaction parameters for ^{35}Cl in conjunction with density functional calculations has concluded that chloride is not directly coordinated to the molybdenum but instead merely bound near the molybdenum center.[305] This latter interpretation is in agreement with the subsequently determined X-ray crystal structure of the recombinant chicken enzyme, showing chloride in the substrate binding site,[269] and with XAS analysis of the analogous bromide and iodide complexes of sulfite oxidase, which indicate that the halide binding site is some 5 Å from the molybdenum.[306] The effect of chloride on the low-pH EPR signal of both human and *A. thaliana* sulfite oxidases (see below), as well as a closely related sulfite dehydrogenase from the bacterium *Starkeya novella*, has also shown that depletion of chloride results in accumulation of a “blocked” form of the low-pH signal that lacks strong proton hyperfine coupling and has sulfate trapped coordinated to the molybdenum in the ligand position otherwise occupied by the catalytically labile equatorial Mo=O.[307] In the human enzyme, the blocked form exhibits rather different g-values ($g_{1,2,3}$ = 1.999, 1.972, and 1.963) than the ordinary low-pH form ($g_{1,2,3}$ = 2.004, 1.973, and 1.966). It appears that chloride somehow promotes hydrolysis of the Mo–OSO_3− bond of the reduced enzyme·product complex and appearance of the characteristic proton doublet of the unblocked low-pH signal with a Mo–OH ligand in place of the Mo–$OSOSO_3$−. The R160Q mutant of the human protein remains locked in the blocked configuration even in the presence of high concentrations of chloride, indicating that, in addition to its dramatically attenuated intramolecular electron transfer rate (above), product dissociation is also much slower.[301] On the basis of the crystal structures of the wildtype and R138Q chicken enzyme,[269] the “blocked” and “unblocked” forms of the enzyme appear to differ principally in the position of Arg 450, with this residue facing into or away from the substrate binding site, respectively. The crystallographically observed binding of chloride in the substrate binding pocket provides an obvious basis by which the anion might influence the position of Arg 450 and product dissociation.

4.2.2. Plant Sulfite Oxidase—In contrast to all vertebrate sulfite oxidases, the enzyme from *A. thaliana* lacks a heme domain.[308] Nevertheless, the remainder of the protein closely resembles the corresponding parts of the chicken enzyme,[97] as shown in Figure 40 (second

from top). The structure thus appears to represent an evolutionarily ancient motif that has remained highly conserved over time (despite sometimes low sequence identity among proteins).[309] As indicated in Figure 40 (right), the active site residues of the plant enzyme corresponding to Arg 138, Arg 190, Trp 204, Tyr 322, and Arg 450 of the chicken enzyme are Arg 51, Arg 103, Trp 117, Tyr 241, and Arg 374 in the *A. thaliana* protein. As pointed out above, with no sulfate in the structure of the (oxidized) plant protein, Arg 374 is found in a substantially different configuration than the corresponding Arg 450 of the chicken enzyme, facing away from the substrate binding cavity rather than into it. From a comparison of the two structures, it appears that Arg 374/450 swings into place only when the substrate binding site is occupied. As discussed above, it has been suggested that chloride, a known inhibitor of sulfite oxidase at higher concentrations, may facilitate this motion of Arg 450/374 and enhance activity at lower concentrations.[310]

The fact that the plant enzyme has no redox-active sites other than the molybdenum center has enabled spectroscopic studies of the enzyme without the complications that arise from the presence of the heme.[311] The absorption spectrum of the oxidized enzyme has maxima at 480 and 360 nm, both of which exhibit positive ellipticity in the circular dichroism spectrum; both bands bleach upon reduction of the enzyme, leaving a single weak shoulder at 400 nm.[308,311] These results corroborate and extend those previously seen for the molybdenum-containing proteolytic fragment of chicken sulfite oxidase.[312] The resonance Raman spectrum of the *A. thaliana* sulfite oxidase has also been examined, taking advantage of the absence of a heme site in the protein.[311] Using 488 nm excitation, three strong bands are observed at 896, 877, and 864 cm^{-1} in the 800–1000 cm^{-1} region where Mo=O stretches are to be expected. By analogy to comparable bands seen at 903 and 881 cm^{-1} with the chicken enzyme,[297] the 896 and 864 cm^{-1} bands have been assigned to symmetric and antisymmetric stretching modes of the MoO_2 unit of the molybdenum center, and the 877 cm^{-1} band to a vibrational mode having mixed enedithiolate and pyran ring character. The symmetric mode has approximately twice the intensity of the antisymmetric mode, which has been interpreted as indicating that the redox-active orbital arises from an antibonding interaction between the Mo d_{xy} and an O p orbital of the equatorial Mo=O.[311] After turning the enzyme over in $H_2{}^{18}O$ to incorporate label into the active site, the 896 and 864 cm^{-1} modes shift to 854 and 825 cm^{-1}, consistent with incorporation of the heavier isotope of oxygen into the molybdenum center. A new band at 910 cm^{-1} is also clearly resolved in the spectrum to the ^{18}O-labeled enzyme (evident as a shoulder on the 896 cm^{-1} mode in the ^{16}O sample), as is a second band at 883 cm^{-1}. Assuming, consistent with the above work with the chicken enzyme, that only the equatorial oxygen is labeled, then the 825 cm^{-1} mode would represent the isotope-sensitive ν_{eq} mode, with a shift of 39 cm^{-1} from the ν_{as} at 864 cm^{-1} that is near the 44 cm^{-1} expected for a simple harmonic oscillator (the analysis explicitly takes into account the fact that substitution of only one of the oxygens in the MoO_2 unit breaks the symmetry of the center, making it necessary to consider equatorial and apical vibrational modes explicitly, rather than symmetric and antisymmetric modes).

While the reductive half-reaction of the catalytic cycle for the vertebrate and plant sulfite oxidases undoubtedly proceeds in fundamentally the same way, the oxidative half-reaction is necessarily different given the absence of the heme in the plant enzyme. It has been shown

that the molybdenum center of the plant enzyme reacts with O_2 directly, with H_2O_2 as the ultimate product of the reaction.[313] It has subsequently been demonstrated, however, that $O_2^{\bullet-}$ is the immediate product of the reaction, and that H_2O_2 is formed only indirectly by the spontaneous disproportionation of $O_2^{\bullet-}$.[314] The observed rate constant for the reaction of reduced enzyme with O_2 exhibits a linear dependence on [O_2] ($k_{ox} = 5.3 \times 10^4\ M^{-1}\ s^{-1}$ at pH 8.0); given that the rate of reduction of the plant enzyme by sulfite exceeds that accessible by stopped-flow,[308] the oxidative half-reaction is clearly rate-limiting for overall turnover with the plant enzyme. Plant sulfite oxidase is localized in the peroxisome, and it is possible that the superoxide it generates is involved in antimicrobial generation of reactive oxygen species, although an appropriate source of sulfite to provide the reducing equivalents necessary for generation of a superoxide burst upon infection has not been identified. In addition to a possible physiological role for plant sulfite oxidase in microbial defense mechanisms, it has been shown that overexpression of the enzyme imparts resistance to air-borne SO_2.[315] The oxygen-reactivity of the plant sulfite oxidase is quite unusual for a molybdenum center, and the structural basis for it has not been elucidated. Among the very few differences in the environments of the molybdenum centers of sulfite oxidase family members, however, Tyr 49 in the plant sulfite oxidase is a Phe in chicken and human sulfite oxidases (and also in nitrate reductase, see section 2.3), and the greater polarity and hydrogen-bonding capacity afforded by tyrosine may impart the reactivity toward O_2 that is observed in the plant enzyme.

A pulsed EPR study using ^{33}S-labeled sulfite to generate the low-pH EPR signal of the *A. thaliana* sulfite oxidase has provided clear evidence for sulfate coordinated to molybdenum. The signal generated under the experimental conditions used (reduction by sulfite followed with partial reoxidation by ferricyanide) also lacks the strongly coupled proton typically seen[316] (which had also been seen previously under at least certain conditions with the chicken enzyme[317]), and the signal-giving species has been interpreted as a $LMo^{V}O(O–SO_3^-)(S–Cys)$ center with product sulfate coordinated to the molybdenum in place of the equatorial Mo=O. The g-values for this signal, in which product is blocked from dissociation, are $g_{1,2,3} = 2.005, 1.974, 1.963$, very similar to the parameters for the ordinary low-pH spectrum (generated by partial reduction of enzyme with Ti^{III}·citrate), $g_{1,2,3} = 2.006, 1.975, 1.968$. It is to be emphasized that this intermediate is expected for a reaction mechanism proceeding via lone-pair attack on the equatorial Mo=O of the oxidized enzyme, as described above. The presence of a bound sulfate accounts for the inability of the *A. thaliana* enzyme to form a phosphate-inhibited EPR signal under many reaction conditions, and also the absence of evident proton coupling in the low-pH signal.[311] As discussed above with regard to the vertebrate sulfite oxidases, a Y343F mutant in human sulfite oxidase also predisposes this blocked low-pH EPR signal (and also results in an increase in the pK_a associated with the low-pH/high-pH interconversion).[318] The implication is that the *A. thaliana* enzyme, crystallized with the corresponding Arg 374 in an open or unblocked position, nevertheless readily forms the blocked state. Extensive DFT calculations on the molybdenum center of the blocked form of the enzyme show that the coupling parameters for ^{33}S, in particular the large quadrupole coupling constant, favor a mono- rather than bidentate sulfite ligand rather than sulfate (sulfite being present in ~20-fold excess in the sample, in contrast to the excess of sulfate present in the X-ray crystal structures).[302]

4.2.3. Bacterial Sulfite Dehydrogenases[319]—Several sulfite dehydrogenases from bacterial sources have been identified, and on the basis of a genomics analysis these are found to fall into several discrete groups based on their amino acid sequences, polypeptide makeup, and the genetic context of the genes encoding them.[320] All are thought to possess the same active site as found in the eukaryotic enzymes, with a conserved cysteine residue coordinating the molybdenum in a square-pyramidal coordination sphere. As an example, the SorAB enzyme from *Starkeya novella* is a periplasmically localized αβ heterodimer that has been crystallographically characterized.[321] As shown in Figure 40 (second from bottom), it has a molybdenum center in the 44.6 kDa SorA subunit and a c-type cytochrome in the 9.7 kDa SorB subunit. Unlike the situation seen in the chicken sulfite oxidase, the cytochrome domain in the *S. novella* sulfite dehydrogenase is clearly positioned for effective electron transfer from the molybdenum center (with an edge-to-edge distance of 6.5 Å and a Mo-to-Fe distance of 15.5 Å). The orientation of the cytochrome subunit in the bacterial enzyme has been used as a model for docking of the molybdenum- and heme-containing domains of the vertebrate sulfite oxidases,[321] a model that is supported by a molecular docking study[322] and by site-directed mutagenesis studies of the human sulfite oxidase in which it is found that mutating either Trp 338 or His 337 at the putative interface of the molybdenum domain results in ~100-fold decreases in electron transfer rates between molybdenum and heme.[323] The molecular dynamics of the heme domain have also been investigated and found to be consistent with the proposed model.[324] Interestingly, although the molybdenum-containing SorA subunit possesses a domain homologous to the dimerization domain of the eukaryotic enzymes, the bacterial protein does not form an $(\alpha\beta)_2$ dimer.[321] The arginine equivalent to the human Arg 160 (whose mutation so dramatically reduces the rate of electron transfer between molybdenum and heme, as discussed above) is Arg 55 in the *S. novella* enzyme (Figure 40, right, second from bottom). An R55Q mutant of the bacterial enzyme is not compromised in intramolecular electron transfer, however,[325] suggesting that the role of the arginine in the human enzyme has more to do with properly orienting the heme domain for electron transfer rather than directly participating in a specific electron transfer pathway. The R55Q mutant of the bacterial enzyme is significantly compromised in substrate binding[285] and hydrolysis of the Mo^{IV}·sulfate complex, resulting in accumulation of the blocked EPR species discussed above in regard to the eukaryotic enzymes;[326] in the crystal structure of the R55 M mutant,[285] sulfate is coordinated to the molybdenum at the equatorial position otherwise occupied by the catalytically labile Mo=O, directly supporting the proposed structure for the blocked enzyme. Thus, as with the vertebrate enzymes, this arginine appears to be involved in facilitating hydrolysis of the $E_{red}{\cdot}SO_4^{2-}$ complex and product dissociation from the molybdenum center.

There are other types of bacterial sulfite dehydrogenases, including the enzymes from *T. thermophilus*,[327] *Deinococcus radiodurans*,[328] and *Sonorhizobium meliloti*[329] that, like the plant enzyme, lack a heme. These proteins can be either monomers or dimers and exhibit the characteristic absorption features of the molybdenum center as manifested by the plant enzyme. They are generally (but not universally) periplasmically localized and do not utilize O_2 or cytochrome *c* as oxidizing substrate, but frequently their genetic context suggests a membrane-bound cytochrome as the oxidizing substrate. The phylogeny of the bacterial sulfite-oxidizing enzymes and related proteins has recently been systematically

examined.[309,320] The sulfite-oxidizing enzymes proper, along with the assimilatory nitrate reductases (below), fall into one major group, with two other clades consisting of proteins that have other, frequently undefined, activities. These include proteins such as YedY from *E. coli*, vertebrate mARC proteins, and the so-called MOSC (for molybdenum cofactor sulfurase C-terminal domain) proteins that are homologous to the molybdenum cofactor-binding portions of proteins such as ABA3 and XdhC, which are involved in cofactor biosynthesis. These systems are considered further below, but it is to be emphasized here that genomics searches based on sulfite oxidases identify many proteins with activities other than sulfite oxidation. As will become evident (section 4.4), the sulfite oxidase family of molybdenum enzymes has proven to be much more diverse, both structurally and catalytically, than long believed.

4.3. Eukaryotic (Assimilatory) Nitrate Reductase

The eukaryotic assimilatory nitrate reductases catalyze the first and rate-limiting step of nitrate assimilation in fungi, algae, and higher plants, the reduction of nitrate to nitrite.[330] Pyridine nucleotides are the source of reducing equivalents required for catalysis by all of these enzymes, those from higher plants utilizing NADH and those from fungal sources NADPH; the algal enzymes usually require NADH, although some nonspecific enzymes able to use either pyridine nucleotide have been described.[330a] The present section focuses on more recent work on these systems, and the reader is referred to other reviews covering earlier work.[330]

Nitrate reductases from a number of higher plants have been characterized to varying degree, and that from *A. thaliana* is typical.[331] The enzyme is a homodimer of 2 × 110 kDa, with each subunit consisting of a large N-terminal domain (~59 kDa) that possesses the active site molybdenum center at which nitrate is reduced to nitrite, a 14 kDa central domain with a *b*-type cytochrome, and a C-terminal domain containing FAD and the NADH binding site (24 kDa). The structure of holo nitrate reductase and the specific orientation of the molybdenum, heme, and flavin domains with respect to one another remain unknown at present, but crystal structures have been reported for the molybdenum domain of the *Pichia angusta* enzyme,[332] for the heme domains of both chicken[265] and human[333] sulfite oxidase (as well as the bovine cytochrome b_5[334]) to which the heme domain of nitrate reductase is highly homologous, and for the flavin domain of the *Zea mays* nitrate reductase[335] (Figure 41). The molybdenum domain from *P. angusta*, consisting of residues 1–484 of the holoenzyme, is strikingly similar to the corresponding portion of the chicken[265] and *A. thaliana*[97] sulfite oxidases, with molybdenum-binding and dimerization subdomains. The molybdenum center itself closely resembles that seen in sulfite oxidase (Figure 41, top right), with a square-pyramidal $LMo^{VI}O_2$(S–Cys) molybdenum center in the oxidized enzyme, with one of the Mo=O groups occupying the apical position. The cysteine residue coordinating the molybdenum is Cys 139 in the *P. angusta* nitrate reductase (equivalent to Cys 191 in the *A. thaliana* nitrate reductase, Cys 98 in *A. thaliana* sulfite oxidase, and Cys 185 in chicken sulfite oxidase). EPR[336] and X-ray absorption[337] studies have provided clear evidence that the equatorial Mo=O becomes protonated upon reduction of the enzyme. As with the sulfite oxidases, the equatorial Mo=O of the oxidized *P. angusta* nitrate reductase faces into the solvent access channel and the substrate binding site (see section 3.3) and is

presumed to be catalytically labile. The substrate binding site in the *P. angusta* nitrate reductase molybdenum domain consists of two arginine residues, Arg 89 and 144, as well as Trp 158 (Figure 41); all three of these residues are conserved with the sulfite oxidases. The substrate binding site also includes three residues conserved among the nitrate reductases but different in the sulfite oxidases: Met 427 (a Val in the sulfite oxidases), Asn 272 (a Tyr in the sulfite oxidases), and Thr 425 (the Arg in the sulfite oxidases involved in formation of the blocked state discussed in section 4.2.1). It is to be noted that the position corresponding to Thr 425 in the *P. angusta* nitrate reductase is more commonly a methionine in other nitrate reductases. The extent to which these residues impart substrate specificity is discussed further below. Very recently, a molybdenum-cofactor free form of the nitrate reductase from *Neurospora crassa* has been successfully cloned and heterologously expressed in *E. coli*.[98] Work with the apoprotein thus obtained has demonstrated that incorporation of the molybdenum center is required for dimerization, and a small region of the dimerization domain (see below) has been identified that is involved in the dimerization process once cofactor is inserted. It is to be hoped that the development of this expression system bodes well for the ultimate expression of holoenzyme.

In the overall structure of the molybdenum-containing fragment of the *P. angusta* nitrate reductase, the first 25 and last six amino acid residues are not resolved. The crystallographically resolved residues 26–37 constitute the end of an N-terminal extension that leads into the molybdenum-binding domain of the fragment, consisting of residues 38–385, which is followed by the dimerization subdomain (residues 385–484). The molybdenum- and heme-containing domains of nitrate reductase are connected by a ~50-residue linker (approximately residues 491–541 in the holoenzyme from *A. thaliana*, which will serve as the point of reference in discussing the structure of the holoenzyme). As indicated above, the heme-containing domain has significant sequence homology to the heme domain of sulfite oxidase and the mammalian cytochromes b_5 (Figure 40). His 577 and 600 in the *A. thaliana* nitrate reductase correspond to His 40 and 65 in the chicken enzyme that coordinate the heme iron. The more negatively charged environment of the heme in nitrate reductase (particularly to the amino terminal side of His 600, where the sequence is $EFEAIH_{600}$ in the *A. thaliana* nitrate reductase but $WALYAVH_{64}$ in chicken sulfite oxidase) accounts for the substantially more negative reduction potential for the heme in nitrate reductases (−123 and −162 mV for spinach and *Chlorella vulgaris* nitrate reductases, respectively) as compared to sulfite oxidases (e.g., +90 mV for the chicken enzyme). The differences in heme potentials are consistent with the differing physiological direction of electron transfer in the two systems (heme → Mo in the nitrate reductases, Mo → heme in the sulfite oxidases).

The heme- and FAD-containing domains of nitrate reductase are connected by a second, ~30-amino acid linker (approximately residues 621–650 in the *A. thaliana* protein). The flavin-binding domain itself is a member the well-characterized family of ferredoxin:$NADP^+$ reductase-like (FNR) flavoproteins,[341] and the crystal structure of the FAD-containing fragment of *Z. mays* nitrate reductase has been determined.[335] It consists of two well-defined FAD- and NADH-binding subdomains (approximately residues 651–757 and 758–917, respectively, in the *A. thaliana* protein). As with other members of the FNR

family, the NADH binding site of nitrate reductase is only poorly defined.[341] By analogy to the structures of various members of the FNR family in complex with their physiological partners,[342] it is very likely that the heme domain interacts with the flavin domain of nitrate reductase at the portion of the surface of the latter where its flavin C-8 methyl protrudes to solvent (Figure 41, bottom right, in green). The flavin C-8 methyl is flanked by His 48 and His 118 in the corn FAD fragment (equivalent to the conserved residues His 698 and His 768 of the *A. thaliana* enzyme), which along with the C-terminus of the enzyme may help position the heme domain (with possible cognate residues Asp 579, Asp 585, and Lys 606) for electron transfer. It is likely that any such complex formed is only transiently as the heme domain must undoubtedly reorient significantly within holo nitrate reductase, once reduced, to present its redox-active face to the molybdenum domain of the enzyme for electron transfer on to the molybdenum center.

In the course of turnover, NADH introduces reducing equivalents into the enzyme at the FAD in the reductive half-reaction of the overall catalytic cycle, and these are subsequently transferred via the heme to the molybdenum center, where nitrate is reduced to nitrite in the oxidative half-reaction. Reduction of the $LMo^{VI}O_2(S–Cys)$ core of the active site yields $LMo^{IV}O(OH)(S–Cys)$, consistent with X-ray absorption studies of the enzyme.[337] The basic chemistry of nitrate reduction is believed to be straightforward, and functionally the reverse of the oxygen atom transfer seen with sulfite oxidase, with nitrate serving as oxygen atom donor and the reduced molybdenum center functioning as the oxygen atom acceptor:

$$\begin{aligned} &O{=}NO_2^- + LMo^{IV}O(OH)(S-Cys) \\ \rightarrow\ &{:}NO_2^- + LMo^{VI}O_2(S-Cys) + HO^- \end{aligned}$$

With each catalytic cycle, the equatorial Mo=O (after reduction, protonation, and displacement by nitrate) is lost to solvent, regenerated with oxygen derived from substrate in the oxygen atom transfer event. It is to be noted, however, that just as with sulfite oxidase, there is to date no explicit experimental evidence for direct oxygen atom transfer in the enzyme mechanism. The basis for the nitrate-utilizing enzyme being a reductase and the sulfite-utilizing enzyme an oxidase has been justified on the basis of the relative thermodynamic stabilities of N=O, S=O, and Mo=O bonds.[343]

For the *A. thaliana* nitrate reductase, the steady-state kinetic parameters are $k_{cat} = 210\ s^{-1}$, $K_m^{nitrate} = 90\ \mu M$, and $K_m^{NADH} = 0.8\ \mu M$ at pH 7.0, 30 °C.[344] A rapid reaction kinetic analysis of the enzyme has also been undertaken, beginning with an examination of the reaction of the flavin fragment of corn nitrate reductase, and also a C242S mutant, with NADH.[345] The rate of reduction of the C242S mutant by NADH is some 7-fold slower than for the wild-type protein ($68\ s^{-1}$ versus $478\ s^{-1}$), and K_d^{NADH} is somewhat larger (6 vs 3 μM), indicating that Cys 242 plays a modest role in facilitating electron transfer from NADH to the flavin but only a minimal role in binding of NADH to the enzyme. A $FADH_2{\cdot}NAD^+$ charge-transfer complex with characteristic long-wavelength absorption ($\varepsilon_{8\ nm} = 2.7\ mM^{-1}\ cm^{-1}$) is formed in the course of the reaction with both forms of the flavin domain.[345] The reaction of a combined flavin-heme fragment of nitrate reductase from spinach with NADH has also been examined.[346] The reaction in this case is triphasic,

with a fast phase whose k_{red} of 560 s^{-1} and K_d of 3 μM agree well with the results using the (corn) flavin fragment alone (478 s^{-1} and 3 μM, respectively). The $FADH_2{\cdot}NAD^+$ charge-transfer complex is formed in this fast phase of the reaction. Surprisingly, the subsequent internal electron transfer from $FADH_2$ to heme in the intermediate phase of the reaction is very slow, 12 s^{-1}, and appears to be rate-limited by dissociation of NAD^+ from the $E_{red}{\cdot}NAD^+$ charge-transfer complex. The slowest phase of the reaction is due a slow intermolecular disproportionation of the two-electron reduced protein formed after reaction with a first equivalent of NADH to yield one equivalent each of the one- and three-electron reduced form (the one-electron reduced enzyme then reacting with a second equivalent of NADH to give full reduction in a process rate-limited by the disproportionation).

The rapid reaction kinetics of recombinant holo nitrate reductase from *A. thaliana* (expressed in *Pichia pastoris*) has also been examined.[344] The kinetics of enzyme reduction by NADH are largely consistent with the above results with the flavin-heme fragment, with a fast phase of ~700 s^{-1} observed at 70 μM NADH corresponding to flavin reduction and a subsequent slower phase at 28 s^{-1} corresponding to electron transfer on to the heme. No evidence is seen with the *A. thaliana* enzyme for formation of an $FADH_2{\cdot}NAD^+$ chargetransfer complex. The kinetics of the reoxidation of prereduced nitrate reductase by nitrate were not examined in this study, perhaps due to the inevitable complications due to the very low level of competent molybdenum center (only ~20%) in the recombinant enzyme. A series of enzyme-monitored turnover experiments were performed, however, in which enzyme at a concentration of, for example, 2 μM enzyme prereduced with 40 μM NADH was reacted with 90 μM nitrate. The kinetics for the approach to steady-state, as followed by the absorbance changes at 460 nm (following changes in the oxidation state of the FAD) and 557 nm (following changes in the oxidation state of the heme), were biphasic with apparent rate constants of 260–270 and 6–8 s^{-1}, respectively. The latter value is unfortunately too slow to support turnover, and the possibility exists that most of the observed kinetics involved the large proportion of enzyme lacking a molybdenum center (which, despite being readily reducible by NADH, could not be reoxidized by nitrate).

The activity of assimilatory nitrate reductases is under tight regulatory control at the transcriptional, translational, and post-translational levels.[330] Post-translational inhibition of nitrate reductase at night, when photosynthetically generated reducing equivalents are not available to reduce nitrite on to ammonia, prevents the deleterious accumulation of nitrite in the plant.[347] Enzyme inhibition involves phosphorylation of a serine in the linker region between the molybdenum and heme domains (Ser 543 in the spinach enzyme, Ser 534 in *A. thaliana*),[348] carried out by any one of several specific protein kinases (including cAMP-activated protein kinase and calcium-dependent protein kinase, CPK[349]). Phosphorylation does not directly result in inhibition, but rather creates a binding site for a specific regulatory element, a member of the 14–3–3 family of proteins, whose binding (in the presence of Mg^{2+}, which is required for inhibition) effectively shuts down activity.[350] Of the several 14–3–3 proteins encoded by the *A. thaliana* genome, the 14–3–3ω isoform is particularly effective in binding to and inhibiting the phosphorylated form of nitrate reductase.[351] The steady-state kinetic properties of *A. thaliana* nitrate reductase as-isolated, phosphorylated, and phosphorylated in complex with 14–3–3ω forms have been investigated.[352] Of the

several calcium-dependent protein kinases encoded by the *A. thaliana* genome, CPK-17 has been found to efficiently phosphorylate nitrate reductase at Ser 534 in vitro. In NADH-nitrate assays, the as-isolated enzyme exhibits a k_{cat} of 20 s^{-1}, $K_m^{nitrate}$ of 197 μM, and K_m^{NADH} of 18 μM, phosphorylated enzyme exhibits a somewhat higher k_{cat} and $K_m^{nitrate}$ of 33 s^{-1} and ~200 μM, respectively, while the phosphorylated enzyme complexed with 14–3–3ω gave a substantially reduced k_{cat} of 1.8 s^{-1} and $K_m^{nitrate}$ of 141 μM. An S534A mutant of the nitrate reductase is not inhibited by 14–3–3ω, underscoring the importance of the phosphorylated site in formation of the inhibitory complex. Significantly, phosphorylation and 14–3–3ω binding have no effect on turnover with NADH and cytochrome *c* as substrate. Cytochrome *c* accepts reducing equivalents from the heme site of nitrate reductase, and the kinetic results indicate that neither the reaction of oxidized enzyme with NADH nor electron transfer from the flavin to the heme are affected by 14–3–3ω binding. Similarly, 14–3–3ω binding does not influence K_i for product nitrite (and presumably also K_d for substrate nitrate), meaning that inhibition is due either to a reduced rate of reduction of nitrate at the reduced molybdenum center or to a slower rate of electron transfer from the heme to the molybdenum in the enzyme. A subsequent rapid kinetic study of the system[353] has shown that phosphorylation and 14–3–3ω binding slows the limiting rate constant for reoxidation of the heme site of a reduced molybdenum-heme fragment of *A. thaliana* nitrate reductase on reaction with saturating concentrations of nitrate by a factor of approximately 10 (from 310 to 35 s^{-1}), but that phosphorylation and 14–3–3ω binding have no discernible effect on the rate of reaction of the molybdenum center of the reduced molybdenum-heme fragment with nitrate. Inhibition of phosphorylated nitrate reductase by 14–3–3ω thus appears to be due to a decrease in the rate of electron transfer from the heme to the molybdenum, rather than a decrease in the rate of nitrate reduction at the molybdenum center per se. It has been suggested that this occurs via a conformational change induced by binding of 14–3–3ω that significantly increases the distance between heme and molybdenum sites.[353]

No site-directed mutagenesis work has yet been done with the molybdenum domain of the assimilatory nitrate reductases, but a study has been reported attempting to reverse the substrate specificity of the molybdenum domain of sulfite oxidase to make it favor nitrate reduction.[354] Mutation of Tyr 343/322 (human and chicken numbering, respectively) to Asn and Arg 472/450 to Met significantly compromises steady-state turnover with sulfite, with k_{cat} and k_{cat}/K_m reduced by factors of 20–30 and 10^4–10^6, respectively. Both double mutants exhibit significant nitrate reductase activity, with k_{cat} 0.4–1.0 s^{-1} and $k_{cat}/K_m \approx 10^3$ $M^{-1}s^{-1}$. Interestingly, for a triple mutant that additionally included switching Val 474/452 to Met, reactivity toward both sulfite and nitrate increased approximately twofold as compared to the double mutants. Rapid-reaction experiments were limited to two single mutants of the human sulfite oxidase, R472Q and R472M, and these examined only the reaction with sulfite. While the trends in k_{red}/K_d and k_{cat}/K_m are indeed very similar, with either mutation compromising both parameters by 10–40-fold, the effect on k_{red}/K_d is a modest 4-fold greater than that on k_{cat}/K_m (where these parameters each reflect the slope of the hyperbolic plot of rate (constant) versus [substrate] in the low-substrate regime). On closer inspection of the data, it is evident that the principal effect of each mutation is on k_{cat} rather than K_m in the steady-state experiments, but on K_d rather than k_{red} in the rapid-reaction studies. It is important to remember that K_d is a proper thermodynamic parameter gauging affinity of

enzyme for substrate, while $K_m^{sulfite}$ is simply the empirical concentration of substrate that yields half-maximal catalytic velocity, and in terms of the microscopic rate constants appearing in the kinetic reaction mechanism is minimally $[(k_{-1} + k_2)/k_1]\cdot[k_{ox}/(k_{red} + k_{ox})]$, where k_1, k_{-1}, and k_2 have their conventional meaning for a one-substrate enzyme reaction, and k_{red} and k_{ox} represent the limiting rate constants at high substrate concentration in the reductive and oxidative half-reactions of the catalytic cycle, respectively. Similarly, the equation for k_{cat} is at least as complicated as $(k_{red} + k_{ox})/(k_{red}\cdot k_{ox})$, assuming that k_{red} is entirely rate-limiting (which is in fact known not to be the case, at least for the chicken sulfite oxidase[276]). In deriving these relationships, it is assumed that electron transfer between the molybdenum center (site of the reductive half-reaction) and heme (site of the oxidative half-reaction) is very rapid, which is generally thought to be the case, but otherwise the equations become even more complicated. This illustrates how difficult it is on the basis of steady-state data alone to parse thermodynamically how an enzyme utilizes the free energy available to it from the interaction between any given active site residue and substrate to simply bind substrate or instead lower the activation barrier for the reaction and thereby accelerate reaction rate.

4.4. More Recently Identified Members of the Sulfite Oxidase Family

For many years, sulfite-oxidizing and nitrate-reducing enzymes (from eukaryotes) were the only known members of the sulfite oxidase family of molybdenum enzymes. Over the past several years, however, a number of proteins have been identified that are clearly members of this family, and that have different (if unidentified in some cases) catalytic activities that expand our understanding of the catalytic repertoire available to the molybdenum centers of these proteins. These include the mitochondrial amidoxime reducing component (mARC) of eukaryotes, the bacterial gene products YedY, YcbX, and YiiM, and the newly recognized and extensive group of homologues of the molybdenum cofactor sulfurase C-terminal (MOSC) domain of ABA3 discussed above. Although genomics analyses indicate that these proteins often have quite divergent amino acid sequences,[309,320] those whose crystal structures have been determined are found to have three-dimensional structures for their molybdenum-binding domains that closely resemble those discussed above for sulfite oxidase and nitrate reductase.

Mitochondria are able to reduce a wide range of hydroxylamines to amines, and the enzyme catalyzing the NADH-dependent reaction has been shown to be a 35 kDa molybdenum-containing enzyme.[261] Termed mitochondrial amidoxime reducing component (mARC), the monomeric enzyme catalyzes the reduction of *N*-hydroxylated substrates such as amidoximes, *N*-hydroxy-sulfonamides, and *N*-hydroxyguanidines, with the reducing equivalents provided by NADH via cytochrome b_5 reductase and cytochrome b_5. Many of the substrates for this system are prodrugs (having been hydroxylated to neutralize the positive charge on the amine so as to increase membrane permeability) that are reductively activated by mARC to the (positively charged and membrane-impermeable) amine.[261a,355] The physiological substrate(s) are as yet unknown, but several of the tested *N*-hydroxylated compounds, including *N*-hydroxy-cytosine[356] and *N*-ω-hydroxy-L-arginine,[357] are likely candidates. *N*-hydroxycytosine is reduced to cytosine with high efficiency by human mARC proteins, providing a mechanism for detoxification of this mutagenic base analogue, which

otherwise would be misincorporated into DNA.[355] The possible involvement of mARC in reduction of *N*-ω-hydroxy-L-arginine, the immediate precursor to nitric oxide, suggests that mARC may play an important role in the regulation of intracellular nitric oxide levels. All annotated eukaryotic genomes of eukaryotes requiring molybdenum encode two discrete mARC genes. Although these exhibit strong similarities in nucleotide and amino acid sequence, the two isoforms, designated mARC-1 and mARC-2, can be distinguished on the basis of substrate preferences[358] and tissue distribution.[355]

The mARC proteins possess a strictly conserved cysteine residue among the MOSC proteins (Cys273 and Cys272 in human mARC-1 and -2, respectively) at the extreme C-terminal end[359] that represents the ligand to the molybdenum seen in members of the sulfite oxidase family. Although initially considered to represent a cysteine converted to a persulfide in an analysis of proteins exhibiting sequence homology to the C-terminal domain of ABA3 and similar molybdenum cofactor sulfurases, it has become increasingly clear that the conserved cysteine instead coordinates a bound molybdenum center having the same structure as seen in the sulfite oxidases. Consistent with this interpretation, both mARC isoforms exhibit EPR signals that closely resemble the low pH and high pH signals characteristic of both sulfite oxidase and nitrate reductase, with the low pH signal exhibiting approximately isotropic superhyperfine coupling to a single exchangeable proton.[355] The *g*-values associated with both types of signal seen with mARC clearly reflect the presence of a third axial sulfur ligand. More recently, it has been demonstrated that mARC-2 has a solvent-exchangeable equatorial oxygen ligand, most likely a Mo=O.[360] mARC proteins represent the simplest vertebrate molybdenum enzymes in that they are monomeric proteins consisting of solely a MOSC domain and bind only one prosthetic group, the molybdenum cofactor. It should be borne in mind, however, that these enzymes do not function as stand-alone proteins but rather act in concert with other redox-active components. Indeed, the complement of redox-active centers in the complete amidoxime-reducing system, consisting of cytochrome b_5 and the FAD-containing NADH:cytochrome b_5 reductase, resembles that seen in the eukaryotic nitrate reductases, and the direction of electron flow in the two systems is the same: NADH $\rightarrow$ FAD $\rightarrow$ cyt b_5 $\rightarrow$ molybdenum $\rightarrow$ substrate. It remains for future structural studies to ascertain whether deeper structural homologies exist between the mARC system and nitrate reductase.

Two other proteins from *E. coli*, YcbX and YiiM, been shown to exhibit activities similar to mARC, catalyzing the dehydroxylation of *N*-hydroxyadenine and thereby imparting resistance to this mutagen.[361] Both proteins have been identified as members of the MOSC family of proteins with sequence homology to the C-terminal domain of ABA3.[359] Additionally, the function of both proteins has been demonstrated to be dependent on the pyranopterin biosynthetic pathway,[75b] and it is evident that these are true molybdenum-containing enzymes. Somewhat surprisingly, reducing equivalents for the reduction of *N*-hydroxyadenine have been shown to come from the diflavin-containing CysJ subunit of sulfite reductase.[362] Unfortunately, neither protein has been purified and biochemically characterized to any degree.

Finally, the *yedYZ* operon of *E. coli* encodes a membraneintegral *b*-type cytochrome (YedZ) and a periplasmically localized and molybdenum-containing YedY. The system, originally

identified on the basis of weak homology to other known molybdenum-containing enzymes, has been crystallographically characterized (Figure 40).[74] YedY lacks the dimerization domain seen in chicken and *A. thaliana* sulfite oxidases, but despite low overall sequence homology the protein fold generally closely resembles that seen in for the molybdenum-binding portions of the eukaryotic enzymes,[309] and the structure of the molybdenum center is essentially identical that seen in the sulfite oxidases, with Cys 102 coordinating the molybdenum. The physiological substrate for YedY has not yet been determined. The enzyme is unable to oxidize sulfite or reduce nitrate, consistent with the absence of conserved arginine residues known to be involved in sulfite binding, but can reduce a variety of *S*- and *N*-oxides, albeit with K_m values in the tens of mM.[74] Unusually, as-isolated YedY exists nearly quantitatively in the Mo(V) oxidation state, and while it can be reduced to Mo(IV), it is not easily oxidized to Mo(VI).[363] The nearly axial EPR signal exhibited by the protein has $g_{1,2,3}$ = 2.030, 1.974, 1.969 with no proton hyperfine, even at low pH. The highly axial *g* tensor has been attributed to the extremely covalent nature of the metal–sulfur ligation (from the enedithiolate as well as the cysteine).[364] Electronic absorption transitions at 11 900 cm^{-1} (840 nm), 19 122 cm^{-1} (523 nm), and 21 578 cm^{-1} (463 nm) have been assigned to the following charge-transfer interactions, respectively: out-of-plane enedithiolate S(p) → Mo(d_{x2-y2}), out-of-plane Cys S(p) → Mo(d_{x2-y2}), and out-of-plane Mo(d_{x2-y2}) + Cys S(p) → Mo(d_{xz}) + Mo(d_{yz}); all three transitions have very weak oscillator strengths below 0.01 (and ε < 1000 M^{-1} cm^{-1}). These assignments may well hold for all members of the sulfite oxidase family, at least for those Mo(V) forms whose EPR do not manifest hyperfine coupling to protons, although the energies of the transitions can be expected to vary. XAS analysis of YedY in the Mo(V) state has provided clear evidence of the two enedithiolate sulfurs and Cys 102 at 2.4 Å, a Mo=O at 1.7 Å, and a Mo–(OH) at 2.1 Å.[365] There is suggestive evidence of a longer O/N at 2.6 Å, possibly Asn 45 or Glu 104 bound to the molybdenum *trans* to the Mo=O, at least in the Mo(V) state. In the reduced state, the equatorial Mo–OH lengthens to 2.20 Å, consistent with protonation to a water molecule.[365] Q-band EPR has provided clear evidence that the broad g_1 feature seen at X band is due to two nearly overlapping signals arising from two distinct species present in the sample in a 40:60 ratio. Fits of both the Q- and the X-band spectra indicate that the three *g*-values for the minor species are consistently shifted to higher *g* by ~0.002 relative to the major species.[365b]

On the basis of the above, it appears that at least three subfamilies of enzymes exist that possess $LMoO_2$(S–Cys) centers.[320] The first consists of the proper sulfite oxidases/dehydrogenases and nitrate reductases, which are broadly distributed in eukarya and bacteria but relatively rare in the archaea. A second subfamily includes enzymes such as mARC and YcbX that catalyze the reduction of other S- and N-hydroxylated compounds, and a third subfamily consists of the MOSC proteins involved in molybdenum cofactor sulfuration and related enzymes; the latter two subfamilies are found in all three domains of life. Genomics analyses indicate that these subfamilies may be further parsed based on the size of the molybdenum-binding domain, the presence or absence of a "dimerization" domain (sometimes identified simply as a "β-strand-rich fold"[359]) regardless of whether the protein in fact dimerizes, the presence of additional domains possessing prosthetic groups (e.g., redox-active centers or pyridoxal phosphate), the presence or absence of a *tat* signaling

sequence for transport to the periplasm, and the detailed manner in which the polypeptide interacts with the pyranopterin.[309,320,359] While the vast majority of the proteins identified have not been isolated and characterized to any significant degree, it is nevertheless evident that the sulfite oxidase family of molybdenum-containing enzymes, until very recently thought to consist of only a very few specific enzymes catalyzing only oxygen atom transfer reactions, is in fact a large and catalytically diverse group of proteins with members that are as broadly distributed in biology as those of the xanthine oxidase family.

5. THE DMSO REDUCTASE FAMILY

The family of molybdenum-containing enzymes epitomized by DMSO reductase from *Rhodobacter sphaeroides*, the first to be structurally characterized, is the most diverse group of molybdenum-containing enzymes from both a structural and a catalytic viewpoint. All of these enzymes are from prokaryotes, and while most catalyze bona fide oxygen atom transfer reactions, others catalyze oxidation/reduction or even hydroxylation/hydration reactions. Here, we cover first the diversity of overall protein architectures found in members of this family, then consider several specific groups of enzymes in turn. As has been pointed out earlier,[3] members of this family of molybdenum-containing enzymes are structurally related to the aldehyde:ferredoxin oxidoreductase family of tungsten-containing enzymes, and at least some members are able to accept either metal. The second family of tungsten-containing enzymes, including archaeal formate dehydrogenases and related enzymes,[4] are occasionally referred to as a fourth family of molybdenum-containing enzymes,[309] but this is misleading: these enzymes are pyranopterin-containing, but none has been found to possess molybdenum. Thus, while it can be considered that there are four families of pyranopterin-containing enzymes, there are only three families of (mononuclear) molybdenum enzymes proper.

5.1. Overview of Protein Architectures and Phylogenetic Relationships

As indicated in the Introduction and Scope, there is considerable diversity among members of the DMSO reductase family of enzymes as regards the identity of the amino acid residue coordinating the molybdenum and the nature of the Mo=Y ligand of oxidized enzyme (Y = O, S, Se). As illustrated in Figure 42, there is also considerable diversity as regards the different types of subunit constitution and complement of redox-active cofactors seen in these enzymes. The simplest of these enzymes are monomeric proteins with an $L_2Mo^{VI}OX$ active site as their sole redox-active center, as exemplified by the periplasmic DMSO reductases from *Rhodobacter sphaeroides* and *R. capsulatus* (with X = O–Ser).[99,366] Next in complexity are enzymes such as the periplasmic formate dehydrogenase H from *E. coli*,[248b] which is a monomer with a [4Fe-4S] cluster in addition to the molybdenum center, followed by enzymes such as arsenite oxidase from *Alcaligenes faecalis*, which has a first subunit with the molybdenum center and a [3Fe-4S] cluster, and a second with a Rieske-like [2Fe-2S] cluster.[367] Similarly, the periplasmic (Nap) or cytoplasmic (Nas) assimilatory nitrate reductases are usually heterodimers with a molybdenum- and [4Fe-4S]-containing subunit as well as a diheme containing one.[368] Even greater complexity is manifested by integral membrane enzymes such as the DMSO reductase,[369] NarGHI nitrate reductase,[370] and the FdnGHI formate dehydrogenase N[371] from *E. coli*, which are heterotrimers with five

iron–sulfurs in addition to their molybdenum centers, and sometimes hemes as well. Finally, the cytoplasmic NAD^+-dependent FdsABG formate dehydrogenases (from aerobic bacteria such as *Ralstonia eutropha*) have the greatest complexity, with a minimum of seven iron–sulfur centers and FMN in addition to the molybdenum center.

Several genomics studies have been made of members of the DMSO reductase family of enzymes that reveal relationships among its members that might not be expected on the basis of Figure 42.[372] One major clade indeed consists of the simple monomeric enzymes possessing a molybdenum center as their sole redox-active group, but a second consists of the Nap and Nas nitrate reductases plus the FdhF formate dehydrogenase H and arsenite oxidase. A third consists of two subgroups containing enzymes such as polysulfide reductase and the *E. coli* DmsABC DMSO reductase, on the one hand, and the NarGHI nitrate reductase, ethylbenzene dehydrogenase, and DMS dehydrogenase, on the other. The polysulfide reductase group is unusual in that it includes members from several different phyla of bacteria as well as archaea, a signature of it having evolved prior to the divergence of these groups.[373] The segregation among clades appears to be most closely correlated with the nature of the additional redox-active centers found in these enzymes. While there is often a correlation with the detailed structure of the molybdenum center, and in particular the nature of the sixth ligand to the metal provided (usually) by the polypeptide, it is not the case that all members of a given clade possess the same type of ligand. Functionality and the nature of the reaction catalyzed would seem to be least correlated; the *Rhodobacter* DorA and *E. coli* DmsABC DMSO reductases are in separate clades, as are the NarGHI and Nap/Nas nitrate reductases; the *E. coli* DmsABC DMSO reductase and R. *sulfidophilum* DdhABC DMS dehydrogenase (which catalyzes the opposite reaction) are in the same major clade, but separate subgroups within that clade. The discussion below is organized according to the reaction catalyzed, and it will become evident that the enzymes under each heading can in fact be quite distinct. The reader is asked to bear this in mind. Given the very large number of enzymes in this family, discussion here focuses on members that are particularly well-characterized from a biochemical standpoint. The interested reader is referred to other reviews dealing with other aspects of enzymes in the DMSO reductase family, particularly more detailed analyses of phylogenetic relationships among these enzymes.[372b,373,374]

5.2. The DMSO Reductases

5.2.1. *Rhodobacter* DMSO Reductases and Related Enzymes—DMSO arises naturally in marine environments from the degradative cleavage of dimethylsulfoniopropionate, the principal osmolyte in seaweeds and phytoplankton. When grown anaerobically on a highly reduced carbon source, and in the presence of DMSO, organisms such as *Rhodobacter sphaeroides* and *R. capsulatus* express a periplasmically localized, monomeric DMSO reductase that has a molybdenum center as its sole redox-active center. The enzyme functions as a dissimilatory terminal reductase, reducing DMSO to dimethyl-sulfide without contributing to the transmembrane proton gradient.[375] The enzymatically generated DMS is volatile and exchanges readily between ocean and atmosphere, where it plays a central role in cloud nucleation. Its concentration has been directly correlated with the number of condensation nuclei in clouds,[376] and DMS thus

serves as an antigreenhouse gas by reducing global albedo (although it is eventually oxidized in the atmosphere by ozone, thereby reducing its beneficial effects).

The crystal structures of the DMSO reductases from both *R. sphaeroides* and *R. capsulatus* have been determined; that for the *R. sphaeroides* enzyme is shown in Figure 43, with the oxidized active site having the L_2MoO^{VI}(O–Ser) coordination indicated in Figure 1.[99] The coordination geometry is trigonal prismatic in the oxidized, six-coordinate state, but reduction results in loss of the Mo=O to give a square-pyramidal coordination geometry with the serine occupying the apical position. The protein consists of four domains, with the polypeptide trace making multiple passes among the first three of these; only the fourth domain (in blue in Figure 43) consists of a contiguous stretch of polypeptide (the C-terminal 150 amino acid residues). In all of those proteins possessing an iron–sulfur cluster in the molybdenum-containing subunit (see Figure 42), the Fe/S domain is a contiguous insert at or near the N-terminus, with the cluster in close proximity to the pyranopterin designated crystallographically as Q. Substrate access to the active site is provided by a wide funnel that provides access to the Mo=O of the molybdenum coordination sphere, which has been shown to be catalytically labile.[377] A cluster of aromatic residues (Tyr 165, Trp 196, Trp 322, and Tyr 360) at the base of the funnel provides a binding site for the methyl groups of substrate. The structure of fully functional enzyme has both equivalents of pyranopterin (present as the dinucleotide of guanine) coordinated to the metal, as shown in Figure 43. The pterin designated Q (below the metal in the structure shown, bound by the domain rendered in yellow) readily dissociates from the metal, however, to give a catalytically inert from of the enzyme. While the initial report of the structure for the *R. sphaeroides* showed the Q pterin fully coordinated to the molybdenum in the oxidized enzyme, one of the sulfur ligands of the Q pterin had dissociated in the reduced state (at a distance of 3.9 Å from the molybdenum).[99] In the structure of the oxidized *R. capsulatus* enzyme, the Q pterin is fully dissociated, with Mo–S distances of 3.5 and 3.9 Å. It is replaced by a second Mo=O group in the molybdenum coordination sphere.[378] Accumulation of this Q pterin-dissociated enzyme form caused some confusion in the earlier crystallographic work with the enzyme, but a 1.3 Å-resolution structure of the *R. sphaeroides* enzyme eventually demonstrated the presence of both forms.[366c] Only the bispterin form of the molybdenum center is catalytically active, and it has been shown that the Q pterin can be readily recoordinated to the molybdenum upon redox-cycling (reducing with sodium dithionite followed by reoxidation with DMSO) to restore full catalytic activity.[379]

The enzyme has been examined by both X-ray absorption[380] and resonance Raman[379] spectroscopy. Overall, the XAS analyses are fully consistent with the structures described above, with a monooxo Mo(VI) center in oxidized enzyme and a desoxo Mo(IV) center in reduced. Indeed, it was on the basis of this XAS work that it was first suggested that the crystal structures known at the time were obtained with heterogeneous protein. In the XAS data, collected at 10 K, the reduced enzyme showed evidence of a second O/N ligand at 2.16 Å in addition to the oxygen of Ser 147,[380a] a point considered further below. The Raman work included an analysis of the spectra of oxidized and reduced enzyme, and an E_{red}·DMSO complex formed by treating oxidized enzyme with DMS.[379] The Mo=O stretching mode of oxidized enzyme was identified at 862 cm^{-1} and shown to be

catalytically labile, oxidation of reduced enzyme with ^{18}O-labeled DMSO resulting in a 43 cm^{-1} red-shift to 819 cm^{-1}. This mode was lost upon reduction of the enzyme with dithionite, but when oxidized enzyme was treated with DMS to generate the E_{red}·DMSO complex a new mode at 862 cm^{-1} appeared that shifted only to 843 cm^{-1} with ^{18}O and was assigned to the S=O stretch of bound DMSO (the latter some 141 cm^{-1} lower in frequency than in free DMSO, reflecting destabilization of the bond). The Mo–O(ser) stretching mode was seen at 536 cm^{-1} in oxidized enzyme and 513 cm^{-1} in reduced. A careful analysis of the enedithiolate stretching modes, including excitation profiles, clearly demonstrated that the two pyranopterins were not equivalent, with one being best represented as a discrete enedithiolate and the other as being highly π-delocalized. The latter more closely resembled that seen previously with sulfite oxidase[297] and was assigned to the crystallographically identified P pterin, with the discrete enedithiolate being the Q pterin.[379] This assignment is consistent with the more recent structural survey discussed above (section 4.1) in which one pterin of the bisenedihiolate-coordinated DMSO reductase family resembles that seen in the sulfite oxidase family (is π-delocalized and presumably a dihydropterin with a flatter structure), while the other more closely resembles that seen in the xanthine oxidase family (is a discrete enedithiolate and presumably a tetrahydropterin with a more twisted structure).[263] As discussed further below, it is the latter that appears to be involved in electron transfer to other redox-active centers, emphasizing again that electron transfer out of the molybdenum involves principally σ rather than π interactions.[115]

The molybdenum centers of the xanthine oxidase[381] and sulfite oxidase[311,312] families absorb only relatively weakly and give only small spectral changes upon reduction, but the molybdenum centers of the DMSO reductase family absorb extensively throughout the visible and have pronounced spectral changes upon reduction.[366a] In the case of the DMSO reductase from *R. sphaeroides*, these absorbance changes have been used to carry out enzyme-monitored turnover experiments in which the absorption spectrum of the enzyme is monitored as it turns over with either DMSO and TMAO as substrate (and sodium dithionite as nonphysiological reductant).[382] With 3 mM DMSO, 25 mM sodium dithionite, and 20–30 μM enzyme (in 500 mM phosphate buffer, pH 6.0, 25 °C), the observed spectrum at any given point in the course of turnover can be fit as the weighted sum of four specific species having well-defined absorption spectra: reduced enzyme, the reduced enzyme complexed with DMSO, oxidized enzyme, and the EPR-active "high-*g* split" Mo(V) form that is an intermediate in the rereduction of the molybdenum center (Figure 44). Deconvolution of the spectrum observed over the course of the reaction permits the time courses for each of the several catalytically relevant species to be determined. With DMSO as substrate, product DMS that accumulates in the course of turnover can rebind to the oxidized enzyme and back the reaction up to the E_{red}·DMSO species, resulting in a significant accumulation of this species and a concomitant reduction in catalytic throughput. This product inhibition does not occur with TMAO as substrate, and the predominant species that accumulates in the steady-state with this substrate is the Mo(V) species, whose reduction on to the fully reduced Mo(IV) species is principally rate-limiting under the reaction conditions.[382] The structure of the E_{red}·DMSO complex has been confirmed both by XAS[380b] and by X-ray crystallography;[383] the structure of the homologous complex with trimethylarsine was examined by XAS.[384]

Mutagenesis studies of Tyr 114[385] and Trp 116[385b] have probed the catalytic roles of these residues. Trp 116 is within hydrogen-bonding distance of the Mo=O of oxidized enzyme, and Tyr 114 (which is a valine in the otherwise closely related TMAO reductase from *Shewanella massilia*, see below) has been proposed to hydrogen bond to the oxygen of DMSO in the course of its reaction with reduced enzyme.[385a,386] In methylviologen:DMSO steady-state assays, the Y114F mutant exhibits a 3-fold higher k_{cat} than wild-type enzyme (180 vs 50 s^{-1}), but a substantially higher K_m for DMSO (180 vs 7 μM).[385a] Breakdown of the E_{red}·DMSO complex is approximately twice as fast with the Y114F mutant than with wild-type enzyme, and rebinding of DMS to oxidized enzyme to regenerate the E_{red}·DMSO species occurs to a significantly lesser degree than with wild-type enzyme. The Y114F mutant also manifests a normal "high-*g* split" EPR signal in the Mo(V) state (indicating that Tyr 114 does not interact with the Mo(V) state of the enzyme to a significant degree), but reduction by sodium dithionite is approximately 4-fold slower than seen with wild-type enzyme, for reduction from both Mo(VI) to Mo(V) and Mo(V) to Mo(IV). Thus, in enzyme-monitored turnover experiments, the E_{red}·DMSO species accumulates much less with the mutant than with the wild-type enzyme. The behavior of the mutant with DMSO as substrate resembles that of wild-type enzyme with TMAO, reflecting compromised substrate specificity in the mutant. The Y114F mutant exhibits essentially the same absorption spectrum as wild-type enzyme in the fully oxidized and reduced states, but the spectrum of the E_{red}·DMSO complex is perturbed, consistent with the proposed role of this residue in interacting with substrate.

The W116F mutant reacts with DMSO at approximately the same rate as wild-type enzyme, but like the Y114F mutant is reduced sluggishly by dithionite. The W116F mutant is particularly prone to have the Q pterin dissociate from the molybdenum. The as-isolated W116F mutant is essentially completely in the five-coordinate form, but like wild-type enzyme can be converted to the functional six-coordinate form by reduction and reoxidation with DMSO; it is this six-coordinate form that is responsible for the observed catalytic activity of the mutant in steady-state assays.[385b] Trp 116 thus appears to play a major role in the active site of wild-type enzyme in minimizing the binding of water to the reduced molybdenum center, a process that would initiate dissociation of the Q pterin. The regenerated, oxidized W116F mutant exhibits a perturbed absorption spectrum, with a long-wavelength band at 680 nm, as compared to 720 nm for wild-type enzyme. Addition of DMS to the oxidized W116F mutant results in conversion to the five-coordinate species rather than formation of the E_{red}·DMSO complex. Interestingly, the reduced W116F mutant exhibits absorption maxima at 470 and 550 nm and resembles the spectrum of the E_{red}·DMSO complex seen with wild-type enzyme. Both enzyme forms are pink to the eye, and the reduced wild-type enzyme also turns pink upon freezing.[387] XAS analysis of the reduced enzyme has suggested a water molecule bound to the molybdenum that is not present in oxidized enzyme,[380a] and the pink color of frozen reduced wild-type enzyme and the reduced W116F mutant at room temperature has been attributed to weak binding of a water molecule to the reduced molybdenum center in a manner that mimics substrate binding.[385b]

The Mo(V) species that forms so extensively in the course of turnover of DMSO reductase with TMAO is that giving rise to the so-called "high-g split" EPR signal,[388] with $g_{1,2,3}$ = 1.9988, 1.9885, 1.9722 and ^{1}H $a_{1,2,3}$ = 15, 11, 12 mT.[382] The Mo hyperfine from the 25% of naturally occurring ^{95,97}Mo having I = 5/2 is $A_{1,2,3}$ = 14.55, 34.1, 53.20 ($\times 10^{-4}$ cm^{-1}), which includes an isotropic A_{iso} of 34.22×10^{-4} cm^{-1} and an anisotropic component of $[-20.9, +3.11, +17.8] \times 10^{-4}$ cm^{-1} that is close to the fully anisotropic limit of $[-A_{aniso}, 0, +A_{aniso}]$.[389] This reflects a very low symmetry for the signal-giving species, neither trigonal prismatic as seen in the fully oxidized enzyme nor square pyramidal as seen in the reduced. The good agreement between calculated *g* and ^{95,97}Mo A tensors from a geometry-optimized model indicates that the signal-giving species is in a relaxed rather than entatic configuration,[389] consistent with its observed accumulation in the course of turnover. The essentially quantitative accumulation of the paramagnetic Mo(V) species in the course of the turnover with TMAO, in conjunction with the absence of other chromophores in the protein, has also made it possible to examine the molybdenum center of the *R. sphaeroides* DMSO reductase by magnetic circular dichroism[389] and XAS.[390] In the MCD analysis, the two absorption maxima observed at 667 and 540 nm in the Mo(V) species (Figure 44, right, in blue) are found to be due to six discrete but overlapping electronic transitions between specific pairs of frontier molecular orbitals of the molybdenum center. Most of the absorption above 400 nm is attributed to four specific ligand-to-metal charge-transfer transitions involving one-electron promotion from either of the two highest doubly occupied orbitals (both of which are principally enedithiolate in character) to the lowest-lying unoccupied orbitals (principally Mo d,p in character). Transitions involving one-electron promotion from the singly occupied orbital to the two lowest unoccupied orbitals, or from a combination of the two highest-energy doubly occupied orbitals into the singly occupied orbital, are also identified, but are relatively weak. The overall energies and intensities of the several electronic transitions observed in both the absorption and the MCD spectra are reproduced using the same conformationally relaxed structural model as was used to analyze the EPR spectrum, providing additional support for the conclusion that the signal-giving species has an inherently stable geometry that is intermediate between that of fully oxidized and reduced enzyme. It is interesting to note that while the two highest-energy doubly occupied frontier orbitals are approximately equally distributed over the enedithiolates of the P and Q pterins, the same is not true of the two lowest-lying unoccupied orbitals: although these lie relatively close together, the lower of the two is principally P pterin in character, while the next lowest is principally Q. Somewhat surprisingly, the XAS results suggest that while the signal-giving species has a *bis*enedithiolate-coordinated molybdenum, Ser 147 has dissociated from the metal and been replaced by a Mo–OH ligand. The signal-giving species has long been associated with functional enzyme, and given that it was generated by catalytic turnover in the XAS work, it is an unquestionable part of the catalytic cycle, but it is possible that using sodium dithionite as a nonphysiological reductant (in a reaction that is quite sluggish) leads to a different form of the partially reduced enzyme than seen with the physiological DorC cytochrome. It is nevertheless clear, however, that the fully reduced form of the functional enzyme has Ser 147 (re)coordinated to the molybdenum.

Unlike the oxygen atom transfer reactions catalyzed by members of the sulfite oxidase family, which cycle between dioxo Mo(VI) and monooxo Mo(IV) species, members of the

DMSOR family cycle between monooxo Mo(VI) and desoxo Mo(IV) species. Work with model compounds for these *bis*pyranopterin enzymes have shown that the preferred coordination geometry of the molybdenum in the oxidized state is octahedral,[391] rather than the trigonal prismatic coordination geometry invariably seen in the enzymes. The implication is that the polypeptide imposes structural constraints on the metal center such that the dihedral angle between the planes of the two enedithiolate ligands to the molybdenum is very small, as is seen in the reduced forms. The observed geometry in the oxidized state appears to represent an entatic state that labilizes the oxo group for dissociation upon reduction, a conclusion supported by the above MCD study of the partially reduced Mo(V) state. A recent XAS/DFT study of a $[Mo^{IV}(OSi)(bdt)_2]$/ $Mo^{VI}O(OSi)(bdt)_2]$ system has shown that the reduced form of the model passes through the same discrete complex with DMSO seen with the enzyme,[392] but this is not inconsistent with the above interpretation because the geometric constraints imposed by the polypeptide in the enzyme-catalyzed reaction are manifested principally in the oxidized rather than reduced state. There are several other important conclusions arising from this latter study: (1) in agreement with the above MCD study of the enzyme,[389] the redox-active orbital is predominantly Mo d in character, and the enedithiolate ligands to the metal are “innocent” (i.e., are not directly involved in the oxidation–reduction chemistry of the reaction); (2) oxygen atom transfer is a concerted process wherein lengthening of the S–O bond stabilizes the S–O p* orbital, which facilitates concomitant electron transfer from the molybdenum; and (3) the enedithiolate ligands directly stabilize a singlet rather than triple ground state in the reduced complex, which facilitates the overall two-electron chemistry. In all, the mechanistic enzymology and model compound work has led to a very clear picture of the chemical course of the reaction catalyzed by DMSO reductase that is likely to be directly relevant to other oxotransferase members of the DMSO reductase family.

Two other enzymes closely related to the *Rhodobacter* DMSO reductases that have been relatively well-characterized are the *Shewanella massilia* trimethylamine-*N*-oxide reductase and biotin sulfoxide reductase (from *R. sphaeroides* or *E. coli*). The crystal structure of the former has been determined,[393] and while the overall fold closely resembles that of the *Rhodobacter* enzymes, including the presence of the pyranopterin as the dinucleotide of guanine, its molybdenum center has a somewhat different environment. Notably, TMAO reductase is quite specific for TMAO as substrate, and the residue equivalent to Tyr 114 in DMSO reductase that hydrogen bonds to bound DMSO is absent in TMAO reductase (it is Thr 116, whose hydroxyl oxygen is 9.8 Å from the molybdenum). The hydrophobic pocket at the base of the substrate access funnel is conserved (residues Tyr 167, Trp 198, Trp 328, and Tyr 366), but on the whole the sides of the funnel are more positively charged in TMAO reductase. Interestingly, an extended loop that was unresolved in the *R. sphaeroides* DMSO reductase structures is clear in the structure of the TMAO reductase. Originally proposed in the case of the DMSO reductase structure to be a flexible lid over the active site, it is now seen to line the outer lip of the substrate access funnel in TMAO reductase and appears unlikely to act as a lid in either enzyme. The molybdenum center itself was originally modeled as having a pair of Mo=O ligands in addition to the two pyranopterins and Ser 149, but it appears that the Q pterin had at least partially dissociated in the crystal. A more recent

XAS analysis of redox-cycled enzyme has clearly demonstrated that the oxidized TMAO reductase (from *E. coli*) possesses only a single Mo=O ligand,[394] as expected.

In addition to its DMSO reductase, *R. sphaeroides* also encodes a very similar biotin-S-oxide (BSO) reductase, and a heterologous expression system in *E. coli* has been developed for the *R. sphaeroides* enzyme.[395] The oxidized enzyme exhibits an absorption spectrum very similar to that of DMSO reductase and, unusually for enzymes of this family, is directly reducible by NADPH.[395b] The EPR signal manifested by BSO reductase[395b] resembles the "low-*g* unsplit" EPR signal manifested by DMSO reductase.[388] An XAS analysis of BSO reductase is fully consistent with the enzyme cycling catalytically between $L_2Mo^{VI}O(O–Ser_{121})$ and $L_2Mo^{VI}(O–Ser_{121})$, although as with DMSO reductase there is evidence of a second long Mo–O ligand in the reduced state.[395b] The Q pterin of BSO reductase appears to be significantly less prone to dissociation from the molybdenum than that in the *R. sphaeroides* DMSO reductase, and the as-isolated enzyme does not require redox-cycling to become activated. The resonance Raman characteristics of BSO reductase are very similar to those of DMSO reductase described above, and fully support a direct oxygen atom transfer mechanism involving the enzyme cycling between monooxo Mo(VI) and desoxoMo(IV) states.[396]

5.2.2. *E. coli* DMSO Reductase and *R. sulfidophilum* DMS Dehydrogenase—

The DMSO reductase from *E. coli*, encoded by the *dmsABC* gene cluster, is an αβγ heterotrimer and is considerably more complex than the *Rhodobacter* enzymes.[397] Even the molybdenum-containing DmsA subunit is more complex in having an N-terminal domain with a [4Fe-4S] cluster designated FS0 in addition to its $MGD_2Mo^{VI}(O–Ser_{176})$ molybdenum center. DmsA also has an N-terminal *tat* signal sequence and, like the *Rhodobacter* enzymes, is translocated to the periplasm.[398] DmsB contains four [4Fe-4S] clusters and is cotranslated to the periplasm with DmsA after maturation in the cytosol. DmsC is a membrane-integral anchor subunit that, while it has no hemes or other redox-active prosthetic groups, has the menaquinol binding site for enzyme reduction.[397c] The *E. coli* DMSO reductase has the same broad substrate specificity as the *Rhodobacter* enzymes, being able to reduce a wide range of *S*- and *N*-oxides. Although no crystal structure is yet available for the enzyme, it is presumed to closely resemble polysulfide reductase, to which it is closely related (see section 5.3). Unlike the *Rhodobacter* enzymes, which simply dissipate "extra" reducing equivalents under certain growth conditions, the *E. coli* enzyme contributes to the membrane protonmotive force through the vectoral generation of protons in the oxidation of menaquinol. Like most other DMSO reductase family members considered below, the *E. coli* DMSO reductase is a representative of the "complex iron–sulfur molybdoenzyme" subfamily whose phylogenetic relationships have recently been reviewed.[372b]

Given the close similarity in amino acid sequence between the molybdenum-binding portion of DmsA and the *Rhodobacter* DMSO reductases, the overall chemistry of oxygen atom transfer is expected to be the same. Indeed, XAS analysis of the *E. coli* enzyme indicates that its molybdenum center is essentially identical to that found in the *Rhodobacter* enzymes (with the notable difference that there is no indication with the *E. coli* enzyme for dissociation of the Q pterin from the molybdenum).[399] While there is as yet no direct

crystallographic or EPR evidence for the FS0 [4Fe-4S] cluster in DmsA, a cluster of four cysteine residues in the amino terminal domain of DmsA (Cys 34, 38, 42, and 75) is highly homologous to those seen in the *E. coli* NarGHI nitrate reductase,[370] FDH-H[248b] and FDH-N[371] formate dehydrogenases, as well as the PsrABC polysulfide reductase from *Thermus thermophilus*,[400] which have been shown crystallographically to coordinate [4Fe-4S] clusters (see below). Further, mutation of Cys 38 in this cluster of cysteines to Ser or Ala results in the appearance of a [3Fe-4S] cluster in DmsA,[401] and the spin–spin interaction between an iron–sulfur cluster in DmsABC with its molybdenum center is perturbed in the DmsA C38S mutant.[402] In those proteins whose crystal structure has been determined, FS0 is always near the tetrahydropterin-like Q pterin that is itself bound by the more N-terminal domain interacting with the pyranopterin ligands to the molybdenum; confusingly, the pyranopterins of DmsA are sometimes referred to as "P" (for proximal) and "D" (distal) rather than P and Q.[263] Here, we will retain the original P and Q nomenclature introduced with the elucidation of the crystal structure for the *R. sphaeroides* DMSO reductase.

Whereas the FS0 cluster of native DmsA has proven refractory by EPR, the FS1–4 clusters of DmsB are all EPR detectable, making it possible to determine their reduction potentials.[403] Again in the context of the crystal structures of homologous enzymes (see below), the four clusters of DmsB are expected to reside in a pair of bacterial 2x[4Fe-4S]-like domains, with consensus sequences of $CxxCx_{2-11}Cx_3C$. In each of the two pairs, three cysteines of a given tetrad coordinate one [4Fe-4S] cluster, with the fourth cysteine of the tetrad coordinating the other [4Fe-4S] cluster of the pair. FS1 and FS2 are coordinated by Cys tetrads I and IV in the amino acid sequence, respectively, and FS3 and FS4 by tetrads II and III. The reduction potentials for the purified protein at pH 6.8 are, from lowest to highest: −330, −240, −120, and −50 mV, vs SHE. The Mo(VI/V) and Mo(V/IV) potentials are quite condition-sensitive, but are in the range of +0 and −140 mV vs SHE, respectively, indicating considerable stabilization of the paramagnetic Mo(V) state; the observed signal[403] is of the type subsequently categorized by Bray and co-workers as "high-*g* unsplit",[388] with $g_{1,2,3}$ = 1.987, 1.976, 1.960. On the basis of the crystal structures of similar proteins, the clusters are arranged FS1–FS2–FS3–FS4 progressively away from the FS0 cluster of DmsA, with the potentials −240, −330, −120, and −50 mV, respectively.[372b] It is thus evident that the clusters are not arranged in uniform thermodynamic order for electron transfer into the molybdenum center in the course of catalysis. Given the likely close proximity of the clusters (e.g., the structure below for the closely related *T. thermophilus* polysulfide reductase; see section 5.3), however, electron transfer among them is likely to be sufficiently rapid to sustain catalytic rates, with electron distributions among the several redox-active centers in partially reduced enzyme best treated using a rapid equilibrium model.[171]

A protein film voltammetric study of *E. coli* DMSO reductase has been undertaken, revealing that the enzyme behaves like a tunnel diode, with the catalytic wave passing through a maximum as the poised potential is increased, with catalytic velocity decreasing beyond this point despite the stronger thermodynamic driving force.[404] The range of poised system potential for optimal catalytic throughput coincides very well with that over which the Mo(V) state accumulates maximally. It has been suggested that the basis for this behavior involves protonation events at the molybdenum center (which are known to occur

upon reduction[405]), with the kinetics of protonation of the Mo(V) state being faster than that for the Mo(IV) state.[404] The model not only accounts for the diodelike behavior of the enzyme at high pH, but for its disappearance as the pH is decreased. It is to be emphasized, however, that the Mo(V) state is only relevant for the reductive half-reaction because, as discussed above, the oxidative half-reaction involving conversion of DMSO to DMS is obligatory two-electron chemistry. Furthermore, reduction of immobilized enzyme on the surface of an electrode may well be considerably different from reduction with the enzyme's physiological reductant, menaquinol. It is unknown at present whether the enzyme manifests such behavior during turnover with menaquinol.

The DmsC membrane anchoring subunit of the *E. coli* DMSO reductase consists of eight transmembrane helices, with the menaquinol binding site exposed to the periplasm (consistent with the enzyme's proposed role in generating a transmembrane potential).[397a,c] Site-directed mutagenesis studies have suggested that His 65[369b,406] and Glu 87[407] contribute to binding of menaquinol. While DmsC does not contain any redox-active prosthetic groups, its menaquinol binding site is presumably in close proximity to the high-potential FS4 of DmsB, as is seen in polysulfide reductase (see Section 5.3), in which case oxidation of menaquinol (in sequential one-electron steps) is expected to be facile.

When grown photoautotrophically in the presence of dimethylsulfide, the purple photosynthetic bacterium *Rhodovulum sulfidophilum* expresses a heterotrimeric DdhABC dimethylsulfide dehydrogenase, encoded by the *ddhABDC* operon, that catalyzes the reverse of the reaction catalyzed by the *E. coli* DMSO reductase, the oxidation of DMS to DMSO; reducing equivalents thus obtained by the enzyme are delivered to cytochrome c_2.[408] The DdhD gene product has high sequence homology to NarJ and TorD, which, as discussed in section 2.3, are known to be chaperones involved in the maturation of TAT-targeted members of the DMSO reductase family. Like the *E. coli* enzyme, the DmsAB catalytic core is localized in the periplasm (being translocated by the TAT system) but is membrane-anchored by the DmsC subunit. A detailed analysis of the predicted amino acid sequences of DdhABC indicates that it is more closely related to the *E. coli* NarGHI nitrate reductase (section 5.5.1) and *A. aromaticum* ethylbenzene dehydrogenase (section 5.7) than to the *E. coli* DMSO reductase, including: a histidine-coordinated [4Fe-4S] cluster in DdhA, a distal [3Fe-4S] cluster in the DdhB subunit, and a *b*-type cytochrome in DdhC (on the basis of sequence alignment, coordinated by His 81 and Met 147).[408a] DdhABC exhibits three distinct Mo(V) EPR signals at 120 K, attributed to Mo–OH, Mo–OH_2, and Mo–X species (with X being an anion such as chloride). The aquo species has $g_{1,2,3}$ = 1.9650, 1.9846, 2.0006, with coupling to two equivalent protons (4×10^{-4} cm^{-1}), while the hydroxy species has $g_{1,2,3}$ = 1.9627, 1.98, 1.9914 and coupling to three protons, two with stronger coupling comparable to that seen in the aquo species and a third with weaker coupling. The anion-complexed species has $g_{1,2,3}$ = 1.9600, 1.9805, 1.9989 and no proton coupling. These signals most closely resemble the Mo(V) signals seen with the NarGHI nitrate reductase (section 5.5.1), suggesting aspartate as the sixth ligand to the molybdenum coordination sphere.[409] The reduction potentials for DdhABC have been examined, it being found (consistent with the reaction catalyzed) that the enzyme operates in a quite high oxidation–reduction regime. The low-temperature EPR spectra of DdhAB are as expected given its

constitution of iron–sulfur centers, with a [3Fe-4S] signal in oxidized enzyme with $g_{1,2,3}$ = 1.9650, 1.9870, 2.0180, and a low-spin *b*-type heme. Upon reduction, signals attributable to the three [4Fe-4S] clusters of DdhB are seen, but (as with the *E. coli* DmsABC) no signal attributable to an FS0 iron–sulfur cluster in DdhA is observed.[410] The potentials for the Mo(VI/V) and MoV/IV) couples are +123 and +55 mV vs NHE, those for FS1–4 (FS4 being the [3Fe-4S] cluster) are +175, −337, +66, and +292 mV, and that for the *b*-type cytochrome in DdhC is +324 mV, reflecting the overall favorability of electron transfer from the molybdenum center to the heme.[410] Interestingly, FS2 also has an unusually low reduction potential in the closely related NarGHI and ethylbenzene dehydrogenase systems (see below).

5.3. Polysulfide Reductase

Polysulfide reductases catalyze the respiratory reduction of inorganic sulfur $(S_n)^{2-}$ to sulfide and $(S_{n-1})^{2-}$, a critical reaction in making sulfur bioavailable and one that is fundamentally different from the oxygen atom transfer reactions catalyzed by many members of the DMSO reductase family of enzymes. The enzyme from *Thermus thermophilus* has been crystallographically characterized, and its overall subunit organization is found to be very similar to that of the *E. coli* DmsABC DMSO reductase discussed above, including the presence of a cofactorless membrane-integral PsrC subunit that binds menaquinol.[400] As shown in Figure 45, polysulfide reductase is organized as an $(\alpha\beta\gamma)_2$ oligomer with the catalytic PsrA subunit periplasmically localized. The active site molybdenum center of PsrA has the structure shown in Figure 46, with the pyranopteirn cofactor present as the guanine dinucleotide. The protein ligand corresponding to Ser 176 in the *E. coli* DMSO reductase is Cys 173 in the *Thermus* polysulfide reductase, and the additional covalency of the Mo–S bond serves to lengthen the Mo–O distance of the sixth ligand to 2.19 (±0.05) Å in each of the two PsrA subunits, indicating that the oxygen has been protonated at least to a hydroxide (and possibly water, but not a Mo=O as originally assigned crystallographically). As is found in all of these more complex enzymes, the [4Fe-4S] FS0 cluster is adjacent to the crystallographically identified Q pterin of the molybdenum center. While the overall fold of the PsrA subunit closely resembles that seen in the *R. sphaeroides* DMSO reductase, the broad funnel providing access to the active site is considerably more constricted in PsrA. In the active site, a second water molecule is found bound by Arg 332 and His 145, which constitute a putative substrate binding site (Figure 46). A reaction mechanism has been proposed based on that of peroxidases (which catalyze similar chemistry in reducing peroxide to water), with the terminal sulfur of polysulfide coordinating the reduced molybdenum center of PsrA, displacing the coordinated oxygen, and placing the penultimate sulfur in the position of the crystallographically observed water between Arg 332 and His 145. Chemical precedent exists for the putative enzyme·substrate complex that has molybdenum coordinated by six sulfurs.[411]

The PsrB subunit contains the four [4Fe-4S] clusters expected on the basis of sequence analysis, and these are organized as two pairs, each of which is similar to the eight-iron bacterial ferredoxins. Similar subunits have been identified in a great many respiratory enzymes.[412] As discussed above in the case of the *E. coli* DMSO reductase, these iron–sulfur clusters are organized FS1–FS2–FS3–FS4 progressively away from the FS0 cluster of

PsrA, but are coordinated by four tetrads of cysteine residues, I–IV, from the amino terminus. The clusters are arranged in two pairs, with FS1 and FS2 coordinated by the cysteine tetrads I and IV, respectively, and with FS2 and FS3 coordinated by cysteine tetrads II and III. Within each pair of clusters, three cysteines are contributed by a first tetrad with the fourth cysteine coming from the other cysteine tetrad of the pair. The iron–sulfur clusters of PsrB are 8.5–10 Å apart, edge-to-edge, with FS1 11.7 Å from FS0 of PsrA. This same arrangement is seen in all homologues whose crystal structures have been determined (including the FdnHI formate dehydrogenase and NarGHI nitrate reductase discussed below in sections 5.4.2 and 5.5.3, respectively). Iron–sulfur cluster FS4 of PsrB lies at the subunit interface immediately adjacent to the membrane-integral PsrC subunit.

As shown in Figure 46, PsrC has eight transmembrane helices arranged as a pair of four-helix bundles; the N-terminal 14 amino acid residues extend into the periplasm and span the length of PsrB (see Figure 45). The menaquinol binding site is located at the periplasmic end of the first (N-terminal) four-helix bundle, with substrate access provided by a cavity between the second and third helices of the bundle (Figure 46, far right). While there are no redox-active centers in PsrC, menaquinol is positioned within 9 Å of FS3 in PsrB in a generally hydrophobic binding pocket that includes Tyr 130 and His 21. The role of the second four-helix bundle, which is always present in the integral membrane subunits of homologous enzymes that lack redox-active centers, is suggested by a set of hydrophilic amino acid residues (Glu 224, Arg 177, Arg 239, Thr 220, Ser 183, Thr 155, 60, and His 21 in PsrC) that extend through the core to the menaquinol binding site in the other bundle and may be part of a proton pump that contributes to the transmembrane proton gradient.[400] Under the most favorable circumstances, given that polysulfide reduction in the periplasm necessarily consumes protons, the loss of protons on oxidation of menaquinol to the periplasm would entail proton-neutral chemistry in the course of turnover, yet a net contribution to the proton gradient of 0.5 H^+/e^- during turnover of polysulfide reductase has been determined experimentally.[413] The involvement of the second four-helix bundle of PsrC in a proton pump such as proposed would account for its strict conservation, and mutation of several of the proposed residues in the highly homologous *Wollinella succinogenes* polysulfide reductase is known to result in loss of activity of the enzyme.[413b] Still, direct experimental evidence for the operation of such a pump is not yet available.

5.4. Formate Dehydrogenases

The bacterial formate dehydrogenases are distinct from the $NAD(P)^+$-dependent (and cofactorless) enzymes from yeasts and higher plants. *E. coli* encodes three different molybdenum-containing formate dehydrogenases: formate dehydrogenase H (FdhF, the product of the *fdhF* gene, but sometimes referred to in the literature as FDH_H or, confusingly, FdhH) that is part of the formate hydrogen lyase complex;[414] formate dehydrogenase N (FdnGHI, or FDH_N), product of the *fdnGHI* operon and expressed in concert with *narGHI* to form an anaerobic formate:nitrate respiratory chain;[415] and formate dehydrogenase O (FdoGHI, product of the *fdoDEGHI* operon) that is expressed in concert with *narZYX* to form a formate:nitrate respiratory system during the transition from aerobic to anaerobic growth. Each of these systems has broadly distributed cognates in other bacteria. In addition, many aerobic bacteria encode a cytoplasmic NAD^+-dependent

FdsABG(D) formate dehydrogenase that, in contrast to the eukaryotic enzymes, has multiple redox-active centers, including a molybdenum center. In addition to their intrinsic biological interest, several of these enzymes readily catalyze the reverse reaction, the reduction of CO_2 to formate, a reaction that is of industrial interest as a convenient storage form of H_2.[416]

5.4.1. Formate Dehydrogenase H (FdhF)—The first of the formate dehydrogenases to be structurally characterized was the 79 kDa formate dehydrogenase H, the FdhF gene product. In the 2.9 Å structure (Figure 47), the monomeric enzyme is seen to have an overall fold similar to the *R. sphaeroides* DMSO reductase discussed above, but with an N-terminal domain containing a [4Fe-4S] cluster as seen in the *T. thermophilus* PsrA subunit of polysulfide reductase.[248b] The active site is an $L_2Mo(OH)(Se–Cys_{140})$ center with a selenocysteine replacing the serine seen in the DMSO reductases (the pyranopterin is present as the dinucleotide of guanine).[248b] As with PsrA and all other enzymes of this family that contain a [4Fe-4S] cluster, that in FdhF is found adjacent to the tetrahydropterin-like Q pterin of the molybdenum center. Reduction of FdhF with formate to the Mo(IV) state results in loss of the oxygen ligand to give a square-pyramidal $L_2Mo(Se–Cys)$ center, analogous to the structure of reduced *R. sphaeroides* DMSO reductase, as discussed in sectio 5.2.1. A structure for the complex of oxidized enzyme with the inhibitor nitrite has also been obtained,[248b] with Arg 333 interacting with the anion as shown in Figure 47 (right). Modeling formate into the active site on the basis of this structure places the Cα hydrogen of formate within 1.5 Å of the selenium of Sec 140. XAS analysis of FdhF largely confirms the molybdenum coordination sphere as defined in the crystallographic work, although there is evidence that an O/N ligand at 2.1 Å persists in the reduced state.[417] There is also evidence for at least a partial Se–S bond between the selenocysteine and one of the enedithiolate sulfurs in the oxidized forms of both the *E. coli*[417] and the *D. desulfuricans* enzymes;[418] at least in the latter case, the Se–S distance increases from 2.12 in oxidized reduced enzyme to 2.57 in reduced, suggesting some ligand-based oxidation–reduction chemistry in the molybdenum center, at least with dithionite as reductant. Interestingly, mutation of Sec 140 to Cys (U140C) results in a significant shortening of the Mo–O bond in oxidized enzyme, from 2.1 to 1.7 Å, consistent with its deprotonation to a Mo=O.[417] This substitution reduced k_{cat} by a factor of 100.[419]

On the basis of the protein structure, particularly that of the nitrite complex with oxidized enzyme, a reaction mechanism has been proposed for FdhF[248b] that involves initial coordination of formate to the molybdenum, displacing the Mo–OH of oxidized enzyme. Subsequent oxidation of formate to CO_2 then occurs either by direct electron transfer to the molybdenum with protonation of His 141 (consistent with the pH dependence of catalytic activity, reflecting general base catalysis with a pK_a of ~7[419]) or alternatively by direct hydride transfer involving Sec 140. Consistent with this, it has subsequently been shown that oxidation of formate to CO_2 does not entail incorporation of oxygen derived from solvent (as would be expected were the enzyme to catalyze the oxidative hydroxylation of formate to bicarbonate, followed by dehydration).[420]

Reduction of FdhF by formate leads to the accumulation of two EPR signals: a Mo(V) signal with $g_{1,2,3}$ = 2.094, 2.001, 1.989 and a reduced [4Fe-4S] signal with $g_{1,2,3}$ = 2.045, 1.957, 1.840.[248a,421] The Mo(V) signal is observed below 130 K, while the [4Fe-4S] signal is

observed only below 50 K; the former signal exhibits coupling to a proton with $A_{1,2,3}$ = 7.5, 19, 21 MHz and, when generated in enzyme substituted with ^{77}Se (I = 1/2) very strong and anisotropic coupling with $A_{1,2,3}$ = 13.2, 75, 240 MHz that reflects considerable spin-delocalization of the unpaired electron onto the selenium.[248a,420] When deuterated formate is used to reduce the enzyme, the proton coupling is initially absent but grows in over 30–300 s, depending on the pH (exchange being slower at higher pH).[420] On the basis of these observations, the signal-giving species has been interpreted as an L_2Mo^V(Se–Cys) species lacking a coordinated water or hydroxide, with the coupled (and substrate-derived) proton residing on His 141.[420]

The electron density and chain trace of formate-reduced FdhF have recently been reassessed, and an alternate orientation identified for the critical loop containing Sec 140, with this residue (coordinated to the molybdenum in oxidized enzyme) oriented away from the molybdenum center; it has also been suggested that the axial ligand to the molybdenum is Mo=S rather than Mo–OH.[422] Absent Sec in the metal coordination sphere, the electron density was better refined using sulfur rather than oxygen, although at the resolution of the electron density (2.3 Å) the improvement in fit was not considered defintive.[422] However, a recent examination of the FdhD gene product has demonstrated that the protein is a sulfur transferase that it inserts a cyanolyzable sulfur (derived from IscS) into the molybdenum coordination sphere of FdhF.[423] Given that FdhD is required for proper maturation of all formate dehydrogenases (at least in *E. coli*), it now seems clear that all have a Mo=S ligand rather than Mo=O or Mo–OH as the sixth ligand to molybdenum in the oxidized enzyme. With regard to the peptide loop proposed to be repositioned in the reexamined crystal structure (consisting of residues 138–146), the newly proposed orientation does indeed improve the crystallographic R/R_{free} factor for this region of the polypeptide trace, albeit only modestly. In both the old and new structures, R/R_{free} for the loop in question is substantially higher than for the structure overall, an inevitable consequence of the poorer quality of the electron density map in this region.

On the basis of the alternate structure for reduced FdhF, a new mechanism has been proposed in which formate binds to the molybdenum and displaces the selenocysteine, with the now-dissociated Sec 140 serving as a general base to abstract the Cα proton of formate. Such a mechanism is difficult to reconcile with the structure of the nitrite complex of FdhF,[248b] however, and is consistent with the available XAS data on FdhF (above) only if it is assumed that dithionite- and formate-reduced FdhF are fundamentally different. A third mechanism, also based on the alternate crystal structure involving Sec 140 dissociation from the molybdenum and Mo=S coordination, has recently been considered in a DFT-based computational study.[424] It is proposed that formate coordination to the molybdenum results in insertion of the sulfur into the Se–Mo bond, yielding a Se–S–Mo moiety with the metal formally reduced to Mo(IV). The Se–S bond is then cleaved, leaving the selenate anion of Sec 140 hydrogen-bonded to His 141, which then abstracts the Cα proton from formate. This ultimately yields thioformate coordinated to the (reduced) molybdenum in a bidentate fashion, which then decays to a Mo(IV)=S species and product CO_2. With CO_2 release, Sec 140 then deprotonates and reorients the loop, with a transient Se–S bond formed in the process.

The poor electron density associated with the loop in the formate-reduced enzyme in fact suggests another interpretation: that the loop exists in at least two alternate configurations in the crystal. The ambiguity is analogous in some respects to that seen in the crystal structure work with the *R. sphaeroides* DMSO reductase discussed above, where quite high-resolution structures were required to identify the presence of two alternate structures for the molybdenum center. If this is the case with FdhF, then the question is (as in the case with the DMSO reductase) whether there is a catalytically relevant conformational change or, alternatively, one or the other of the two configurations is not catalytically relevant. It is evident that additional crystallographic and XAS work is needed to resolve the structural ambiguities that have been raised with regard to FdhF, and it is only at that point that alternate mechanistic possibilities can be critically evaluated.

Physiologically in the formate:hydrogen lyase complex, FdhF passes the reducing equivalents obtained from oxidation of formate to one of two hydrogenases (Hyd3 or Hyd4, depending on growth conditions) that reduce protons to H_2.[414] Hyd3 is encoded by the complex *hycABCDEFGHI* operon and consists minimally of the HycBCDEFG structural genes. At least the HycB and HycF subunits possess iron–sulfur clusters that shuttle reducing equivalents to the Ni–Fe active site located in the HycE subunit. Hyd4 is encoded by the similarly complex *hyfABCDEFGHIJR* operon, the enzyme itself being HyfACEFGHI with the active site Ni/Fe center present in the HyfG subunit. Both Hyd3 and Hyd4 are localized on the cytosolic side of the cell membrane, and with FdhF in the periplasm the formate:hydrogen lyase complex contributes to the transmembrane proton gradient by generating protons in the periplasm and consuming them in the cytosol. Hyd3 and Hyd4, along with the primary Hyd1 and Hyd2 hydrogenases of *E. coli* and other organisms, have been extensively reviewed elsewhere.[414]

5.4.2. Formate Dehydrogenases N and O (FdnGHI and FdoGHI)—The *E. coli* formate dehydrogenase N (FdnGHI) is coexpressed with the NarGHI nitrate reductase (section 5.5) to form a formate:nitrate oxidoreductase system under appropriate growth conditions (specifically, in the absence of O_2 and presence of formate and NO_3^-). Both enzymes have integral membrane diheme-containing subunits, and the menaquinone pool mediates electron transfer between them. The 1.6 Å crystal structure of FdnGHI has been reported,[371] and the enzyme is found to be considerably more complex than the monomeric FdhF. It is organized as an $(\alpha\beta\gamma)_3$ trimer of trimers as shown in Figure 48, with the overall organization of the αβγ protomer resembling that seen in the NarGHI nitrate reductase (see section 5.4.1), this despite the latter being a dimer of trimers rather than a trimer of trimers. Importantly, the catalytic subunits of FdnGHI and NarGHI are on opposite sides of the cell membrane, with NarGH being cytosolic[425] and FdnGH being periplasmic (by virtue of the presence of a tat signal sequence on FdnG).[371] As a result, protons are generated in the periplasm (with the oxidation of formate) and consumed in the cytosol (with the reduction of nitrate) so that, like the formate:hydrogen lyase system, FdnGHI:NarGHI contributes to the transmembrane proton gradient.[426]

The substrate access funnel is predominantly positively charged in FdnG, as compared to the more negatively charged channel in NarG. The molybdenum center of oxidized FdnG again has the guanine dinucleotide form of the pyranopterin cofactor, with the molybdenum

additionally coordinated by Sec 196. A sixth ligand in oxidized enzyme has been modeled as a Mo–OH (at 2.2 Å), but in light of the recent work referred to above demonstrating that FdhD inserts a Mo=S group into the molybdenum centers of the formate dehydrogenases,[423] the sixth ligand is most likely a terminal sulfido rather than a hydroxy ligand, at least in functional enzyme. Overall the molybdenum coordination sphere closely resembles that seen in oxidized FdhF.[248b] Given the overall hydrogen-bonding network observed crystallographically in the vicinity of His 197 of FdnG, the orientation of its imidazole ring is unambiguous, with its $N\delta_1$ oriented toward the substrate binding site. The opposite orientation has been assigned in the original FdnF structure, but the FdnG structure clearly positions His 197 appropriately to abstract the Cα proton of substrate in the course of formate oxidation.[371] FdnG has a molybdenum center and FS0 [4Fe-4S] cluster in an overall fold closely resembling that described for the PsrA subunit of polysulfide reductase above (section 5.3), but is larger than the DmsA subunit of *E. coli* DMSO reductase or the FdnF formate dehydrogenase H due to the addition of a small C-terminal fifth domain.

As predicted on the basis of the amino acids sequence discussed above for DmsABC, and in agreement with the structure of the PsrABC polysulfide reductase, the four [4Fe-4S] clusters of FdnH are arranged in pairs that are related by a pseudo two-fold axis of symmetry and similar to the eight-iron bacterial ferredoxins, despite the fact that the subdomain containing FS1 and FS2 consists of discontinuous strands of polypeptide. The structure of FdnH is generally very similar to the PsrB subunit of polysulfide reductase (see section 5.3), but has a unique C-terminal transmembrane anchoring α-helix.[371] The arrangement of the four [4Fe-4S] clusters in FdnH also closely resembles that seen for iron–sulfur components of other systems, including the [NiFe] hydrogenases[427] and NADH dehydrogenase,[428] and is evidently an evolutionarily ancient motif.[372b]

The FdnI membrane anchor has two *b*-type cytochromes embedded in a four-helix bundle that constitutes the membrane-integral core of the $(\alpha\beta\gamma)_3$ complex; a fifth C-terminal α-helix lies approximately parallel to the surface of the membrane on the cytosolic side of the membrane. With the C-terminal membrane-integral helix of FdnH and one equivalent of cardiolipin at the subunit interface, FdnI forms a tightly packed trimer within the membrane that holds the overall structure together. The two cytochromes are stacked vertically in the core of the four-helix bundle at an angle of approximately 45° to one another; one lies closer to the periplasm and FS4 of FdnH (heme b_P) and the other closer to the cytoplasm (heme b_C); the latter is the site of menaquinone reduction.[371] In both hemes, the planes of the two ligating histidine residues lie at approximately 45° to one another. There is again significant homology to the corresponding HyaC subunit of the *E. coli* [NiFe] hydrogenase.[412b] The arrangement of the hemes in FdnI also resembles, at least superficially, that seen in the four-helix bundle core of the cytochrome bc_1 complex,[429] although the ratio of proton translocation to electron transfer in FdnGHI indicates that it does not operate via a Q cycle.[426,430]

In addition to the FdnGHI nitrate reductase coexpressed with the NarGHI nitrate reductase, *E. coli* encodes another formate dehydrogenase in the *fdoGHI* operon (FdoGHI, but also referred to as FDH-Z or FDH-O) that is coexpressed with the NarZYX nitrate reductase in the transition from aerobic to anaerobic growth.[431] The similarity in structure to FdnGHI is

high, with ~75% sequence identity in the FdoGH and FdnGH subunits, and 45% identity between FdoI and FdnI.[432] The key difference between FdoGHI and FdnGHI appears to lie not in their structure or activity, but in the manner in which their expression is regulated. Specifically, FdnGHI is under tight regulatory control of the FNR O_2 sensor and is not expressed in the presence of even low concentrations of O_2. On the other hand, FdoGHI is not regulated by FNR, which allows *E. coli* to express some constitutive nitrate reductase activity in the aerobic:anaerobic transition.[431]

5.4.3. NAD^+-Dependent Bacterial Formate Dehydrogenases (FdsABG)—In addition to the enzymes considered above, a number of aerobic bacteria express an O_2-tolerant and soluble NAD^+-dependent formate dehydrogenase that has a molybdenum center as the active site; the enzyme is distinct from both the extremely O_2-sensitive systems considered above and the cofactor-less eukaryotic NAD^+-dependent formate dehydrogenases. In *Ralstonia eutropha*, genetic analysis has predicted that the *fdsGBACD* operon encodes a complex trimeric FdsABG enzyme (sometimes referred to as S-FDH in the literature, for soluble) that contains a molybdenum center, multiple iron–sulfur clusters, and FMN, with each subunit bearing strong sequence homology to subunits of NADH dehydrogenase.[433,434] The 105 kDa FdsA exhibits 51–62% sequence similarity to the catalytic subunits of a variety of known molybdenum-containing formate dehydrogenases, with Cys 378 and His 379 occupying the positions equivalent to Sec 140 and His 141 in FdnG; Cys 378 binds to the molybdenum in lieu of a selenocysteine residue, which presumably contributes to the air-stability of the molybdenum center. In addition, FdsA has a 240-aa N-terminal extension exhibiting homology to regions of the HoxU and HndD subunits of the *R. eutropha* $NAD(P)^+$-reducing hydrogenases and the C-terminal portion of NuoG subunit of *E. coli* NADH dehydrogenase (Nqo3 in the crystallographically characterized *T. thermophilus* NADH dehydrogenase[428a,c]). On the basis of its amino acid sequence, the N-terminal region of FdsA is predicted to have four [4Fe-4S] clusters and one [2Fe-2S] cluster; the final (most C-terminal) [4Fe-4S] cluster in this N-terminal extension is conserved with NuoG and occupies a position in the amino acid sequence of FdsA equivalent to FS0 in FdnF and FdnG (and NarG, see section 5.4.1).[434] The 55 kDa FdsB subunit has some 45% sequence identity to the FMN^- and [4Fe-4S] containing NuoF subunit of *E. coli* NADH dehydrogenase and HoxF of $NAD(P)^+$-dependent hydrogenase, and includes the NAD^+ binding site. The 19 kDa FdsG subunit has 34% sequence identity to the NuoE subunit of NADH dehydrogenase, and is expected to have a [2Fe-2S] cluster. FdsC and FdsD appear not part of the holoenzyme enzyme (although FdsD was initially reported to be so), but seem to be involved in its maturation, possibly being involved in sulfuration as several of the NAD^+-dependent formate dehydrogenases, including those from *R. eutropha*,[433a] *Methylosinus trichosporium*,[435] and *Pseudomonas oxalaticus*,[436] have been shown to contain a cyanolyzable sulfur that is presumably a Mo=S group such as is found in xanthine oxidase family members.

The NAD^+-dependent formate dehydrogenase exhibits the spectroscopic properties expected on the basis of the constitution of redox-active centers predicted above. The *R. eutropha*[433a] and *M. trichosporium*[435] enzymes absorb throughout the visible, with absorption maxima (or well-resolved shoulders) at 450 nm indicative of the FMN cofactor. The *M.*

trichosporium enzyme, which is organized as $(\alpha\beta\delta\gamma)_2$, also exhibits at least five readily resolvable EPR signals attributable to at least one [2Fe-2S] and four [4Fe-4S] clusters, with evidence of magnetic interactions among them such as seen in NADH dehydrognase.[435] A Mo(V) signal with $g_{1,2,3}$ = 2.005, 1.091, 1.984 and evident ^{95,97}Mo hyperfine is also observed, but no $FMN^{\bullet}$ signal is seen (indicating that the semiquinone is simply thermodynamically destabilized, with the $FMN/FMNH^{\bullet}$ couple having a lower potential than the $FMNH^{\bullet}/FMNH_2$ couple).

On the basis of the observation that the last [4Fe-4S] cluster (N7) of subunit NuoG/Nqo3 of the bacterial NADH dehydrogenases is equivalent to FS0 in FdsA,[434] and the observation of both sequence[437] and structural[428a] similarities of the (cofactorless) C-terminal region of Nqo3 of the *T. thermophilus* enzyme[428a,c] to bisMGD molybdenum enzymes, a model can be assembled for FdsABG based on the structures of Nqo1–3 of the *Thermus thermophilus* NADH dehydrogenase[428a,c] and FdhF[248b] with the respective N7 and FS0 domains are simply overlaid as shown in Figure 49. Proper orientation is assured by including the vestigial molybdenum-binding region of Nqo3. It is noteworthy that iron-sulfur cluster N7 of the *T. thermophilus* Nqo3 is some 20 Å removed from the nearest cluster (N4), but that the alignment with FdsA provides clear evidence that an intervening [4Fe-4S] cluster is present in FdsA; the approximate position of this additional cluster in the structure of Nqo3 is defined by a residual helix-turn motif that in Nqo3 has only a single cysteine contributing the final ligand to the N4 [4Fe-4S] cluster, but in the sequence of FdaA clearly has the full complement of cysteines for formation of an additional [4Fe-4S] cluster. The position of this motif, reflecting the position of the additional iron–sulfur cluster present in FdsA, is indicated by the brown sphere in Figure 49, lower left. The homology between FdsA and Nqo3 extends to the presence of a histidine ligand to the N5 [4Fe-4S] cluster (at extreme bottom in Figure 49, lower left). The overall oblong shape of the FdsABG model is consistent with sedimentation studies of the NAD^+-dependent formate dehydrogenase from *M. trichosporium*, which indicates that the protein is distinctly nonspherical.[435] While the detailed nature of the structure of FdsABG must await crystallographic work, the model shown in Figure 49 provides important insight into the likely disposition of the several redox-active of the enzyme. The structural homologies that make such a model feasible underscore the fact, elaborated upon elsewhere,[372b] that the NAD^+-dependent formate dehydrogenases, NAD^+-dependent hydrogenases, and NADH dehydrogenase have all evolved from a common ancestor. In this regard, it is important to emphasize that the alignment of FdhH with Nqo3 extends beyond the common [4Fe-4S]-containing domain, to the entirety of the C- terminus of the latter.[428a] It is evident that this cofactorless C-terminus of Nqo3 (i.e., the region beyond the structural motif coordinating the N7 iron–sulfur cluster) is in fact a vestigial molybdenum-binding domain, further illustrating how closely the two systems are related. It is also noteworthy that loss of the molybdenum center and the iron–sulfur cluster intervening between N7 and N4 in the evolution of NADH dehydrogenase resulted in a redirection of electron flow away from rather than toward the FMN (Figure 49, lower left).

Very recently, the NAD^+-dependent FdsABG formate dehydrogenase from *R. capsulatus* has been cloned and heterologously expressed in *E. coli*.[438] The enzyme appears to be ca.

50% replete of all prosthetic groups, and exhibits UV/visible absorption (and absorption change upon reduction by substrate) similar to that described above for the *M. trichosporium* enzyme. k_{cat} in the forward reaction is 36.5 s^{-1} (reported as 2189 min^{-1}), with a surprisingly high pH optimum of 9. Significantly, like the selenocysteine-containing FdhF from *Clostridium carboxidovorans*[416b] and the tungsten- and selenocysteine-containing formate dehydrogenase from *Syntrophobacter fumaroxidans*,[416c] the enzyme also catalyzes the reduction of CO_2 to formate, in the case of the *R. capsulatus* enzyme with a k_{cat} of 1.5 s^{-1} (reported as 89 min^{-1}). The enzyme thus has considerable potential as an air-stable catalyst for the bioindustrially important interconversion of CO_2 and formate. Not surprisingly given the homologies to NADH dehydrogenase, the flavin-containing FdsBG unit, absent the molybdenum-containing FdsA, exhibits diapohorase (NADH:O_2 oxidoreductase) activity. It has also been shown that FdsC and FdsD, products of the final two genes of the *fdsGBACD* operon, are required for maturation of FdsABG. FdsC is homologous to FdsD of *E. coli*, which as mentioned above is likely involved in insertion of a Mo=S group into the molybdenum coordination sphere and which can genetically complement the *R. capsulatus* FdsC. With the development of this expression system, rapid progress can be expected in our understanding of this system.

Although little mechanistic work has been done with any soluble formate dehydrogenase, formate oxidation at the molybdenum center may proceed analogously to that seen FdhF (with all of the issues discussed above in section 5.4.1 regarding structural ambiguities, compounded by the caveat that the less covalent Mo–S–Cys as compared to the Mo–Se–Cys seen in FdhF may alter the chemical course of the reaction).

5.5. The Bacterial Nitrate Reductases

There are three principal reasons for an organism to reduce nitrate to nitrite: to incorporate nitrogen into a biomolecule, to generate energy for cellular function, and to dissipate excess energy. All known nitrate reductases are molybdenum-dependent enzymes and they catalyze the same reaction, the reduction of nitrate to nitrite. However, they differ in physiological function, subcellular location, and the coordination sphere about the molybdenum center.[439] Nitrate reductases have been divided into four major groups: eukNR, Nas, Nap, and Nar.[439] Eukaryotic nitrate reductases (eukNR) isolated from plants and fungi have been discussed in section 4.3; the primary function of these enzymes is to assimilate nitrogen into cellular components (especially proteins). Animals do not encode a classical nitrate reductase, although bovine xanthine oxidase (XO) can reduce nitrate into nitrite.[186,440] The three prokaryotic nitrate reductases, Nar, Nap and Nas, can reduce nitrate to nitrite for respiration (Nar), dissimilation (Nap) or assimilation (Nas).

The location of nitrate reductases in the cell correlates with their function. Both eukNR and Nas are involved in nitrogen assimilation and are soluble proteins in the cytoplasm where the bulk of biosynthesis occurs. Nap and Nar are involved in respiratory or dissimilatory nitrate reduction, respectively, and are usually membrane-associated. The Nap protein is oriented to the periplasmic side of the cell membrane, while the Nar protein is oriented to face the cytoplasm in bacteria, and periplasm in archaea, hence the latter is called pNar.[441] The dissimilatory nitrate reductases are typically involved in energy generation,

detoxification, and redox regulation. The classical respiratory nitrate reductase, Nar, couples nitrate respiration to proton translocation across the inner membrane of bacteria, thereby contributing to the transmembrane proton gradient that is subsequently used to drive ATP synthesis.[442] The periplasmically localized complexes, that is, Nap and pNar, are more complex and functionally diverse. Neither by itself can contribute to the proton gradient across the inner membrane, although when nitrate reduction is coupled with formate oxidation, they can contribute to the transmembrane proton gradient.[443] The contribution in this case may be less than that of the cytoplasm-facing Nar complex, although this can be compensated for by the higher affinity for nitrate typically observed for periplasmic nitrate reductases. Additional subunits associated with the different Nap complexes may further increase the contribution to the transmembrane proton gradient.

In general, the nitrate reductase operons (i.e., *nar, nap*, and *nas*) are chromosomal, although plasmid-borne *nap* operons are known. In some organisms, more than one copy of the *nap* and *nar* operons have been identified, for example, *Shewanella* for *nap*[444] and *Geobacter* for *nar*.[445] In many cases, however, operons of otherwise similar nitrate reductases are not similarly composed or organized. Of these, the *nap* operon is the most heterogeneous. As many as 11 *nap* genes, that is, *napA, B, C, D, E, F, G, H, L, M*, and *S*, are known, although the function of the gene products is not always clear. These genes are organized into four distinct operon structures: *napEDABC, napDAGHB, napCMADGH*, and *napAGHBFLD.* Most *Shewanella* species have two distinct nap operons, *napEDABC* and *napDAGHB*, that encode two functionally distinct Naps.[444,446] What follows is a consideration of each of these three major types of bacterial nitrate reductase in turn.

5.5.1. Respiratory Nar Enzymes—The Nar system is best characterized in *E. coli*, which has two operons encoding two different Nars, NarGHI and NarZYW, encoded by the *narKGHJI* and *narUZYWV* operons, respectively. The enzymes are very similar but have distinct physiological roles. Both operons have regulatory elements *narX* (or *narP)* and *narL* (or *narQ*), and their regulation in *E. coli* has been investigated in detail.[58a,447] Transcriptionally, the two-component systems (NarX-NarL and NarP-NarQ), in conjunction with the O_2 sensor FNR (for fumarate nitrate reductase regulator), control the expression of NarGHI, with FNR directly activating *narKGHJI* (but not *narUZYWV).* Both NarX-NarL and NarP-NarQ are specific for nitrate regulation, and in most cases they work in concert. In some cases, they function asymmetrically antagonizing each other.[448] Unlike the *narKGHJI* operon, *narUZYWV* is not under control by FNR in *E. coli*, and is expressed under aerobic conditions in the presence of nitrate. It appears to play a role in transitioning from aerobic to anaerobic growth. The *Shewanella oneidensis* genome encodes for one NarQ/NarX homologue and two NarP/NarL homologues, but only the latter is transcriptionally active.[449]

As shown in Figure 50, the crystal structure of the membrane-bound respiratory nitrate reductase NarGHI from *E. coli* at 1.9 Å resolution shows the protein organized as a $(\alpha\beta\gamma)_2$ heterotrimer (PDB 1Q16).[370a,450] The NarG catalytic subunit has the molybdenum center and a [4Fe-4S] cluster adjacent to its Q pyranopterin (very similar to the corresponding formate dehydrogenase H, FdhF, and PsrA subunit of polysulfide reductase discussed above in sections 5.3 and 5.4.1). The iron–sulfur cluster differs, however, in having one of the coordinating cysteines replaced with as histidine, thereby increasing its reduction potential.

Although unique to molybdenum-containing enzymes, similar His-substituted clusters have been observed in the [NiFe] hydrogenase from *D. gigas*[427] and Fe-only hydrogenase from *C. pasteurianum.*[451] Mutation of the histidine to serine in FS0 causes loss of enzymatic activity, demonstrating the importance of the substitution.[452] NarH harbors four additional iron–sulfur clusters analogous to FdnH and PsrB, but with the distal cluster a [3Fe-4S] rather than a [4Fe-4S] cluster due to the absence of a fourth cysteine in the protein sequence to coordinate the cluster. The interaction between NarG and NarH involves two N-terminal helices in NarG, one of which extends completely through NarH. Finally, the cytoplasmically exposed NarGH subunits connect to the membrane-integral NarI, which has two *b*-type cytochromes. The hemes are oriented quite differently than is seen in FdnI (section 5.4.2), being perpendicular to each other and displaced such that the iron of one heme does not lie in-plane with the other heme. Also, the histidines are aligned almost perpendicular to each other rather than at the 45° angle seen in FdnI. A structure of NarGHI in complex with the quinone analogue pentachlorophenol clearly shows the substrate analogue bound near the distal heme of NarI (indicated by the asterisk in Figure 50, center).[450]

The structure reveals the eight redox-active centers aligned in a single chain approximately 75 Å in length indicating the path of electron flow (Figure 50, right). Thus, electrons flow from the distal heme of NarI (the site of menaquinol reduction) to the proximal heme (5.4 Å apart edge-to-edge) to the [3Fe-4S] cluster of NarH (8.9 Å apart, edge-to-edge), then on through the four [4Fe-4S] clusters (three in NarH and one in NarG, each 9–11 Å apart). By analogy to the iron–sulfur assignments in the DMSO reductase based on the order of the cysteine motifs in the amino acid sequence, the electron transfer sequence for the iron–sulfur clusters is FS2 → FS3 → FS4 → FS1 → FS0. Finally, electrons pass individually from FS0 to the molybdenum center via its proximal Q pyranopterin, over a distance of 6 Å. Arg 94 of NarG lies close to the distal amino group of the Q pyranopterin and occupies the space between it and FS0.

The molybdenum center of NarG has two equivalents of the pyranopterin cofactor (present as the guanine dinucleotide) as expected for a member of the DMSO reductase family of enzymes, but has two distinctive features. First, Asp 222 is found coordinated to the metal in a bidentate fashion, and there is no terminal oxo or sulfido ligand. Second, the pyran ring of the P pyranopterin (the one away from the proximal) FS0 has opened. This mode of binding confirms that a bicyclic molybdopterin can bind to the metal ion. Opening and closing of the pyran ring has been discussed in the context of enzymatic function,[453] perhaps being involved in a catalytic proton transfer process. A separate structure of just the soluble NarGH subunits (PDB 1R27) has also been reported, showing a very similar overall protein architecture. At the molybdenum center, however, Asp 222 is clearly coordinated to the molybdenum in a monodentate fashion, with a terminal oxo group completing the sixth coordination position in a trigonal prismatic geometry similar to that seen in most other members of the DMSO reductase family.[370b] It is noteworthy that while the second Mo–O distance in the bidentate structure for the active site is rather long at 2.5 Å, the orientation of Asp 222 with respect to the remainder of the molybdenum coordination sphere is clearly different in the two structures. Interestingly, ethylbenzene dehydrogenase also has a

monodentate coordination of aspartate (section 5.7).[454] In reconciling the structures of the two active sites in nitrate reductase, it seems likely that the NarGHI crystal had become reduced in the synchrotron beam, whereas the NarGH crystal remained oxidized, which could account for the different binding modes for Asp 222.

The active sites of Nar from different species have been investigated by EPR spectroscopy.[455] Nar's typically exhibit two pH-dependent EPR signals, where a "low pH" signal ($g_{1,2,3}$ = 2.001, 1.986, 1.964) distinguishes itself from the "high-pH" signal ($g_{1,2,3}$ = 1.987, 1.981, 1.962) in the magnitude of the observed hyperfine splitting, a_{av} = 9.6 G for the low-pH form and a_{av} = 3.4 G for the high-pH form; in both signals, the protons are solvent-exchangeable.[455d] It has been suggested that only the low-pH form is catalytically competent,[455e] but more recent studies suggest that both forms may be important in catalysis.[452] A detailed investigation with the *M. hydrocarbonoclasticus* 617 Nar has demonstrated the formation of both high- and low-pH forms in the as-isolated enzyme.[455f] At a molecular level, the different hyperfine coupling may be due to different orientations of the proton either via hydrogen bonding with nearby amino acid residue or a network created by water molecules. Such a scenario has been observed in sulfite oxidase. Alternatively, the different hyperfine coupling may result from different binding modes (Figure 51) for substrate, as has been observed crystallographically.[455f] Interestingly, different binding modes have been invoked in explaining a different rhombic signal ($g_{1,2,3}$ = 2.007, 1.987, 1.970) in *P. pantothrophus* Nar.[456]

George et al. have reported a thorough EPR and EXAFS study of the Nar from *E. coli*,[455d] with low- and high-pH forms of the enzyme again observed. The high-pH Mo(V) species exhibits a small hyperfine with ^{17}O ($A_{av} \approx 2.38$ G), which they suggest is consistent with an Mo=^{17}O unit. For the low-pH species, the presence of a coordinated hydroxyl group was proposed to be responsible for the more strongly coupled proton, but no ^{17}O hyperfine was detected. In the presence of fluoride, a well-resolved ^{19}F coupling is observed suggestive of direct coordination to molybdenum,[455d] although in light of the discussion above concerning halide binding to sulfite oxidase it seems more likely that fluoride instead simply binds near the molybdenum center of Nar rather than coordinating directly to the metal. In the reduced Mo(IV) state, a substantial amount of a desoxo molybdenum species is seen with Nar, and in the oxidized Mo(VI) state, only a single terminal oxo group is observed at a distance of 1.73 Å. Thus, the low-pH form may be a desoxo-Mo species, while the high-pH species has one terminal oxo-group. Structural studies of DMSO reductase have established that monooxo-Mo(VI) and desoxo-Mo(IV) transformation is an accepted mechanism in these cases, as discussed in section 5.1. Subsequent studies have demonstrated such chemistry in discrete inorganic compounds.[7m,457]

The kinetic properties of the soluble NarGH fragment from *P. pantotrophus* have been investigated using protein film voltammetry (PFV).[458] At pH 6, the enzyme is catalytically active at potentials lower than +100 mV, and at that pH the Mo(VI/V) and Mo(V/IV) reduction potentials have been determined to be +470 ± 20 and −50 ± 20 mV, respectively. The [3Fe-4S] cluster has the highest reduction potential among the iron–sulfur clusters at +24 ± 20 mV, and the reduction potential for the [4Fe-4S] $^{2+/1+}$ cluster ($g \approx 1.833$) is −34 ± 20 mV. To account for the observed dependence of k_{cat} on applied potential, it has been

suggested that substrate can bind to both the Mo(V) and the Mo(IV) states, with the enzyme–substrate complex dissociating 5 times more slowly in the Mo(V) state than the Mo(IV) state. Such preferential binding of nitrate to Mo(V) has also been observed for the *E. coli* NarGHI.[459] At higher substrate concentrations, the pathway involving the Mo(V) state becomes dominant. k_{cat} of the *P. pantotrophus* NarGH is 100 s^{-1} for both nitrate and chlorate, and the rate of each electron transfer step, that is, Mo(VI/V) and Mo(V/IV), is much faster, at 1×10 s^{-1}. Substrate binding is potential-dependent with K_m = 5 μM and 20 μM at 30 and −130 mV, respectively. Thus, there appears to be a redox switch between the two forms of the enzyme that can catalyze substrate reduction, which may reflect geometric reorganization at the active site. While the exact nature of the structural change is not clear, in a discrete oxo-molybdenum(V) model compound, switching the position of a coordinated oxygen donor from an equatorial to an axial position changes the Mo(V/IV) reduction potential by 25 mV.[460] The pH-dependent PFV identified an ionizable proton with a pK_a of ~7.9, which, once ionized, reduces the catalytic efficiency.

The *E. coli* Nar GHI complex has also been investigated by PFV,[461] and is found to behave similarly to the *P. pantotrophus* enzyme over the pH range of 5.0–9.0, with catalytic activity being a function of applied potential (with higher activity at −25 mV and lower activity at −400 mV). The k_{cat} for the low-potential activity is approximately twice that observed at high potential, whereas the K_m is 4 times lower. It has been proposed that the redox switch of the catalytic activity may involve the participation of the pterin ring either via direct participation in the redox process or by a pyran ring-opening-closing mechanism. The PFV work has also provided evidence for the involvement of a proton in the catalytic process with pK_a of 7.8. Marangon et al.[462] have also investigated the enzymatic activity of NarGHI from *Marinobacter hydrocarbonoclasticus* 617 (previously known as *Pseudomonas nautica* 617) both by PFV and spectrophotometrically. The kinetic parameters are again comparable to those obtained in the case of *E. coli* and *P. pantotrophus* Nar. In particular, two catalytically distinct potential-dependent forms of the enzyme are differentially affected by pH and inhibitors, with the activity at low potential shown to be carried out by the protonated form of the enzyme; similar behavior is observed for *Synecococcus* Nas (section 5.5.3).[456]

Interestingly, a tungsten-containing Nar from *Pyrobaculum aerophilum*, an archaeon, has been reported.[463] It has a very high specific activity (V_{max} 1162 s^{-1} and K_m 58 μM) in 50 mM phosphate buffer (pH 7.0; 75 °C) and functions optimally at temperatures greater than 95 °C. Even this enzyme, purified from cells grown in the presence of molybdenum and tungsten, was reported to contain mostly Mo, indicating a natural selection of molybdenum in nitrate reductases.

5.5.2. Dissimilatory Nap Enzymes—In *Shewanella gelidimarina*, two different NapA enzymes have been characterized from aerobically grown cells; that encoded by the *napEDABC* operon (and sometimes designated as NapA-α) is found to be more stable than that from the *napDAGHB* operon (designated NapA-β). Whether the Nap produced from two different operons in the same organism be monomeric (e.g., NapA in *D. desulfuricans*) or heterodimeric (as in NapAB in *R. sphaeroides*) depends on their ability to form salt bridges at the NapA:NapB interface. Two residues (PDB 1OGY: E47 and S772) have been

identified as critical for formation of the heterodimer.[444] The two forms may be under different regulatory control, particularly with regard to the presence or absence of oxygen. For example, in *Bradyrhizobium japonicum*, expression of the sole Nap operon, *napEDABC*, is upregulated by nitrate and the presence of small amounts of O_2 through the regulatory cascade of FixLJ-FixK2-NnR.[464] In contrast, in *P. pantothrophus*, Nap is only expressed aerobically,[465] while the *R. sphaeroides* Nap is expressed anaerobically as well as aerobically.[466] When different types of nitrate reductases are present in the same organism (e.g., *E. coli* has both NarGHI and NapA), some of the regulatory elements may have dual controls. For example, in *E. coli* the cyclic AMP receptor protein (Crp) is involved in the regulation of both Nap and Nar expression.

All NapA enzymes possess a molybdenum center and a [4Fe-4S] cluster. The first crystal structure of the catalytic subunit of any nitrate reductase was reported for the monomeric NapA from *Desulfovibrio desulfuricans.*[368] As shown in Figure 51, the water-soluble protein was crystallized in the oxidized form, and the structure was solved to a 1.9 Å resolution (PDB 2NAP). The overall fold is very similar to that seen in FdhF of *E. coli* (PDB 1FDO; see Figure 47).[248b] The two enzymes share a high degree of sequence similarity, and each can catalyze the reaction of the other enzyme (although less efficiently). Both enzymes are also compositionally similar, containing a catalytic molybdenum center and a [4Fe-4S] cluster as prosthetic groups. In NapA, the distal amino group of the Q pyranopterin of the molybdenum center is 7.6 Å from the nearest iron atom of the [4Fe-4S], comparable to the distance seen in FdhF (Figure 52). In both cases, there is a highly conserved lysine residue (Lys 49 in the *D. desulfuricans* enzyme) lying between the two. These distances place the two metal centers within the 14 Å limit generally considered necessary for efficient electron transfer.[131]

The molybdenum center is deeply buried within the protein matrix approximately 15 Å from the surface, and is coordinated by two enedithiolates from the pyranopterin cofactor (present as the guanine dinucleotide) and Cys 140. The sixth coordination position had originally been assigned to a terminal oxo-group, but recently this has been revised due to the long molybdenum-ligand distance and a low thermal (*B*) parameter for the ligand.[467] A careful examination of the anomalous scattering parameters of oxygen and sulfur suggests that the ligand is a terminal sulfur rather than oxygen. The terminal sulfur is proposed to form a partial persulfide bond with the cysteine sulfur as the S···S distance of ~2.2 Å is shorter than the sum of the van der Waals radii, as shown in Figure 53, right. Structures with different substrates (e.g., nitrate, perchlorate, and cyanide) have also been examined. The active site structure with cyanide (PDB 2JIR) shows a cyanide bound to molybdenum at a distance of 2.2 Å away (Figure 53). Perchlorate ions from the crystallization mother liquor are found in the active site channel. A new crystal structure of the dimeric NapAB from *Cupriavidus necator* (also known as *Ralstonia eutropha* and *Alcaligenes eutrophus*) at 1.6 Å resolution (PDB 3ML1) has provided additional support for the overall description of the molybdenum coordination sphere (Figure 54).[468] The protein environment surrounding the molybdenum center is comprised of highly conserved residues (in the *C. necator* NapA – Arg 400, Arg 392, Glu 168, Asp 167, and Arg 150). Arg 392 and Asp 167 form a salt bridge and are directed toward the active site. Mutation of Asp 167 to alanine abolishes catalytic activity,

demonstrating its importance in the overall reaction.[469] Jepson et al. have also reported the crystal structure of *Escherichia coli* of NapA (2NYA) at 2.5 Å resolution.[470] The *E. coli* NapA forms a dimer with its electron transfer partner protein, the diheme NapB, but weakly with a K_d of 15 and 32 μM for oxidized and reduced complexes, respectively. The molybdenum center of NapA is coordinated by dithiolenes from two pyranopterin cofactors, one cysteine sulfur donor, and an oxygen donor forming a longer bond (2.6 Å). The two hemes of NapB are parallel to one another but displaced such that the two iron atoms are 10 Å apart. The porphyrin rings are in van der Waals contact. The proximal heme (heme I) iron is 7.6 Å from a tyrosine residue (Tyr 58), which in turn is 7.9 Å away from the [4Fe-4S] cluster.

Prior to the crystal structure of the *C. necator* NapAB referred to above, that of the dimeric NapAB from *Rhodobacter sphaeroides* was solved at 3.2 Å resolution (PDB 1OGY).[471] The NapB is a cytochrome-containing partner electron transfer protein that harbors two hemes. Complex formation alters the structure and also the reduction potential of the [4Fe-4S] cluster in NapA. The potential of one of the hemes (in NapB) is stabilized (i.e., lowered) by 40 mV, while that for the [4Fe-4S] cluster (in NapA) is stabilized by 180 mV upon forming the NapAB complex. The two subunits have a strong affinity for one another with an estimated dissociation constant (K_d) of 0.5 nM. As in the case of the *C. necator* NapAB, the molybdenum center is ~7.5 Å from the closest Fe in [4Fe-4S] cluster, and the opposite Fe on the same face of the cluster is 9.1 Å (edge-to-edge) from the nearer (proximal) heme of NapB, with the highly conserved Tyr 58 from NapB (*C. necator* numbering) intervening. It is the potential of this heme that is changed upon complex formation. The proximal heme is parallel to and in van der Waals contact with the distal heme, although the two are displaced with respect to one another such that the iron–iron distance is 10.0 Å; the distal heme is solvent-exposed. Both hemes are coordinated by a pair of histidine residues as is typical of *b*-type cytochromes, rather than the histidine–methionine coordination that is more common for c-type cytochromes.[472] In addition, in both hemes of NapB the histidines are parallel to one another, as distinct from the perpendicular orientation found in the heme of chicken liver sulfite oxidase.[265] The parallel arrangement is also seen in the structure of NapB from *Haemophilus influenzae* (PD: 1JNI).[473] The relative orientation of the histidines is well-known to impact the electronic structure of the heme and hence its reduction potential.[474] The reduction potentials of the heme in the *C. necator* NapAB are +50 and +160 mV, respectively, for the proximal and distal hemes. Interestingly, the orientation of the histidines in the *R. sphaeroides* NapAB is somewhat different, with the imidazole rings at an angle of ~45° with respect to one another. The reduction potentials of the heme center in *R. sphaeroides* NapAB are −210 and −65 mV, respectively, for the proximal and distal hemes.

The Nap proteins from *P. pantothrophus*,[475] *D. desulfuricans*,[467,476] *E. coli*,[470] *Shewanella gelidimarina*,[444] and *R. sphaeroides*[471,477] have each been investigated by EPR spectroscopy, extensively so in the case of the NapAB complex from *P. pantothrophus*.[475] Three distinct EPR signals are observed, distinguished on the basis of their average *g* values ($\langle g \rangle$): "very high-*g*", "low-*g*", and "high-*g*". All three forms are rhombic with $g_1 > 2$ for the "very high-*g*" signal ($g_{1,2,3} = 2.022, 1.999, 1.994$) suggesting substantial sulfur contributions to the HOMO. This "very high-*g*" species is thought to originate from an inactive form of

the enzyme.[475a,477a] The "low-*g*" signal, with $g_{av} \approx 1.97$ ($g_{1,2,3} = 1.996, 1.969, 1.961$), is observed when the enzyme is partially reduced with dithionite and is similar to that of the xanthine oxidase rapid type 1 signal, which has only one dithiolene moiety. The species giving this signal is thus also considered to be inactive. The high-*g* species (also called high-*g* split, and high-*g* resting) with a $g_{av} \approx 1.99$ ($g_{1,2,3} = 1.999, 1.991, 1.981$) is the most commonly observed signal and is insensitive to pH and ligands (i.e., nitrate, nitrite, cyanide, azide, and thiocyanate).[475a,478] XAS analysis indicates the presence of at least one terminal oxo group in each of the EPR-active forms of *P. pantotrophus* NapA.[475a] It also suggests direct binding of azide to Mo(IV). Proposed structures for the several EPR-active forms of the molybdenum center are shown in Figure 55. The fully oxidized state shows ligation by five sulfur donors, while the reduced form shows three. Another signal, "high-*g* nitrate" ($g_{1,2,3} = 1.999, 1.982, 1.990$) with lower *g*-anisotropy, has been reported from samples reduced with dithionite under turnover conditions.[475a,478] A similar signal from viologen-reduced samples has raised questions about the catalytic relevance of the "high-*g*-nitrate" signal.[479] EPR studies with *D. denitrificans* NapA indicate that the "high-*g* nitrate" signal does not come from catalytically relevant species,[467,476a] but a spectroscopic investigation by Fourmond et al. on the *R. sphaeroides* NapA suggests otherwise.[477a] A QM/MM investigation by Biaso et al. provides structural rationale for the different species detected for NapA.[480] They suggest a MoS_6 core in "high *g*-resting", "high-*g* nitrate", and "high-*g* turnover" species with the signals very similar to each other. The "high-*g*" species is considered to be a more reduced state where the proposed persulfide bond between the sulfido and S–Cys of the molybdenum is reduced, while the "low-*g*" signal is attributed to a species coordinated by only one pterin cofactor, as proposed before. Certainly small perturbations in structure even in simple $[MoOCl_4]^-$ can give rise to different EPR parameters.[481] The differences in the signal-giving species may have to do with the presence of different ions, and/or a structure distortion in the molybdenum coordination sphere, although their catalytic relevance remains unclear.

An initial catalytic mechanism for the Nap enzymes has been proposed[368] on the basis of the crystal structure of *D. desulfuricans* NapA, in which nitrate binds to the five-coordinate molybdenum center via one oxygen atom to give a six-coordinate center. The nitrate is reduced to nitrite and the bridging oxygen is transferred to molybdenum, becoming a terminal oxo group of the now-oxidized molybdenum center. Rereduction of the molybdenum with reducing equivalents from menaquinol results in protonation of the Mo=O to water, leading to its dissociation to regenerate the pentacoordinate reduced Mo(IV) center. The overall reaction is essentially the reverse of that shown above for the *Rhodobacter* DMSO reductase. The recent conclusion that the terminal ligand to molybdenum in oxidized NapA of both *D. desulfuricans* and *C. necator* is a sulfido rather than oxo group has led to a revision of this mechanism. Specifically, a putative persulfide bond between the terminal sulfide and cysteine sulfur has been proposed that reacts with substrate to generate an oxo-sulfido intermediate and a sulfide species, with Cys 140 (in the *D. desulfuricans* enzyme) dissociated from the molybdenum center. Support for this mechanism has been provided by density functional theory calculations,[480] but as yet no direct experimental support has been forthcoming.

The steady-state kinetics of NapA from *D. desulfuricans* have been investigated using reduced methyl viologen as an electron donor. The K_m is found to be 32 μM with a specific activity of 18.8 μmol [NO_3] mg^{-1} min^{-1} (phosphate buffer, 37 °C, pH 8.0).[482] The optimal pH range for this enzyme is 8.0–9.5; both phosphate and cyanide stimulate the activity, but ferricyanide inhibits activity. For the NapAB from *Paracoccus pantotrophus* (sometimes called *Paracoccus denitrificans*), K_m is 1.3 ± 0.2 mM and k_{cat} is 240 ± 32 s^{-1} (and k_{cat}/K_m = 1.84 × 10^5 M^{-1} s^{-1}) at pH ≈ 7.5 (24 °C, 50 mM Hepes buffer),[475a] The *P. pantotrophus* enzyme is specific for nitrate and cannot reduce chlorate, iodate, bromate, arsenate, formate, tellurite, nitrite, selenite, sulfate, or sulfite. Cyanide is a noncompetitive inhibitor, while azide is a competitive inhibitor (K_i =11 ± 1 mM, an order of magnitude greater than seen with NarGHI).[483] The enzyme is also competitively inhibited by thiocyanate with a K_i 4.0 mM.[478] Thiocyanate inhibition occurs by direct binding of the inhibitor to the molybdenum center with displacement of one of the pyranopterin cofactors (presumably the Q pyranopterin, by analogy to the situation seen in the *R. sphaeroides* DMSO reductase). The mechanism of azide inhibition is not clear, but it may directly bind to the molybdenum center. Periplasmic fractions isolated from *P. pantotrophus* cells grown on tungsten-containing media have a much higher K_m, 3.91 ± 0.45 mM (in 50 mM Hepes-NaOH, pH 7.5, 24 °C), but the intrinsic activity is very low.[484]

The steady-state kinetics of the *R. sphaeroides* NapAB yield a K_m of 170 μM, somewhat higher than the value of 45 μM for the monomeric NapA; the V_{max} values are 25 μmol [NO_3] mg^{-1} min^{-1} and 5.9 μmol [NO_3] mg^{-1} min^{-1} assayed at 30 °C in a 50 mM Tris-HCl buffer (pH 7.0), for the NapAB and NapA, respectively, indicating that the heterodimeric enzymes are considerably more efficient. Consistent with a “ping-pong” mechanism, nitrate binding to the active site is controlled by prior reduction of the Mo-center.[471] Interestingly, *napB* gene deletion mutants in *R. sphaeroides*[485] and *E. coli*[486] exhibit very little activity in NapA, indicating an essential role of NapB in these organisms. As mentioned before, the NapAB complex formation may be oxidation-state dependent, and a redox-modulated binding may control the flow of electrons in the reduced state.

Frangioni et al.[487] have reported that the *R. sphaeroides* NapAB complex exhibits maximum catalytic activity in PFV experiments at applied potentials close to the reduction potential of the nitrate-saturated Mo(V/IV) couple even under nonsaturating substrate concentrations, suggesting a strong affinity for substrate.[488] Under turnover conditions, the enzyme is thought to exist in active and inactive forms that interconvert on a time scale slower than the catalytic turnover. As mentioned earlier, under reducing conditions and in the presence of excess nitrate, the inactive form accumulates, resulting in inhibition of the enzyme. This is particularly interesting as such heterogeneity is now recognized to be a problem with several members of the DMSO reductase family.[7k,366c] A redox switch such as thought to operate in NarGHI has also been invoked in the case of the NapAB from *P. pantotrophus*, but in this case the redox switch is thought to be associated with the [4Fe-4S] cluster, not the molybdenum center.[489] In this case, the activity of the enzyme has been linked to a single protonation event with a pK_a =7.8; the enzyme exhibits a higher catalytic current at pH ≈ 6.[489] Because NapAB operates at a lower potential than NarGH, electron transfer to Nar

through the quinone pool would be thermodynamically more favorable and thus the dominant process. At high quinol concentrations, NapAB becomes activated.[490]

5.5.3. Assimilatory Nas Enzymes—The ability of bacteria to assimilate nitrate is well-known, and assimilatory nitrate reductases (Nas) catalyze the first step of this process by reducing nitrate to nitrite. The Nas enzymes are quite diverse and have been investigated from organisms ranging from the cyanobacterium *Synechococcus* sp. PCC7942 to heterotrophs such as *Rhodobacter capsulatus*,[491] *Klebsiella oxytoca*,[492] *Azotobacter vinelandii*,[493] *Paracoccus denitrificans*,[494] as well as the Gram-positive *Bacillus subtilis*.[495] The majority of work, however, has focused on genetic aspects. The molybdenum-containing catalytic subunit has been designated variously in these organisms as NarB (in cyanobacteria), NasA (in *Klebsiella oxytoca*), NasB (in *A. vinelandii*), and NasC (in *B. subtilis* and *P. denitrificans*). The *nas* genes are in the same operon as nitrite reductase and nitrate transporters, with the nitrite reductases genes designated as *nirA* in cyanobacteria; *nasB* in *K. oxytoca* and *P. denitrificans; nasA* in *A. vinelandii*; and *nasD* in *B. subtilis*. The transporters are designated as *nrtA*, *nrtB*, *nrtC*, and *nrtD*, in *Synechococcus* sp PCC7942; but *nasA* in *B. subtilis; nasF*, *nasE*, and *nasD* in *K. oxytoca; nasA* and *nasH* in *P. denitrificans*; and *narK* in *A. vinelandii*. It is not surprising that nitrate and nitrite reductase genes are part of the operon with transporter genes as the overall process is tightly regulated. In Gram-positive bacteria, nitrate reduction is controlled by regulatory proteins in a pathway-specific manner, while Gram-negative bacteria have a dual control, a general nitrate regulatory control as well as repression by ammonia.[494b]

Initial kinetic studies suggested that Nas exhibited bimodal behavior,[496] but more recent work has indicated the presence of only one catalytically active form.[497] As with other nitrate reductases, most studies have focused on steady-state kinetics, but Jepson et al.[498] have investigated the Nas from *Synechococcus* sp. (reported as NarB) by PFV. The Mo(VI/V) reduction potential is −150 mV, while that for the Mo(V/IV) couple is lower than −550 mV, indicating the accumulation of large amounts of the Mo(V) state below −150 mV. At −450 mV, where the maximal catalytic current is observed, the K_m is 0.08 mM, consistent with the K_m of 0.05 mM determined in steady-state assays using reduced methyl viologen ($MV^{+\bullet}$) as reductant (25 °C, 25 mM Hepes, 100 mM NaCl, 10% glycerol, pH 8.0). At a more reducing potential of −650 mV, the K_m increased to 0.350 mM, indicating redox-dependent binding of nitrate, perhaps associated with a structural change at the molybdenum center. Again using $MV^{+\bullet}$-reducing substrate, k_{cat} for nitrate (0.05 mM) reduction was 80 s^{-1}, yielding a k_{cat}/K_m of 1.6×10^6 M^{-1} s^{-1}. The specificity of the same enzyme was similarly evaluated using chlorate (2.5 mM) and selenate (2.5 mM), with k_{cat}/K_m of 2000 M^{-1} s^{-1} for chlorate (k_{cat} = 5 s^{-1}) and 400 M^{-1} s^{-1} for selenate (k_{cat} = 1 s^{-1}), respectively, clearly indicating a high specificity for nitrate. Azide acts as a competitive inhibitor with a K_i of 13 mM.

The ferredoxin (Fd)-dependent activity of Nas from *Synechococcus* sp. PCC 7942 has also been examined by Hirasawa et al. who demonstrated the importance of positively charged amino acid residue(s) in binding to the negatively charged Fd.[499] The catalytic subunit of Nas (called NarB in this case) forms a 1:1 complex with Fd, and at high ionic strength binding becomes weaker, underscoring the electrostatic nature of the interaction. Treatment

of Nas with chemical modifying agents specific for arginine or lysine reduces the affinity for Fd without affecting turnover with the nonphysiological electron donor $MV^{+\bullet}$. The reduced affinity has been attributed to modification of Arg 44 and Lys 23 of Nas, identifying a candidate region for interaction with Fd. In more recent site-directed mutagenesis studies, Srivastava et al.[500] have identified four positively charged residues near the molybdenum center that are conserved among the Nas proteins. Lys 58, for example, intervenes between the Q pyranopterin of the molybdenum center and the [4Fe-4S] cluster and is essential for effective electron transfer because even a K58R mutation significantly reduces activity. Mutation of Lys 58 also compromises cofactor insertion, suggesting that lysine may play a role in stabilizing the cofactors. Mutation of Arg 70 to Gln also abolishes activity, but the role of this residue is less clear. Another conserved arginine, Arg 146, does not impact the catalytic activity of the enzyme at all, regardless of whether it is mutated to a positively charged residue or a neutral residue. On the other hand, a positive charge at Lys 130 is important for catalysis as its mutation to an arginine only minimally affects activity. While homology models have been used in guiding the mutational studies, a crystal structure is not yet available and obviously would help immensely in placing the mutagenesis results in a structural context.

The Nas proteins give EPR signals similar to those observed with the Nap proteins. Two different signals, "very high *g*" ($g_{1,2,3}$ = 2.023, 1.998, 1.993) and "high *g*-split" ($g_{1,2,3}$ = 1.997, 1.990, 1.982, 1.990) have been reported from *Synechococcus* sp. PCC 7942 Nas.[498] Here, also the very high-*g* signal is likely due to an inactive form of the enzyme, and the "high-*g*" signal is the major signal arising from functional enzyme. In addition, Nas from *Cyanothece* sp. PCC 8801 exhibits a rhombic Mo(V) signal ($g_{1,2,3}$ = 2.0167, 1.988, 1.962) accounting for 3–10% of Mo(V) signal; this signal is not observable in K58Qand K58R mutants.[497] The origin of this signal is not clear at present. Very high-*g* and high-*g*-nitrate signals have also been observed in Nas isolated from *Azotobacter v*in*elan*dii.[501] The high-*g* signal ($g_{1,2,3}$ = 2.023, 1.998, 1.993) is observed in as isolated sample that accounts for ~10% of total Mo, and the high-g nitrate signal ($g_{1,2,3}$ = 1.998, 1.989, 1.981) was observed in dithionite reduced sample oxidized by nitrate that accounted for *7%* of total Mo. The as-isolated *Cyanothece* enzyme shows a fast-relaxing species (observable below 30 K) with $g_{\|} \approx 2.02$ and $g_{\perp} \approx 2.00$, characteristics of an oxidized [3Fe-4S] cluster presumably originating from degradation of the [4Fe-4S] cluster. The dithionite-reduced sample at 20 K showed a fast relaxing rhombic signal ($g_{1,2,3}$ = 2.06, 1.95, 1.91) due to the reduced [4Fe-4S] cluster.

5.6. Arsenite Oxidase and Arsenate Reductase

The metabolism of arsenicals, and in particular that of the environmentally widely encountered and water-soluble arsenite and arsenate ions, has recently received a great deal of attention as the broad distribution of enzymes able to oxidize arsenite and/or reduce arsenate has become appreciated.[373,502] These include not only detoxifying systems found in all three domains of life but also respiratory systems that use the oxidation of arsenite or the reduction of arsenate to generate energy; they are thought to be evolutionarily ancient, present in the last universal common ancestor to all present life forms.[373,503] These enzymes fall into three distinct groups: the Aio arsenite oxidases (formerly referred to variously as

Aox, Aro, or Aso[504]) that provide reducing equivalents for the respiratory chain (and simultaneously transform arsenite to the much less cytotoxic arsenate); the Arr arsenate reductases that utilize arsenate as a terminal respiratory substrate; and the recently identified Arx arsenite oxidases that are closely related to the Arr enzymes but function physiologically to oxidize arsenite rather than reduce arsenate.

5.6.1. AioAB Arsenite Oxidases—The AioAB arsenite oxidases are phylogenetically broadly distributed and encoded by a minimal *aioBA* operon that frequently also includes genes encoding a *c*-type cytochrome, a two-component AioS/AioR sensor histidine kinase, and regulatory element, a periplasmic AioX arsenite binding protein and/or an ArsA ATPase arsenite pump.[505] The enzyme is membrane-associated but in the periplasm. Unusually, the twin arginine leader sequence that targets the protein for TAT-dependent export to the periplasm is on the AioB rather than AioA subunit. Crystal structures exist for two AioAB arsenite oxidases, that from *Alcaligenes faecalis*[367] and the *Rhizobium* strain NT-26.[506] The structure of the *A. faecalis* enzyme is shown in Figure 56. The AioA subunit has a [3Fe-4S] cluster in its N-terminal domain and an active site molybdenum center in a four-domain motif resembling that first seen in the *R. sphaeroides* DMSO reductase. The molybdenum center, which has apparently become reduced in the synchrotron beam, has two equivalents of the pyranopterin (present as the guanine dinucleotide) and an apical Mo=O (at a distance of 1.6 Å) in a square-pyramidal coordination geometry. Unique to the enzyme, no molybdenum ligand is provided by the polypeptide (the position homologous to the molybdenum-binding amino acid residues in other enzymes of the DMSO reductase family is Ala 199, which lies in a polypeptide strand that loops away from the molybdenum center). As shown in Figure 56, Lys 450 lies very close to the apical oxo group and is flanked by Arg 419 and Glu 203 that define the substrate binding site. Again, the iron–sulfur cluster is adjacent to the Q pyranopterin. X-ray absorption analysis of the oxidized *A. faecalis* arsenite oxidase shows four sulfurs with Mo–S distances in the 2.37–2.47 range, consistent with the crystallographically observed bisenedithiolate coordination of the metal, and two additional oxygen atoms.[507] The data were best fit with a Mo=O at 1.72 Å and a Mo–O(H) at 1.84 Å, but the possibility of two Mo=O at 1.78 Å could not be excluded.[507] The AioB subunit is oblong-shaped, with a six-strand β-barrel at one end and a four-stranded sheet containing a Rieske-type [2Fe-2S] center at the other. The Rieske-containing end is inserted into a shallow depression on the surface of AioA near its [3Fe-4S] cluster, with the cluster's histidine-coordinated iron proximal to the [3Fe-4S] cluster; the edge-to-edge distance between the two iron–sulfur cluster is approximately 10 Å. The Rieske center is buried in AioB, but lies immediately beneath a disulfide bond between Cys 65 and Cys 80, which is on the protein surface.

The *A. faecalis* arsenite oxidase is able to use either azurin or a *c*-type cytochrome as oxidizing substrate, and steady-state analysis yields k_{cat} = 27 s^{-1}, $K_m^{arsenite}$ = 3 μM, K_m^{azurin} = 68 μM in 50 mM MES buffer, pH 6.0, 25 °C.[508] The enzyme from other organisms, notably *Ralstonia* isolate 22, appear to be specific for soluble *c*-type cytochromes.[509] The purified enzyme absorbs broadly throughout the visible, with pronounced shoulders at 680 and 450 nm that bleach upon reduction. The oxidized enzyme manifests the expected EPR signal of a [3Fe-4S] cluster ($g_{1,2,3}$ = 2.03, 2.01, 2.00), and the reduced of a Rieske-type

center ($g_{1,2,3}$ = 2.03, 1.89, 1.76).[508] In the course of reductive titrations, the [3Fe-4S] signal disappears before that for the Rieske center emerges, reflecting its more positive reduction potentials. Unusually, no EPR signal attributable to a Mo(V) state of the molybdenum center has ever been observed. The electrochemical behavior of the enzyme has been examined by protein film voltammetry, with reduction potentials for the [3Fe-4S] and Rieske cluster of +260 and +160 mV, respectively, being found.[510] The midpoint potential for the molybdenum center is +292 mV at pH 6.0, and it behaves as an obligate two-electron system, consistent with the failure to observe a Mo(V) EPR signal. Although these reduction potentials indicate that electron transfer out of the molybdenum center is thermodynamically uphill, they are considerably more positive than that for the arsenite/arsenate couple, at +60 mV. The pH dependence of E_{mid}^{Mo} indicates the uptake of two protons with the two electrons, consistent with the oxidized enzyme having an L_2MoO_2 structure, with one of the oxo groups being protonated and dissociating upon reduction of the molybdenum. Indeed, redox-cycling the enzyme by reducing with arsenite followed by reoxidation in $H_2{}^{18}O$ results in incorporation of oxygen into a Mo=O group of the enzyme, as reflected in a 39 cm^{-1} red-shift in the 822 cm^{-1} Mo=O stretching mode of oxidized enzyme to 784 cm^{-1}. These results are all consistent with the enzyme operating via a simple oxygen atom transfer mechanism as envisaged for DMSO reductase, with a substrate lone pair attacking a catalytically labile Mo=O to initiate catalysis. In the presence of substrate, the onset of the catalytic wave in the voltammogram correlates with the Mo(VI/IV) potential, indicating that electron transfer among the redox-active centers is rapid and that catalytic electron transport is entirely limited by turnover at the molybdenum center, with a k_{cat} of ~50 s^{-1} at pH 6.0, 25 °C.[510] The *Rhizobium* NT-26 arsenite oxidase[511] appears to behave somewhat differently from the *A. faecalis* enzyme. Most significantly, the pH dependence of the catalytic wave for this enzyme is −30 mV/pH unit, indicating a two-electron/one-proton process. Such an interpretation would be more consistent with an $L_2MoO(OH)$ formulation for the oxidized molybdenum center, the preferred interpretation of the XAS analysis. As with the *A. faecalis* enzyme, that from *Rhizobium* does not exhibit a Mo(V) EPR signal under any conditions thus far examined.

Ralstonia sp. S22 also possesses an AioAB arsenite oxidase, and an *E. coli* heterologous expression system for recombinant expression system for this enzyme has recently been reported, with the recombinant enzyme exhibiting EPR properties similar to those of the *A. faecalis* enzyme.[512] Interestingly, the reduction potential for the Rieske cluster of the *Ralstonia* enzyme is considerably higher than that for the *A. faecalis* enzyme at +210 mV.[503a] The *Ralstonia* enzyme possesses the disulfide bond adjacent to the Rieske cluster that is seen in the *A. faecalis* enzyme (but the *Rhizobium* enzyme does not). A C106A mutant has been prepared that exhibits EPR and reduction potential similar to that of the wild-type enzyme, indicating that the presence of the disulfide bond itself does not influence the reduction potential of the cluster, as had long been assumed.[512] Conflicting results have been recently obtained in this regard with the *Rhizobium* NT26 arsenite oxidase, however, where it is reported that introduction of a disulfide bond results in a 35 mV decrease in reduction potential of the Rieske cluster.[506] The overexpressed *Ralstonia* enzyme is found to spontaneously associate with the membrane, indicating that it does not need a membrane-

anchoring protein to so associate. A Δ*tat* AioB construct has been prepared that, as expected, is localized to the cytosol rather than periplasm.

5.6.2. Arr Arsenate Reductase and Arx Alternate Arsenite Oxidase—Although not as well-characterized from a biochemical standpoint as the AioAB arsenite oxidases discussed above, the Arr arsenate reductases have been extensively analyzed genetically and phylogenetically.[373] The operons encoding Arr arsenate reductases are generally organized *arrCABD* (although other arrangements are sometimes observed), with the ArrD gene product predicted to be a Tat-associated chaperone analogous to TorD (section 2.3).[373,513] The gene sequences predict that ArrABC has strong sequence homology to the PsrABC polysulfide reductase discussed in section 5.3, and presumably has a similar complement of redox-active centers: a molybdenum- and [4Fe-4S]-containing ArrA (and a conserved Cys homologous to Cys 173 of PsrA that coordinates the molybdenum in the active site), a 4x[4Fe-4S]-containing ArrB, and a cofactorless membrane-integral ArrC possessing a site for oxidation of menaquinol adjacent to the distal [4Fe-4S] cluster of ArrB.[373] Given the conserved and distinctive double four-helix bundle structure of PsrC and the role of this subunit in dimerization of polysulfide reductase, it is likely that ArrABC also dimerizes into an $(\alpha\beta\gamma)_2$ oligomer. As with the arsenite oxidases, the catalytic ArrA subunit is periplasmically localized, although the TAT leader sequence is found in the ArrA subunit rather than ArrB.[513] ArrABC is expressed only in the presence of arsenate and in most organisms is under the additional regulatory control of FNR, being expressed only under anaerobic conditions.[514] The *arrA* gene has been shown to be a reliable marker for the ability of a microorganism to respire on arsenate and has been used successfully to greatly expand the number of organisms known to be able to do so.[515]

As seen with the NarGHI system, a soluble ArrAB unit can be isolated from, for example, *Chrysiogenes arsenatis*,[516] the *Shewanella* strain ANA-3,[517] or *Bacilllus selenitireducens*,[517] which has electron donor:arsenate oxidoreductase activity; both enzymes are specific for arsenate as substrate and do not utilize, for example, nitrate effectively. In contrast to the AioAB arsenite oxidases, the ArrABC arsenate reductases appear capable of catalyzing the reverse of their physiological reaction, the oxidation of arsenite to arsenate.[518]

Quite recently, an alternate ArxABC arsenite oxidase has been identified[518] that more closely resembles the ArrABC arsenate reductases than the AioAB arsenite oxidases described above.[519] Interestingly, the operons from three different organisms are minimally organized *arxB′ABC*, with a redundant copy of the *arxB′* gene; in two of the three organisms, an *arxD* gene encoding a putative chaperone is also present. The ArxABC enzyme functions physiologically as an arsenite oxidase during anaerobic respiration on nitrate[520] or selenate,[521] and under photoautotrophic conditions as well.[522] It has been suggested that, depending on growth conditions, a given organism will express either an ArrABC enzyme that reduces arsenate utilizing menaquinol as substrate or an ArxABC enzyme that oxidizes arsenite, reducing ubiquinone.[373] The similarity in protein architecture and reversible arsenite/arsenate interconversion notwithstanding, it must be borne in mind that the ArrA and ArxA catalytic subunits occupy distinct subgroups within the polysulfide

reductase clade of molybdenum-containing enzymes (although the two are more closely related to one another than to AioA clade).[519c]

5.7. Ethylbenzene Dehydrogenase

Aromatoleum aromaticum (formerly *Azoarcus* strain EbN1) is a β-proteobacterium and an obligate anaerobe that is able to grow on ethylbenzene (a major component of crude oil) as sole carbon source. Ethylbenzene dehydrogenase, encoded by the *ebdABC* operon, catalyzes the first step in the degradative pathway, the hydroxylation of ethylbenzene to (*S*)-1-phenyl-ethanol, which involves the remarkable hydroxylation of an aromatic hydrocarbon without utilizing O_2 (i.e., the enzyme is neither a mono- nor dioxygenase).[523] The enzyme thus catalyzes the hydroxylation of a very unactivated substrate, in contrast to the case of those enzymes of the xanthine oxidase family that hydroxylate only on more activated heterocyclic compounds or aldehydes. Ethylbenzene dehydrogenase acts on a wide range of alkylaromatics and alkylheterocyclics, but requires an ethyl (or substituted ethyl) side chain since toluene and related compounds are inhibitors.[524] The enzyme also catalyzes the dehydrogenation of reduced, bicyclic aromatics such as indane to conjugated products (indene in the case of the reaction with indane), possibly by hydroxylating then dehydrating the substrate.

Ethylbenzene dehydrogenase is a soluble, periplasmically localized αβγ trimer whose architecture (Figure 57) generally resembles individual protomers of DmsABC, PsrABC, FdnGHI, and NarGHI systems discussed above.[454] The EbdA subunit has a *bis*pyranopterin active site (with the pterin present as the dinucleotide of guanine) with Asp 223 and an acetate ligand from the crystallization mother liquor coordinated to the (presumably reduced) molybdenum in a distorted trigonal prismatic coordination geometry, as well as a [4Fe-4S] cluster proximal to the Q pyranopterin that, as seen in NarG, has a histidine ligand replacing one of the cysteines. The P pyranopterin has a ring-opened pyran ring as seen in NarGHI (see section 5.4.1), although the geometry of the cofactor suggests that it is a dihydropterin rather than the tetrahydropterin proposed for NarGHI. Asp 223 is hydrogen-bonded to Lys 450, an arrangement similar to the Arg-Asp predicted to be conserved in selenate reductase[525] and chlorate reductase[526] on the basis of sequence homology. The tunnel providing access to the active site is principally hydrophobic, as might be expected given the nature of the substrate. The EbdB subunit has 46% sequence identity with NarH, with three [4Fe-4S] and one [3Fe-4S] clusters (with the last being distal to the EbdA subunit, as seen in NarGHI). The clusters are again organized as two pairs, with a similar cysteine coordination scheme as found in DmsB, PsrB, FdnH, and NarH. The EbdC subunit of the soluble ethylbenzene dehydrogenase is distinct from the membrane-integral subunits of DmsABC and so on, with a secondary structure dominated by two sandwiched five-stranded β-sheets. It possesses a single *b*-type cytochrome, coordinated by Met 108 and Lys 201, in an otherwise very hydrophobic environment, and is related to the heme-binding domain of the flavocytochrome cellobiose dehydrogenase.[527] The physiological electron acceptor for ethylbenzene dehydrogenase is unknown.

A model of product (*S*)-1-phenylethanol coordinated to the molybdenum center of ethylbenzene dehydrogenase via the catalytically introduced hydroxylate has been

generated, with substrate in place of the acetate ligand seen crystallographically.[454] Assuming a Mo=O group in place of the bound acetate in oxidized enzyme, the reaction is proposed[454,524] to proceed with proton abstraction from the methyl group of substrate by Asp 223 with concomitant hydride transfer to the Mo=O to give a Mo(IV)(OH) intermediate with a carbocation at C-2 of substrate. This breaks down by hydroxyl transfer from the molybdenum coordination sphere to substrate to give the hydroxylated product, His 192, proposed to play a role in facilitating the hydride transfer. Although an initial quantum mechanical study of the reaction mechanism discretely comparing a carbocation versus radical mechanism suggested that the carbocation reaction coordinate is preferred,[528] a more detailed density functional study has indicated that a two-step radical-based mechanism is in fact preferred, and is more consistent with an observed pH-dependent primary kinetic isotope effect with 2-^{2}H-ethylbenzene as substrate of 3–10 (with the larger values observed at higher pH, where the initial hydrogen atom transfer from substrate to the molybdenum center becomes rate-limiting).[529] Experimental support for this mechanism has recently been obtained from a detailed product analysis of enzyme with over 40 substrate analogues and inhibitors,[530] the upshot being that, in contrast to xanthine oxidase,[132] C–H bond cleavage in the ethylbenzene dehydrogenase reaction appears to be homolytic rather than heterolytic.

5.8. Pyrogallol:Phloroglucinol Transhydroxylase

Pelobacter acidigallici is able to grow on phloroclucinol (1,3,5-trihydroxybenzene), pyrogallol (1,2,3-trihydroxybenzene), and related polyhydroxylated aromatics as the sole carbon source, reductively cleaving the aromatic ring prior to further degradation to acetate.[531] The first step in the degradation of pyrogallol is the transhydroxylation reaction shown in Figure 58, in which the 2-hydroxyl group of the cosubstrate 1,2,3,5-tetrahydroxybenzene is transferred to the 5 position of pyrogallol to generate a new equivalent of the tetrahydroxybenzene and phloroglucinol derived from the cores of pyrogallol and 1,2,3,5-tetrahydroxybenzene, respectively. The hydroxyl group that is transferred is not derived from solvent, nor does it equilibrate with solvent in the course of turnover.[532] The crystal structure of the transhydroxylase (Figure 59) shows the enzyme to be an αβ heterodimer, with a molybdenum-containing large subunit and a smaller subunit with three [4Fe-4S] clusters.[533] The large subunit consists of four domains as seen in the *Rhodobacter* DMSO reductases (Figure 43), although segments of the chain trace (mostly in regions involved in substrate binding) differ significantly from that seen in DMSO reductase. The pyranopterin cofactors of the molybdenum center are present as the guanine dinucleotide, and the molybdenum (which under the strongly reducing crystallization conditions used is most likely present as Mo(IV)) is also coordinated by Ser 175 and an acetate ion from the crystallization mother liquor. The position occupied by acetate is thought normally to be occupied by a water/ hydroxide ligand. The small subunit consists of three domains: a normal bacterial ferredoxin domain with two [4Fe-4S] clusters, a second ferredoxin-like domain that has only a single iron–sulfur cluster, and a third domain consisting of a fibronectin-like seven-stranded β-barrel that may be involved in attaching the enzyme to the inner surface of the cell membrane. The overall layout of the iron–sulfur clusters in the small subunit resembles that seen in the tungsten-containing formate dehydrogenase from *D. gigas*.[534] The reduced enzyme exhibits two iron–sulfur EPR signals

with $g_{1,2,3}$ = 2.08, 1.94, 1.87 and 2.06, 1.95, 1.87 in an approximately 2:1 ratio,[535] consistent with the makeup of the enzyme. Absent an FS0 cluster in the large subunit, the nearest [4Fe-4S] cluster of the small subunit is 12.4 Å from the distal amino group of the Q pyranopterin, but because the reaction does not involve electron transfer per se, so large a distance does not appear likely to compromise turnover.

The crystal structure of the complex of reduced enzyme with the substrate pyrogallol has also been determined.[533] As shown in Figure 59 (right), pyrogallol coordinates to the molybdenum via its C1 hydroxyl group, in the position occupied by the acetate seen in the absence of substrate. Trp 176, Trp 354, and Phe 468 provide a hydrophobic substrate binding pocket, with Arg 153 hydrogen interacting with the 3-hydroxyl group of substrate and His 144 hydrogen bonding to the coordinating 1-hydroxyl group. Interestingly, C1 of bound pyrogallol is clearly sp^3-hybridized and tetrahedral. A model of the ternary complex of enzyme with both substrates places phloroglucinol between His 154, Cys 557, and Tyr 404, and positioned such that its 2-hydroxyl group is adjacent to C5 of pyrogallol.[533] A reaction mechanism has been proposed that involves oxidation of pyrogallol by the molybdenum center to give the orthoquinone, followed by nucleophilic attack of the 5-hydroxyl of phloroglucinol to give a diphenylether intermediate. Cleavage of the C–O bond of phloroglucinol substrate occurs by formation of an orthoquinone on the pyrogallol moiety, which upon reduction by the molybdenum center yields the rearomatized product phloroglucinol (from the aromatic ring of the pyrogallol substrate) and the now reoxidized molybdenum center. This mechanism is quite distinct from another that is proposed to involve a simpler hydroxyl group transfer, in which the reduced enzyme first accepts the 2-hydroxyl from 1,2,3,5-tetrahydroxybenzene to afford phloroglucinol and oxidized enzyme, which then reductively hydroxylates pyrogallol to phloroglucinol.[532]

6. CONCLUSIONS

It should be evident from the above that progress in our understanding of molybdenum-containing enzymes over the past 15 years or so has been impressive. Genomics and proteomics studies have greatly expanded our appreciation of the distribution, interrelationships, and diversity of molybdenum-containing enzymes, and have helped to identify promising new gene products for future investigation. This work has also underscored the evolutionary ancient origins of molybdenum-containing enzymes and their relationship to other systems (e.g., NADH dehydrogenase and the Ni/Fe hydrogenases) that had not been previously recognized. Our understanding of the biosynthetic pathway for the pyranopterin cofactor has now advanced to the point that we not only understand the key intermediates in the pathway but in many cases have a detailed grasp of the structural basis for their interconversion by the enzymes involved. Again, new aspects of molybdenum cofactor biosynthesis continue to emerge, and it is evident that its genetic regulation and intracellular trafficking is far more intricate than might have been expected. With respect to each of the major families of molybdenum-containing enzyme considered here, it is evident that while many interesting variations on the common themes of structure and reactivity have been identified, it is very likely that more will come to light in the near future. Progress in understanding the three-dimensional structures of molybdenum-containing enzymes has been enormous, and our understanding of the reaction mechanisms of many of these

enzymes has been informed by the inspired synthesis of active site models and by the application of the most advanced spectroscopic and theoretical methods available to inorganic chemists.

Having said this, it should be evident from this account that a number of areas remain incompletely understood at present. While it is possible that cofactor simply binds to apoprotein in the case of members of the sulfite oxidase family from free solution, for example, it is evident that the process is much more complicated for members of the xanthine oxidase and DMSO reductase families. It remains for future work to ascertain whether and how auxiliary proteins such as XdhC and TorD participate in cofactor insertion, and to determine the structural changes that occur in the course of the process. The relationship of the extensive MOSC family of proteins to other members of the sulfite oxidase family also remains to be explored, and the reactions catalyzed by some these proteins (e.g., YedY, mARC) to be ascertained. While the reaction mechanisms of enzymes such as xanthine oxidoreductase, sulfite oxidase, and DMSO reductase are now well-understood, the same cannot be said of many of the more recently discovered enzymes. Specific and testable hypotheses concerning the reaction mechanisms of enzymes such as CO dehydrogenase, 4-hydroxybenzoyl-CoA reductase, and ethylbenzene dehydrogenase have been proposed, but have yet to be experimentally confirmed (or refuted). Particularly in the cases of the formate dehydrogenases and (bacterial) nitrate reductases, present ambiguities in the structures of the active sites make it virtually impossible to discriminate among the several reaction mechanisms that have been proposed. For these enzymes, much work remains to be done.

Biographies

Russ Hille was born in Tyler, TX, in 1951. He received a B.S. in Chemistry from Texas Tech University in 1974 and a Ph.D. in Biochemistry from Rice University in 1979. After postdoctoral work at the University of Michigan, in affiliation with the Department of Biological Chemistry and the Michigan Society of Fellows, he took a faculty position in the Department of Molecular and Cellular at The Ohio State University. In 2007 he moved to the Department of Biochemistry at the University of California, Riverside. His principal research interests concern the mechanism of action of molybdenum-and flavin-containing enzymes, and biological electron transfer.

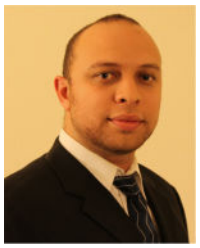

James Hall was born in Redlands, CA in 1985. He received a B.S. in Biochemistry from University of California, Riverside in 2007 and a M.S. in Biochemistry from University of California, Riverside in 2011. He is currently a Ph.D. student in the Biochemistry and Molecular Biology graduate program at the University of California, Riverside, where he is studying structure–function relationships in xanthine oxidase and related enzymes in the laboratory of Dr. Russ Hille.

Partha Basu grew up in West Bengal, India. He received his B.Sc. (Honors) in Chemistry and M.Sc in Inorganic Chemistry from Calcutta University, and a Ph.D. from Jadavpur University. He was a recipient of the Indian National Science Academy's Young Scientist award. After postdoctoral work at the University of Arizona, in 1998 he joined the faculty of Duquesne University, where he is now Professor of Chemistry and Biochemistry. His research interest is in metals in biology, specifically the role of metallobiomolecules in nitrate and arsenic metabolism. His group designs and develops new molecules for detailed kinetic, spectroscopic, and structural studies, as well as sensors of heavy metal ions.

References

1. (a) Derenzo EC, Heytler PG, Kaleita E. Arch Biochem Biophys. 1954; 49:242. [PubMed: 13139688] (b) Mahler HR, Mackler B, Green DE, Bock RM. J Biol Chem. 1954; 210:465. [PubMed: 13201608] (c) Nicholas DJD, Nason A, McElroy WD. J Biol Chem. 1954; 207:341. [PubMed: 13152109] (d) Cohen HJ, Fridovich I, Rajagopalan K. J Biol Chem. 1971; 246:374. [PubMed: 5100417] (e) Richert DA, Westerfeld WW. J Biol Chem. 1953; 203:915. [PubMed: 13084661]
2. (a) Cvetkovic A, Menon AL, Thorgersen MP, Scott JW, Poole FL II, Jenney FE Jr, Lancaster WA, Praissman JL, Shanmukh S, Vaccaro BJ, Trauger SA, Kalisiak E, Apon JV, Siuzdak G, Yannone SM, Tainer JA, Adams MWW. Nature. 2010; 466:779. [PubMed: 20639861] (b) Zhang Y, Gladyshev VN. J Biol Chem. 2011; 286:23623. [PubMed: 21566146] (c) Zhang Y, Rump S, Gladyshev VN. Coord Chem Rev. 2011; 255:1206. [PubMed: 22451726]
3. Hille R. Chem Rev. 1996; 96:2757. [PubMed: 11848841]
4. Johnson MK, Rees DC, Adams MWW. Chem Rev. 1996; 96:2817. [PubMed: 11848842]
5. Chan MK, Mukund S, Kletzin A, Adams MWW, Rees DC. Science. 1995; 267:1463. [PubMed: 7878465]

6. (a) Hille R. Trends Biochem Sci. 2002; 27:360. [PubMed: 12114025] (b) Hille, R. Molybdenum and Tungsten: Their Roles in Biological Processes. Vol. 39. CRC Press; New York: 2002.
7. (a) Magalon A, Fedor JG, Walburger A, Weiner JH. Coord Chem Rev. 2011; 255:1159.(b) Holm RH, Solomon EI, Majumdar A, Tenderholt A. Coord Chem Rev. 2011; 255:993.(c) Dobbek H. Coord Chem Rev. 2011; 255:1104.(d) Mendel RR, Schwarz G. Coord Chem Rev. 2011; 255:1145. (e) Leimkuehler S, Wuebbens MM, Rajagopalan KV. Coord Chem Rev. 2011; 255:1129. [PubMed: 21528011] (f) Metz S, Thiel W. Coord Chem Rev. 2011; 255:1085.(g) Kirk ML, McNaughton RL, Helton ME. Prog Inorg Chem. 2004; 52:111.(h) Basu P, Burgmayer SJN. Coord Chem Rev. 2011; 255:1016. [PubMed: 21607119] (i) Brondino CD, Rivas MG, Romao MJ, Moura JJG, Moura I. Acc Chem Res. 2006; 39:788. [PubMed: 17042479] (j) Brondino CD, Romao MJ, Moura I, Moura JJG. Curr Opin Chem Biol. 2006; 10:109. [PubMed: 16480912] (k) Pushie MJ, George GN. Coord Chem Rev. 2011; 255:1055.(l) Klein EL, Astashkin AV, Raitsimring AM, Enemark JH. Coord Chem Rev. 2013; 257:110. [PubMed: 23440026] (m) Enemark JH, Cooney JJA. Chem Rev. 2004; 104:1175. [PubMed: 14871153] (n) Zhang Y, Gladyshev VN. J Mol Biol. 2008; 379:881. [PubMed: 18485362] (o) Leimkuhler S, Wuebbens MM, Rajagopalan KV. Coord Chem Rev. 2011; 255:1129. [PubMed: 21528011] (p) Mendel RR. J Biol Chem. 2013; 288:13165. [PubMed: 23539623] (q) Iobbi-Nivol C, Leimkuhler S. Biochim Biophys Acta, Bioenerg. 2013; 1827:1086.
8. (a) Vey JL, Drennan CL. Chem Rev. 2011; 111:2487. [PubMed: 21370834] (b) Dowling DP, Vey JL, Croft AK, Drennan CL. Biochim Biophys Acta, Proteins Proteomics. 2012; 1824:1178.(c) Marsh ENG, Patterson DP, Li L. ChemBioChem. 2010; 11:604. [PubMed: 20191656]
9. Hanzelmann P, Schindelin H. Proc Natl Acad Sci USA. 2004; 101:12870. [PubMed: 15317939]
10. (a) Lees NS, Haenzelmann P, Hernandez HL, Subramanian S, Schindelin H, Johnson MK, Hoffman BM. J Am Chem Soc. 2009; 131:9184. [PubMed: 19566093] (b) Hanzelmann P, Schindelin H. Proc Natl Acad Sci USA. 2006; 103:6829. [PubMed: 16632608]
11. Hanzelmann P, Hernandez HL, Menzel C, Garcia-Serres R, Huynh BH, Johnson MK, Mendel RR, Schindelin H. J Biol Chem. 2004; 279:34721. [PubMed: 15180982]
12. (a) Wuebbens MM, Rajagopalan KV. J Biol Chem. 1995; 270:1082. [PubMed: 7836363] (b) Rieder C, Eisenreich W, O'Brien J, Richter G, Gotze E, Boyle P, Blanchard S, Bacher A, Simon H. Eur J Biochem. 1998; 255:24. [PubMed: 9692897]
13. (a) Mehta AP, Hanes JW, Abdelwahed SH, Hilmey DG, Hanzelmann P, Begley TP. Biochemistry. 2013; 52:1134. [PubMed: 23286307] (b) Mehta AP, Abdelwahed SH, Begley TP. J Am Chem Soc. 2013; 135:10883. [PubMed: 23848839]
14. Hover BM, Loksztejn A, Ribeiro AA, Yokoyama K. J Am Chem Soc. 2013; 135:7019. [PubMed: 23627491]
15. Wuebbens MM, Liu MTW, Rajagopalan KV, Schindelin H. Struct Folding Des. 2000; 8:709.
16. Kanaujia SP, Jeyakanthan J, Nakagawa N, Balasubramaniam S, Shinkai A, Kuramitsu S, Yokoyama S, Sekar K. Acta Crystallogr, Sect D: Biol Crystallogr. 2010; 66:821. [PubMed: 20606263]
17. Clinch K, Watt DK, Dixon RA, Baars SM, Gainsford GJ, Tiwari A, Schwarz G, Saotome Y, Storek M, Belaidi AA, Santamaria-Araujo JA. J Med Chem. 2013; 56:1730. [PubMed: 23384403]
18. (a) Rudolph MJ, Wuebbens MM, Rajagopalan KV, Schindelin H. Nat Struct Biol. 2001; 8:42. [PubMed: 11135669] (b) Rudolph MJ, Wuebbens MM, Turque O, Rajagopalan KV, Schindelin H. J Biol Chem. 2003; 278:14514. [PubMed: 12571227]
19. Daniels JN, Wuebbens MM, Rajagopalan KV, Schindelin H. Biochemistry. 2008; 47:615. [PubMed: 18092812]
20. Santamaria-Araujo JA, Wray V, Schwarz G. J Biol Inorg Chem. 2012; 17:113. [PubMed: 21877100]
21. (a) Pitterle DM, Rajagopalan KV. J Biol Chem. 1993; 268:13499. [PubMed: 8514782] (b) Gutzke G, Fischer B, Mendel RR, Schwarz G. J Biol Chem. 2001; 276:36268. [PubMed: 11459846]
22. Wuebbens MM, Rajagopalan KV. J Biol Chem. 2003; 278:14523. [PubMed: 12571226]
23. Leimkuhler S, Freuer A, Araujo JAS, Rajagopalan KV, Mendel RR. J Biol Chem. 2003; 278:26127. [PubMed: 12732628]
24. Zhang W, Urban A, Mihara H, Leimkuehler S, Kurihara T, Esaki N. J Biol Chem. 2010; 285:2302. [PubMed: 19946146]

25. Marelja Z, Stoecklein W, Nimtz M, Leimkuehler S. J Biol Chem. 2008; 283:25178. [PubMed: 18650437]
26. Zheng LM, White RH, Cash VL, Jack RF, Dean DR. Proc Natl Acad Sci USA. 1993; 90:2754. [PubMed: 8464885]
27. Cupp-Vickery JR, Urbina H, Vickery LE. J Mol Biol. 2003; 330:1049. [PubMed: 12860127]
28. (a) Lake MW, Wuebbens MM, Rajagopalan KV, Schindelin H. Nature. 2001; 414:325. [PubMed: 11713534] (b) Hochstrasser M. Nat Cell Biol. 2000; 2:E153. [PubMed: 10934491]
29. (a) Matthies A, Rajagopalan KV, Mendel RR, Leimkuhler S. Proc Natl Acad Sci USA. 2004; 101:5946. [PubMed: 15073332] (b) Matthies A, Nimtz M, Leimkuhler S. Biochemistry. 2005; 44:7912. [PubMed: 15910006]
30. Dahl J-U, Urban A, Bolte A, Sriyabhaya P, Donahue JL, Nimtz M, Larson TJ, Leimkuehler S. J Biol Chem. 2011; 286:35801. [PubMed: 21856748]
31. Schwarz G. Cell Mol Life Sci. 2005; 62:2792. [PubMed: 16261263]
32. Chowdhury MM, Dosche C, Lohmannsroben HG, Leimkuhler S. J Biol Chem. 2012; 287:17297. [PubMed: 22453920]
33. (a) Rees DC, Johnson E, Lewinson O. Nat Rev Mol Cell Biol. 2009; 10:218. [PubMed: 19234479] (b) Hollenstein K, Dawson RJP, Locher KP. Curr Opin Struct Biol. 2007; 17:412. [PubMed: 17723295]
34. Hollenstein K, Frei DC, Locher KP. Nature. 2007; 446:213. [PubMed: 17322901]
35. Lawson DM, Williams CE, White DJ, Choay AP, Mitchenall LA, Pau RN. J Chem Soc, Dalton Trans. 1997:3981.
36. Wagner UG, Stupperich E, Kratky C. Structure. 2000; 8:1127. [PubMed: 11080635]
37. Stallmeyer B, Nerlich A, Schiemann J, Brinkmann H, Mendel RR. Plant J. 1995; 8:751. [PubMed: 8528286]
38. (a) Stallmeyer B, Schwarz G, Schulze J, Nerlich A, Reiss J, Kirsch J, Mendel RR. Proc Natl Acad Sci USA. 1999; 96:1333. [PubMed: 9990024] (b) Smolinsky B, Eichler SA, Buchmeier S, Meier JC, Schwarz G. J Biol Chem. 2008; 283:17370. [PubMed: 18411266] (c) Feng GP, Tintrup H, Kirsch J, Nichol MC, Kuhse J, Betz H, Sanes JR. Science. 1998; 282:1321. [PubMed: 9812897]
39. (a) Llamas A, Mendel RR, Schwarz N. J Biol Chem. 2004; 279:55241. [PubMed: 15504727] (b) Llamas A, Otte T, Multhaup G, Mendel RR, Schwarz G. J Biol Chem. 2006; 281:18343. [PubMed: 16636046]
40. Liu MTW, Wuebbens MM, Rajagopalan KV, Schindelin H. J Biol Chem. 2000; 275:1814. [PubMed: 10636880]
41. Sola M, Kneussel M, Heck IS, Betz H, Weissenhorn W. J Biol Chem. 2001; 276:25294. [PubMed: 11325967]
42. (a) Kuper J, Llamas A, Hecht HJ, Mendel RR, Schwarz G. Nature. 2004; 430:803. [PubMed: 15306815] (b) Schwarz G, Schrader N, Mendel RR, Hecht HJ, Schindelin H. J Mol Biol. 2001; 312:405. [PubMed: 11554796]
43. Neumann M, Leimkuehler S. FEBS J. 2008; 275:5678. [PubMed: 18959753]
44. Morrison MS, Cobine PA, Hegg EL. J Biol Inorg Chem. 2007; 12:1129. [PubMed: 17687573]
45. (a) Leimkuhler S, Rajagopalan KV. J Biol Chem. 2001; 276:1837. [PubMed: 11042213] (b) Joshi MS, Johnson JL, Rajagopalan KV. J Bacteriol. 1996; 178:4310. [PubMed: 8763964]
46. Mendel RR, Alikulov ZA, Lvov NP, Muller A. J Mol Gen Genet. 1981; 181:395.
47. Schwarz G, Schulze J, Bittner F, Eilers T, Kuper J, Bollmann G, Nerlich A, Brinkmann H, Mendel RR. Plant Cell. 2000; 12:2455. [PubMed: 11148290]
48. (a) Xiang S, Nichols J, Rajagopalan KV, Schindelin H. Structure. 2001; 9:299. [PubMed: 11525167] (b) Schrag JD, Huang WJ, Sivaraman J, Smith C, Plamondon J, Larocque R, Matte A, Cygler M. J Mol Biol. 2001; 310:419. [PubMed: 11428898]
49. Kim EY, Schrader N, Smolinsky B, Bedet C, Vannier C, Schwarz G, Schindelin H. EMBO J. 2006; 25:1385. [PubMed: 16511563]
50. Belaidi AA, Schwarz G. Biochem J. 2013; 450:149. [PubMed: 23163752]
51. Rivers SL, McNairn E, Blasco F, Giordano G, Boxer DH. Mol Microbiol. 1993; 8:1071. [PubMed: 8361352]

52. Anderson LA, McNairn E, Leubke T, Pau RN, Boxer DH. J Bacteriol. 2000; 182:7035. [PubMed: 11092866]
53. McNicholas PM, Chiang RC, Gunsalus RP. Mol Microbiol. 1998; 27:197. [PubMed: 9466267]
54. (a) Hall DR, Gourley DG, Duke EMH, Leonard GA, Anderson LA, Pau RN, Boxer DH, Hunter WN. Acta Crystallogr, Sect D: Biol Crystallogr. 1999; 55:542. [PubMed: 10089372] (b) Gourley DG, Schuttelkopf AW, Anderson LA, Price NC, Boxer DH, Hunter WN. J Biol Chem. 2001; 276:20641. [PubMed: 11259434] (c) Schuttelkopf AW, Boxer DH, Hunter WN. J Mol Biol. 2003; 326:761. [PubMed: 12581638] (d) Anderson LA, Palmer T, Price NC, Bornemann S, Boxer DH, Pau RN. Eur J Biochem. 1997; 246:119. [PubMed: 9210473]
55. Self WT, Grunden AM, Hasona A, Shanmugam KT. Microbiology-UK. 1999; 145:41.
56. Grunden AM, Ray RM, Rosentel JK, Healy FG, Shanmugam KT. J Bacteriol. 1996; 178:735. [PubMed: 8550508]
57. Schuttelkopf AW, Harrison JA, Boxer DH, Hunter WN. J Biol Chem. 2002; 277:15013. [PubMed: 11836258]
58. (a) Constantinidou C, Hobman JL, Griffiths L, Patel MD, Penn CW, Cole JA, Overton TW. J Biol Chem. 2006; 281:4802. [PubMed: 16377617] (b) Green J, Crack JC, Thomson AJ, LeBrun NE. Curr Opin Microbiol. 2009; 12:145. [PubMed: 19246238] (c) Unden G, Achebach S, Holighaus G, Tran HQ, Wackwitz B, Zeuner Y. J Mol Microbiol Biotechnol. 2002; 4:263. [PubMed: 11931557]
59. Korner H, Sofia HJ, Zumft WG. FEMS Microbiol Rev. 2003; 27:559. [PubMed: 14638413]
60. (a) Crack J, Green J, Thomson AJ. J Biol Chem. 2004; 279:9278. [PubMed: 14645253] (b) Mettert EL, Kiley PJ. J Bacteriol. 2007; 189:3036. [PubMed: 17293415]
61. Serganov A, Patel DJ. Biochim Biophys Acta, Gene Regul Mech. 2009; 1789:592.
62. Weinberg Z, Barrick JE, Yao Z, Roth A, Kim JN, Gore J, Wang JX, Lee ER, Block KF, Sudarsan N, Neph S, Tompa M, Ruzzo WL, Breaker RR. Nucleic Acids Res. 2007; 35:4809. [PubMed: 17621584]
63. Regulski EE, Moy RH, Weinberg Z, Barrick JE, Yao Z, Ruzzo WL, Breaker RR. Mol Microbiol. 2008; 68:918. [PubMed: 18363797]
64. (a) Johnson JL, Jones HP, Rajagopalan KV. J Biol Chem. 1977; 252:4994. [PubMed: 873926] (b) Amy NK, Rajagopalan KV. J Bacteriol. 1979; 140:114. [PubMed: 387715] (c) Johnson JL, Hainline BE, Rajagopalan KV. J Biol Chem. 1980; 255:1783. [PubMed: 6892571]
65. (a) Witte CP, Igeno MI, Mendel R, Schwarz G, Fernandez E. FEBS Lett. 1998; 431:205. [PubMed: 9708903] (b) Ataya FS, Witte CP, Galvan A, Igeno MI, Fernandez E. J Biol Chem. 2003; 278:10885. [PubMed: 12519777]
66. Fisher K, Llamas A, Tejada-Jimenez M, Schrader N, Kuper J, Ataya FS, Galvan A, Mendel RR, Fernandez E, Schwarz G. J Biol Chem. 2006; 281:30186. [PubMed: 16873364]
67. Kruse T, Gehl C, Geisler M, Lehrke M, Ringel P, Hallier S, Haensch R, Mendel RR. J Biol Chem. 2010; 285:6623. [PubMed: 20040598]
68. Jeon WB, Allard STM, Bingman CA, Bitto E, Han BW, Wesenberg GE, Phillips GN. Proteins: Struct, Funct, Bioinf. 2006; 65:1051.
69. (a) Gehl C, Waadt R, Kudla J, Mendel RR, Hansch R. Mol Plant. 2009; 2:1051. [PubMed: 19825679] (b) Lardi-Studler B, Smolinsky B, Petitjean CM, Koenig F, Sidler C, Meier JC, Fritschy JM, Schwarz G. J Cell Sci. 2007; 120:1371. [PubMed: 17374639] (c) Mendel RR. BioFactors. 2009; 35:429. [PubMed: 19623604]
70. Teschner J, Lachmann N, Schulze J, Geisler M, Selbach K, Santamaria-Araujo J, Balk J, Mendel RR, Bittner F. Plant Cell. 2010; 22:468. [PubMed: 20164445]
71. Marelja Z, Chowdhury MM, Dosche C, Hille C, Baumann O, Lohmannsroben HG, Leimkuhler S. PLoS One. 2013; 8:e60869. [PubMed: 23593335]
72. Fischer K, Llamas A, Tejada-Jimenez M, Schrader N, Kuper J, Ataya FS, Galvan A, Mendel RR, Fernandez E, Schwarz G. J Biol Chem. 2006; 281:30186. [PubMed: 16873364]
73. (a) Johnson JL, Bastian NR, Rajagopalan KV. Proc Natl Acad Sci USA. 1990; 87:3190. [PubMed: 2326278] (b) Borner G, Karrasch M, Thauer RK. FEBS Lett. 1991; 290:31. [PubMed: 1915887]
74. Loschi L, Brokx SJ, Hills TL, Zhang G, Bertero MG, Lovering AL, Weiner JH, Strynadka NCJ. J Biol Chem. 2004; 279:50391. [PubMed: 15355966]

75. (a) Xi HL, Schneider BL, Reitzer L. J Bacteriol. 2000; 182:5332. [PubMed: 10986234] (b) Kozmin SG, Schaaper RM. Mutat Res, Fundam Mol Mech Mutagen. 2007; 619:9.(c) Neumann M, Mittelstadt G, Iobbi-Nivol C, Saggu M, Lendzian F, Hildebrandt P, Leimkuhler S. FEBS J. 2009; 276:2762. [PubMed: 19368556]

76. (a) Palmer T, Goodfellow IPG, Sockett RE, McEwan AG, Boxer DH. Biochim Biophys Acta, Gene Struct Expression. 1998; 1395:135.(b) Palmer T, Santini CL, IobbiNivol C, Eaves DJ, Boxer DH, Giordano G. Mol Microbiol. 1996; 20:875. [PubMed: 8793883] (c) Guse A, Stevenson CEM, Kuper J, Buchanan G, Schwarz G, Giordano G, Magalon A, Mendel RR, Lawson DM, Palmer T. J Biol Chem. 2003; 278:25302. [PubMed: 12719427]

77. Neumann M, Mittelstaedt G, Seduk F, Iobbi-Nivol C, Leimkuehler S. J Biol Chem. 2009; 284:21891. [PubMed: 19542235]

78. Neumann M, Stocklein W, Leimkuhler S. J Biol Chem. 2007; 282:28493. [PubMed: 17686778]

79. (a) Lake MW, Temple CA, Rajagopalan KV, Schindelin H. J Biol Chem. 2000; 275:40211. [PubMed: 10978347] (b) Stevenson CEM, Sargent F, Buchanan G, Palmer T, Lawson DM. Structure. 2000; 8:1115. [PubMed: 11080634]

80. Neumann M, Seduk F, Iobbi-Nivol C, Leimkuehler S. J Biol Chem. 2011; 286:1400. [PubMed: 21081498]

81. Vergnes A, Gouffi-Belhabich K, Blasco F, Giordano G, Magalon A. J Biol Chem. 2004; 279:41398. [PubMed: 15247236]

82. Temple CA, Rajagopalan KV. J Biol Chem. 2000; 275:40202. [PubMed: 10978348]

83. (a) Johnson JL, Indermaur LW, Rajagopalan KV. J Biol Chem. 1991; 266:12140. [PubMed: 1648082] (b) McLuskey K, Harrison JA, Schuttelkopf AW, Boxer DH, Hunter WN. J Biol Chem. 2003; 278:23706. [PubMed: 12682065]

84. Reschke S, Sigfridsson KGV, Kaufmann P, Leidel N, Horn S, Gast K, Schulzke C, Haumann M, Leimkuhler S. J Biol Chem. 2013; 288:29736. [PubMed: 24003231]

85. (a) Genest O, Mejean V, Iobbi-Nivol C. FEMS Microbiol Lett. 2009; 297:1. [PubMed: 19519768] (b) Iobbi-Nivol C, Leimkuhler S. Biochim Biophys Acta. 2013; 1827:1086. [PubMed: 23201473]

86. Palmer T, Berks BC. Nat Rev Microbiol. 2012; 10:483. [PubMed: 22683878]

87. (a) Vergnes A, Pommier J, Toci R, Blasco F, Giordano G, Magalon A. J Biol Chem. 2006; 281:2170. [PubMed: 16286471] (b) Genest O, Neumann M, Seduk F, Stocklein W, Mejean V, Leimkuhler S, Iobbi-Nivol C. J Biol Chem. 2008; 283:21433. [PubMed: 18522945] (c) Hatzixanthis K, Clarke TA, Oubrie A, Richardson DJ, Turner RJ, Sargent F. Proc Natl Acad Sci USA. 2005; 102:8460. [PubMed: 15941830]

88. (a) Kirillova O, Chruszcz M, Shumilin IA, Skarina T, Gorodichtchenskaia E, Cymborowski M, Savchenko A, Edwards A, Minor W. Acta Crystallogr, Sect D: Biol Crystallogr. 2007; 63:348. [PubMed: 17327672] (b) Stevens CM, Winstone TML, Turner RJ, Paetzel M. J Mol Biol. 2009; 389:124. [PubMed: 19361518] (c) Tranier S, Iobbi-Nivol C, Birck C, Ilbert M, Mortier-Barriere I, Mejean V, Samama JP. Structure. 2003; 11:165. [PubMed: 12575936] (d) Maillard J, Spronk CAEM, Buchanan G, Lyall V, Richardson DJ, Palmer T, Vuister GW, Sargent F. Proc Natl Acad Sci USA. 2007; 104:15641. [PubMed: 17901208]

89. (a) Bordas J, Bray RC, Garner CD, Gutteridge S, Hasnain SS. J Inorg Biochem. 1979; 11:181. [PubMed: 501352] (b) Bordas J, Bray RC, Garner CD, Gutteridge S, Hasnain SS. Biochem J. 1980; 191:499. [PubMed: 6894537] (c) Massey V, Edmondso D. J Biol Chem. 1970; 245:6595. [PubMed: 5536559]

90. Leimkuhler S, Kern M, Solomon PS, McEwan AG, Schwarz G, Mendel RR, Klipp W. Mol Microbiol. 1998; 27:853. [PubMed: 9515710]

91. (a) Neumann M, Stocklein W, Walburger A, Magalon A, Leimkuhler S. Biochemistry. 2007; 46:9586. [PubMed: 17649978] (b) Leimkuhler S, Angermuller S, Schwarz G, Mendel RR, Klipp W. J Bacteriol. 1999; 181:5930. [PubMed: 10498704] (c) Neumann M, Schulte M, Junemann N, Stocklein W, Leimkuhler S. J Biol Chem. 2006; 281:15701. [PubMed: 16597619]

92. Neumann M, Leimkuhler S. Biochem Res Int. 2011; 2011:13.

93. Lima CD. J Mol Biol. 2002; 315:1199. [PubMed: 11827487]

94. (a) Watanabe T, Ihara N, Itoh T, Fujita T, Sugimoto Y. J Biol Chem. 2000; 275:21789. [PubMed: 10801779] (b) Komoto N, Sezutsu H, Yukuhiro K, Banno Y, Fujii H. Insect Biochem Mol Biol.

2003; 33:417. [PubMed: 12650690] (c) Bittner F, Oreb M, Mendel RR. J Biol Chem. 2001; 276:40381. [PubMed: 11553608] (d) Sagi M, Scazzocchio C, Fluhr R. Plant J. 2002; 31:305. [PubMed: 12164810] (e) Scazzocc C, Holl FB, Foguelma A. Eur J Biochem. 1973; 36:428. [PubMed: 4581274] (f) Scazzocc C. Mol Gen Genet. 1973; 125:147. [PubMed: 4149466] (g) Warner CK, Finnerty V. Mol Gen Genet. 1981; 184:92. [PubMed: 6950197]

95. Ichida K, Matsumura T, Sakuma R, Hosoya T, Nishino T. Biochem Biophys Res Commun. 2001; 282:1194. [PubMed: 11302742]
96. Schwarz G, Mendel RR, Ribbe MW. Nature. 2009; 460:839. [PubMed: 19675644]
97. Schrader N, Fischer K, Theis K, Mendel RR, Schwarz G, Kisker C. Structure. 2003; 11:1251. [PubMed: 14527393]
98. Ringel P, Krausze J, van den Heuvel J, Curth U, Pierik AJ, Herzog S, Mendel RR, Kruse T. J Biol Chem. 2013; 288:14657. [PubMed: 23539622]
99. Schindelin H, Kisker C, Hilton J, Rajagopalan KV, Rees DC. Science. 1996; 272:1615. [PubMed: 8658134]
100. (a) Leimkuhler S, Klipp W. J Bacteriol. 1999; 181:2745. [PubMed: 10217763] (b) Schumann S, Saggu M, Moller N, Anker SD, Lendzian F, Hildebrandt P, Leimkuhler S. J Biol Chem. 2008; 283:16602. [PubMed: 18390908]
101. (a) Schwartz SH, LeonKloosterziel KM, Koornneef M, Zeevaart JAD. Plant Physiol. 1997; 114:161. [PubMed: 9159947] (b) Wollers S, Heidenreich T, Zarepour M, Zachmann D, Kraft C, Zhao YD, Mendel RR, Bittner F. J Biol Chem. 2008; 283:9642. [PubMed: 18258600]
102. Hille R, Nishino T, Bittner F. Coord Chem Rev. 2011; 255:1179. [PubMed: 21516203]
103. Dobbek H, Gremer L, Meyer O, Huber R. Proc Natl Acad Sci USA. 1999; 96:8884. [PubMed: 10430865]
104. Dixon M, Thurlow S. Biochem J. 1924; 18:976. [PubMed: 16743383]
105. Montero-Moran GM, Li M, Rendon-Huerta E, Jourdan F, Lowe DJ, Stumpff-Kane AW, Feig M, Scazzocchio C, Hausinger RP. Biochemistry. 2007; 46:5293. [PubMed: 17429948]
106. (a) Pope SD, Chen L-L, Stewart V. J Bacteriol. 2009; 191:1006. [PubMed: 19060149] (b) de la Riva L, Badia J, Aguilar J, Bender RA, Baldoma L. J Bacteriol. 2008; 190:7892. [PubMed: 18849434]
107. Santiago B, Schubel U, Egelseer C, Meyer O. Gene. 1999; 236:115. [PubMed: 10433972]
108. Enroth C, Eger BT, Okamoto K, Nishino T, Pai EF. Proc Natl Acad Sci USA. 2000; 97:10723. [PubMed: 11005854]
109. Romao MJ, Archer M, Moura I, Moura JJG, Legall J, Engh R, Schneider M, Hof P, Huber R. Science. 1995; 270:1170. [PubMed: 7502041]
110. Ormejohn W, Beinert H. Biochem Biophys Res Commun. 1969; 36:337. [PubMed: 4309781]
111. Hille R, Hagen WR, Dunham WR. J Biol Chem. 1985; 260:569.
112. Iwasaki T, Okamoto K, Nishino T, Mizushima J, Hori H. J Biochem. 2000; 127:771. [PubMed: 10788785]
113. (a) Lowe DJ, Bray RC. Biochem J. 1978; 169:471. [PubMed: 25647] (b) Coffman RE, Buettner GR. J Phys Chem. 1979; 83:2392.
114. Romao MJ, Hubert R. Biochem Soc Trans. 1997; 25:755. [PubMed: 9388539]
115. Jones RM, Inscore FE, Hille R, Kirk ML. Inorg Chem. 1999; 38:4963. [PubMed: 11671238]
116. Dobbek H, Gremer L, Kiefersauer R, Huber R, Meyer O. Proc Natl Acad Sci USA. 2002; 99:15971. [PubMed: 12475995]
117. Bonin I, Martins BM, Purvanov V, Fetzner S, Huber R, Dobbek H. Structure. 2004; 12:1425. [PubMed: 15296736]
118. Okamoto K, Matsumoto K, Hille R, Eger BT, Pai EF, Nishino T. Proc Natl Acad Sci USA. 2004; 101:7931. [PubMed: 15148401]
119. Doonan CJ, Stockert A, Hille R, George GN. J Am Chem Soc. 2005; 127:4518. [PubMed: 15783235]
120. Xia M, Dempski R, Hille R. J Biol Chem. 1999; 274:3323. [PubMed: 9920873]
121. Murray KN, Watson JG, Chaykin S. J Biol Chem. 1966; 241:4798. [PubMed: 4224474]

122. Hille R, Sprecher H. J Biol Chem. 1987; 262:10914. [PubMed: 3611096]
123. Greenwood RJ, Wilson GL, Pilbrow JR, Wedd AG. J Am Chem Soc. 1993; 115:5385.
124. Albert A, Brown DJ. J Chem Soc. 1954:2060.
125. Kim JH, Ryan MG, Knaut H, Hille R. J Biol Chem. 1996; 271:6771. [PubMed: 8636099]
126. Huber R, Hof P, Duarte RO, Moura JJG, Moura I, Liu MY, LeGall J, Hille R, Archer M, Romao M. J Proc Natl Acad Sci USA. 1996; 93:8846.
127. Skibo EB, Gilchrist JH, Lee CH. Biochemistry. 1987; 26:3032. [PubMed: 3607009]
128. Gutteridge S, Tanner SJ, Bray RC. Biochem J. 1978; 175:869. [PubMed: 217353]
129. McWhirter RB, Hille R. J Biol Chem. 1991; 266:23724. [PubMed: 1660883]
130. Tanner SJ, Bray RC, Bergmann F. Biochem Soc Trans. 1978; 6:1328. [PubMed: 217783]
131. Page CC, Moser CC, Chen XX, Dutton PL. Nature. 1999; 402:47. [PubMed: 10573417]
132. Stockert AL, Shinde SS, Anderson RF, Hille R. J Am Chem Soc. 2002; 124:14554. [PubMed: 12465963]
133. Lorigan GA, Britt RD, Kim JH, Hille R. Biochim Biophys Acta, Bioenerg. 1994; 1185:284.
134. Howes BD, Bray RC, Richards RL, Turner NA, Bennett B, Lowe DJ. Biochemistry. 1996; 35:1432. [PubMed: 8634273]
135. Manikandan P, Choi EY, Hille R, Hoffman BM. J Am Chem Soc. 2001; 123:2658. [PubMed: 11456936]
136. Pauff JM, Zhang J, Bell CE, Hille R. J Biol Chem. 2008; 283:4818. [PubMed: 18063585]
137. (a) Palmer G, Bray RC, Beinert H. J Biol Chem. 1964; 239:2657. [PubMed: 14235550] (b) Bray RC, Vanngard T. Biochem J. 1969; 114:725. [PubMed: 4310055]
138. (a) Bray RC, Palmer G, Beinert H. J Biol Chem. 1964; 239:2667. [PubMed: 14235551] (b) Edmondso D, Ballou D, Vanheuve A, Palmer G, Massey V. J Biol Chem. 1973; 248:6135. [PubMed: 4353632]
139. Hille R, Kim JH, Hemann C. Biochemistry. 1993; 32:3973. [PubMed: 8385992]
140. Mondal MS, Mitra S. Biochemistry. 1994; 33:10305. [PubMed: 8068667]
141. Dardenne SC, Edmondson DE. Biochemistry. 1990; 29:9046. [PubMed: 2271576]
142. Voityuk AA, Albert K, Romao MJ, Huber R, Rosch N. Inorg Chem. 1998; 37:176.
143. (a) Ilich P, Hille RJ. Phys Chem B. 1999; 103:5406.(b) Morpeth FF, George GN, Bray RC. Biochem J. 1984; 220:235. [PubMed: 6331408]
144. Howes BD, Bennett B, Bray RC, Richards RL, Lowe DJ. J Am Chem Soc. 1994; 116:11624.
145. (a) Ilich P, Hille RJ. Am Chem Soc. 2002; 124:6796.(b) Wagener N, Pierik AJ, Ibdah A, Hille R, Dobbek H. Proc Natl Acad Sci USA. 2009; 106:11055. [PubMed: 19549881]
146. (a) McNaughton RL, Helton ME, Cosper MM, Enemark JH, Kirk ML. Inorg Chem. 2004; 43:1625. [PubMed: 14989655] (b) Doonan CJ, Rubie ND, Peariso K, Harris HH, Knottenbelt SZ, George GN, Young CG, Kirk ML. J Am Chem Soc. 2008; 130:55. [PubMed: 18062689]
147. (a) Zhang XH, Wu YD. Inorg Chem. 2005; 44:1466. [PubMed: 15732988] (b) Amano T, Ochi N, Sato H, Sakaki S. J Am Chem Soc. 2007; 129:8131. [PubMed: 17564439]
148. Bayse CA. Dalton Trans. 2009:2306. [PubMed: 19290363]
149. Yamaguchi Y, Matsumura T, Ichida K, Okamoto K, Nishino T. J Biochem. 2007; 141:513. [PubMed: 17301077]
150. (a) Metz S, Thiel W. J Am Chem Soc. 2009; 131:14885. [PubMed: 19788181] (b) Metz S, Thiel W. J Phys Chem B. 2010; 114:1506. [PubMed: 20050623]
151. Pauff JM, Cao H, Hille R. J Biol Chem. 2009; 284:8751.
152. Sempombe J, Stein B, Kirk ML. Inorg Chem. 2011; 50:10919. [PubMed: 21972782]
153. Truglio JJ, Theis K, Leimkuhler S, Rappa R, Rajagopalan KV, Kisker C. Structure. 2002; 10:115. [PubMed: 11796116]
154. Leimkuhler S, Stockert AL, Igarashi K, Nishino T, Hille R. J Biol Chem. 2004; 279:40437. [PubMed: 15265866]
155. Ilich P, Hille R. Inorg Chim Acta. 1997; 263:87.

156. Pauff JM, Hemann CF, Juenemann N, Leimkuehler S, Hille R. J Biol Chem. 2007; 282:12785. [PubMed: 17327224]
157. Pauff JM, Hille R. J Nat Prod. 2009; 72:725. [PubMed: 19388706]
158. Dietzel U, Kuper J, Doebbler JA, Schulte A, Truglio JJ, Leimkuhler S, Kisker C. J Biol Chem. 2009; 284:8759.
159. Nishino T, Okamoto K, Eger BT, Pai EF. FEBS J. 2008; 275:3278. [PubMed: 18513323]
160. Okamoto K, Kawaguchi Y, Eger BT, Pai EF, Nishino T. J Am Chem Soc. 2010; 132:17080. [PubMed: 21077683]
161. Cao H, Pauff JM, Hille R. J Biol Chem. 2010; 285:28044. [PubMed: 20615869]
162. Pick FM, McGartol M, Bray RC. Eur J Biochem. 1971; 18:65. [PubMed: 4322209]
163. Tanner SJ, Bray RC. Biochem Soc Trans. 1978; 6:1333. [PubMed: 217784]
164. Lowe DJ, Barber MJ, Pawlik RT, Bray RC. Biochem J. 1976; 155:81. [PubMed: 180983]
165. Williams JW, Bray RC. Biochem J. 1981; 195:753. [PubMed: 6274312]
166. (a) Hille R, Stewart RC, Fee JA, Massey V. J Biol Chem. 1983; 258:4849. [PubMed: 6300101] (b) George GN, Bray RC. Biochemistry. 1983; 22:1013. [PubMed: 6301534] (c) Barber MJ, Siegel LM. Biochemistry. 1983; 22:618. [PubMed: 6301524]
167. Shanmugam M, Zhang B, McNaughton RL, Kinney RA, Hille R, Hoffman BM. J Am Chem Soc. 2010; 132:14015. [PubMed: 20860357]
168. (a) Stiefel EI, Newton WE, Pariyadath NJ. Less-Common Met. 1977; 54:513.(b) Miller GA, McClung RED. Inorg Chem. 1973; 12:2552.
169. Boer DR, Thapper A, Brondino CD, Romao MJ, Moura JJG. J Am Chem Soc. 2004; 126:8614. [PubMed: 15250689]
170. Cramer SP, Hille R. J Am Chem Soc. 1985; 107:8164.
171. Olson JS, Ballou DP, Palmer G, Massey V. J Biol Chem. 1974; 249:4363. [PubMed: 4367215]
172. (a) Hille R, Massey V. J Biol Chem. 1986; 261:1241. [PubMed: 3753700] (b) Hille R. Biochemistry. 1991; 30:8522. [PubMed: 1888720]
173. (a) Hille R, Anderson RF. J Biol Chem. 1991; 266:5608. [PubMed: 2005100] (b) Hille R, Anderson RF. J Biol Chem. 2001; 276:31193. [PubMed: 11395485]
174. Lim LW, Shamala N, Mathews FS, Steenkamp DJ, Hamlin R, Xuong NH. J Biol Chem. 1986; 261:5140.
175. Rohlfs RJ, Huang LX, Hille R. J Biol Chem. 1995; 270:22196. [PubMed: 7673198]
176. (a) Hille R, Massey V. J Biol Chem. 1981; 256:9090. [PubMed: 6894924] (b) Porras AG, Olson JS, Palmer G. J Biol Chem. 1981; 256:9096.
177. Olson JS, Ballou DP, Palmer G, Massey V. J Biol Chem. 1974; 249:4350. [PubMed: 4367214]
178. Hitzert MM, Bos AF, Bergman KA, Veldman A, Schwarz G, Santamaria-Araujo JA, Heiner-Fokkema R, Sival DA, Lunsing RJ, Arjune S, Kosterink JGW, van Spronsen FJ. Pediatrics. 2012; 130:E1005. [PubMed: 22987873]
179. (a) Dellacor E, Stirpe F. Biochem J. 1972; 126:739. [PubMed: 4342395] (b) Stirpe F, Dellacor E. J Biol Chem. 1969; 244:3855. [PubMed: 4308738] (c) Battelli MG, Lorenzon E, Stirpe F. Biochem J. 1973; 131:191. [PubMed: 4352904] (d) Waud WR, Rajagopalan KV. Arch Biochem Biophys. 1976; 172:365. [PubMed: 176940] (e) Nakamura M, Yamazaki I. J Biochem. 1982; 92:1279. [PubMed: 6959993]
180. Nishino T, Okamoto K, Kawaguchi Y, Hori H, Matsumura T, Eger BT, Pai EF. J Biol Chem. 2005; 280:24888. [PubMed: 15878860]
181. (a) Hille R, Nishino T. FASEB J. 1995; 9:995. [PubMed: 7649415] (b) McCord JM. N Engl J Med. 1985; 312:159. [PubMed: 2981404] (c) Berry CE, Hare JM. J Physiol (Oxford, UK). 2004; 555:589.
182. (a) Harris CM, Massey V. Flavins and Flavoproteins. 1993; 1994:723.(b) Nishino T, Schopfer LM, Massey V. J Biol Chem. 1989; 264:2518. [PubMed: 2914919] (c) Schopfer LM, Massey V, Nishino T. J Biol Chem. 1988; 263:13528. [PubMed: 3166459] (d) Turner NA, Doyle WA, Ventom AM, Bray RC. Eur J Biochem. 1995; 232:646. [PubMed: 7556219]
183. Vorbach C, Scriven A, Capecchi MR. Genes Dev. 2002; 16:3223. [PubMed: 12502743]

184. Godber BLJ, Doel JJ, Sapkota GP, Blake DR, Stevens CR, Eisenthal R, Harrison R. J Biol Chem. 2000; 275:7757. [PubMed: 10713088]

185. (a) Godber BLJ, Doel JJ, Goult TA, Eisenthal R, Harrison R. Biochem J. 2001; 358:325. [PubMed: 11513730] (b) Ichimori K, Fukahori M, Nakazawa H, Okamoto K, Nishino T. J Biol Chem. 1999; 274:7763. [PubMed: 10075667] (c) Li HT, Samouilov A, Liu XP, Zweier JL. J Biol Chem. 2001; 276:24482. [PubMed: 11312267]

186. Li HT, Samouilov A, Liu XQ, Zweier JL. Biochemistry. 2003; 42:1150. [PubMed: 12549937]

187. Li HT, Samouilov A, Liu XP, Zweier JL. J Biol Chem. 2004; 279:16939. [PubMed: 14766900]

188. (a) Bueno M, Wang J, Mora AL, Gladwin MT. Antioxid Redox Signaling. 2013; 18:1797.(b) Raedschelders K, Ansley DM, Chen DDY. Pharmacol Ther. 2012; 133:230. [PubMed: 22138603]

189. Elion GB. Science. 1989; 244:41. [PubMed: 2649979]

190. (a) Henderson J, Khoo MKY. J Biol Chem. 1965; 240:3104. [PubMed: 14342339] (b) Caskey CT, Wynagaar J, Ashton DM. J Biol Chem. 1964; 239:2570. [PubMed: 14235537]

191. (a) Elion GB, Singer S, Hitchings GH. J Biol Chem. 1954; 208:477. [PubMed: 13174557] (b) Massey V, Komai H, Palmer G, Elion GB. J Biol Chem. 1970; 245:2837. [PubMed: 5467924]

192. Okamoto K, Eger BT, Nishino T, Kondo S, Pai EF. J Biol Chem. 2003; 278:1848. [PubMed: 12421831]

193. Fukunari A, Okamoto K, Nishino T, Eger BT, Pai EF, Kamezawa M, Yamada I, Kato N. J Pharmacol Exp Ther. 2004; 311:519. [PubMed: 15190124]

194. Matsumoto K, Okamoto K, Ashizawa N, Nishino T. J Pharmacol Exp Ther. 2011; 336:95. [PubMed: 20952484]

195. Kikuchi H, Fujisaki H, Furuta T, Okamoto K, Leimkuhler S, Nishino T. Sci Rep. 2012; 2:331. [PubMed: 22448318]

196. Santos-Silva T, Ferroni F, Thapper A, Marangon J, Gonzalez PJ, Rizzi AC, Moura I, Moura JJG, Romao MJ, Brondino CD. J Am Chem Soc. 2009; 131:7990. [PubMed: 19459677]

197. Cao H, Hall J, Hille R. J Am Chem Soc. 2011; 133:12414. [PubMed: 21761899]

198. More C, Asso M, Roger G, Guigliarelli B, Caldeira J, Moura J, Bertrand P. Biochemistry. 2005; 44:11628. [PubMed: 16114900]

199. Neumann M, Mittelstadt G, Seduk F, Iobbi-Nivol C, Leimkuhler S. J Biol Chem. 2009; 284:21891. [PubMed: 19542235]

200. Badalyan A, Neumann-Schaal M, Leimkuhler S, Wollenberger U. Electroanalysis. 2013; 25:101.

201. (a) Rajagopalan KV, Handler P. J Biol Chem. 1964; 239:2027. [PubMed: 14213393] (b) Felsted RL, Chu AEY, Chaykin S. J Biol Chem. 1973; 248:2580. [PubMed: 4698232]

202. Huang DY, Furukawa A, Ichikawa Y. Arch Biochem Biophys. 1999; 364:264. [PubMed: 10190983]

203. (a) Yamamoto T, Moriwaki Y, Takahashi S, Tsutsumi Z, Tuneyoshi K, Matsui K, Cheng JD, Hada T. Metab, Clin Exp. 2003; 52:1501. [PubMed: 14624414] (b) Peretz H, Naamati MS, Levartovsky D, Lagziel A, Shani E, Horn I, Shalev H, Landau D. Mol Genet Metab. 2007; 91:23. [PubMed: 17368066]

204. Terao M, Kurosaki M, Barzago MM, Fratelli M, Bagnati R, Bastone A, Giudice C, Scanziani E, Mancuso A, Tiveron C, Garattini E. Mol Cell Biol. 2009; 29:357. [PubMed: 18981221]

205. Sigruener A, Buechler C, Orso E, Hartmann A, Wild PJ, Terracciano L, Roncalli M, Bornstein SR, Schmitz G. Horm Metab Res. 2007; 39:781. [PubMed: 17992631]

206. (a) Rajagopalan KV, Handler P, Fridovich I. J Biol Chem. 1962; 237:922. [PubMed: 14489970] (b) Rajagopalan KV, Handler P. J Biol Chem. 1964; 239:2022. [PubMed: 14213392] (c) Barber MJ, Coughlan MP, Rajagopalan KV, Siegel LM. Biochemistry. 1982; 21:3561. [PubMed: 6288079] (d) Branzoli U, Massey V. J Biol Chem. 1974; 249:4339.(e) Hall WW, Krenitsky TA. Arch Biochem Biophys. 1986; 251:36. [PubMed: 3789740] (f) Krenitsky TA. Biochem Pharmacol. 1978; 27:2763. [PubMed: 736972] (g) Rajagopa, Kv; Handler, P.; Palmer, G.; Beinert, H. J Biol Chem. 1968; 243:3784. [PubMed: 4298512] (h) Rajagopa, Kv; Handler, P.; Palmer, G.; Beinert, H. J Biol Chem. 1968; 243:3797. [PubMed: 4298513]

207. Bray RC, George GN, Gutteridge S, Norlander L, Stell JGP, Stubley C. Biochem J. 1982; 203:263. [PubMed: 6285895]

208. Li Calzi M, Raviolo C, Ghibaudi E, De Gioia L, Salmona M, Cazzaniga G, Kurosaki M, Terao M, Garattini E. J Biol Chem. 1995; 270:31037. [PubMed: 8537361]

209. Terao M, Kurosaki M, Demontis S, Zanotta S, Garattini E. Biochem J. 1998; 332:383. [PubMed: 9601067]

210. Wright RM, Clayton DK, Riley MG, McManaman JL, Repine JE. J Biol Chem. 1999; 274:3878. [PubMed: 9920943]

211. (a) Terao M, Kurosaki M, Saltini G, Demontis S, Marini M, Salmona M, Garattini E. J Biol Chem. 2000; 275:30690. [PubMed: 10893244] (b) Terao M, Kurosaki M, Marini M, Vanoni MA, Saltini G, Bonetto V, Bastone A, Federico C, Saccone S, Fanelli R, Salmona M, Garattini E. J Biol Chem. 2001; 276:46347. [PubMed: 11562361]

212. (a) Garattini E, Fratelli M, Terao M. Cell Mol Life Sci. 2008; 65:1019. [PubMed: 18066686] (b) Garattini E, Mendel R, Romao MJ, Wright R, Terao M. Biochem J. 2003; 372:15. [PubMed: 12578558]

213. Schumann S, Terao M, Garattini E, Saggu M, Lendzian F, Hildebrandt P, Leimkuhler S. PLoS One. 2009; 4:e5348. [PubMed: 19401776]

214. Pauff JM, Hemann CF, Junemann N, Leimkuhler S, Hille R. J Biol Chem. 2007; 282:12785. [PubMed: 17327224]

215. Coelho C, Mahro M, Trincao J, Carvalho ATP, Ramos MJ, Terao M, Garattini E, Leimkuhler S, Romao MJ. J Biol Chem. 2012; 287:40690. [PubMed: 23019336]

216. Nishino T. J Biol Chem. 1989; 264:5468. [PubMed: 2925614]

217. Torres RA, Korzekwa KR, McMasters DR, Fandozzi CM, Jones JP. J Med Chem. 2007; 50:4642. [PubMed: 17718551]

218. Alfaro JF, Joswig-Jones CA, Ouyang W, Nichols J, Crouch GJ, Jones JP. Drug Metab Dispos. 2009; 37:2393. [PubMed: 19741035]

219. (a) Kundu TK, Hille R, Velayutham M, Zweier JL. Arch Biochem Biophys. 2007; 460:113. [PubMed: 17353002] (b) Kundu TK, Velayutham M, Zweier JL. Biochemistry. 2012; 51:2930. [PubMed: 22404107]

220. (a) Li HT, Cui HM, Kundu TK, Alzawahra W, Zweier JL. J Biol Chem. 2008; 283:17855. [PubMed: 18424432] (b) Li HT, Kundu TK, Zweier JL. J Biol Chem. 2009; 284:33850. [PubMed: 19801639]

221. Zdunek-Zastocka E. Plant Physiol Biochem. 2008; 46:19. [PubMed: 18006324]

222. (a) Seo M, Peeters AJM, Koiwai H, Oritani T, Marion-Poll A, Zeevaart JAD, Koornneef M, Kamiya Y, Koshiba T. Proc Natl Acad Sci USA. 2000; 97:12908. [PubMed: 11050171] (b) Hoff T, Frandsen GI, Rocher A, Mundy J. Biochim Biophys Acta, Gene Struct Expression. 1998; 1398:397.

223. Akaba S, Seo M, Dohmae N, Takio K, Sekimoto H, Kamiya Y, Furuya N, Komano T, Koshiba T. J Biochem. 1999; 126:395. [PubMed: 10423535]

224. (a) Seo M, Aoki H, Koiwai H, Kamiya Y, Nambara E, Koshiba T. Plant Cell Physiol. 2004; 45:1694. [PubMed: 15574845] (b) Zarepour M, Simon K, Wilch M, Nielander U, Koshiba T, Seo M, Lindel T, Bittner F. Plant Mol Biol. 2012; 80:659. [PubMed: 23065119] (c) Koiwai H, Nakaminami K, Seo M, Mitsuhashi W, Toyomasu T, Koshiba T. Plant Physiol. 2004; 134:1697. [PubMed: 15064376]

225. Badwey JA, Robinson JM, Karnovsky MJ, Karnovsky ML. J Biol Chem. 1981; 256:3479. [PubMed: 6259169]

226. Meyer O, Frunzke K, Mordorf G. Microb Growth C1 Compd. 1993:27.

227. Jacobitz S, Meyer O. J Bacteriol. 1989; 171:6294. [PubMed: 2808305]

228. Cypionka H, Meyer O. J Bacteriol. 1983; 156:1178. [PubMed: 6315679]

229. (a) Moxley JM, Smith KA. Soil Biol Biochem. 1998; 30:65.(b) Moersdorf G, Frunzke K, Gadkari D, Meyer O. Biodegradation. 1992; 3:61.

230. Ragsdale SW, Kumar M. Chem Rev. 1996; 96:2515. [PubMed: 11848835]

231. (a) Kraut M, Hugendieck I, Herwig S, Meyer O. Arch Microbiol. 1989; 152:335. [PubMed: 2818128] (b) Kang BS, Kim YM. J Bacteriol. 1999; 181:5581. [PubMed: 10482497]

232. Pelzmann A, Ferner M, Gnida M, Meyer-Klaucke W, Maisel T, Meyer O. J Biol Chem. 2009; 284:9578. [PubMed: 19189964]

233. Spreitler F, Brock C, Pelzmann A, Meyer O, Koehler J. ChemBioChem. 2010; 11:2419. [PubMed: 20979125]

234. Hanzelmann P, Dobbek H, Gremer L, Huber R, Meyer O. J Mol Biol. 2000; 301:1221. [PubMed: 10966817]

235. Meyer-Klaucke W, Gnida M, Ferner R, Gremer L, Meyer O. J Inorg Biochem. 2001; 86:339.

236. Zhang B, Hemann CF, Hille R. J Biol Chem. 2010; 285:12571. [PubMed: 20178978]

237. (a) Siegbahn PEM, Shestakov AF. J Comput Chem. 2005; 26:888. [PubMed: 15834924] (b) Hofmann M, Kassube JK, Graf T. J Biol Inorg Chem. 2005; 10:490. [PubMed: 15971074]

238. Gourlay C, Nielsen DJ, White JM, Knottenbelt SZ, Kirk ML, Young CG. J Am Chem Soc. 2006; 128:2164. [PubMed: 16478141]

239. Resch M, Dobbek H, Meyer O. J Biol Inorg Chem. 2005; 10:518. [PubMed: 16091936]

240. Wilcoxen J, Snider S, Hille R. J Am Chem Soc. 2011; 133:12934. [PubMed: 21774528]

241. Shanmugam M, Wilcoxen J, Habel-Rodriguez D, Cutsail GEI, Kirk ML, Hoffman BM, Hille R. J Am Chem Soc. 2013; 135:17775. [PubMed: 24147852]

242. Wilcoxen J, Hille R. J Biol Chem. 2013:288.

243. Kemper PR, Weis P, Bowers MT, Maitre P. J Am Chem Soc. 1998; 120:13494.

244. Hulley EB, Welch KD, Appel AM, DuBois DL, Bullock RM. J Am Chem Soc. 2013; 135:11736. [PubMed: 23889300]

245. Wilcoxen J, Zhang B, Hille R. Biochemistry. 2011; 50:1910. [PubMed: 21275368]

246. (a) Holcenbe, Js; Stadtman, ER. J Biol Chem. 1969; 244:1194. [PubMed: 4388026] (b) Imhoff D, Andreesen JR. FEMS Microbiol Lett. 1979; 5:155.(c) Dilworth GL. Arch Biochem Biophys. 1982; 219:30. [PubMed: 7181513]

247. (a) Stadtman TC. Annu Rev Biochem. 1990; 59:111. [PubMed: 2142875] (b) Gladyshev, VN. Molybdenum and Tungsten: Their Roles in Biological Processes. Vol. 39. CRC Press; New York: 2002. p. 655

248. (a) Gladyshev VN, Khangulov SV, Axley MJ, Stadtman TC. Proc Natl Acad Sci USA. 1994; 91:7708. [PubMed: 8052647] (b) Boyington JC, Gladyshev VN, Khangulov SV, Stadtman TC, Sun PD. Science. 1997; 275:1305. [PubMed: 9036855]

249. Self WT, Stadtman TC. Proc Natl Acad Sci USA. 2000; 97:7208. [PubMed: 10860985]

250. Wagner R, Cammack R, Andreesen JR. Biochim Biophys Acta. 1984; 791:63.

251. Schrader T, Rienhofer A, Andreesen JR. Eur J Biochem. 1999; 264:862. [PubMed: 10491134]

252. Gladyshev VN, Lecchi P. BioFactors. 1995; 5:93. [PubMed: 8722123]

253. Gladyshev VN, Khangulov SV, Stadtman TC. Proc Natl Acad Sci USA. 1994; 91:232. [PubMed: 8278371]

254. Tshisuaka B, Kappl R, Huttermann J, Lingens F. Biochemistry. 1993; 32:12928. [PubMed: 8251516]

255. Frerichs-Deeken U, Goldenstedt B, Gahl-Janssen R, Kappl R, Huttermann J, Fetzner S. Eur J Biochem. 2003; 270:1567. [PubMed: 12654012]

256. Gibson J, Dispensa M, Harwood CS. J Bacteriol. 1997; 179:634. [PubMed: 9006014]

257. Boll M, Fuchs G. Eur J Biochem. 1998; 251:946. [PubMed: 9490071]

258. Unciuleac M, Warkentin E, Page CC, Boll M, Ermler U. Structure. 2004; 12:2249. [PubMed: 15576037]

259. Boll M, Fuchs G, Meier C, Trautwein A, El Kasmi A, Ragsdale SW, Buchanan G, Lowe DJ. J Biol Chem. 2001; 276:47853. [PubMed: 11602591]

260. (a) Bergmann F, Dikstein S. J Biol Chem. 1956; 223:765. [PubMed: 13385225] (b) Kalimuthu P, Leimkuehler S, Bernhardt PV. J Phys Chem B. 2011; 115:2655. [PubMed: 21361328]

261. (a) Havemeyer A, Bittner F, Wollers S, Mendel R, Kunze T, Clement B. J Biol Chem. 2006; 281:34796. [PubMed: 16973608] (b) Gruenewald S, Wahl B, Bittner F, Hungeling H, Kanzow S,

Kotthaus J, Schwering U, Mendel RR, Clement B. J Med Chem. 2008; 51:8173. [PubMed: 19053771]

262. Schwarz G, Mendel RR. Annu Rev Plant Biol. 2006; 57:623. [PubMed: 16669776]
263. Rothery RA, Stein B, Solomonson M, Kirk ML, Weiner JH. Proc Natl Acad Sci USA. 2012; 109:14773. [PubMed: 22927383]
264. Williams BR, Fu YC, Yap GPA, Burgmayer SJN. J Am Chem Soc. 2012; 134:19584. [PubMed: 23157708]
265. Kisker C, Schindelin H, Pacheco A, Wehbi WA, Garrett RM, Rajagopalan KV, Enemark JH, Rees DC. Cell. 1997; 91:973. [PubMed: 9428520]
266. Klein JM, Schwarz G. J Cell Sci. 2012; 125:4876. [PubMed: 22854042]
267. Astashkin AV, Rajapakshe A, Cornelison MJ, JohnsonWinters K, Enemark JH. J Phys Chem B. 2012; 116:1942. [PubMed: 22229742]
268. (a) Cramer SP, Gray HB, Rajagopalan KV. J Am Chem Soc. 1979; 101:2772.(b) George GN, Garrett RM, Prince RC, Rajagopalan KV. J Am Chem Soc. 1996; 118:8588.
269. Karakas E, Wilson HL, Graf TN, Xiang S, Jaramillo-Buswuets S, Rajagopalan KV, Kisker C. J Biol Chem. 2005; 280:33506. [PubMed: 16048997]
270. (a) Berg JM, Holm RHJ. Am Chem Soc. 1984; 106:3035.(b) Berg JM, Holm RH. J Am Chem Soc. 1985; 107:917.(c) Berg JM, Holm RH. J Am Chem Soc. 1985; 107:925.(d) Xiao ZG, Young CG, Enemark JH, Wedd AG. J Am Chem Soc. 1992; 114:9194.(e) Roberts SA, Young CG, Kipke CA, Cleland WE, Yamanouchi K, Carducci MD, Enemark JH. Inorg Chem. 1990; 29:3650.(f) Basu P, Kail BW, Young CG. Inorg Chem. 2010; 49:4895. [PubMed: 20433155] (g) Basu P, Nemykin VN, Sengar RS. Inorg Chem. 2009; 48:6303. [PubMed: 19485389] (h) Nemykin VN, Basu P. Inorg Chem. 2005; 44:7494. [PubMed: 16212375]
271. (a) Brody MS, Hille R. Biochim Biophys Acta, Protein Struct Mol Enzymol. 1995; 1253:133.(b) Hille R. Biochim Biophys Acta, Bioenerg. 1994; 1184:143.(c) Kail BW, Perez LM, Zaric SD, Millar AJ, Young CG, Hall MB, Basu P. Chem Eur J. 2006; 12:7501. [PubMed: 16865754]
272. (a) Pietsch MA, Hall MB. Inorg Chem. 1996; 35:1273. [PubMed: 11666318] (b) Thomson LM, Hall MB. J Am Chem Soc. 2001; 123:3995. [PubMed: 11457150]
273. Rappe AK, Goddard WA. Nature. 1980; 285:311.
274. Peariso K, McNaughton RL, Kirk ML. J Am Chem Soc. 2002; 124:9006. [PubMed: 12148977]
275. Kirk ML, Berhane A. Chem Biodiversity. 2012; 9:1756.
276. Brody MS, Hille R. Biochemistry. 1999; 38:6668. [PubMed: 10350486]
277. Wilson HL, Rajagopalan KV. J Biol Chem. 2004; 279:15105. [PubMed: 14729666]
278. Garrett RM, Rajagopalan KV. J Biol Chem. 1996; 271:7387. [PubMed: 8631762]
279. Lamy MT, Gutteridge S, Bray RC. Biochem J. 1980; 185:397. [PubMed: 6249254]
280. George GN, Garrett RM, Prince RC, Rajagopalan KV. Inorg Chem. 2004; 43:8456. [PubMed: 15606194]
281. Qiu JA, Wilson HL, Pushie MJ, Kisker C, George GN, Rajagopalan KV. Biochemistry. 2010; 49:3989. [PubMed: 20356030]
282. Reschke S, Niks D, Wilson H, Sigfridsson KGV, Haumann M, Rajagopalan KV, Hille R, Leimkuhler S. Biochemistry. 2013; 52:8295. [PubMed: 24147957]
283. Garrett RM, Johnson JL, Graf TN, Feigenbaum A, Rajagopalan KV. Proc Natl Acad Sci USA. 1998; 95:6394. [PubMed: 9600976]
284. Strickland S, Palmer G, Massey V. J Biol Chem. 1975; 250:4048. [PubMed: 1126943]
285. Bailey S, Rapson T, Johnson-Winters K, Astashkin AV, Enemark JH, Kappler U. J Biol Chem. 2009; 284:2053. [PubMed: 19004819]
286. Pacheco A, Hazzard JT, Tollin G, Enemark JH. J Biol Inorg Chem. 1999; 4:390. [PubMed: 10555573]
287. Feng CJ, Kedia RV, Hazzard JT, Hurley JK, Tollin G, Enemark JH. Biochemistry. 2002; 41:5816. [PubMed: 11980485]
288. Johnson-Winters K, Nordstrom AR, Emesh S, Astashkin AV, Rajapakshe A, Berry RE, Tollin G, Enemark JH. Biochemistry. 2010; 49:1290. [PubMed: 20063894]

289. Feng CJ, Wilson HL, Hurley JK, Hazzard JT, Tollin G, Rajagopalan KV, Enemark JH. J Biol Chem. 2003; 278:2913. [PubMed: 12424234]

290. Feng CJ, Wilson HL, Hurley JK, Hazzard JT, Tollin G, Rajagopalan KV, Enemark JH. Biochemistry. 2003; 42:12235. [PubMed: 14567685]

291. Feng CJ, Wilson HL, Tollin G, Astashkin AV, Hazzard JT, Rajagopalan KV, Enemark JH. Biochemistry. 2005; 44:13734. [PubMed: 16229463]

292. Elliott SJ, McElhaney AE, Feng CJ, Enemark JH, Armstrong FA. J Am Chem Soc. 2002; 124:11612. [PubMed: 12296723]

293. Dronov R, Kurth DG, Mohwald H, Spricigo R, Leimkuehler S, Wollenberger U, Rajagopalan KV, Scheller FW, Lisdat F. J Am Chem Soc. 2008; 130:1122. [PubMed: 18177044]

294. (a) Raitsimring AM, Pacheco A, Enemark JH. J Am Chem Soc. 1998; 120:11263.(b) Astashkin AV, Mader ML, Pacheco A, Enemark JH, Raitsimring AM. J Am Chem Soc. 2000; 122:5294.(c) George GN. J Magn Reson. 1985; 64:384.

295. Astashkin AV, Raitsimring AM, Feng CJ, Johnson JL, Rajagopalan KV, Enemark JH. J Am Chem Soc. 2002; 124:6109. [PubMed: 12022845]

296. Cramer SP, Johnson JL, Rajagopalan KV, Sorrell TN. Biochem Biophys Res Commun. 1979; 91:434. [PubMed: 229850]

297. Garton SD, Garrett RM, Rajagopalan KV, Johnson MK. J Am Chem Soc. 1997; 119:2590.

298. Astashkin AV, Feng CJ, Raitsimring AM, Enemark JH. J Am Chem Soc. 2005; 127:502. [PubMed: 15643856]

299. Astashkin AV, Neese F, Raitsimring AM, Cooney JJA, Bultman E, Enemark JH. J Am Chem Soc. 2005; 127:16713. [PubMed: 16305262]

300. Astashkin AV, Klein EL, Ganyushin D, Johnson-Winters K, Neese F, Kappler U, Enemark JH. Phys Chem Chem Phys. 2009; 11:6733. [PubMed: 19639147]

301. Astashkin AV, Johnson-Winters K, Klein EL, Feng CJ, Wilson HL, Rajagopalan KV, Raitsimring AK, Enemark JH. J Am Chem Soc. 2008; 130:8471. [PubMed: 18529001]

302. (a) Enemark JH, Raitsimring AM, Astashkin AV, Klein EL. Faraday Discuss. 2011; 148:249. [PubMed: 21322488] (b) Klein EL, Raitsimring AM, Astashkin AV, Rajapakshe A, Johnson-Winters K, Arnold AR, Potapov A, Goldfarb D, Enemark JH. Inorg Chem. 2012; 51:1408. [PubMed: 22225516]

303. Bray RC, Gutteridge S, Lamy MT, Wilkinson T. Biochem J. 1983; 211:227. [PubMed: 6307274]

304. (a) Doonan CJ, Wilson HL, Bennett B, Prince RC, Rajagopalan KV, George GN. Inorg Chem. 2008; 47:2033. [PubMed: 18271529] (b) Astashkin AV, Klein EL, Enemark JHJ. Inorg Biochem. 2007; 101:1623.

305. Klein EL, Astashkin AV, Ganyushin D, Riplinger C, Johnson-Winters K, Neese F, Enemark JH. Inorg Chem. 2009; 48:4743. [PubMed: 19402624]

306. Pushie MJ, Doonan CJ, Wison HL, Rajagopalan KV, George GN. Inorg Chem. 2011; 50:9406. [PubMed: 21894921]

307. Rajapakshe A, Johnson-Winters K, Nordstrom AR, Meyers KT, Emesh S, Astashkin AV, Enemark JH. Biochemistry. 2010; 49:5154. [PubMed: 20491442]

308. Eilers T, Schwarz G, Brinkmann H, Witt C, Richter T, Nieder J, Koch B, Hille R, Hansch R, Mendel RRJ. Biol Chem. 2001; 276:46989.

309. Workun GJ, Moquin K, Rothery RA, Weiner JH. Microbiol Mol Biol Rev. 2008; 72:228. [PubMed: 18535145]

310. Astashkin AV, Johnson-Winters K, Klein EL, Byrne RS, Hille R, Raitsimring AM, Enemark JHJ. Am Chem Soc. 2007; 129:14800.

311. Hemann C, Hood BL, Fulton M, Hansch R, Schwarz G, Mendel RR, Kirk ML, Hille RJ. Am Chem Soc. 2005; 127:16567.

312. Johnson JL, Rajagopalan KVJ. Biol Chem. 1977; 252:2017.

313. Haensch R, Lang C, Riebeseel E, Lindigkeit R, Gessler A, Rennenberg H, Mendel RRJ. Biol Chem. 2006; 281:6884.

314. Byrne RS, Haensch R, Mendel RR, Hille RJ. Biol Chem. 2009; 284:35479.

315. (a) Haensch R, Lang C, Rennenberg H, Mendel RR. Plant Biol (Stuttgart). 2007; 9:589.(b) Brychkova G, Xia Z, Yang G, Yesbergenova Z, Zhang Z, Davydov O, Fluhr R, Sagi M. Plant J. 2007; 50:696. [PubMed: 17425719]
316. Astashkin AV, Hood BL, Feng CJ, Hille R, Mendel RR, Raitsimring AM, Enemark JH. Biochemistry. 2005; 44:13274. [PubMed: 16201753]
317. (a) Bray RC, Lamy MT, Gutteridge S, Wilkinson T. Biochem J. 1982; 201:241. [PubMed: 6282260] (b) Cohen HJ, Rajagopalan KV. Fed Proc. 1972; 31:850.
318. Raitsimring AM, Astashkin AV, Feng C, Wilson HL, Rajagopalan KV, Enemark JH. Inorg Chim Acta. 2008; 361:941.
319. According to the Commission on Enzyme Nomenclature, any enzyme that reduces its name substrate can be called a “reductase”, regardless of the source of treducing equivalents. The same is not the case for the term “oxidase”, which by convention can be used only to refer to those enzymes that utilize O_2 as the oxidizing substrate. The plant enzyme discusssed above is therefore to be considered an oxidase, while the vertebrate enzymes are not. The recommended term for an enzyme that oxidizes its substrate but uses an oxidizing substrate other than O_2 is “dehydrogenase”. The lunacy of this quirk of nomenclature is manifested in those enzymes considered here, which are consistently referred to as sulfite dehydrogenases in the literature despite the fact that the substrate has no hydrogen to be removed in the course of the reaction.
320. (a) Kappler, U. Microbial Sulfur Metabolism. Dahl, CAF.; Cornielius, G., editors. Springer; Berlin: 2008. (b) Kappler U. Biochim Biophys Acta, Bioenerg. 2011; 1807:1.
321. Kappler U, Bailey SJ. Biol Chem. 2005; 280:24999.
322. Utesch T, Mroginski MAJ. Phys Chem Lett. 2010; 1:2159.
323. Rajapakshe A, Meyers KT, Berry RE, Tollin G, Enemark JHJ. Biol Inorg Chem. 2012; 17:345.
324. Pushie MJ, George GNJ. Phys Chem B. 2010; 114:3266.
325. Emesh S, Rapson TD, Rajapakshe A, Kappler U, Bernhardt PV, Tollin G, Enemark JH. Biochemistry. 2009; 48:2156. [PubMed: 19226119]
326. Rapson TD, Astashkin AV, Johnson-Winters K, Bernhardt PV, Kappler U, Raitsimring AM, Enemark JHJ. Biol Inorg Chem. 2010; 15:505.
327. Di Salle A, D’Errico G, La Cara F, Cannio R, Rossi M. Extremophiles. 2006; 10:587. [PubMed: 16830073]
328. D’Errico G, Di Salle A, La Cara F, Rossi M, Cannio R. J Bacteriol. 2006; 188:694. [PubMed: 16385059]
329. Wilson JJ, Kappler U. Biochim Biophys Acta, Bioenerg. 2009; 1787:1516.
330. (a) Solomonson LP, Barber M. J Annu Rev Plant Physiol Plant Mol Biol. 1990; 41:225.(b) Campbell WH. Annu Rev Plant Physiol Plant Mol Biol. 1999; 50:277. [PubMed: 15012211] (c) Campbell WH. Cell Mol Life Sci. 2001; 58:194. [PubMed: 11289301]
331. Crawford NM, Smith M, Bellissimo D, Davis RW. Proc Natl Acad Sci USA. 1988; 85:5006. [PubMed: 3393528]
332. Fischer K, Barbier GG, Hecht HJ, Mendel RR, Campbell WH, Schwarz G. Plant Cell. 2005; 17:1167. [PubMed: 15772287]
333. Rudolph MJ, Johnson JL, Rajagopalan KV, Kisker C. Acta Crystallogr, Sect D: Biol Crystallogr. 2003; 59:1183. [PubMed: 12832761]
334. Durley RCE, Mathews FS. Acta Crystallogr, Sect D: Biol Crystallogr. 1996; 52:65. [PubMed: 15299727]
335. Lu GG, Campbell WH, Schneider G, Lindqvist Y. Structure. 1994; 2:809. [PubMed: 7812715]
336. (a) Gutteridge S, Bray RC, Notton BA, Fido RJ, Hewitt EJ. Biochem J. 1983; 213:137. [PubMed: 6311159] (b) Solomonson LP, Barber MJ, Howard WD, Johnson JL, Rajagopalan KV. J Biol Chem. 1984; 259:849. [PubMed: 6319388]
337. (a) Cramer SP, Solomonson LP, Adams MWW, Mortenson LE. J Am Chem Soc. 1984; 106:1467.(b) George GN, Mertens JA, Campbell WH. J Am Chem Soc. 1999; 121:9730.
338. Kay CJ, Barber MJ, Notton BA, Solomonson LP. Biochem J. 1989; 263:285. [PubMed: 2604699]
339. Kay CJ, Barber MJ, Solomonson LP. Biochemistry. 1988; 27:6142. [PubMed: 2847786]
340. Spence JT, Kipke CA, Enemark JH, Sunde RA. Inorg Chem. 1991; 30:3011.

341. Karplus PA, Faber HR. Photosynth Res. 2004; 81:303. [PubMed: 16034534]
342. Mayoral T, Martinez-Julvez M, Perez-Dorado I, Sanz-Aparicio J, Gomez-Moreno C, Medina M, Hermoso JA. Proteins: Struct, Funct, Bioinf. 2005; 59:592.
343. Holm RH, Donahue JP. Polyhedron. 1993; 12:571.
344. Skipper L, Campbell WH, Mertens JA, Lowe DJ. J Biol Chem. 2001; 276:26995. [PubMed: 11356830]
345. Ratnam K, Shiraishi N, Campbell WH, Hille R. J Biol Chem. 1995; 270:24067. [PubMed: 7592606]
346. Ratnam K, Shiraishi N, Campbell WH, Hille R. J Biol Chem. 1997; 272:2122. [PubMed: 8999912]
347. Sherameti I, Sopory SK, Trebicka A, Pfannschmidt T, Oelmuller R. J Biol Chem. 2002; 277:46594. [PubMed: 12244040]
348. (a) Huber JL, Huber SC, Campbell WH, Redinbaugh MG. Arch Biochem Biophys. 1992; 296:58. [PubMed: 1605645] (b) Bachmann M, Shiraishi N, Campbell WH, Yoo BC, Harmon AC, Huber SC. Plant Cell. 1996; 8:505. [PubMed: 8721752]
349. Douglas P, Moorhead G, Hong Y, Morrice N, MacKintosh C. Planta. 1998; 206:435. [PubMed: 9763711]
350. Moorhead G, Douglas P, Morrice N, Scarabel M, Aitken A, MacKintosh C. Curr Biol. 1996; 6:1104. [PubMed: 8805370]
351. Shen W, Huber SC. Plant Cell Physiol. 2006; 47:764. [PubMed: 16621845]
352. Lambeck I, Chi J-C, Krizowski S, Mueller S, Mehlmer N, Teige M, Fischer K, Schwarz G. Biochemistry. 2010; 49:8177. [PubMed: 20690630]
353. Lambeck IC, Fischer-Schrader K, Niks D, Roeper J, Chi J-C, Hille R, Schwarz G. J Biol Chem. 2012; 287:4562. [PubMed: 22170050]
354. Qiu JA, Wilson HL, Rajagopalan KV. Biochemistry. 2012; 51:1134. [PubMed: 22263579]
355. Wahl B, Reichmann D, Niks D, Krompholz N, Havemeyer A, Clement B, Messerschmidt T, Rothkegel M, Biester H, Hille R, Mendel RR, Bittner F. J Biol Chem. 2010; 285:37847. [PubMed: 20861021]
356. Krompholz N, Krischkowski C, Reichmann D, GarbeSchonberg D, Mendel RR, Bittner F, Clement B, Havemeyer A. Chem Res Toxicol. 2012; 25:2443. [PubMed: 22924387]
357. Kotthaus J, Wahl B, Havemeyer A, Schade D, GarbeSchonberg D, Mende R, Bittner F, Clement B. Biochem J. 2011; 433:383. [PubMed: 21029045]
358. (a) Kotthaus J, Wahl B, Havemeyer A, Kotthaus J, Schade D, Garbe-Schoenberg D, Mende R, Bittner F, Clement B. Biochem J. 2011; 433:383. [PubMed: 21029045] (b) Havemeyer A, Grunewald S, Wahl B, Bittner F, Mendel R, Erdelyi P, Fischer J, Clement B. Drug Metab Dispos. 2010; 38:1917. [PubMed: 20699408]
359. Anantharaman V, Aravind L. FEMS Microbiol Lett. 2002; 207:55. [PubMed: 11886751]
360. Rajapakshe A, Astashkin AV, Klein EL, Reichmann D, Mendel RR, Bittner F, Enemark JH. Biochemistry. 2011; 50:8813. [PubMed: 21916412]
361. Kozmin SG, Leroy P, Pavlov YI, Schaaper RM. Mol Microbiol. 2008; 68:51. [PubMed: 18312271]
362. Kozmin SG, Wang J, Schaaper RM. J Bacteriol. 2010; 192:2026. [PubMed: 20118259]
363. Pushie MJ, Doonan CJ, Moquin K, Weiner JH, Rothery R, George GN. Inorg Chem. 2011; 50:732. [PubMed: 21190336]
364. Yang J, Rothery R, Sempombe J, Weiner JH, Kirk ML. J Am Chem Soc. 2009; 131:15612. [PubMed: 19860477]
365. (a) George GN, Doonan CJ, Rothery RA, Boroumand N, Weiner JH. Inorg Chem. 2007; 46:2. [PubMed: 17198404] (b) Havelius KGV, Reschke S, Horn S, Doerlng A, Niks D, Hille R, Schulzke C, Leimkuehler S, Haumann M. Inorg Chem. 2011; 50:741. [PubMed: 21190337]
366. (a) Bastian NR, Kay CJ, Barber MJ, Rajagopalan KV. J Biol Chem. 1991; 266:45. [PubMed: 1845974] (b) Schneider F, Lowe J, Huber R, Schindelin H, Kisker C, Knablein J. J Mol Biol. 1996; 263:53. [PubMed: 8890912] (c) Li HK, Temple C, Rajagopalan KV, Schindelin H. J Am Chem Soc. 2000; 122:7673.

367. Ellis PJ, Conrads T, Hille R, Kuhn P. Structure. 2001; 9:125. [PubMed: 11250197]
368. Dias JM, Than ME, Humm A, Huber R, Bourenkov GP, Bartunik HD, Bursakov S, Calvete J, Caldeira J, Carneiro C, Moura JJG, Moura I, Romao MJ. Structure. 1999; 7:65. [PubMed: 10368307]
369. (a) Rothery RA, Weiner JH. Biochemistry. 1991; 30:8296. [PubMed: 1653010] (b) Rothery RA, Weiner JH. Biochemistry. 1996; 35:3247. [PubMed: 8605160]
370. (a) Bertero MG, Rothery RA, Palak M, Hou C, Lim D, Blasco F, Weiner JH, Strynadka NCJ. Nat Struct Biol. 2003; 10:681. [PubMed: 12910261] (b) Jormakka M, Richardson D, Byrne B, Iwata S. Structure. 2004; 12:95. [PubMed: 14725769]
371. Jormakka M, Tornroth S, Byrne B, Iwata S. Science. 2002; 295:1863. [PubMed: 11884747]
372. (a) McEwan AG, Ridge JP, McDevitt CA, Hugenholtz P. Geomicrobiol J. 2002; 19:3.(b) Rothery RA, Workun GJ, Weiner JH. Biochim Biophys Acta, Biomembr. 2008; 1778:1897.(c) Kappler U, Nouwens AS. Metallomics. 2013; 5:325. [PubMed: 23310928]
373. van Lis R, Nitschke W, Duval S, Schoepp-Cothenet B. Biochim Biophys Acta, Bioenerg. 2013; 1827:176.
374. Gonzalez PJ, Rivas MG, Mota CS, Brondino CD, Moura I, Moura JJG. Coord Chem Rev. 2013; 257:315.
375. (a) Yamamoto I, Wada N, Ujiiye T, Tachibana M, Matsuzaki M, Kajiwara H, Watanabe Y, Hirano H, Okubo A, Satoh T, Yamazaki S. Biosci, Biotechnol, Biochem. 1995; 59:1850. [PubMed: 8534974] (b) Barber MJ, Vanvalkenburgh H, Trimboli AJ, Pollock VV, Neame PJ, Bastian NR. Arch Biochem Biophys. 1995; 320:266. [PubMed: 7625833] (c) Satoh T, Kurihara FN. J Biochem. 1987; 102:191. [PubMed: 2822679]
376. Turner SM, Nightingale PD, Spokes LJ, Liddicoat MI, Liss PS. Nature. 1996; 383:513.
377. Schultz BE, Hille R, Holm RH. J Am Chem Soc. 1995; 117:827.
378. Bray RC, Adams B, Smith AT, Bennett B, Bailey S. Biochemistry. 2000; 39:11258. [PubMed: 10985771]
379. Garton SD, Hilton J, Oku H, Crouse BR, Rajagopalan KV, Johnson MK. J Am Chem Soc. 1997; 119:12906.
380. (a) George GN, Hilton J, Rajagopalan KV. J Am Chem Soc. 1996; 118:1113.(b) George GN, Hilton J, Temple C, Prince RC, Rajagopalan KV. J Am Chem Soc. 1999; 121:1256.
381. Ryan MG, Ratnam K, Hille R. J Biol Chem. 1995; 270:19209. [PubMed: 7642590]
382. Cobb N, Conrads T, Hille R. J Biol Chem. 2005; 280:11007. [PubMed: 15649898]
383. Bray RC, Adams B, Smith AT, Richards RL, Lowe DJ, Bailey S. Biochemistry. 2001; 40:9810. [PubMed: 11502174]
384. George GN, Nelson KJ, Harris HH, Doonan CJ, Rajagopalan KV. Inorg Chem. 2007; 46:3097. [PubMed: 17361996]
385. (a) Johnson KE, Rajagopalan KV. J Biol Chem. 2001; 276:13178. [PubMed: 11278798] (b) Cobb N, Hemann C, Polsinelli GA, Ridge JP, McEwan AG, Hille R. J Biol Chem. 2007; 282:35519. [PubMed: 17921142]
386. Ridge JP, Aguey-Zinsou KF, Bernhardt PV, Brereton IM, Hanson GR, McEwan AG. Biochemistry. 2002; 41:15762. [PubMed: 12501205]
387. Bell AF, He X, Ridge JP, Hanson GR, McEwan AG, Tonge PJ. Biochemistry. 2001; 40:440. [PubMed: 11148038]
388. Bennett B, Benson N, McEwan AG, Bray RC. Eur J Biochem. 1994; 225:321. [PubMed: 7925452]
389. Mtei RP, Lyashenko G, Stein B, Rubie N, Hille R, Kirk ML. J Am Chem Soc. 2011; 133:9762. [PubMed: 21648481]
390. Pushie MJ, Cotelesage JJH, Lyashenko G, Hille R, George GN. Inorg Chem. 2013; 52:2830. [PubMed: 23445435]
391. (a) Sung KM, Holm RH. J Am Chem Soc. 2001; 123:1931. [PubMed: 11456814] (b) Sung KM, Holm RH. Inorg Chem. 2001; 40:4518. [PubMed: 11511194] (c) Wang JJ, Kryatova OP, Rybak-Akimova EV, Holm RH. Inorg Chem. 2004; 43:8092. [PubMed: 15578849]

392. Tenderholt AL, Wang J-J, Szilagyi RK, Holm RH, Hodgson KO, Hedman B, Solomon EI. J Am Chem Soc. 2010; 132:8359. [PubMed: 20499905]

393. Czjzek M, Dos Santos JP, Pommier J, Giordano G, Mejean V, Haser R. J Mol Biol. 1998; 284:435. [PubMed: 9813128]

394. Zhang L, Nelson KJ, Rajagopalan KV, George GN. Inorg Chem. 2008; 47:1074. [PubMed: 18163615]

395. (a) Pollock VV, Barber MJ. J Biol Chem. 1997; 272:3355. [PubMed: 9013576] (b) Temple CA, George GN, Hilton JC, George MJ, Prince RC, Barber MJ, Rajagopalan KV. Biochemistry. 2000; 39:4046. [PubMed: 10747793]

396. Garton SD, Temple CA, Dhawan IK, Barber MJ, Rajagopalan KV, Johnson MK. J Biol Chem. 2000; 275:6798. [PubMed: 10702237]

397. (a) Sambasivarao D, Scraba DG, Trieber C, Weiner JH. J Bacteriol. 1990; 172:5938. [PubMed: 2170332] (b) Weiner JH, Rothery RA, Sambasivarao D, Trieber CA. Biochim Biophys Acta. 1992; 1102:1. [PubMed: 1324728] (c) Weiner JH, Shaw G, Turner RJ, Trieber CA. J Biol Chem. 1993; 268:3238. [PubMed: 8429002]

398. (a) Stanley NR, Sargent F, Buchanan G, Shi JR, Stewart V, Palmer T, Berks BC. Mol Microbiol. 2002; 43:1005. [PubMed: 11929547] (b) Rothery RA, Kalra N, Turner RJ, Weiner JH. J Mol Microbiol Biotechnol. 2002; 4:133. [PubMed: 11873909]

399. Graham N, Doonan CJ, Rothery RA, Boroumand N, Weiner JH. Inorg Chem. 2007; 46:2. [PubMed: 17198404]

400. Jormakka M, Yokoyama K, Yano T, Tamakoshi M, Akimoto S, Shimamura T, Curmi P, Iwata S. Nat Struct Mol Biol. 2008; 15:730. [PubMed: 18536726]

401. Trieber CA, Rothery RA, Weiner JH. J Biol Chem. 1996; 271:4620. [PubMed: 8617723]

402. Rothery RA, Trieber CA, Weiner JH. J Biol Chem. 1999; 274:13002. [PubMed: 10224050]

403. Cammack R, Weiner JH. Biochemistry. 1990; 29:8410. [PubMed: 2174699]

404. Heffron K, Leger C, Rothery RA, Weiner JH, Armstrong FA. Biochemistry. 2001; 40:3117. [PubMed: 11258926]

405. Stiefel EI. Proc Natl Acad Sci USA. 1973; 70:988. [PubMed: 4515630]

406. Zhao ZW, Weiner JH. J Biol Chem. 1998; 273:20758. [PubMed: 9694819]

407. Geijer P, Weiner JH. Biochim Biophys Acta, Biomembr. 2004; 1660:66.

408. (a) McDevitt CA, Hugenholtz P, Hanson GR, McEwan AG. Mol Microbiol. 2002; 44:1575. [PubMed: 12067345] (b) Hanlon SP, Holt RA, Moore GR, McEwan AG. Microbiology-UK. 1994; 140:1953.(c) Hanlon SP, Toh TH, Solomon PS, Holt RA, McEwan AG. Eur J Biochem. 1996; 239:391. [PubMed: 8706745]

409. McDevitt CA, Hanson GR, Noble CJ, Cheesman MR, McEwan AG. Biochemistry. 2002; 41:15234. [PubMed: 12484761]

410. Creevey NL, McEwan AG, Hanson GR, Bernhardt PV. Biochemistry. 2008; 47:3770. [PubMed: 18298089]

411. Nagarajan K, Joshi HK, Chaudhury PK, Pal K, Cooney JJA, Enemark JH, Sarkar S. Inorg Chem. 2004; 43:4532. [PubMed: 15257571]

412. (a) Berks BC, Ferguson SJ, Moir JWB, Richardson DJ. Biochim Biophys Acta, Bioenerg. 1995; 1232:97.(b) Berks BC, Page MD, Richardson DJ, Reilly A, Cavill A, Outen F, Ferguson SJ. Mol Microbiol. 1995; 15:319. [PubMed: 7746153]

413. (a) Hedderich R, Klimmek O, Kroger A, Dirmeier R, Keller M, Stetter KO. FEMS Microbiol Rev. 1998; 22:353.(b) Dietrich W, Klimmek O. Eur J Biochem. 2002; 269:1086. [PubMed: 11856339]

414. Bagramyan K, Trchounian A. Biochemistry-Moscow. 2003; 68:1159. [PubMed: 14640957]

415. Jormakka M, Byrne B, Iwata S. Curr Opin Struct Biol. 2003; 13:418. [PubMed: 12948771]

416. (a) Ruschig U, Muller U, Willnow P, Hopner T. Eur J Biochem. 1976; 70:325. [PubMed: 12947] (b) Alissandratos A, Kim H-K, Matthews H, Hennessy JE, Philbrook A, Easton CJ. Appl Environ Microbiol. 2013; 79:741. [PubMed: 23144135] (c) Reda T, Plugge CM, Abram NJ, Hirst J. Proc Natl Acad Sci USA. 2008; 105:10654. [PubMed: 18667702]

417. George GN, Colangelo CM, Dong J, Scott RA, Khangulov SV, Gladyshev VN, Stadtman TC. J Am Chem Soc. 1998; 120:1267.

418. George GN, Costa C, Moura JJG, Moura I. J Am Chem Soc. 1999; 121:2625.

419. Axley MJ, Bock A, Stadtman TC. Proc Natl Acad Sci USA. 1991; 88:8450. [PubMed: 1924303]

420. Khangulov SV, Gladyshev VN, Dismukes GC, Stadtman TC. Biochemistry. 1998; 37:3518. [PubMed: 9521673]

421. Gladyshev VN, Boyington JC, Khangulov SV, Grahame DA, Stadtman TC, Sun PD. J Biol Chem. 1996; 271:8095. [PubMed: 8626495]

422. Raaijmakers HCA, Romao MJ. J Biol Inorg Chem. 2006; 11:849. [PubMed: 16830149]

423. Thome R, Gust A, Toci R, Mendel R, Bittner F, Magalon A, Walburger A. J Biol Chem. 2012; 287:4671. [PubMed: 22194618]

424. Mota CS, Rivas MG, Brondino CD, Moura I, Moura JJG, Gonzalez PJ, Cerqueira NMFSA. J Biol Inorg Chem. 2011; 16:1255. [PubMed: 21773834]

425. Blasco F, Guigliarelli B, Magalon A, Asso M, Giordano G, Rothery RA. Cell Mol Life Sci. 2001; 58:179. [PubMed: 11289300]

426. Jones RW, Lamont A, Garland PB. Biochem J. 1980; 190:79. [PubMed: 6255943]

427. Volbeda A, Charon MH, Piras C, Hatchikian EC, Frey M, Fontecillacamps JC. Nature. 1995; 373:580. [PubMed: 7854413]

428. (a) Sazanov LA, Hinchliffe P. Science. 2006; 311:1430. [PubMed: 16469879] (b) Hunte C, Zickermann V, Brandt U. Science. 2010; 329:448. [PubMed: 20595580] (c) Efremov RG, Baradaran R, Sazanov LA. Nature. 2010; 465:441. [PubMed: 20505720]

429. Iwata S, Lee JW, Okada K, Lee JK, Iwata M, Rasmussen B, Link TA, Ramaswamy S, Jap BK. Science. 1998; 281:64. [PubMed: 9651245]

430. Jones RW. FEMS Microbiol Lett. 1980; 8:167.

431. Abaibou H, Pommier J, Benoit S, Giordano G, Mandrandberthelot MA. J Bacteriol. 1995; 177:7141. [PubMed: 8522521]

432. Plunkett G, Burland V, Daniels DL, Blattner FR. Nucleic Acids Res. 1993; 21:3391. [PubMed: 8346018]

433. (a) Friedebold J, Bowien BJ. Bacteriol. 1993; 175:4719.(b) Friedebold J, Mayer F, Bill E, Trautwein AX, Bowien B. Biol Chem Hoppe-Seyler. 1995; 376:561. [PubMed: 8561915]

434. Oh JI, Bowien B. J Biol Chem. 1998; 273:26349. [PubMed: 9756865]

435. Jollie DR, Lipscomb JD. J Biol Chem. 1991; 266:21853. [PubMed: 1657982]

436. Muller U, Willnow P, Ruschig U, Hopner T. Eur J Biochem. 1978; 83:485. [PubMed: 631130]

437. Finel M. Biochim Biophys Acta, Bioenerg. 1998; 1364:112.

438. Hartmann T, Leimkuhler S. FEBS J. 2013; 280:6083. [PubMed: 24034888]

439. Stolz JF, Basu P. ChemBioChem. 2002; 3:198. [PubMed: 11921398]

440. Millar TM, Stevens CR, Benjamin N, Eisenthal R, Harrison R, Blake DR. FEBS Lett. 1998; 427:225. [PubMed: 9607316]

441. (a) Martinez-Espinosa RM, Dridge EJ, Bonete MJ, Butt JN, Butler CS, Sargent F, Richardson DJ. FEMS Microbiol Lett. 2007; 276:129. [PubMed: 17888006] (b) Kraft B, Strous M, Tegetmeyer HE. J Biotechnol. 2011; 155:104. [PubMed: 21219945] (c) Lowe EC, Bydder S, Hartshorne RS, Tape HLU, Dridge EJ, Debieux CM, Paszkiewicz K, Singleton I, Lewis RJ, Santini JM, Richardson DJ, Butler CS. J Biol Chem. 2010; 285:18433. [PubMed: 20388716]

442. Kern M, Simon J. Microbiology-Sgm. 2009; 155:2784.

443. Potter L, Angove H, Richardson D, Cole J. Adv Microb Physiol. 2001; 45:51. [PubMed: 11450112]

444. (a) Simpson PJL, Richardson DJ, Codd R. Microbiology-Sgm. 2010; 156:302.(b) Simpson PJL, McKinzie AA, Codd R. Biochem Biophys Res Commun. 2010; 398:13. [PubMed: 20547139]

445. (a) Aklujkar M, Krushkal J, DiBartolo G, Lapidus A, Land ML, Lovley DR. BMC Microbiol. 2009; 9:109. [PubMed: 19473543] (b) Chovanec P, Stolz JF, Basu P. Metallomics. 2010; 2:133. [PubMed: 21069144]

446. (a) Simpson PJL, Codd R. Biochem Biophys Res Commun. 2011; 414:783. [PubMed: 22005463] (b) Chen CA, Lin CH, Druhan LJ, Wang TY, Chen YR, Zweier JL. J Biol Chem. 2011; 286:29098. [PubMed: 21666221]

447. (a) Tuanh NH, Noriega CE, Stewart V. Proc Natl Acad Sci USA. 2010; 107:21140. [PubMed: 21078995] (b) Darwin AJ, Tyson KL, Busby SJW, Stewart V. Mol Microbiol. 1997; 25:583. [PubMed: 9302020] (c) Rabin RS, Collins LA, Stewart V. Proc Natl Acad Sci USA. 1992; 89:8701. [PubMed: 1528882]

448. (a) Noriega CE, Lin H-Y, Chen L-L, Williams SB, Stewart V. Mol Microbiol. 2010; 75:394. [PubMed: 19968795] (b) Laub, MT.; Shapiro, L.; McAdams, HH. Annual Review of Genetics. Vol. 41. Annual Reviews; CA: 2007.

449. Dong YY, Wang JX, Fu HH, Zhou GQ, Shi MM, Gao HC. PLoS One. 2012:7.

450. Bertero MG, Rothery RA, Boroumand N, Palak M, Blasco F, Ginet N, Weiner JH, Strynadka NCJ. J Biol Chem. 2005; 280:14836. [PubMed: 15615728]

451. Peters JW, Lanzilotta WN, Lemon BJ, Seefeldt LC. Science. 1998; 282:1853. [PubMed: 9836629]

452. Magalon A, Asso M, Guigliarelli B, Rothery RA, Bertrand P, Giordano G, Blasco F. Biochemistry. 1998; 37:7363. [PubMed: 9585550]

453. Enemark JH, Garner CD. J Biol Inorg Chem. 1997; 2:817.

454. Kloer DP, Hagel C, Heider J, Schulz GE. Structure. 2006; 14:1377. [PubMed: 16962969]

455. (a) Bray RC, Vincent SP, Lowe DJ, Clegg RA, Garland PB. Biochem J. 1976; 155:201. [PubMed: 180982] (b) Clegg RA. Biochem J. 1976; 153:533. [PubMed: 782444] (c) Hettmann T, Anemuller S, Borcherding H, Mathe L, Steinrucke P, Diekmann S. FEBS Lett. 2003; 534:143. [PubMed: 12527376] (d) George GN, Bray RC, Morpeth FF, Boxer DH. Biochem J. 1985; 227:925. [PubMed: 2988508] (e) Vincent SP, Bray RC. Biochem J. 1978; 171:639. [PubMed: 27168] (f) Correia C, Besson S, Brondino CD, Gonzalez PJ, Fauque G, Lampreia J, Moura I, Moura JJG. J Biol Inorg Chem. 2008; 13:1321. [PubMed: 18704520]

456. Field SJ, Thornton NP, Anderson LJ, Gates AJ, Reilly A, Jepson BJN, Richardson DJ, George SJ, Cheesman MR, Butt JN. Dalton Trans. 2005:3580. [PubMed: 16234941]

457. (a) Majumdar A, Sarkar S. Coord Chem Rev. 2011; 255:1039.(b) Sung KM, Holm RH. J Am Chem Soc. 2002; 124:4312. [PubMed: 11960460] (c) Sugimoto H, Tsukube H. Chem Soc Rev. 2008; 37:2609. [PubMed: 19020675] (d) Sugimoto H, Tatemoto S, Suyama K, Miyake H, Mtei RP, Itoh S, Kirk ML. Inorg Chem. 2010; 49:5368. [PubMed: 20491454] (e) Nemykin VN, Davie SR, Mondal S, Rubie N, Kirk ML, Somogyi A, Basu P. J Am Chem Soc. 2002; 124:756. [PubMed: 11817943]

458. Anderson LJ, Richardson DJ, Butt JN. Biochemistry. 2001; 40:11294. [PubMed: 11560477]

459. Leger C, Elliott SJ, Hoke KR, Jeuken LJC, Jones AK, Armstrong FA. Biochemistry. 2003; 42:8653. [PubMed: 12873124]

460. (a) Kail B, Nemykin VN, Davie SR, Carrano CJ, Hammes B, Basu P. Inorg Chem. 2002; 41:1281. [PubMed: 11874366] (b) Davie SR, Rubie ND, Hammes BS, Carrano CJ, Kirk ML, Basu P. Inorg Chem. 2001; 40:2632. [PubMed: 11375669]

461. Elliott SJ, Hoke KR, Heffron K, Palak M, Rothery RA, Weiner JH, Armstrong FA. Biochemistry. 2004; 43:799. [PubMed: 14730985]

462. Marangon J, Paes de Sousa PM, Moura I, Brondino CD, Moura JJG, Gonzalez PJ. Biochim Biophys Acta, Bioenerg. 2012; 1817:1072.

463. (a) de Vries S, Momcilovic M, Strampraad MJF, Whitelegge JP, Baghai A, Schroeder I. Biochemistry. 2010; 49:9911. [PubMed: 20863064] (b) Afshar S, Johnson E, de Vries S, Schroder I. J Bacteriol. 2001; 183:5491. [PubMed: 11544209]

464. (a) Robles EF, Sanchez C, Bonnard N, Delgado MJ, Bedmar E. J Biochem Soc Trans. 2006; 34:108.(b) Mesa S, Hauser F, Friberg M, Malaguti E, Fischer HM, Hennecke H. J Bacteriol. 2008; 190:6568. [PubMed: 18689489]

465. Sears HJ, Sawers G, Berks BC, Ferguson SJ, Richardson DJ. Microbiology-Uk. 2000; 146:2977.

466. Gavira M, Roldan MD, Castillo F, Moreno-Vivian C. J Bacteriol. 2002; 184:1693. [PubMed: 11872721]

467. Najmudin S, Gonzalez PJ, Trincao J, Coelho C, Mukhopadhyay A, Cerqueira N, Romao CC, Moura I, Moura JJG, Brondino CD, Romao MJ. J Biol Inorg Chem. 2008; 13:737. [PubMed: 18327621]

468. Coelho C, Gonzalez PJ, Moura JJG, Moura I, Trincao J, Romao MJ. J Mol Biol. 2011; 408:932. [PubMed: 21419779]

469. Hettmann T, Siddiqui RA, Frey C, Santos-Silva T, Romao MJ, Diekmann S. Biochem Biophys Res Commun. 2004; 320:1211. [PubMed: 15249219]

470. Jepson BJN, Mohan S, Clarke TA, Gates AJ, Cole JA, Butler CS, Butt JN, Hemmings AM, Richardson DJ. J Biol Chem. 2007; 282:6425. [PubMed: 17130127]

471. Arnoux P, Sabaty M, Alric J, Frangioni B, Guigliarelli B, Adriano JM, Pignol D. Nat Struct Biol. 2003; 10:928. [PubMed: 14528294]

472. Zoppellaro G, Bren KL, Ensign AA, Harbitz E, Kaur R, Hersleth HP, Ryde U, Hederstedt L, Andersson KK. Biopolymers. 2009; 91:1064. [PubMed: 19536822]

473. Brige A, Leys D, Meyer TE, Cusanovich MA, Van Beeumen J. J Biochemistry. 2002; 41:4827.

474. (a) Basu P, Shokhirev NV, Enemark JH, Walker FA. J Am Chem Soc. 1995; 117:9042.(b) Walker FA. Chem Rev. 2004; 104:589. [PubMed: 14871136]

475. (a) Butler CS, Charnock JM, Bennett B, Sears HJ, Reilly AJ, Ferguson SJ, Garner CD, Lowe DJ, Thomson AJ, Berks BC, Richardson DJ. Biochemistry. 1999; 38:9000. [PubMed: 10413473] (b) Bennett B, Berks BC, Ferguson SJ, Thomson AJ, Richardson DJ. Eur J Biochem. 1994; 226:789. [PubMed: 7813468]

476. (a) Gonzalez PJ, Rivas MG, Brondino CD, Bursakov SA, Moura I, Moura JJG. J Biol Inorg Chem. 2006; 11:609. [PubMed: 16791644] (b) Gonzalez PJ, Correia C, Moura I, Brondino CD, Moura JJG. J Inorg Biochem. 2006; 100:1015. [PubMed: 16412515]

477. (a) Fourmond V, Burlat B, Dementin S, Arnoux P, Sabaty M, Boiry S, Guigliarelli B, Bertrand P, Pignol D, Leger C. J Phys Chem B. 2008; 112:15478. [PubMed: 19006273] (b) Bertrand P, Frangioni B, Dementin S, Sabaty M, Arnoux P, Guigliarelli B, Pignol D, Leger C. J Phys Chem B. 2007; 111:10300. [PubMed: 17676894]

478. Butler CS, Charnock JM, Garner CD, Thomson AJ, Ferguson SJ, Berks BC, Richardson DJ. Biochem J. 2000; 352:859. [PubMed: 11104696]

479. Butler CS, Fairhurst SA, Ferguson SJ, Thomson AJ, Berks BC, Richardson DJ, Lowe DJ. Biochem J. 2002; 363:817. [PubMed: 11964184]

480. Biaso F, Burlat B, Guigliarelli B. Inorg Chem. 2012; 51:3409. [PubMed: 22397692]

481. Nemykin VN, Basu P. Inorg Chem. 2003; 42:4046. [PubMed: 12817960]

482. Bursakov SA, Carneiro C, Almendra MJ, Duarte RO, Caldeira J, Moura I, Moura JJG. Biochem Biophys Res Commun. 1997; 239:816. [PubMed: 9367852]

483. Craske A, Ferguson SJ. Eur J Biochem. 1986; 158:429. [PubMed: 3732277]

484. Berks BC, Richardson DJ, Robinson C, Reilly A, Aplin RT, Ferguson SJ. Eur J Biochem. 1994; 220:117. [PubMed: 8119278]

485. Reyes F, Gavira M, Castillo F, Moreno-Vivian C. Biochem J. 1998; 331:897. [PubMed: 9560320]

486. Potter LC, Cole JA. Biochem J. 1999; 344:69. [PubMed: 10548535]

487. Frangioni B, Arnoux P, Sabaty M, Pignol D, Bertrand P, Guigliarelli B, Leger C. J Am Chem Soc. 2004; 126:1328. [PubMed: 14759176]

488. Fourmond V, Burlat B, Dementin S, Sabaty M, Arnoux P, Etienne E, Guigliarelli B, Bertrand P, Pignol D, Leger C. Biochemistry. 2010; 49:2424. [PubMed: 20146468]

489. Gates AJ, Richardson DJ, Butt JN. Biochem J. 2008; 409:159. [PubMed: 17900239]

490. (a) Gates AJ, Luque-Almagro VM, Goddard AD, Ferguson SJ, Roldan MD, Richardson DJ. Biochem J. 2011; 435:743. [PubMed: 21348864] (b) Gates AJ, Butler CS, Richardson DJ, Butt JN. Biochem Soc Trans. 2011; 39:236. [PubMed: 21265780]

491. Olmo-Mira MF, Cabello P, Pino C, Martinez-Luque M, Richardson DJ, Castillo F, Roldan MD, Moreno-Vivan C. Arch Microbiol. 2006; 186:339. [PubMed: 16897035]

492. Lin, JT.; Stewart, V. Advances in Microbial Physiology. Poole, RK., editor. Vol. 39. Elsevier; New York: 1998.

493. (a) Wang BM, Pierson LS, Rensing C, Gunatilaka MK, Kennedy C. Appl Environ Microbiol. 2012; 78:6558. [PubMed: 22773651] (b) Ramos F, Blanco G, Gutierrez JC, Luque F, Tortolero M. Mol Microbiol. 1993; 8:1145. [PubMed: 8361359]

494. (a) Gates AJ, Luque-Almagro VM, Goddard AD, Ferguson SJ, Dolores Roldan M, Richardson DJ. Biochem J. 2011; 435:743. [PubMed: 21348864] (b) Luque-Almagro VM, Gates AJ, Moreno-Vivian C, Ferguson SJ, Richardson DJ, Roldan MD. Biochem Soc Trans. 2011; 39:1838. [PubMed: 22103536]

495. Ogawa KI, Akagawa E, Yamane K, Sun ZW, Lacelle M, Zuber P, Nakano MM. J Bacteriol. 1995; 177:1409. [PubMed: 7868621]

496. Martinnieto J, Flores E, Herrero A. Plant Physiol. 1992; 100:157. [PubMed: 16652939]

497. Wang T-H, Chen Y-H, Huang J-Y, Liu K-C, Ke S-C, Chu H-A. Plant Physiol Biochem. 2011; 49:1369. [PubMed: 21821424]

498. Jepson BJN, Anderson LJ, Rubio LM, Taylor CJ, Butler CS, Flores E, Herrero A, Butt JN, Richardson DJ. J Biol Chem. 2004; 279:32212. [PubMed: 15166246]

499. Hirasawa M, Rubio LM, Griffin JL, Flores E, Herrero A, Li J, Kim SK, Hurley JK, Tollin G, Knaff DB. Biochim Biophys Acta, Bioenerg. 2004; 1608:155.

500. Srivastava AP, Hirasawa M, Bhalla M, Chung J-S, Allen JP, Johnson MK, Tripathy JN, Rubio LM, Vaccaro B, Subramanian S, Flores E, Zabet-Moghaddam M, Stitle K, Knaff DB. Biochemistry. 2013; 52:4343. [PubMed: 23692082]

501. Gangeswaran R, Lowe DJ, Eady RR. Biochem J. 1993; 289:335. [PubMed: 8380991]

502. Heinrich-Salmeron A, Cordi A, Brochier-Armanet C, Halter D, Pagnout C, Abbaszadeh-Fard E, Montaut D, Seby F, Bertin PN, Bauda P, Arsene-Ploetze F. Appl Environ Microbiol. 2011; 77:4685. [PubMed: 21571879]

503. (a) Duval S, Santini JM, Nitschke W, Hille R, Schoepp-Cothenet B. J Biol Chem. 2010; 285:20442. [PubMed: 20421651] (b) Lebrun E, Brugna M, Baymann F, Muller D, Lievremont D, Lett MC, Nitschke W. Mol Biol Evol. 2003; 20:686. [PubMed: 12679550]

504. Lett MC, Muller D, Lievremont D, Silver S, Santini J. J Bacteriol. 2012; 194:207. [PubMed: 22056935]

505. Osborne TH, Jamieson HE, Hudson-Edwards KA, Nordstrom DK, Walker SR, Ward SA, Santini JM. BMC Microbiol. 2010; 10:205. [PubMed: 20673331]

506. Warelow TP, Oke M, Schoepp-Cothenet B, Dahl JU, Bruselat N, Sivalingam GN, Leimkuhler S, Thalassinos K, Kappler U, Naismith JH, Santini JM. PLoS One. 2013; 8:e72535. [PubMed: 24023621]

507. Conrads T, Hemann C, George GN, Pickering IJ, Prince RC, Hille R. J Am Chem Soc. 2002; 124:11276. [PubMed: 12236735]

508. Anderson GL, Williams J, Hille R. J Biol Chem. 1992; 267:23674. [PubMed: 1331097]

509. Lieutaud A, van Lis R, Duval S, Capowiez L, Muller D, Lebrun R, Lignon S, Fardeau M-L, Lett M-C, Nitschke W, Schoepp-Cothenet B. J Biol Chem. 2010; 285:20433. [PubMed: 20421652]

510. Hoke KR, Cobb N, Armstrong FA, Hille R. Biochemistry. 2004; 43:1667. [PubMed: 14769044]

511. Bernhardt PV, Santini JM. Biochemistry. 2006; 45:2804. [PubMed: 16503635]

512. van Lis R, Nitschke W, Warelow TP, Capowiez L, Santini JM, Schoepp-Cothenet B. Biochim Biophys Acta, Bioenerg. 2012; 1817:1701.

513. Saltikov CW, Newman DK. Proc Natl Acad Sci USA. 2003; 100:10983. [PubMed: 12939408]

514. Saltikov CW, Cifuentes A, Venkateswaran K, Newman DK. Appl Environ Microbiol. 2003; 69:2800. [PubMed: 12732551]

515. Malasarn D, Saltikov W, Campbell KM, Santini JM, Hering JG, Newman DK. Science. 2004; 306:455. [PubMed: 15486292]

516. Krafft T, Macy JM. Eur J Biochem. 1998; 255:647. [PubMed: 9738904]

517. Malasarn D, Keeffe JR, Newman DK. J Bacteriol. 2008; 190:135. [PubMed: 17951391]

518. Richey C, Chovanec P, Hoeft SE, Oremland RS, Basu P, Stolz JF. Biochem Biophys Res Commun. 2009; 382:298. [PubMed: 19285953]

519. (a) Zargar K, Hoeft S, Oremland R, Saltikov CW. J Bacteriol. 2010; 192:3755. [PubMed: 20453090] (b) Sultana M, Vogler S, Zargar K, Schmidt A-C, Saltikov C, Seifert J, Schloemann

M. Arch Microbiol. 2012; 194:623. [PubMed: 22350109] (c) Zargar K, Conrad A, Bernick DL, Lowe TM, Stolc V, Hoeft S, Oremland RS, Stolz J, Saltikov CW. Environ Microbiol. 2012; 14:1635. [PubMed: 22404962]

520. Hoeft SE, Blum JS, Stolz JF, Tabita FR, Witte B, King GM, Santini JM, Oremland RS. Int J Syst Evol Microbiol. 2007; 57:504. [PubMed: 17329775]
521. Fisher JC, Hollibaugh JT. Appl Environ Microbiol. 2008; 74:2588. [PubMed: 18326681]
522. Kulp TR, Hoeft SE, Asao M, Madigan MT, Hollibaugh JT, Fisher JC, Stolz JF, Culbertson CW, Miller LG, Oremland RS. Science. 2008; 321:967. [PubMed: 18703741]
523. (a) Kniemeyer O, Heider J. J Biol Chem. 2001; 276:21381. [PubMed: 11294876] (b) Johnson HA, Pelletier DA, Spormann AM. J Bacteriol. 2001; 183:4536. [PubMed: 11443088]
524. Szaleniec M, Hagel C, Menke M, Nowak P, Witko M, Heider J. Biochemistry. 2007; 46:7637. [PubMed: 17542621]
525. Schroder I, Rech S, Krafft T, Macy JM. J Biol Chem. 1997; 272:23765. [PubMed: 9295321]
526. Thorell HD, Stenklo K, Karlsson J, Nilsson T. Appl Environ Microbiol. 2003; 69:5585. [PubMed: 12957948]
527. Hallberg BM, Bergfors T, Backbro K, Pettersson G, Henriksson G, Divne C. Struct Folding Des. 2000; 8:79.
528. Szaleniec M, Witko M, Heider J. J Mol Catal A: Chem. 2008; 286:128.
529. (a) Szaleniec M, Borowski T, Schuehle K, Witko M, Heider J. J Am Chem Soc. 2010; 132:6014. [PubMed: 20387836] (b) Szaleniec M, Salwinski A, Borowski T, Heider J, Witko M. Int J Quantum Chem. 2012; 112:1990.
530. Knack D, Hagel C, Szaleniec M, Dudzik A, Salwinski A, Heider J. Appl Environ Microbiol. 2012; 78:6475. [PubMed: 22773630]
531. (a) Schnell S, Brune A, Schink B. Arch Microbiol. 1991; 155:511.(b) Brune A, Schnell S, Schink B. Appl Environ Microbiol. 1992; 58:1861. [PubMed: 16348719]
532. Reichenbecher W, Schink B. Biochim Biophys Acta, Protein Struct Mol Enzymol. 1999; 1430:245.
533. Messerschmidt A, Niessen H, Abt D, Einsle O, Schink B, Kroneck PMH. Proc Natl Acad Sci USA. 2004; 101:11571. [PubMed: 15284442]
534. Raaijmakers H, Macieira S, Dias JM, Teixeira S, Bursakov S, Huber R, Moura JJG, Moura I, Romao MJ. Structure. 2002; 10:1261. [PubMed: 12220497]
535. Kisker C, Schindelin H, Baas D, Retey J, Meckenstock RU, Kroneck PMH. FEMS Microbiol Rev. 1998; 22:503. [PubMed: 9990727]
536. Solomon EI, Baldwin MJ, Lowery MD. Chem Rev. 1992; 92:521.

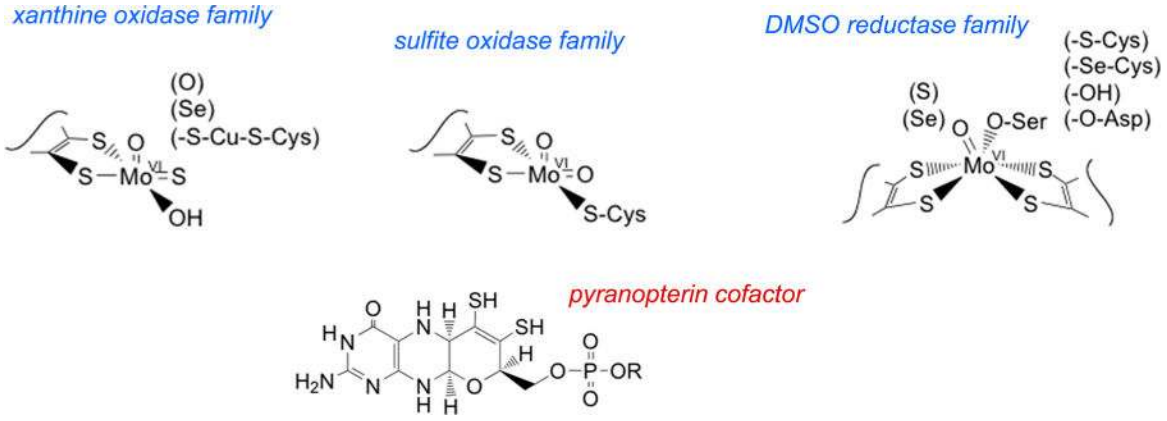

Figure 1.

Active site structures for the three families of mononuclear molybdenum enzymes. The structures shown are, from left to right, for xanthine oxidase, sulfite oxidase, and DMSO reductase. The structure of the pyranopterin cofactor common to all of these enzymes (as well as the tungsten-containing enzymes) is given at the bottom.

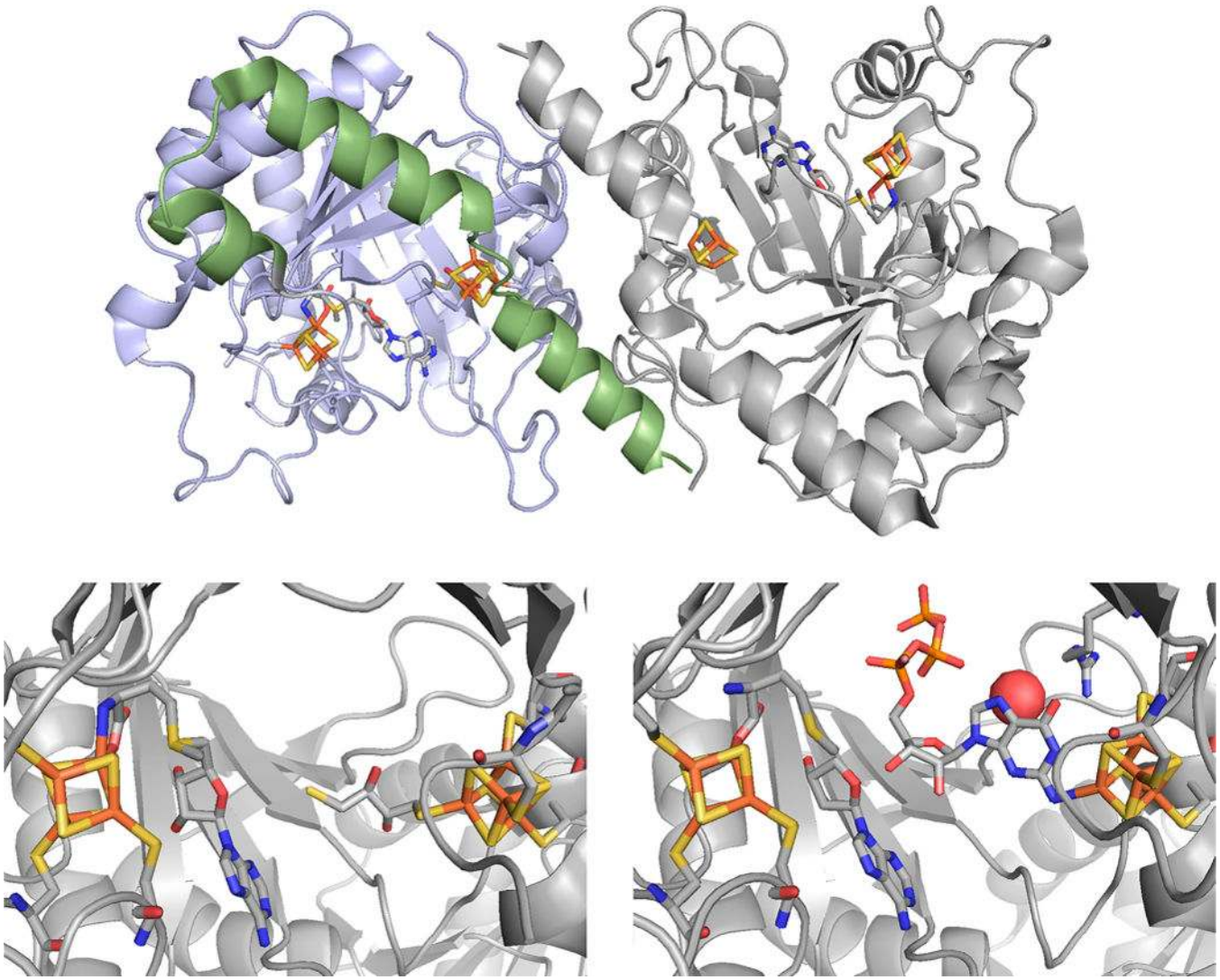

Figure 2.

The structure of MoaA from *S. aureus*. Top, the structure of the dimeric enzyme, with the N- and C-terminal domains of the subunit on the left shaded in blue and green, respectively. Bottom left, a close-up of the active site with S-adenosylmethionine bound to the N-terminal [4Fe-4S] cluster and dithiothreitol bound to the C-terminal [4Fe-4S] (PDB 1TV8). Bottom right, a close-up of the active site of GTP bound to the C-terminal cluster, and methionine bound at the N-terminal cluster; 5′deoxyadenosine is also present in the active site (PDB 2FB3).

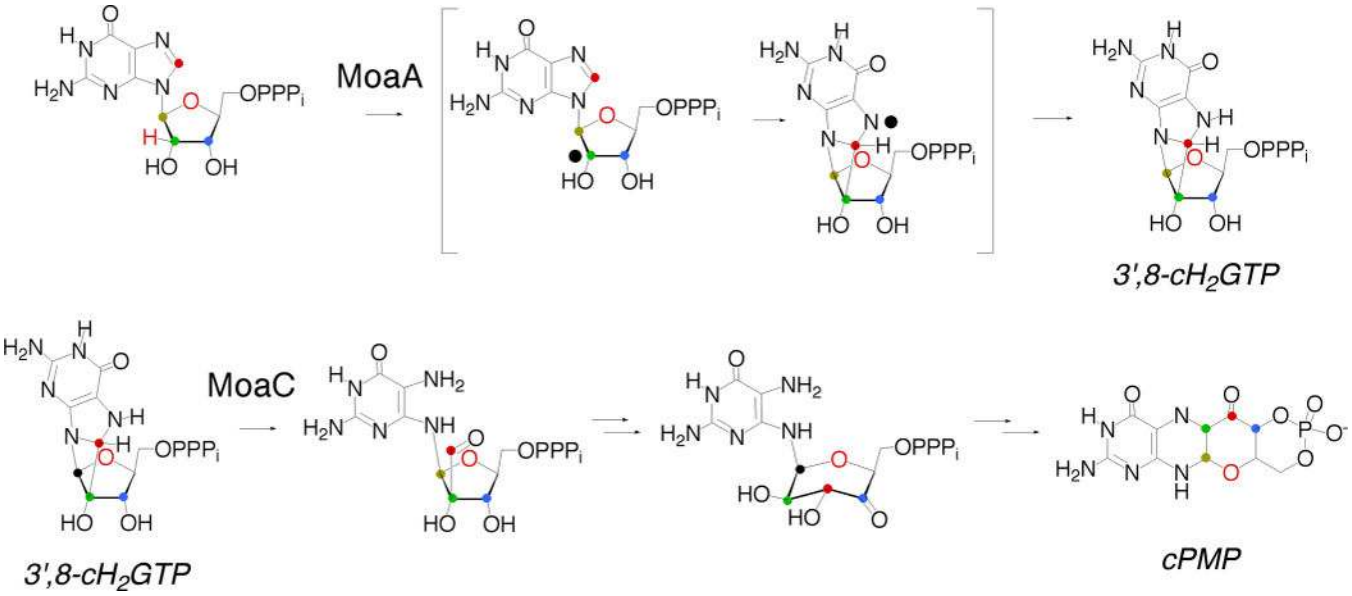

Figure 3.

The reactions catalyzed by MoaA and MoaC. It is possible that the MoaA reaction proceeds without opening of the ribose ring.

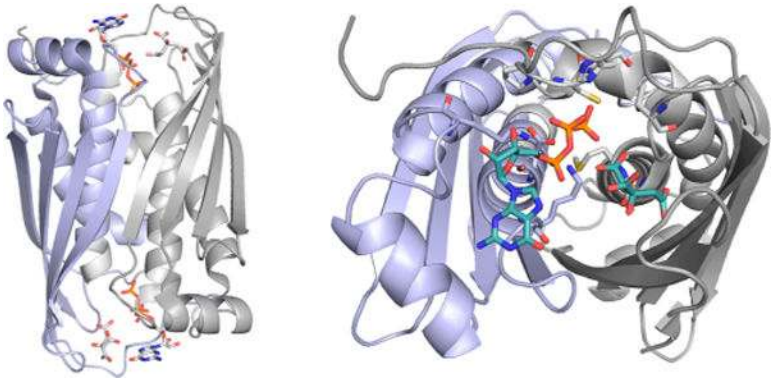

Figure 4.

The structure of MoaC in complex with GTP and citrate (PDB 3JQM). Left, overall structure of the dimer, with the two subunits in blue and gray. The GTP/citrate binding sites are at the top and bottom. Right, a close-up of one binding site, showing the bound GTP and citrate in teal.

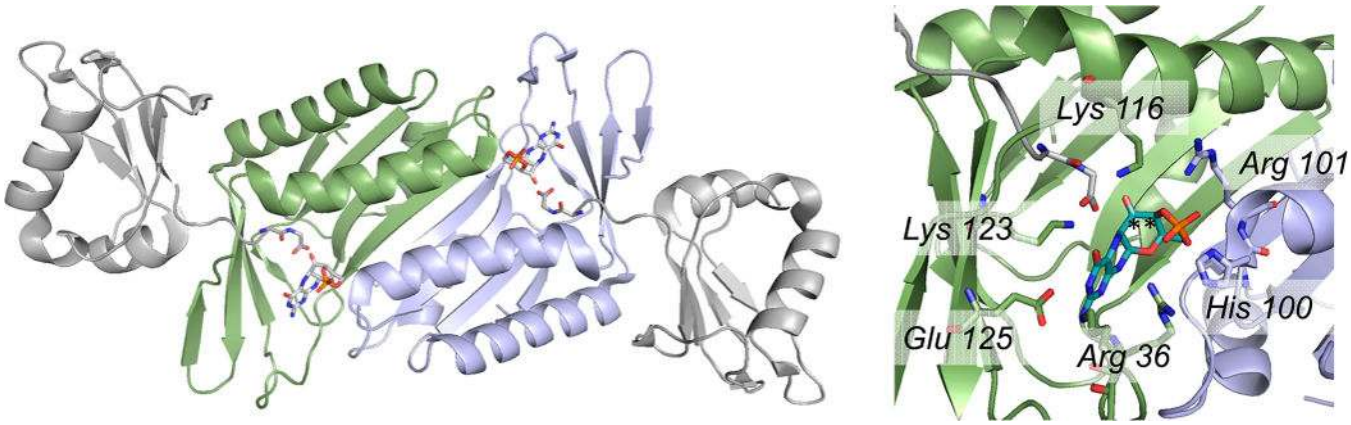

Figure 5.

The structure of *S. aureus* MoaDE in complex with cPMP (PDB 2QIE). Left, the overall structure of the $(\alpha\beta)_2$ heterotetramer, with the two MoaD subunits in gray, and the two MoaE subunits, with cPMP bound in each active site, in blue and green. The C-terminal tails of the MoaD subunits, ending in a highly conserved GG, are seen extending into the MoaD active sites. Right, a close-up of one active site showing the several amino acid residues interacting with the bound cPMP, and the proximity of the MoaD C-terminus to the positions to become sulfurated (indicated by asterisks).

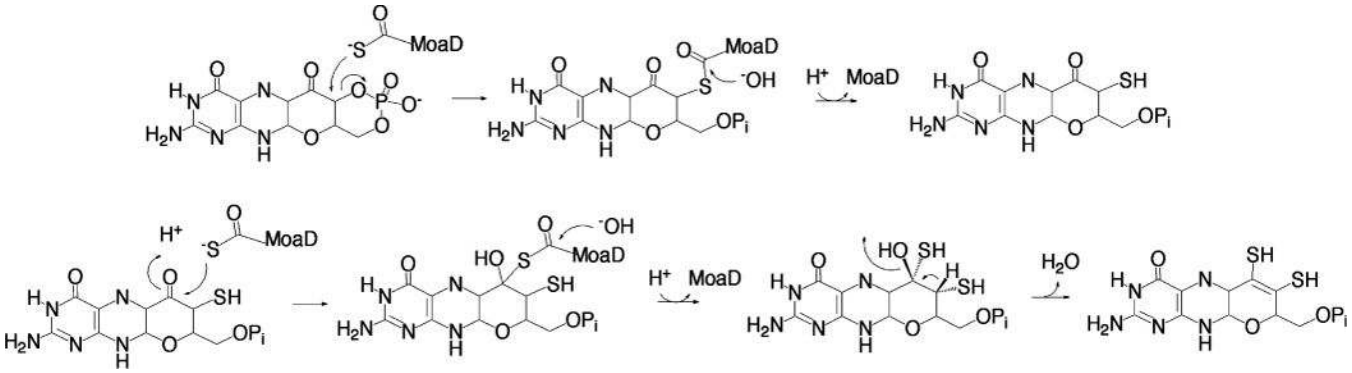

Figure 6.

The proposed reaction mechanism of MPT synthase (after ref 16). In the second sulfuration step (bottom), the stereochemistry of the pyran ring is inferred from the spatial disposition of cPMP relative to the C-terminus of MoaD (see Figure 5).

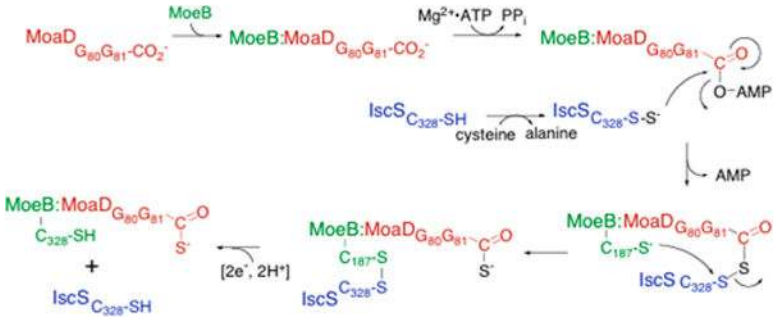

Figure 7.

The sulfuration of the carboxy terminus of MoaD. As shown, MoaD is in red, MoeB in green, and IscS in blue. Numbering is for the *E. coli* system.

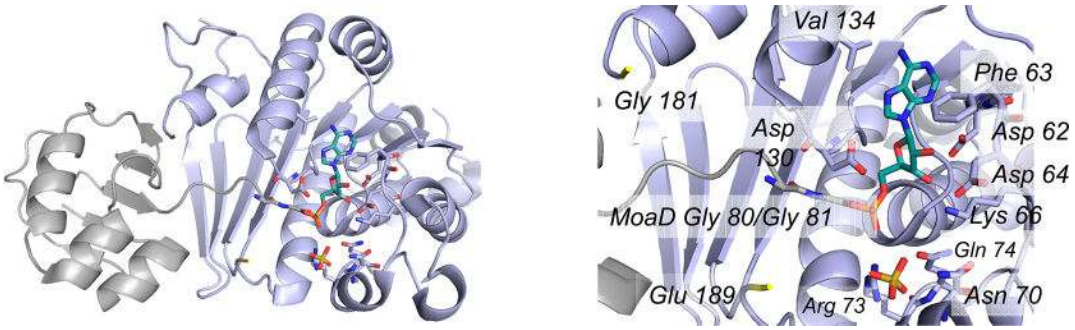

Figure 8.

The structure of the complex of adenylylated MoaD with MoeB (PDB 1JWB). Left, one functional αβ dimer of the overall $(\alpha\beta)_2$ tetramer, with MoeB in blue and MoaD in gray with its C-terminal GG rendered in CPK colors; the covalently attached adenylate is in teal. Residues 181 and 189 are indicated in yellow to demarcate the unresolved loop of MoeB that spans the C-terminus of MoaD (immediately above the four-stranded β-sheet at the far left of MoeB). Right, a close-up of the MoaD acyl adenylate bound in the active site of MoeB, showing amino acid residues interacting with it (including Phe 63 and Val 134, which lie on either side of the adenine, and Arg 73 that interacts with the phosphate). A sulfate ion from the crystallization mother liquor is also bound in the active site. Gly 181 and Glu 189, yellow, delimit the unresolved loop in the crystal structure that includes Cys 187.

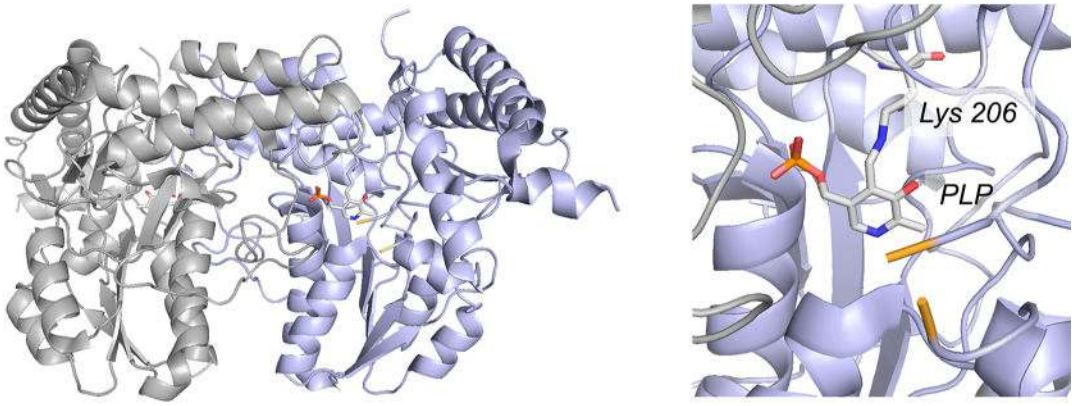

Figure 9.

The structure of the *E. coli* cysteine desulfurase IscS (PDB 1P3W). Right, the overall fold of the dimer, with the two subunits shown in gray and blue and the pyridoxal phosphate rendered in CPK colors. Left, a close-up of the active site, showing the pyridoxal phosphate present as a Schiff base with Lys 206. Residues 327 and 334, which delimit the unresolved residues 328–333 (including Cys 328 that is made of a persulfide in the course of the desulfurase reaction), are shown in yellow.

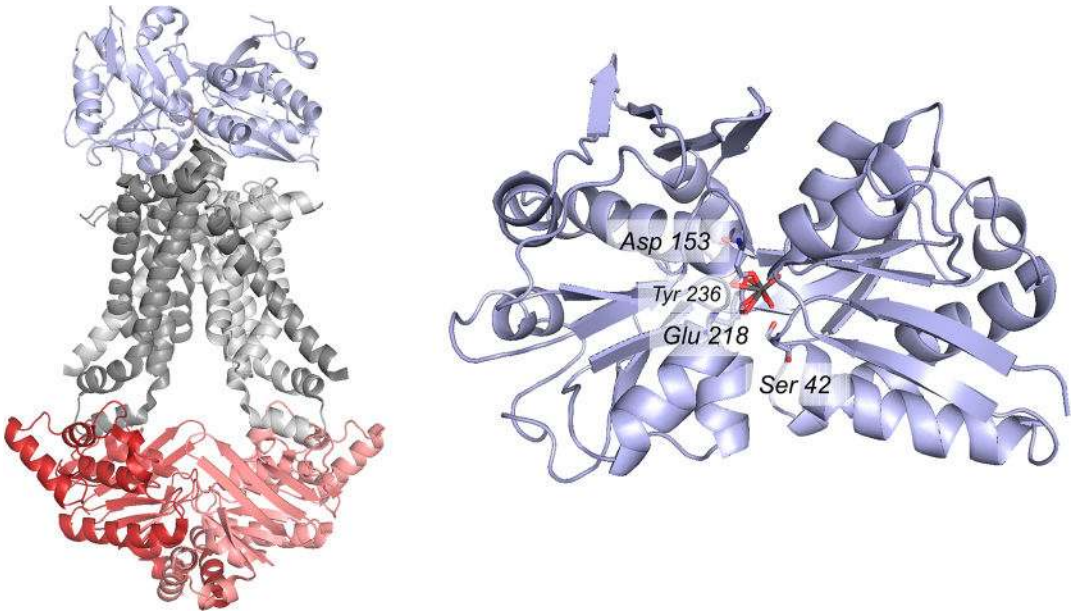

Figure 10.

The structure of the *A. fulgidus* molybdate transporter (PDB 2ONK). Left, the overall structure of the $ModAB_2C_2$ heteropentamer, with ModA in blue, ModB in gray, and ModC in red; the two subunits of ModB and ModC are indicated in dark and light shading. Right, the molybdate binding site of ModA, as seen from the face that interacts with the $ModB_2$ dimer. The anion binding site consists of Asp 153 and Glu 218, both bound in a bidentate fashion, plus Tyr 236 and Ser 42 that hydrogen bond to the bound anion (in the case of the crystal structure tungstate, rather than molybdate, from the crystallization mother liquor).

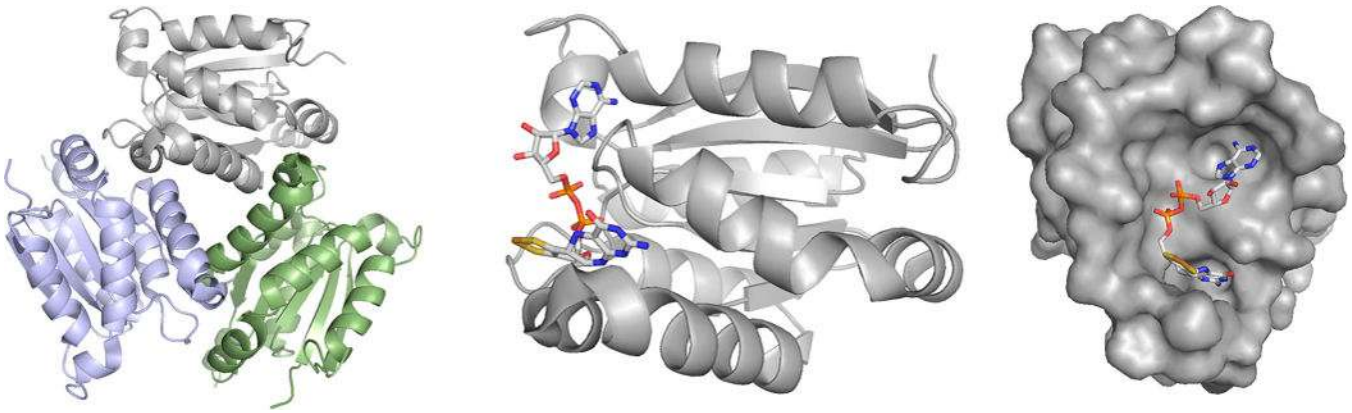

Figure 11.

The structure of MogA homologues. Left, the common trimeric structure of the proteins, as illustrated by the G domain of human gephyrin (PDB 1JLJ). Center, a single subunit of the *A. thaliana* Cnx1-G domain (shown in approximately the same orientation as the gray subunit of the trimer at left), in complex with its product, the adenylylated pyranopterin cofactor (MPT·AMP). The structure is of a fully functional S583A mutant (PDB 1UUY). Right, the surface of the *A. thaliana* G domain showing the deep crevice in which the product binds (the orientation is rotated 90° about the vertical as compared to that seen at center).

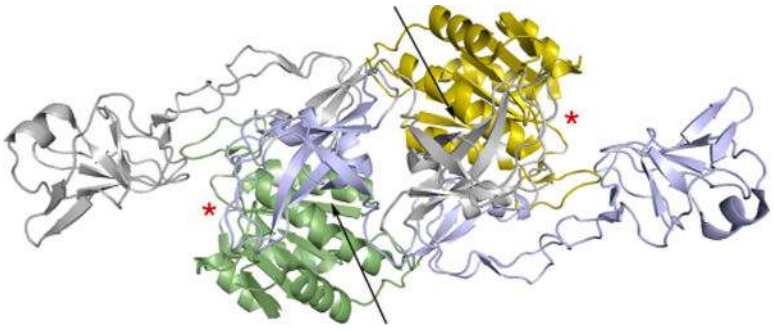

Figure 12.

The structure of the E domain of *A. thaliana* Cnx1 (PDB 1G8L). One subunit of the dimer is gray, with its Cnx1-G-like subdomain III in yellow, the other blue with its subdomain III in green. The two subdomains I are at extreme left (gray) and right (blue). The presumed active sites of the two MogA-like subdomains, based on homologies to the structure for MogA complexed with MPT-AMP, are indicated by the red asterisks. The cleft between subdomains III and IV of each subunit where the β-loop of the glycine receptor binds is indicated by the arrows. In the model for full-length gephyrin proposed by Belaidi and Schwarz,[50] the G domain of the monomer shown here in gray and yellow is assumed to occupy a position comparable that seen for the MogA-like subdomain III shown in green.

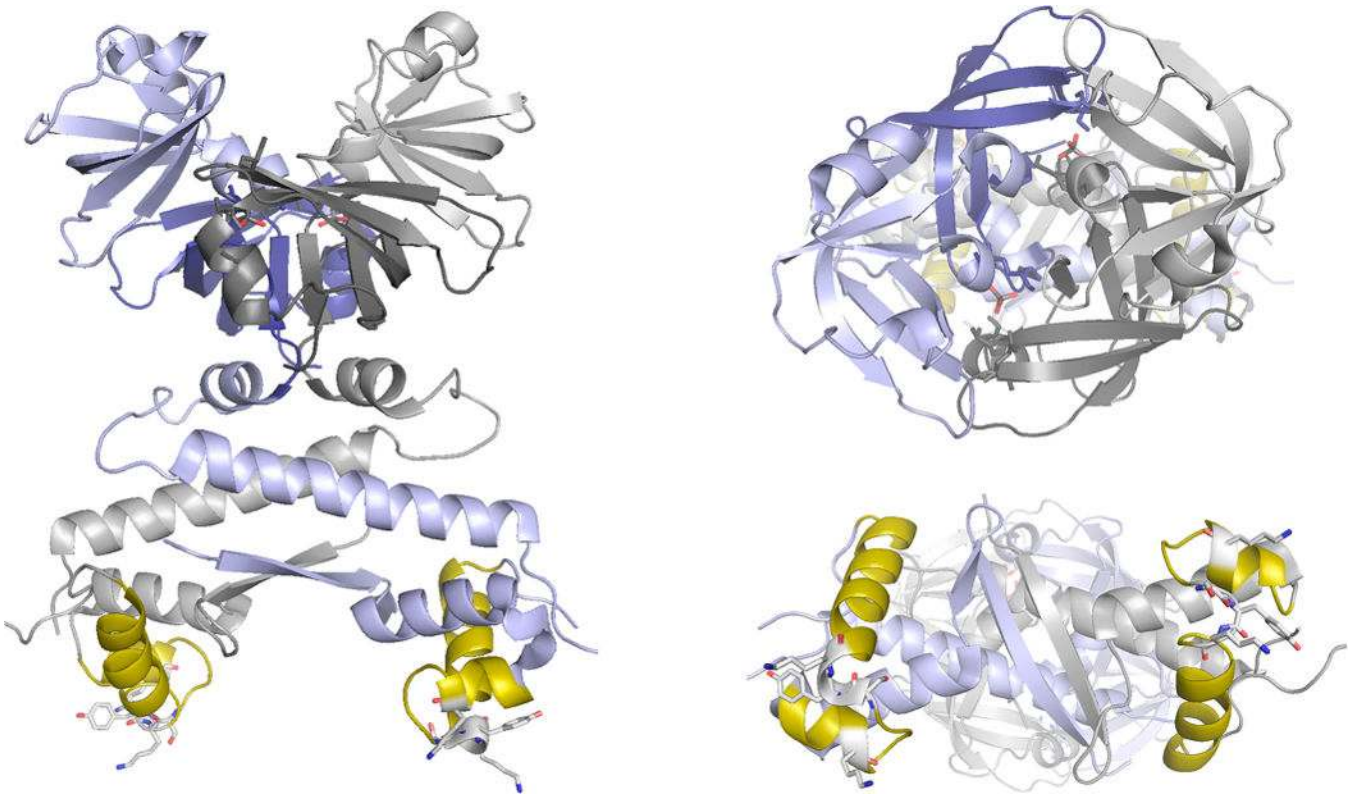

Figure 13.

The structure of molybdate-bound ModE from *E. coli* (PDB 1O7L). Left, the homodimer with subunits in blue and gray. The DNA-binding helix-turn-helix is shown in yellow, with residues likely to intercalate into the DNA major groove shown protruding out from the motif. Upper right, a close-up of the molybdenum-binding C-termini, with the two equivalents of bound molybdate indicated. The two molbindin subdomains of each subunit are indicated in light and dark shading. Bottom right, the N-terminal domains, showing the DNA-binding face of the protein.

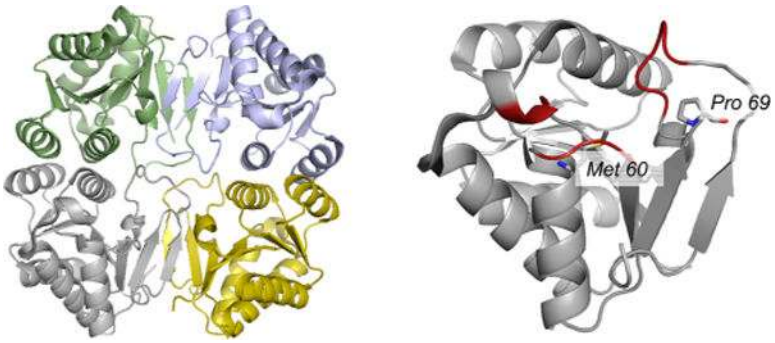

Figure 14.

The structure of the molybdenum cofactor carrier protein from *Chlamydomonas reinhardtii* (PDB 2IZ6). Left, the overall architecture of the $(\alpha_2)_2$ tetramer, with one α_2 dimer in blue and green, and the other in gray and yellow. Right, an enlargement of the gray subunit at left with the region identified as the possible cofactor binding site delimited by the regions in red, including Met 60 and Pro 69.

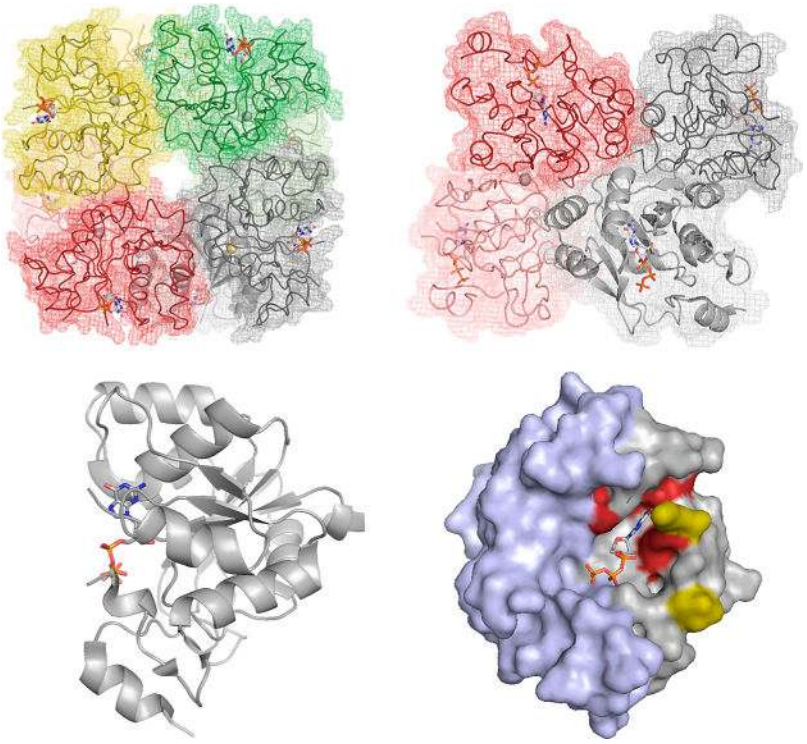

Figure 15.

The structure of *E. coli* MobA in complex with GTP (PDB 1FRW). Top left, the overall arrangement of the octamer, with the zinc ions indicated demarking the subunit interface of dimers (the subunits of which are shown in dark and light shades of the same color). Bound GTP is indicated shown in CPK. Top right, a side view of the octamer, illustrating the disposition of the GTP binding sites with respect to one another. Bottom left, a ribbon representation of one subunit shown from the side. Right, a space-filling representation looking into the GTP binding site. The N-terminal nucleotide-binding domains are in gray, and the C-terminal domain that interacts with apoenzymes requiring the dinucleotide product is in blue. Residues imparting specificity for GTP as opposed to MCD are shown in red.[80] It is to be noted that a seven-residue stretch between Lys 16 and Val 23 (yellow) is unresolved in the crystal structure, and the substrate is likely more protected from solvent than the image implies.

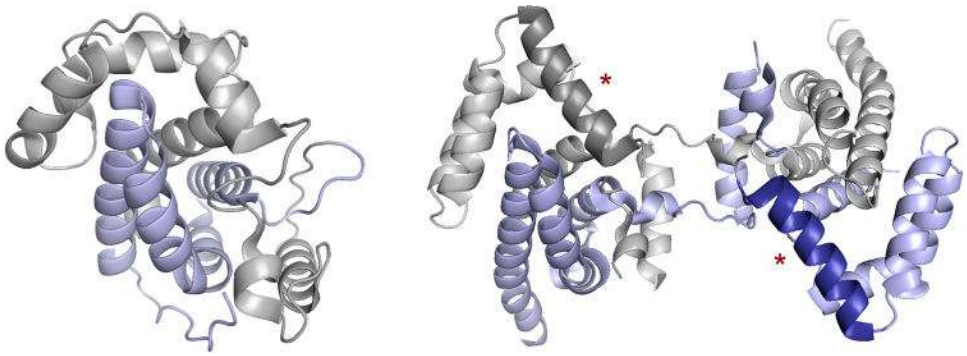

Figure 16.

Structures of molybdenum enzyme chaperones. Left, the monomeric *E. coli* DmsD (PDB 3EFP), with the N- and C-terminal domains colored gray and blue, respectively. Right, the dimeric *Shewanella massilia* TorD (PDB 1N1C), with subunits colored gray and blue, emphasizing the unique domain swapping that has occurred. The two helices shaded more darkly (red asterisks) are implicated in binding to the core of apo TMAO reductase.

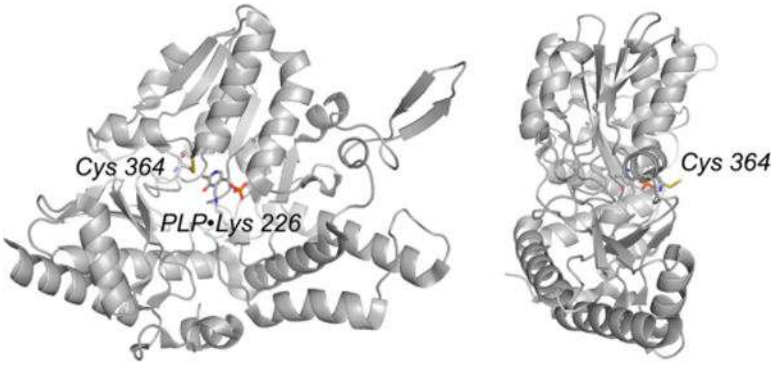

Figure 17.

Structure of the NifS with a persulfide at Cys 364 (PDB 1KMJ). The orientation at right is rotated approximately 90° about the vertical relative to the orientation at left.

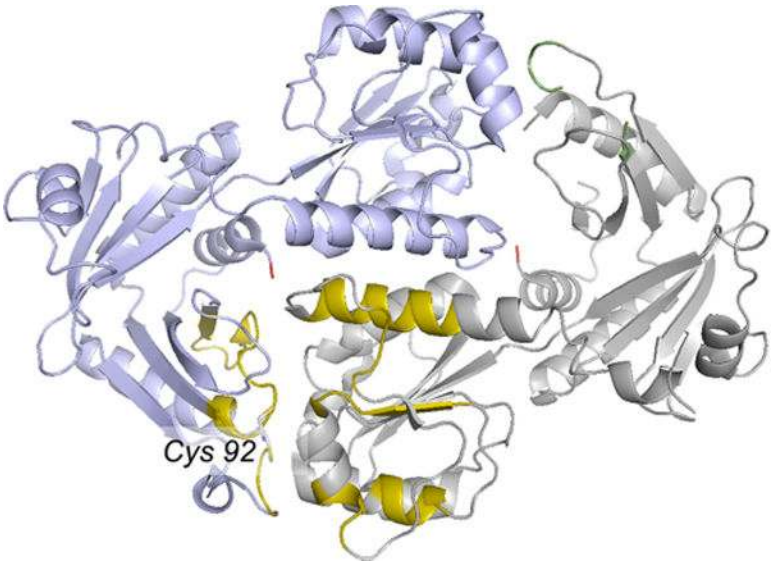

Figure 18.

Structure of the XdhC homologue from *Bacillus halodurans* (PDB 3ON5). One subunit of the homodimer is in light blue, the other in gray. The putative active site cysteine 92 is at the subunit interface at lower left, surrounded by conserved regions of polypeptide as identified by Neumann and Leimkuhler[92] in yellow. The corresponding region on the other side of the molecule is unresolved in the crystal structure.

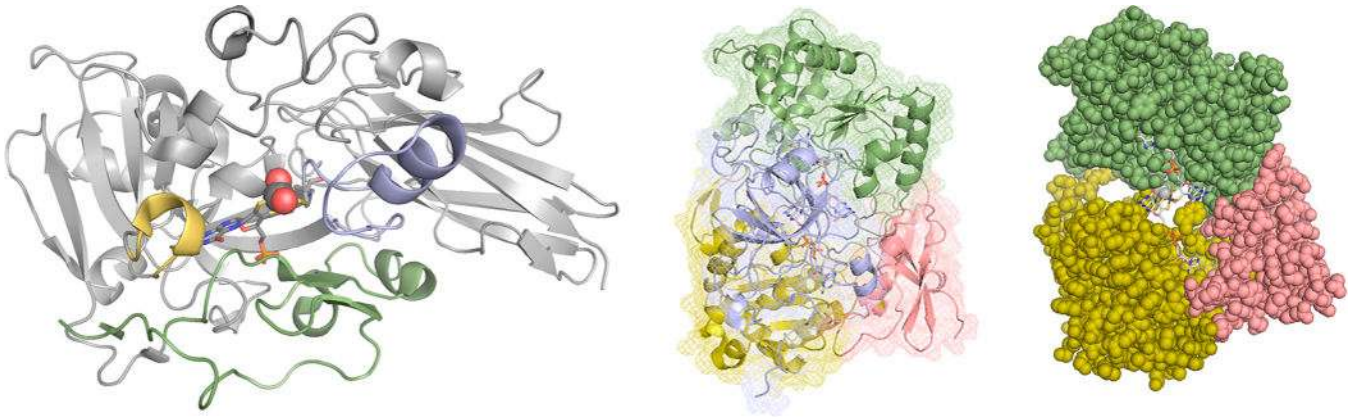

Figure 19.

Protein structure and cofactor insertion in sulfite oxidase and TMAO reductase. Left, the backbone trace of the *A. thaliana* sulfite oxidase (PDB 1OGP). The structural elements shown in yellow, blue, and green are in positions that could allow them to transiently swing away in a largely folded apoprotein to accommodate the incoming cofactor. Center, the structure of *S. massilia* TMAO reductase (PDB 1TMO), as seen from the back of the protein opposite the substrate access funnel, with Domains I-IV in red, yellow, green, and blue, respectively. Right, a space-filling representation with Domain IV removed, exposing the enzyme's molybdenum center from the back.

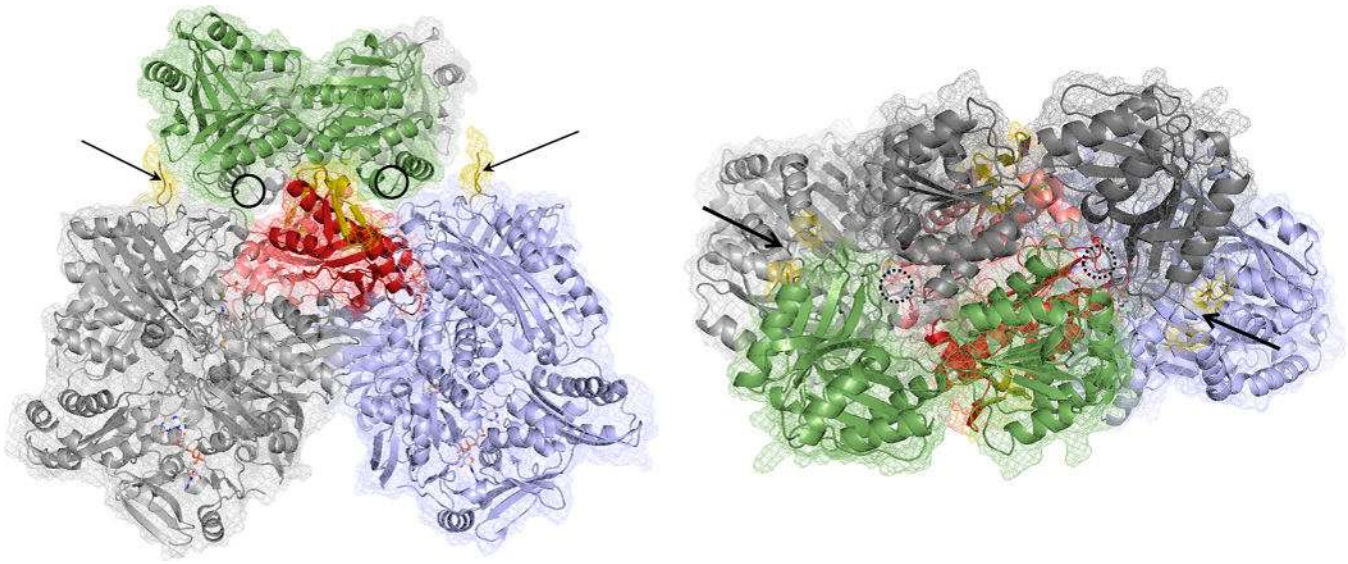

Figure 20.

A model for the interaction between *R. capsulatus* xanthine dehydrogenase (PDB 2W3R) and the *B. halodurans* XdhC homologue (PDB 3ON5). The xanthine dehydrogenase has its two αβ protomers colored light gray and blue, with the previously identified interaction motif of each protomer in red. The redox-active centers of the dehydrogenase are rendered as CPK-colored spheres. The XdhC homologue is rendered with its subunits in dark gray and green. The insets present in the bacterial members of the xanthine oxidase family (but absent in eukaryotic members) are indicated in yellow. The general locations of the cofactor binding sites in the latter are indicated by the circles. The orientation at right is rotated 90° about the horizontal relative to that at left.

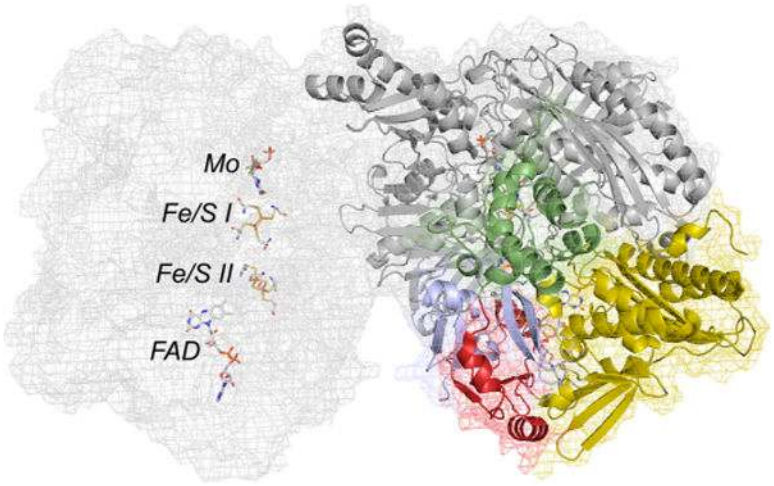

Figure 21.

The structure of bovine xanthine dehydrogenase (PDB 1FO4). From the N-terminus in the subunit at right, the domains are colored blue and green for the two [2Fe-2S] clusters (Fe/S II and Fe/S I, respectively), yellow for the FAD, and gray for the molybdenum-binding portion of the protein. The linker region between iron–sulfur-and FAD-binding domains is in red at the bottom left of the subunit. The subunit on the left is rendered in mesh to illustrate the spatial layout of the several redox-active centers within the subunit to illustrate the electron transfer pathway Mo → Fe/S I → Fe/S II → FAD. The two molybdenum centers are 52 Å apart.

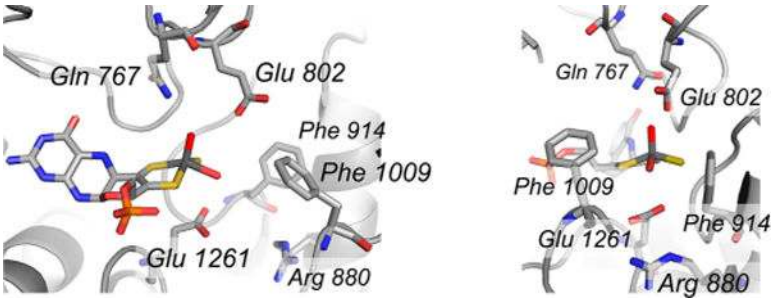

Figure 22.

The active site of xanthine dehydrogenase (PDB 1FO4). The several active site residues referred to in the text are indicated. The orientation at right is rotated 90° about the vertical from that at left, and represents the view from the solvent access channel. The PDB file has been modified to show the catalytically essential Mo=S ligand in an equatorial rather than apical position.

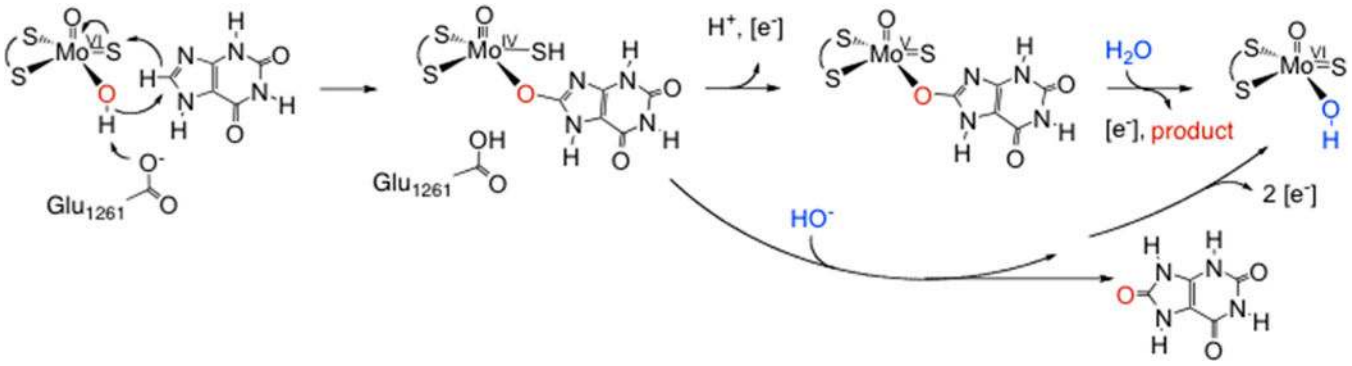

Figure 23.
The reaction mechanism of xanthine oxidase.

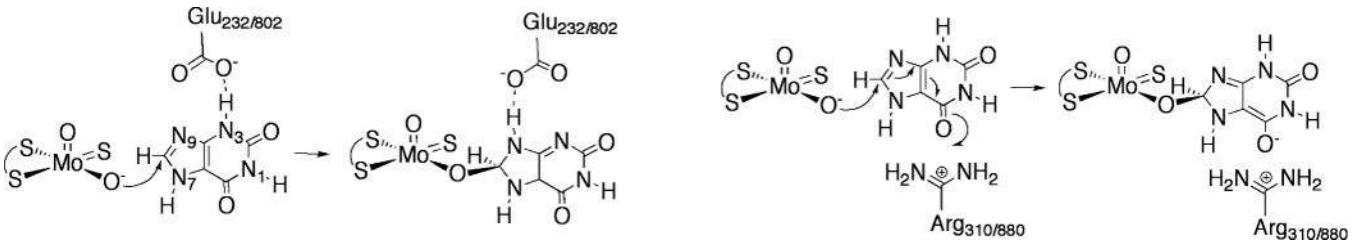

Figure 24.

The proposed mechanism whereby Glu 232/802 facilitates tautomerization (left) and Arg 880 stabilizes charge accumulation on the C_6=O of the heterocycle in the course of catalysis.

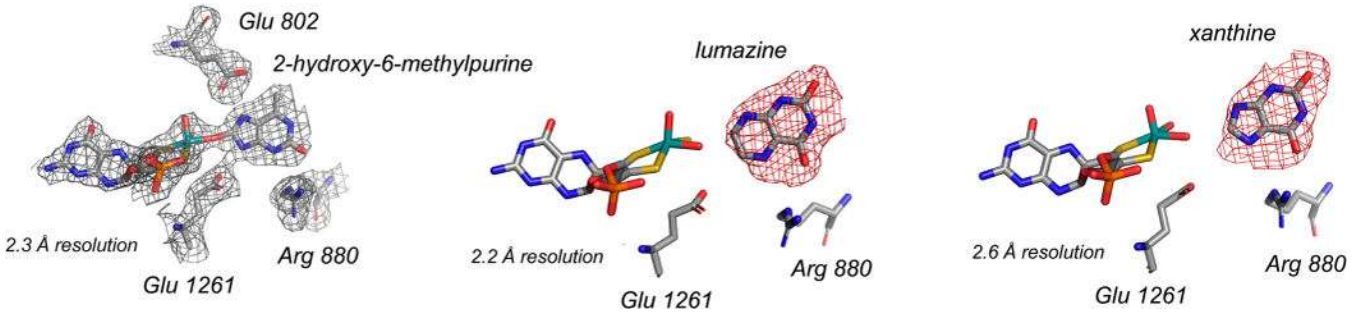

Figure 25.

Substrate orientation in the active site of xanthine oxidase. Left, 2-hydroxy-6-methylpurine, a poor substrate (3B9J); center, lumazine, a good substrate (3ETR); and right, xanthine (3EUB).

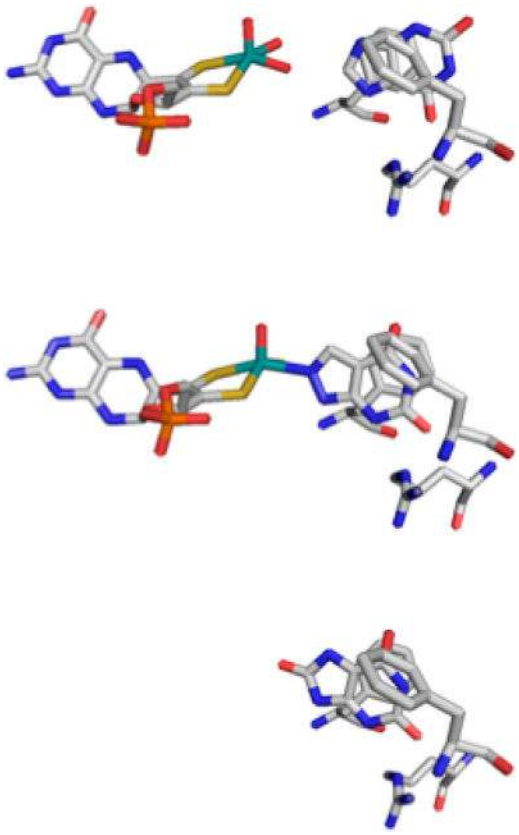

Figure 26.

Heterocycle position in the active site of xanthine oxidase. Top, xanthine bound to desulfo bovine enzyme (3EUB). Center, alloxanthine bound to functional bovine enzyme (3BDJ). Bottom, uric acid bound to the demolybdo form of the rat D428A mutant enzyme (3AN1). A comparison clearly shows that uric acid in the bottom structure sits deeper into the enzyme (further to the left) than does xanthine in the top structure.

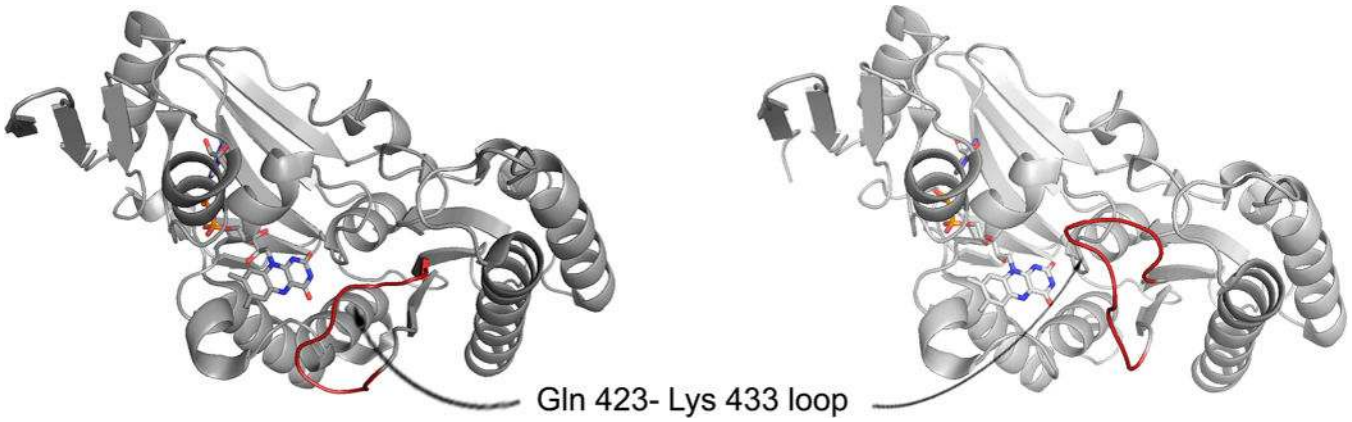

Figure 27.

Structures of the flavin domains of the dehydrogenase (left; PDB 1FO4) and oxidase (right; 1FIQ) forms of bovine xanthine oxidoreductase. The loop that rearranges and occludes NAD^+ binding upon proteolytic nicking or cysteine oxidation is indicated in red.

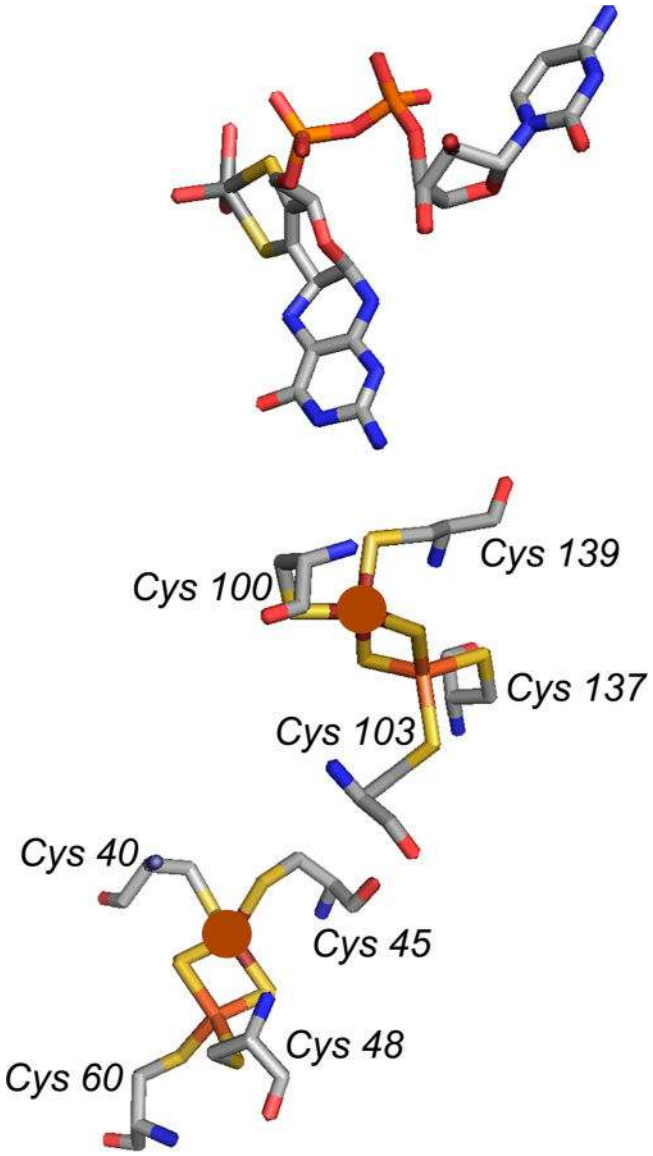

Figure 28.

The redox-active irons in the iron–sulfur clusters of aldehyde oxidoreductase (based on PDB 1VLB). The redox-active iron in Fe/S I (that is proximal to the molybdenum center) is coordinated by Cys 100 and Cys 139, while that in Fe/S II is coordinated by Cys 40 and Cys 45 (in brown sphere).

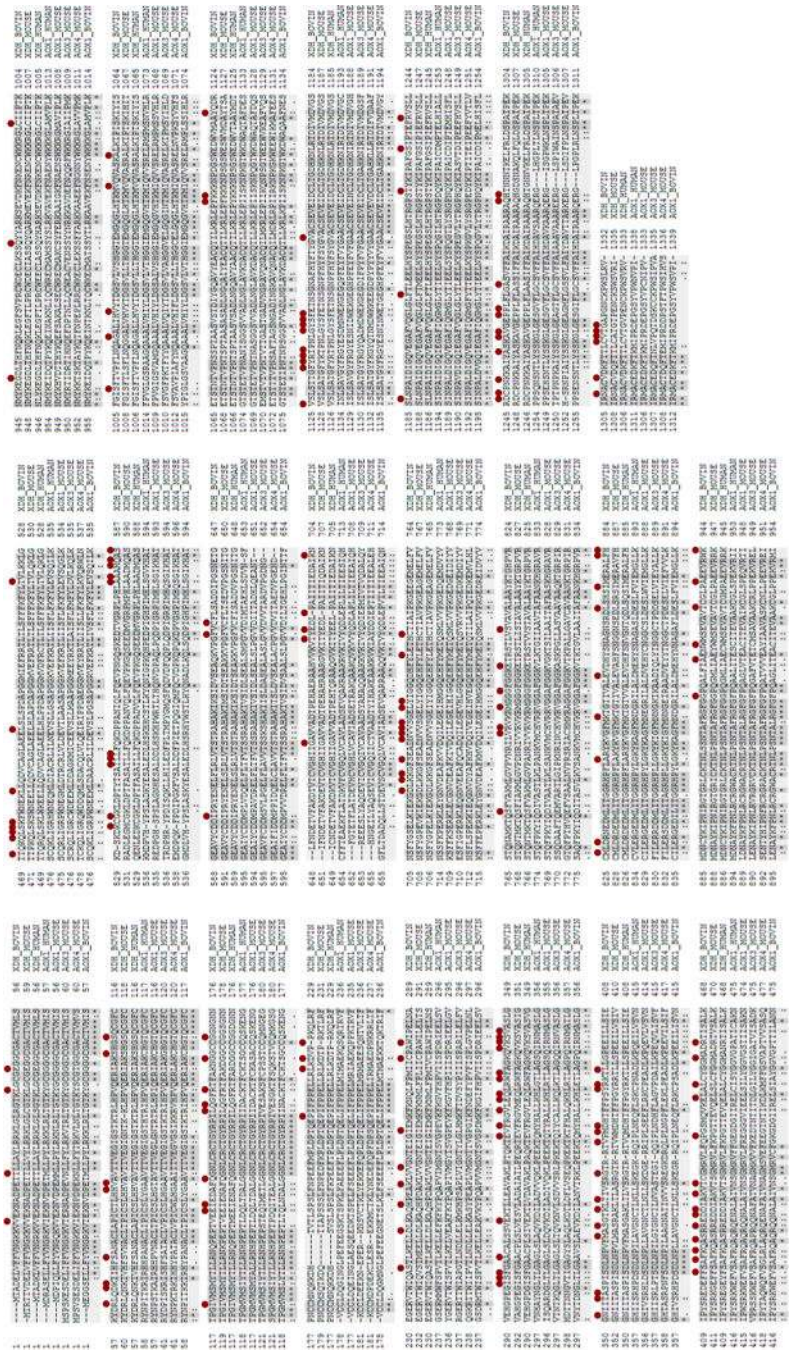

Figure 29.

Sequence alignment of mammalian aldehyde- and xanthine-oxidizing enzymes. Conserved residues common to both subfamilies are shaded and indicated with a black asterisk or colon at below the sequences. Residues conserved within each subfamily but not between the two are indicated with a red dot.

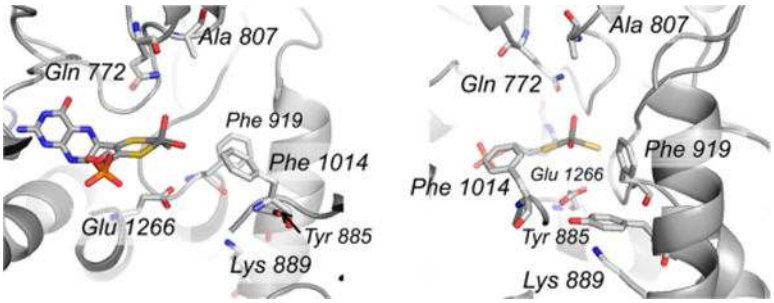

Figure 30.

The active site of murine aldehyde oxidase 3 (PDB 3ZYV). Conserved residues with the bovine xanthine oxidase include Phe 914/919 (bovine/murine numbering), Phe 1009/1014, Glu 1261/1266, and Gln 767/772. Amino acid residues that are not conserved include Glu 802/Ala 807, Arg 880/Tyr 885 (a methionine in most other aldehyde oxidases), His 884/Lys 889, and Leu 1014/Tyr 1019. Compare with Figure 22.

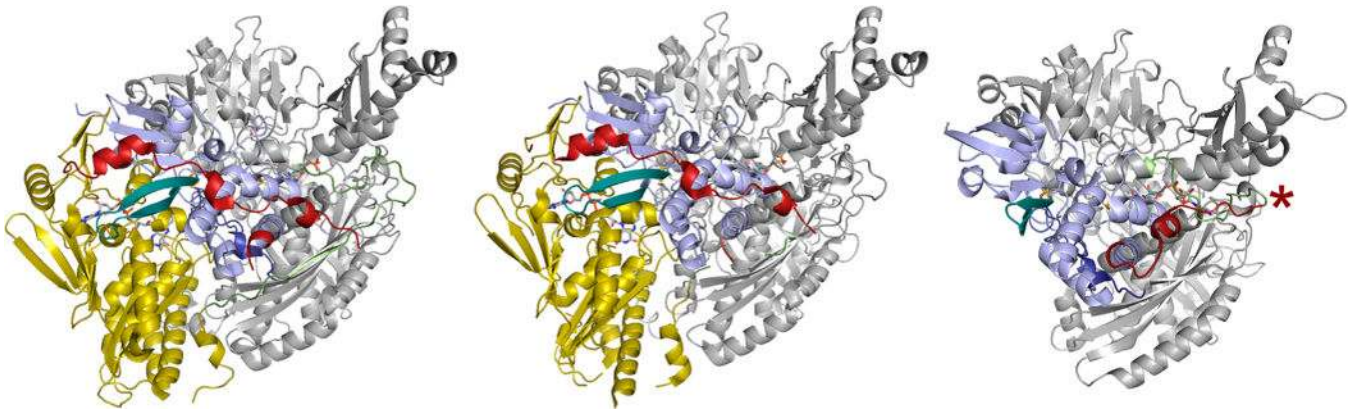

Figure 31.

A comparison of the polypeptide trace in bovine xanthine dehydrogenase (PDB F1O4), mouse aldehyde oxidase (PDB 3ZYV), and *D. gigas* aldehyde oxidoreductase (PDB 1VLB). The iron–sulfur domains (of one subunit each of the homodimers) are in blue, the FAD domains (when present) are in yellow, and the molybdenum domains are in gray. The linker between the Fe/S and FAD domains in the first two structures is in red, and the linker between the FAD and Mo domains is in green. In the bacterial enzyme at right, the single linker between the Fe/S and Mo domains is in red and green, with the approximate point of insertion of the FAD domain indicated by the red asterisk (far right). The β-turn of the first Fe/S domain that is elongated in the eukaryotic enzymes is shown in teal.

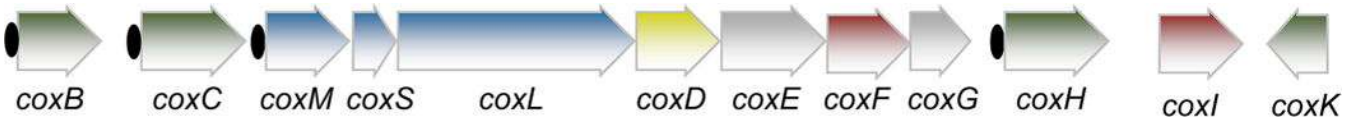

Figure 32.

Gene organization of the coxBCMSLDEFGHIK cluster of *O. carboxidovorans*. In addition to the structural genes coxMSL (blue), the gene cluster encodes the four membrane-associated proteins CoxB, CoxC, CoxH, and CoxK (green) and the two XdhC-like proteins CoxF and CoxI (red). CoxD (yellow) is a membrane-associated AAA+ ATPase thought to be involved in incorporation of the μ-sulfido bridge and copper of the binuclear center. Identified promoter regions are indicated as black ovals.[107]

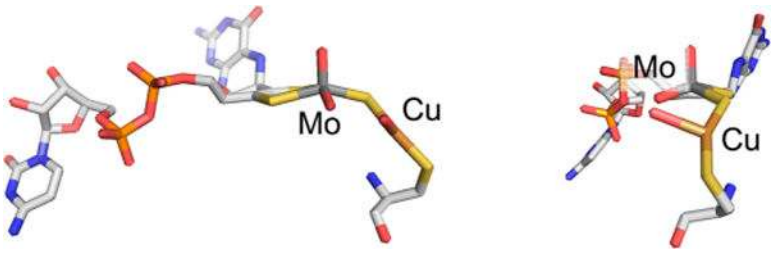

Figure 33.

The structure of the binuclear Mo^{VI}/Cu^{I} cluster of CO dehydrogenase (PDB 1N5W). The perspective at right is rotated approximately 90° about the vertical from that at left.

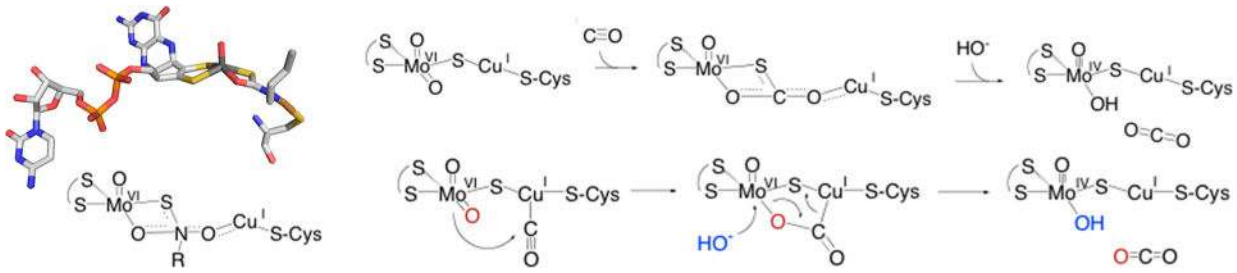

Figure 34.

Possible reaction mechanisms for CO dehydrogenase. Left, the crystal structure (top) and model (bottom) for the *n*-butylisonitrile complex of *O. carboxidovorans* CO dehydrogenase (PDB 1N62). Upper right, a reaction mechanism proposed on the basis of the structure of the isonitrile complex; lower right, an alternate reaction mechanism based on an initial copper carbonyl complex.

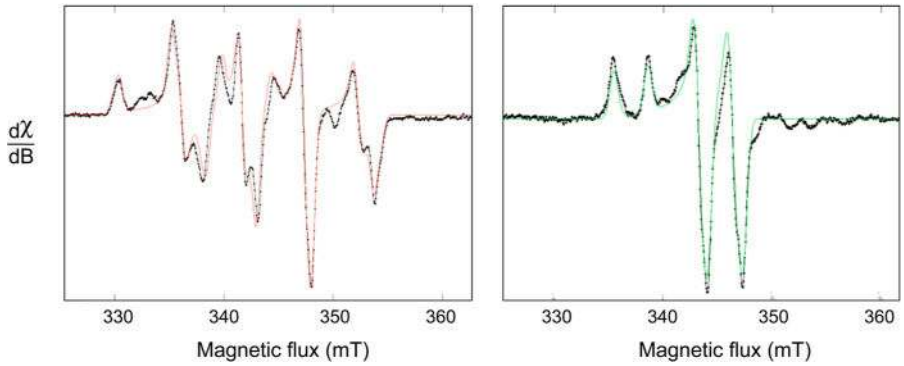

Figure 35.

EPR of as-isolated Mo/Cu CO dehydrogenase (left) and Ag-substituted enzyme (right). Experimental spectra are in black, and simulations are in color. For the native enzyme, the fitting parameters used were $g_{1,2,3}$ = 2.0010, 1.9604, 1.9549 and $A_{1,2,3}$ = 117, 164, 132 MHz; for the silver-substituted, the parameters were $g_{1,2,3}$ = 2.0043, 1.9595, 1.9540 and $A_{1,2,3}$ = 82.0, 78.9, 81.9 MHz.[240]

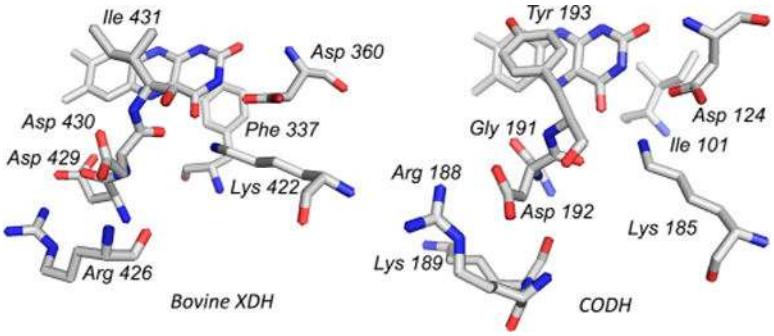

Figure 36.

A comparison of the FAD site of bovine xanthine dehydrogenase (PDB 1FO4) and CO dehydrogenase (PDB 1N5W). Structural elements in common include the Asp/Lys pair adjacent to the pyrimidine ring of the FAD and the Asp/Arg pair below the dimethylbenzene ring. By contrast, in CO dehydrogenase the aromatic residue lies above the isoalloxazine ring and the isoleucine behind, the reverse of that seen in xanthine dehydrogenase. Also, the immediate vicinity of the dimethylbenzene is acidic in xanthine dehydrogenase, and alkaline in CO dehydrogenase.

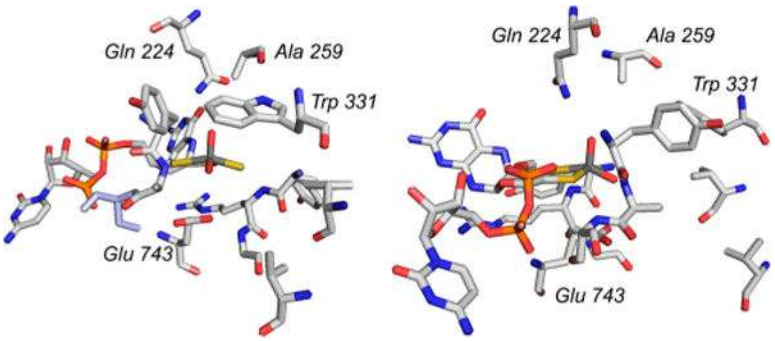

Figure 37.

The active site of quinoline 2-oxidoreductase (PDB 1T3Q). The amino acid residues discussed in the text are indicated.

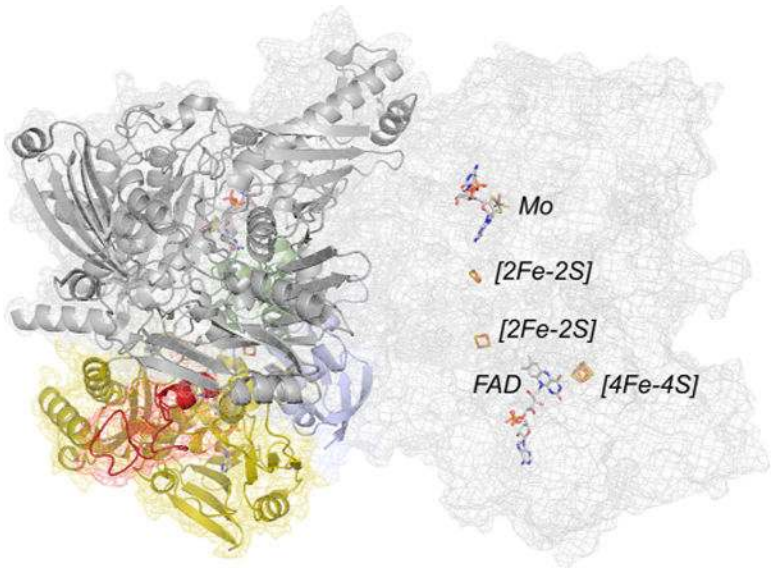

Figure 38.

The structure of 4-hydroxybenzoyl-CoA reductase (PDB 1RM6). The protomer at left is color coded with the two domains of the iron–sulfur-containing subunit in blue and green, the FAD-containing subunit in yellow (with the [4Fe-4S]-containing inset in red), and the molybdenum-containing subunit in gray. The protomer at right is shown in mesh so as to more clearly illustrate the disposition of the several redox-active centers with respect to one another (rendered in CPK coloring).

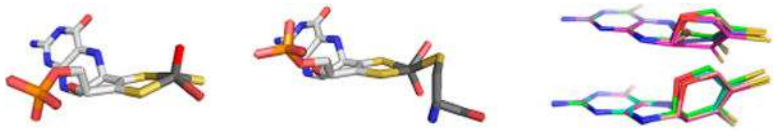

Figure 39.

A comparison of conformations of molybdenum centers in members of the xanthine oxidase and sulfite oxidase families. Left, the molybdenum center of bovine xanthine oxidase (PDB 1FO4), with the apical oxo group oriented up; center, the molybdenum center of chicken sulfite oxidase (PDB 1SOX) with the apical oxo group oriented down; right, a comparison of the extent of pyranopterin distortion in representative members of the sulfite oxidase (top)[36] and xanthine oxidase (bottom)[536] families. After Rothery et al.[263]

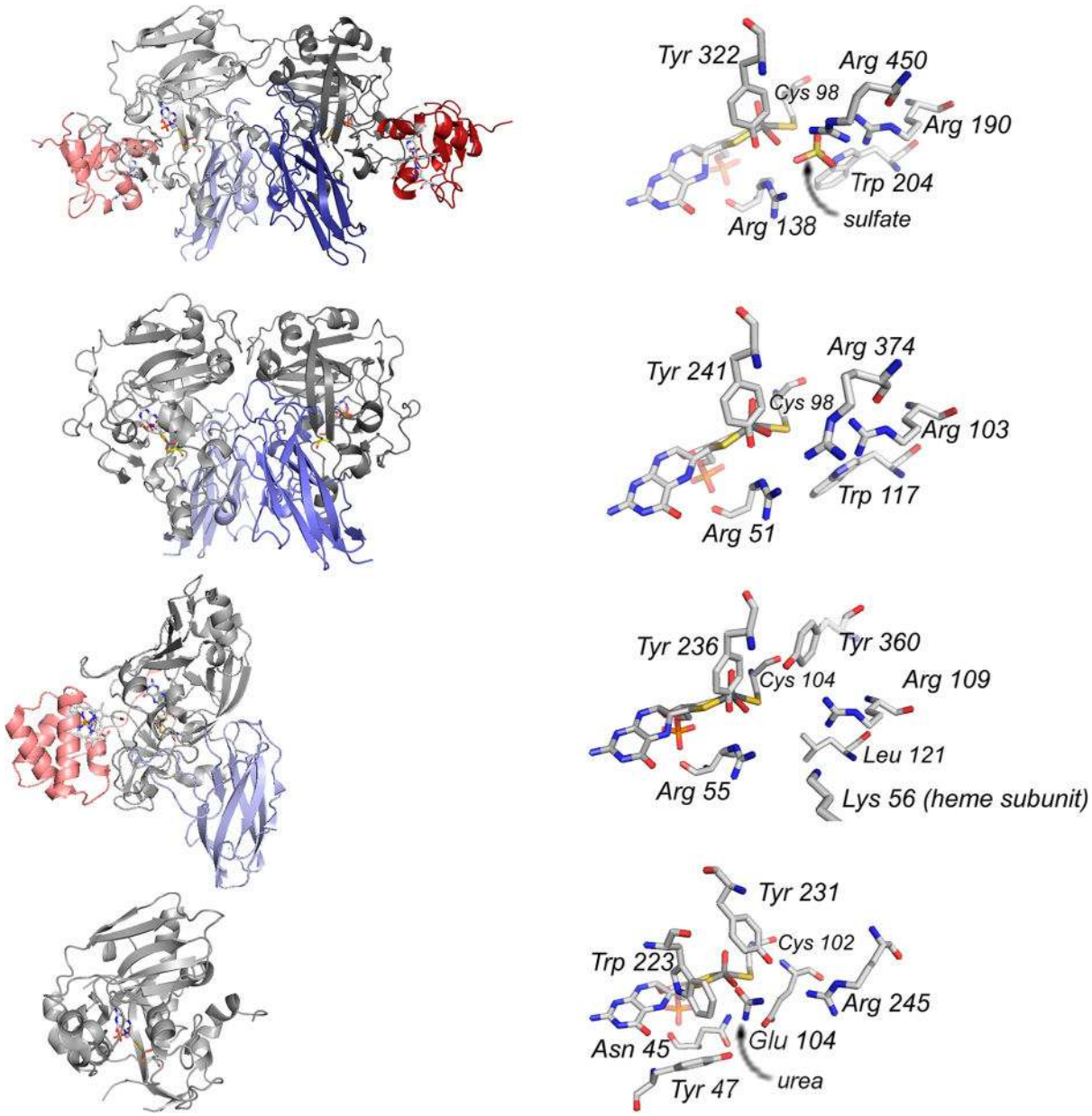

Figure 40.

Structures of sulfite-oxidizing enzymes. From top to bottom: chicken sulfite oxidase (PDB 1SOX), *A. thaliana* sulfite oxidase (PDB 1OGP), *S. novella* sulfite dehydrogenase (PDB 2BPB), and *E. coli* YedY (PDB 1XDQ). Left, the overall protein folds, with heme domains/subunits in red and interface domain in blue (when present). Right, the enzyme active sites, with homologous residues labeled as discussed in the text.

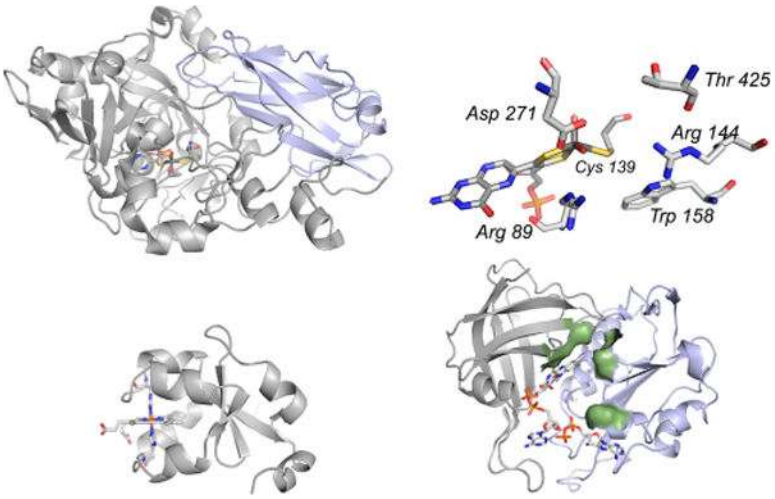

Figure 41.

Domain structures for the assimilatory nitrate reductases. Top left, the molybdenum fragment from *P. angusta* (PDB 2BIH), with the dimerization domain common to the sulfite oxidases (Figure 40) in blue. Top right, the active site molybdenum center, with residues referred to in the text indicated. Bottom left, bovine cytochrome b_5 (PDB 1CYO); and bottom right, the FAD fragment of *Z. mays* nitrate reductase (PDB 1CNF), with bound ADP to indicate the NAD^+ binding site. The NAD^+ binding domain is in blue.

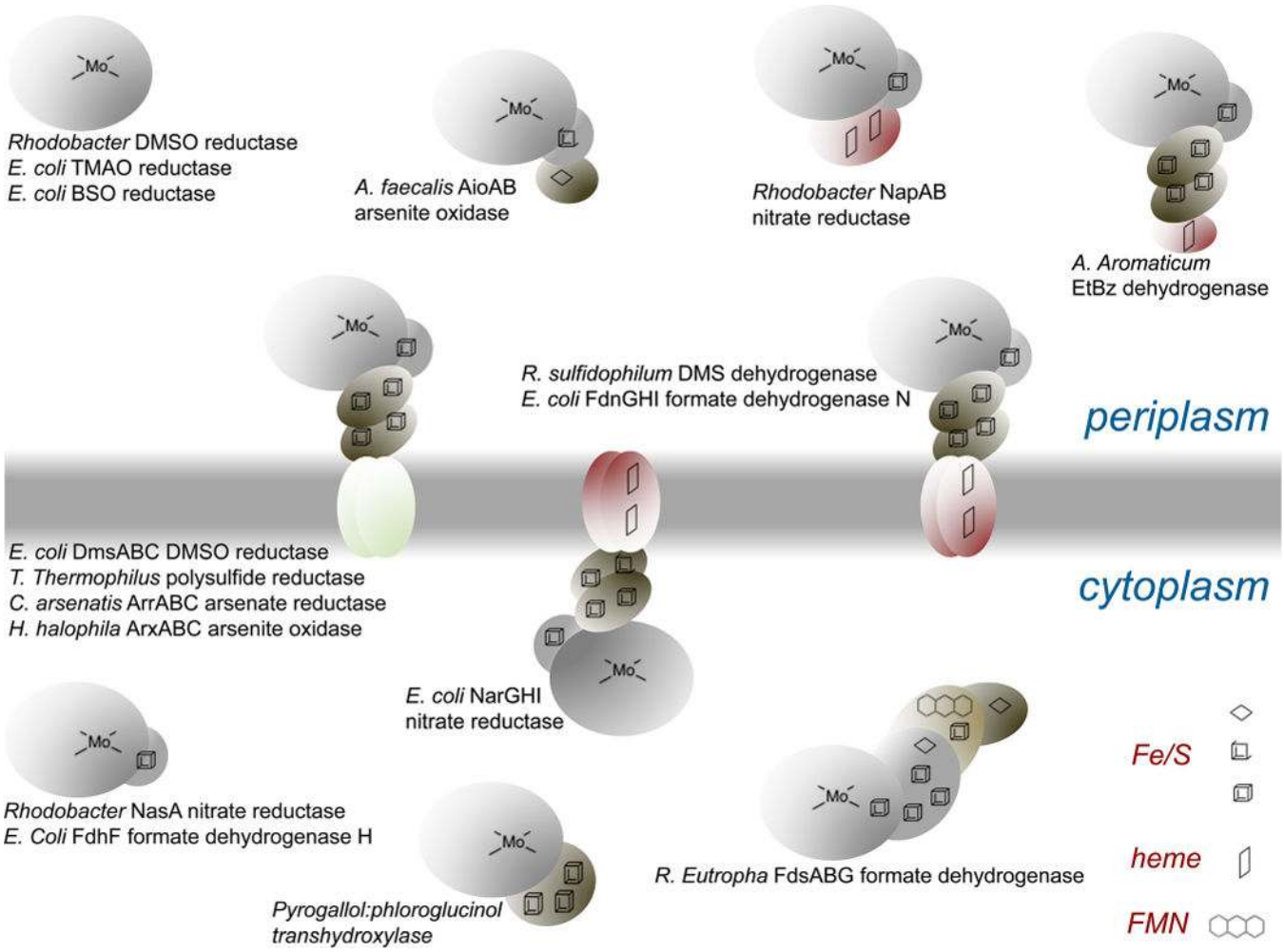

Figure 42.

Examples of protein architectures seen for members of the DMSO reductase family of enzymes. The membrane-integral enzymes can exist as oligomers of the structures shown; only the functional protomers are indicated. A key to the types of redox-active centers found in these proteins is given at bottom right.

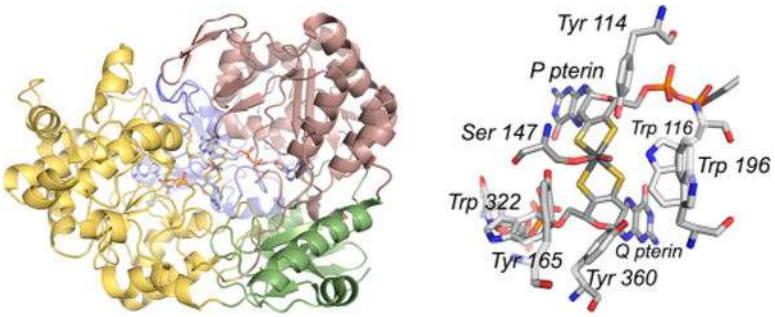

Figure 43.

The structure of *R. sphaeroides* DMSO reductase (PDB 1EU1). Left, the overall fold of the protein. The four domains of the polypeptide are color-coded for clarity, with those colored yellow and red related by a pseudo two-fold axis of symmetry. The pyranopterin designated Q is associated for the most part with the yellow domain, and that designated P is with the red domain. Right, a close-up of the active, with Ser 147 coordinated to the molybdenum, and other residues of the active site as indicated.

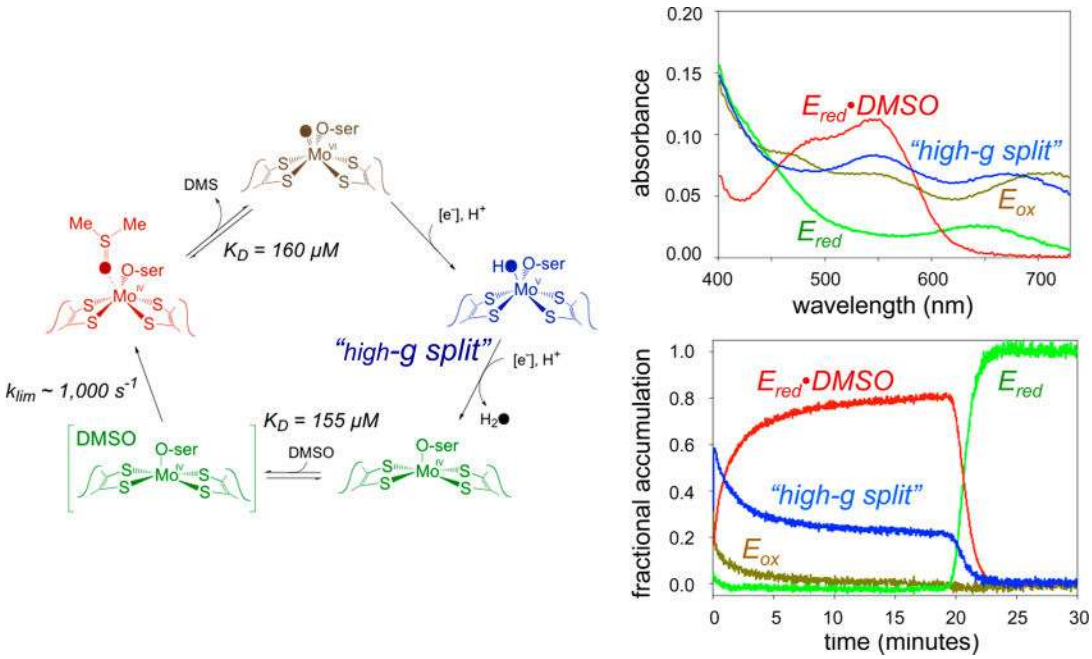

Figure 44.

The catalytic cycle of DMSO reductase. Left, the overall catalytic cycle. Upper right, the deconvoluted absorption spectra for each of the four spectroscopically distinct species. Lower right, the time course for each species in the course of turnover with DMSO as substrate.

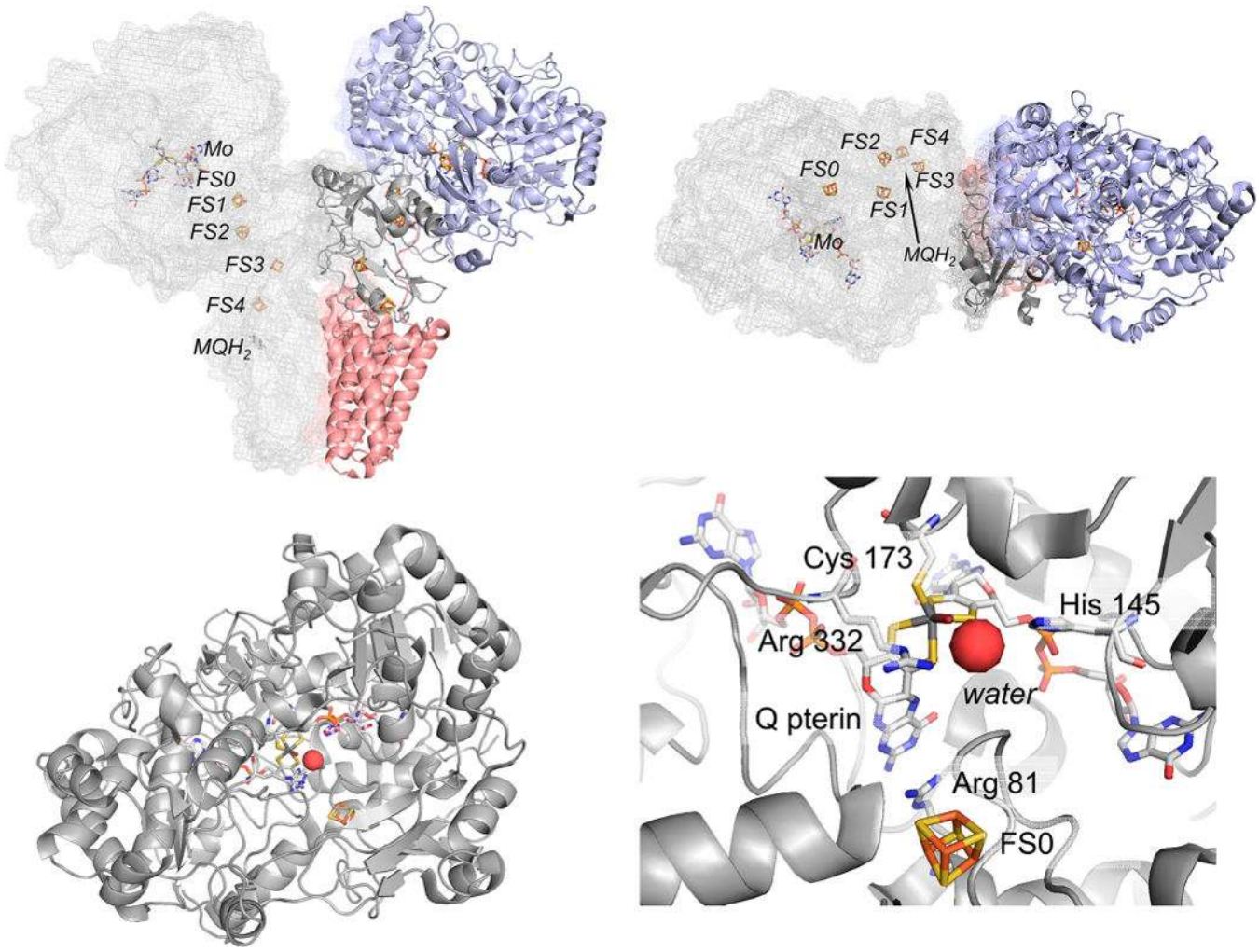

Figure 45.

The structure of the PsrABC polysulfide reductase from *T. thermophilus* (PDB 2VPW). Top, the overall organization of the subunits in the $(\alpha\beta\gamma)_2$ oligomer. One protomer at left is in gray and shown in mesh to illustrate the disposition of the redox-active centers within the protomer, the other has PsrA, PsrB, and PsrC in blue, dark gray, and red, respectively. The orientation at right is rotated 90° about the horizontal compared to that at left. Bottom left, the PsrA subunit, looking down the solvent access channel to the active site. Bottom right, the active site molybdenum center, with Cys 173 coordinating the molybdenum and Arg 81 intervening between the Q pterin and FS0. Arg 332 and His 145 H-bond to a bound water.

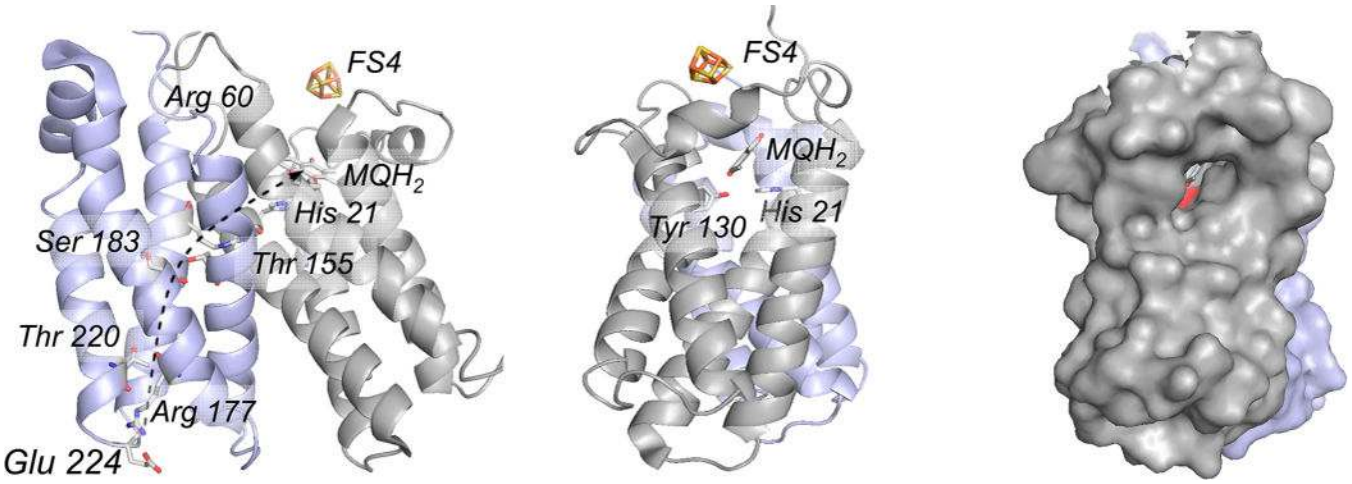

Figure 46.

The membrane-integral PsrC subunit of *T. thermophilus* polysulfide reductase (PDB 2VPW). The N- and C-terminal four-helix bundles referred to in the text are shown in gray and blue, respectively. The orientation in center is rotated 90° about the vertical relative to that at left. The protein channel providing menaquinol access to the binding site is indicated at right. The proximal FS4 of PsrB is also shown, indicating its position relative to the bound menaquinol. In the orientation at left, a putative proton channel through the second four-helix bundle is indicated by the dashed arrow, involving Glu 224, Arg 177, Arg 239, Thr 220, Ser 183, and Thr 155 as shown, leading to Asp 60 and His 21 in the first bundle.

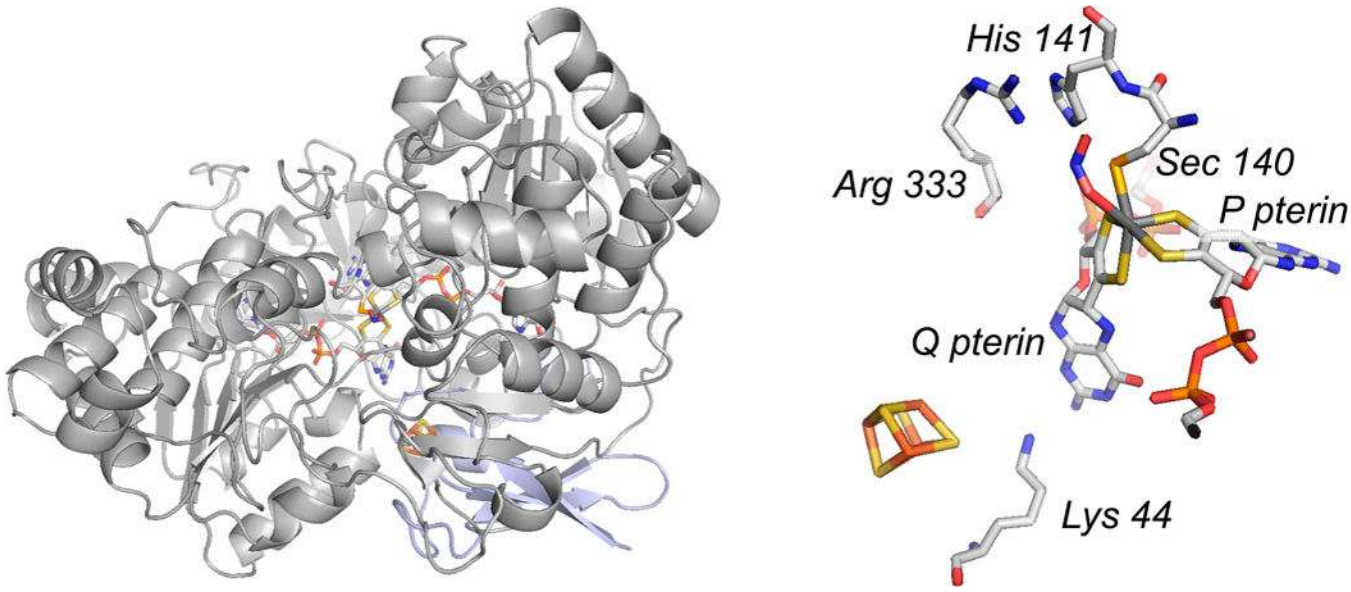

Figure 47.

The structure of *E. coli* FdhF (PDB 1FDI). Left, the overall protein fold, with the N-terminal [4Fe-4S]-containing domain in blue (at rear). The orientation shown is approximately the same as that in Figure 43 for the *R. sphaeroides* DMSO reductase. Right, a close-up of the active site, showing the inhibitor nitrite bound at the molybdenum (displacing the hydroxide seen in free, oxidized enzyme), with Arg 333 adjacent to the molybdenum-coordinated Sec 140.

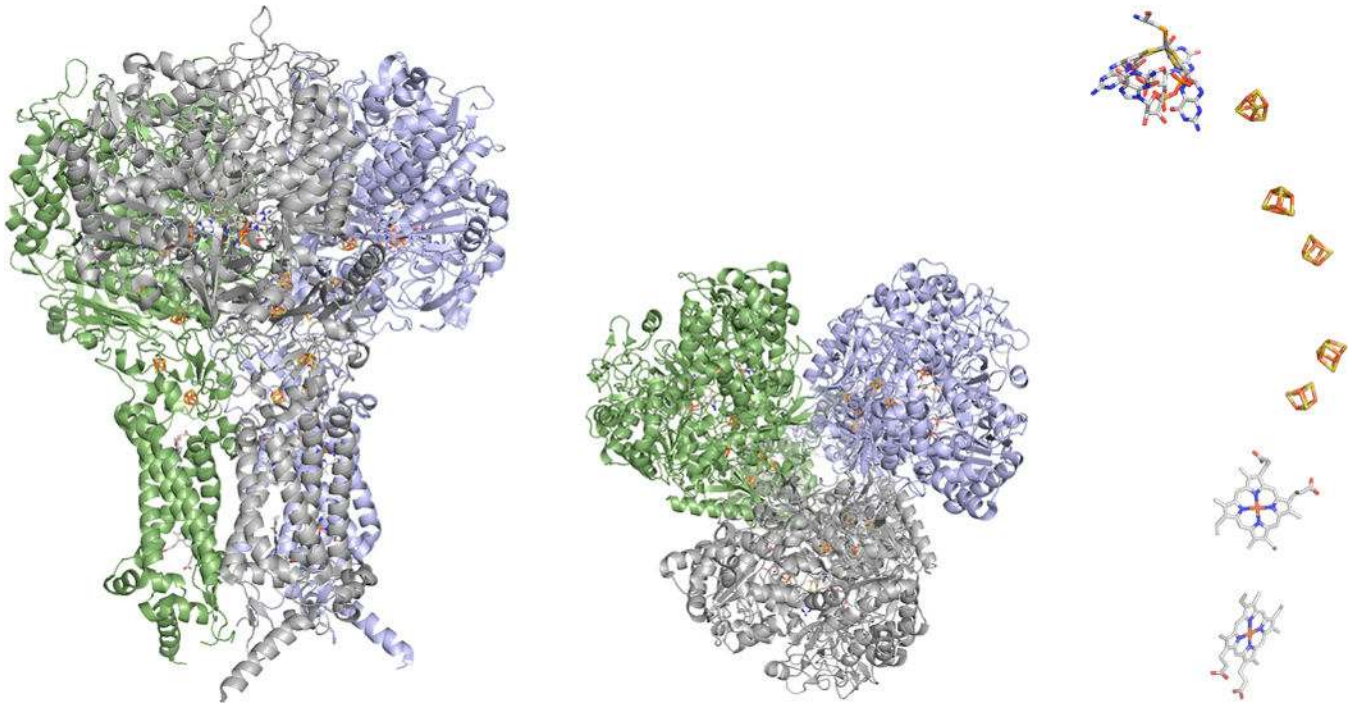

Figure 48.

The structure of *E. coli* formate dehydrogenase N (PDB 1KQF). Left, a side view of the complex; center, the view from the periplasmic side of the membrane, illustrating the trimeric nature of the protein; and right, the arrangement of redox-active centers in one αβγ protomer of the enzyme, illustrating the approximately linear electron transfer chain leading from the membrane-integral hemes at bottom to the molybdenum center (site of nitrate reduction) at top.

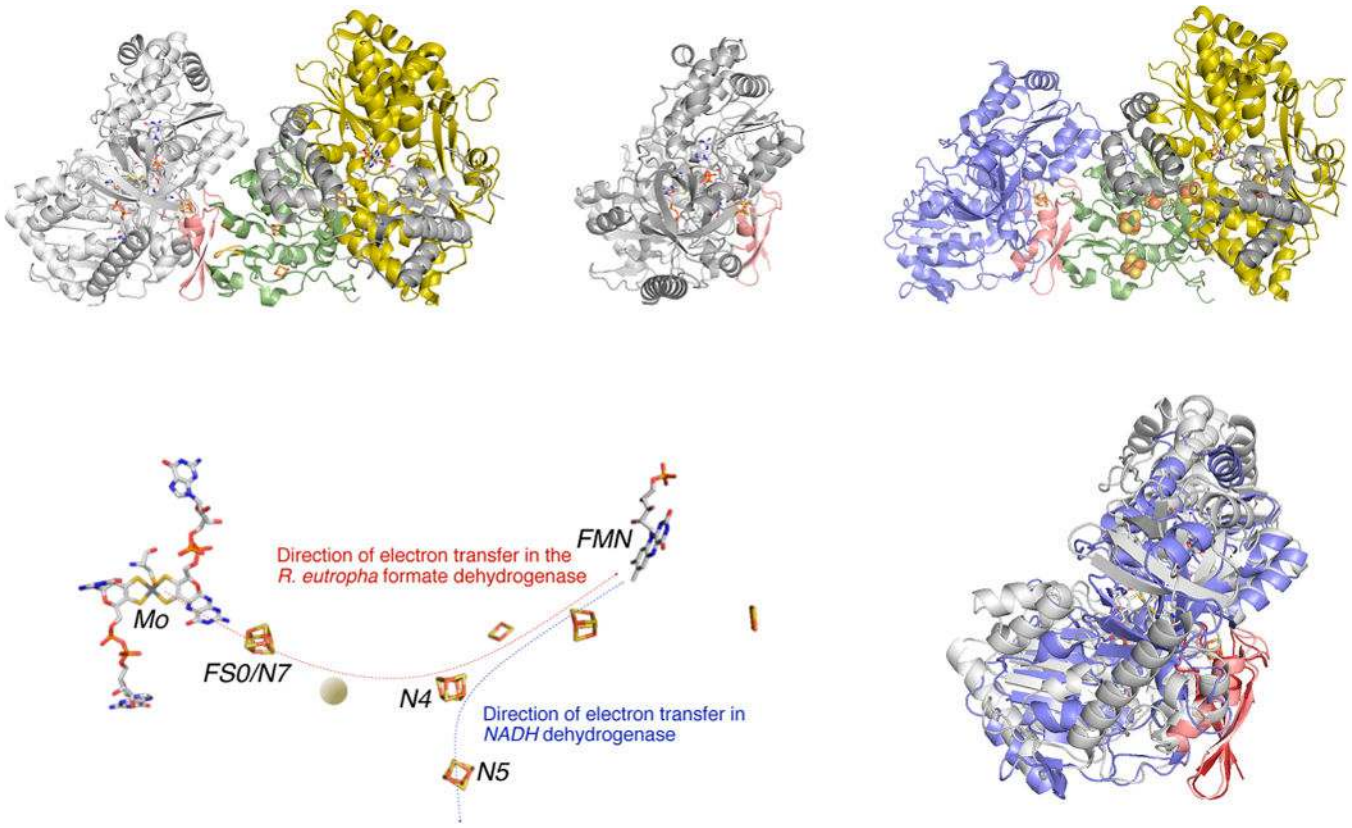

Figure 49.

A model for the structure of the FdsGBA formate dehydrogenases. The model was obtained by superimposing the FS0 [4Fe-4S] cluster of FdhF from *E. coli* (PDB 1AA6) with the N7 [4Fe-4S] cluster of the Nqo3 subunit of *T. thermophilus* NADH dehydrogenase (PDB 3IAM), with the Nqo1 and Nqo2 subunits (which have strong homologies to FdsB and G, respectively) included in the model. Upper left, the model for FdsGBA; upper right, the structures of FdhF (with the molybdenum-binding portion of the protein in gray) and Nqo1–3 (in yellow, gra,y and green/blue, respectively), with the putative overlap region in red from which the model was constructed. This region contains iron–sulfur cluster FS0 in FdhF and N7 in the Nqo3 subunit of NADH dehydrogenase. Lower left, the disposition of the redox-active centers in the model, with the approximate position of the additional iron–sulfur cluster known to be present in the *R. eutropha* enzyme indicated by the orange ball. The orientation of the overall complex is the same as in upper left. Lower right, an alignment of the molybdenum-binding portion of FdhF with the C-terminal domain of Nqo3 (in blue, upper right). The rms deviation is 2.7 Å over 428 Cα atoms.[428a]

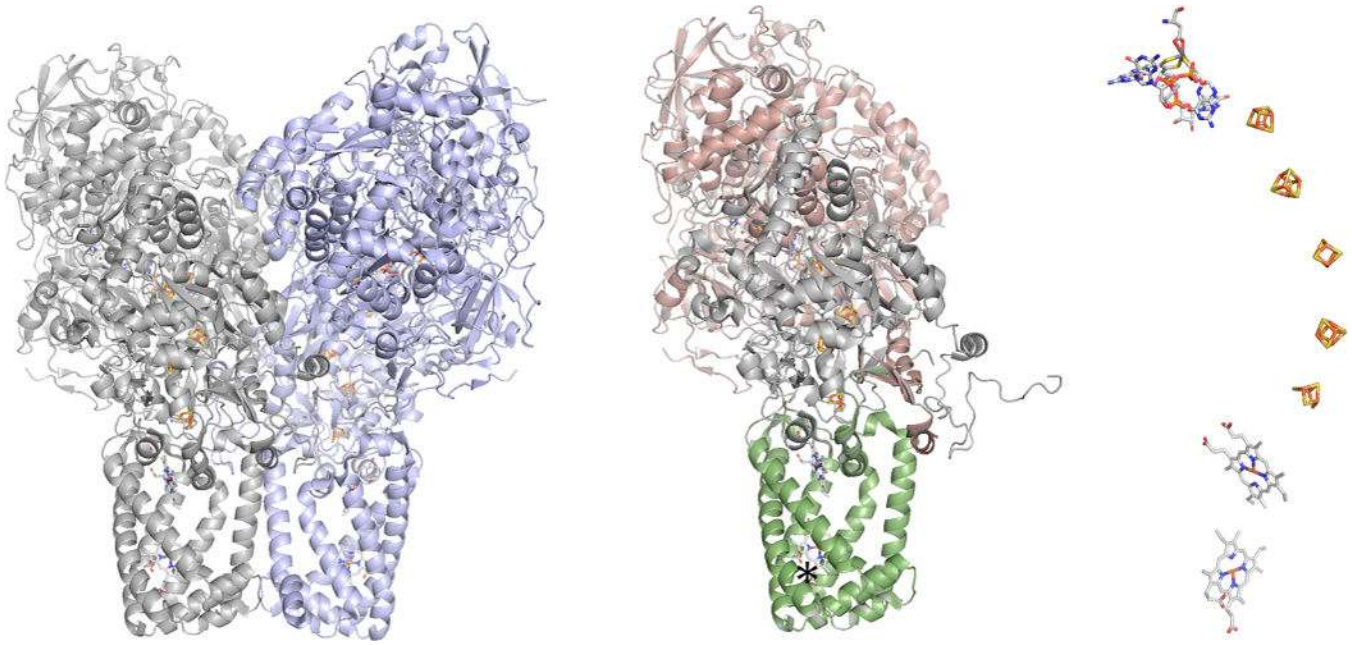

Figure 50.

NarGHI from *E. coli* (PDB 1Q16). Left, the overall of the organization of the $(\alpha\beta\gamma)_2$ enzyme with the membrane integral NarI subunits at bottom. Center, the organization of the left-hand protomer, with the catalytic NarG in red, the iron–sulfur containing NarH in gray, and the membrane integral NarI in green. The approximate position of the menaquinol binding site near the distal heme is indicated by the asterisk. Right, the layout of the eight redox-active centers in the protomer (the perspective is rotated approximately 90° about the vertical relative to that at center).

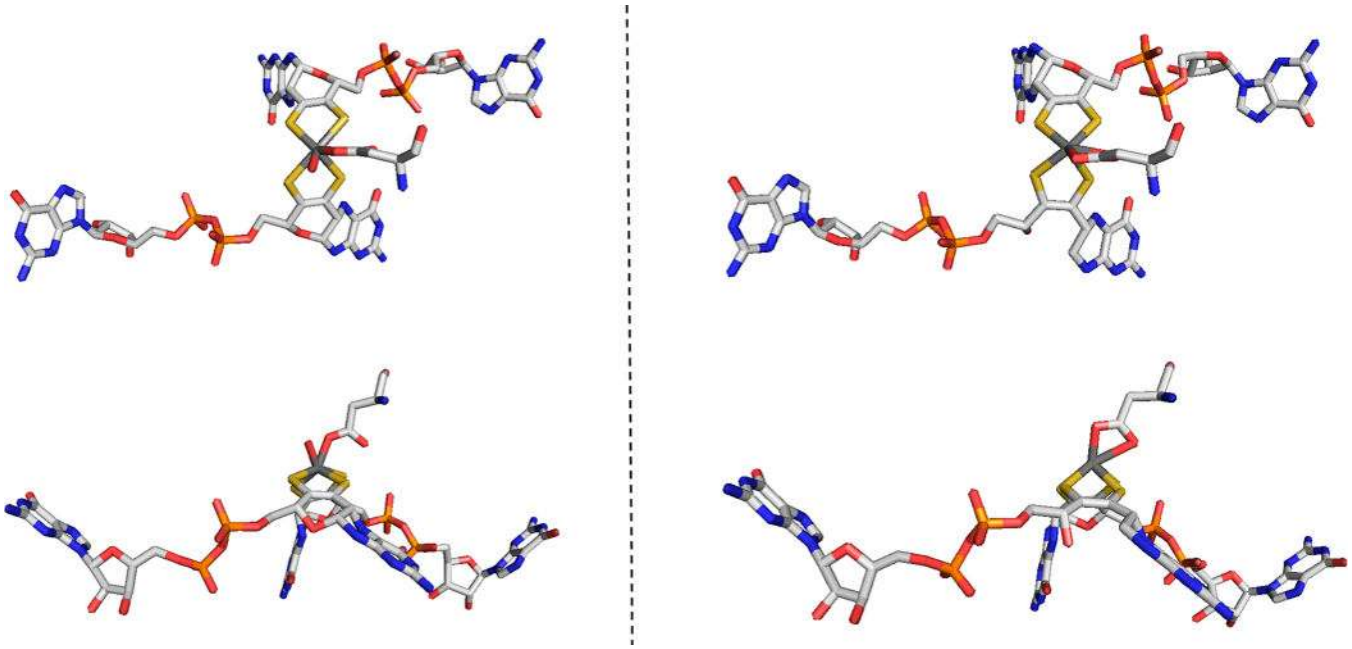

Figure 51.

Alternate coordination modes for Asp 222 in *E. coli* NarG. Left, the monodentate mode with a Mo=O ligand as seen in PDB 1R27,[370b] and right, the bidentate binding mode seen in PDB 1Q16.[370a] In both cases, the lower images are rotated about the horizontal by approximately 90° relative to the upper images.

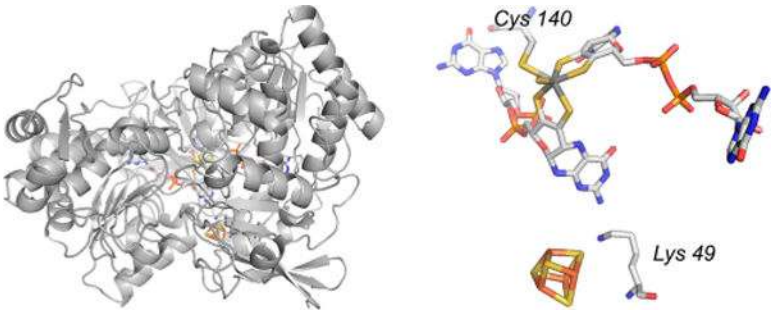

Figure 52.

The structure of the periplasmic Nap nitrate reductase from *D. desulfuricans*. Left, the overall structure (PDB 2NAP), demonstrating the close similarity in overall fold to formate dehydrogenase-H, FdhF (Figure 43). Right, a close-up of the structure of the molybdenum center in the cyanide-inhibited enzyme (PDB 2JIR).

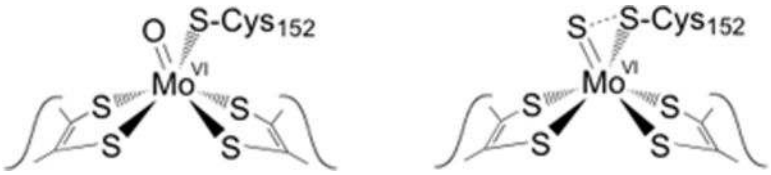

Figure 53.

Alternate structures proposed for the molybdenum center of Nap enzymes. Left, that originally proposed on the basis of the initial structure of the *Desulfovibrio desulfuricans* NapA.[368] Right, that later suggested[467] after examination of anomalous scattering parameters.

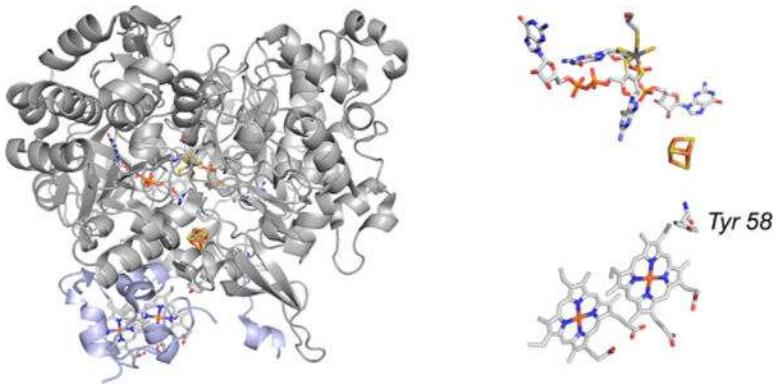

Figure 54.

The structure of the NapAB from *C. necator* (PDB 3ML1). Left, the overall fold, with the molybdenum-containing NapA in gray and the diheme NapB in blue. A close-up of the redox-active centers of the enzyme (rotated approximately 45° counterclockwise about the vertical relative to the perspective at left), showing the position of Tyr 58 of NapB that intervenes between the proximal heme and [4Fe-4S] cluster of NapA.

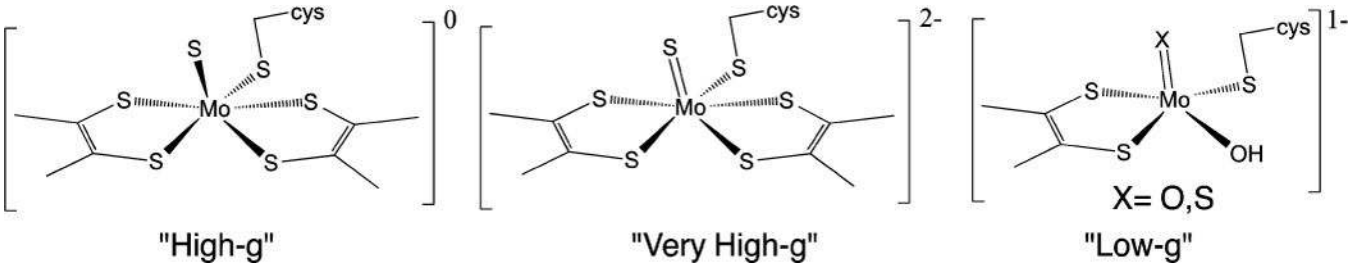

Figure 55.

Proposed structures of the Mo-site giving different EPR signals for the NapA nitrate reductase of *P. pantotrophus*.[480]

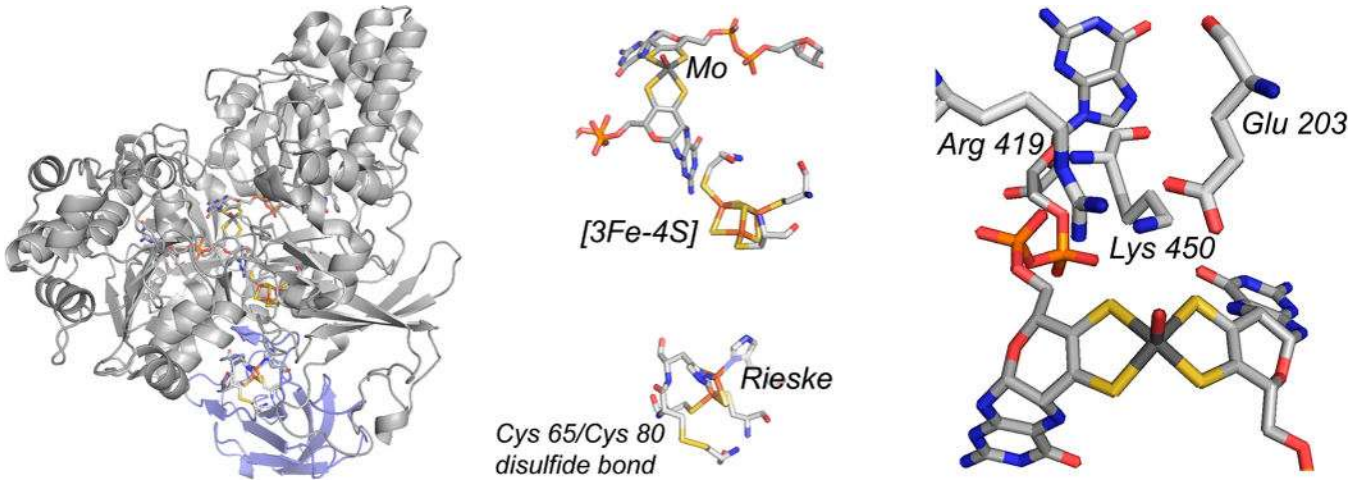

Figure 56.

The structure of the *A. faecalis* AioAB arsenite oxidase (PDB 1G8J). Left, the overall fold of the dimeric enzyme, with the AioA subunit in gray and the AioB subunit in blue. Center, an enlargement of the structure from the same perspective showing the disposition of the molybdenum center (top), [3Fe-4S] cluster (center), and Rieske [2Fe-2S] cluster (bottom). Also shown is the disulfide bond between Cys 65 and Cys 80 in AioB, adjacent to the Rieske cluster. Right, the environment of the molybdenum center, showing Arg 419, Lys 450, and Glu 203 that define the substrate binding site.

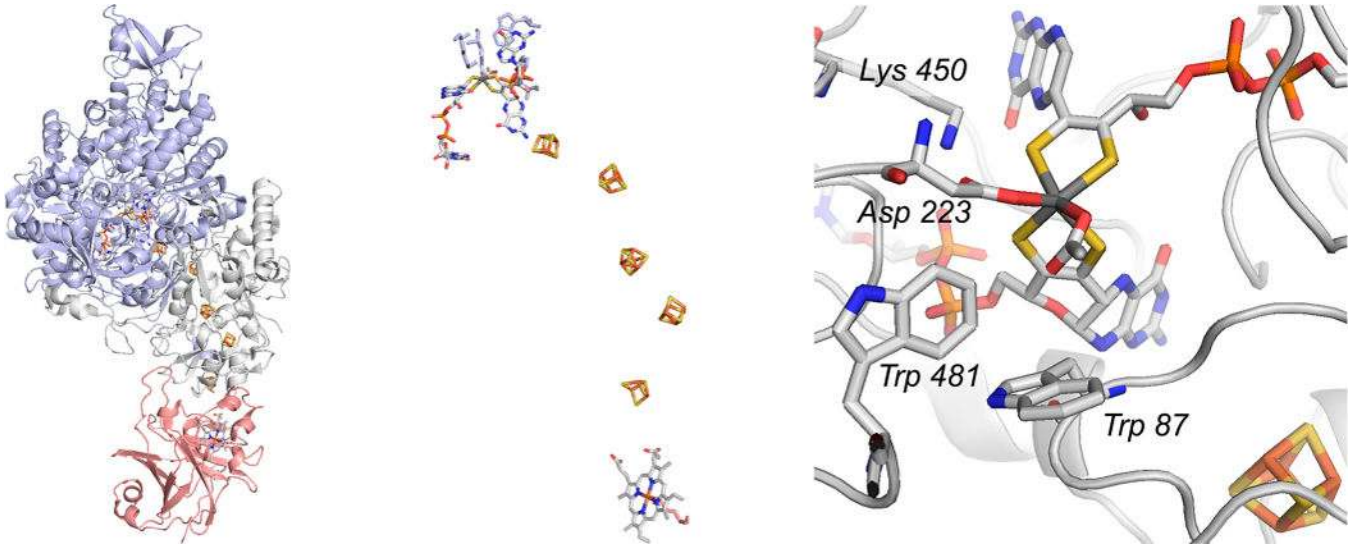

Figure 57.

The structure of ethylbenzene dehydrogenase from *Aromatoleum aromaticum* (PDB 2IVF). Left, the overall structure of the trimeric enzyme, with the α, β, and γ subunits in blue, gray, and red, respectively. Center, an enlargement of the enzyme's electron transfer chain, with the molybdenum center at top and the heme at bottom. Right, the active site of the enzyme, with residues referred to in the text indicated.

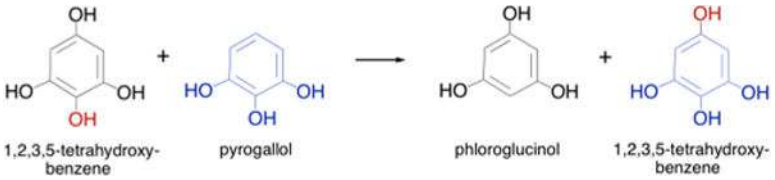

Figure 58.
The reaction catalyzed by pyrogallol:phloroglucinol transhydroxylase.

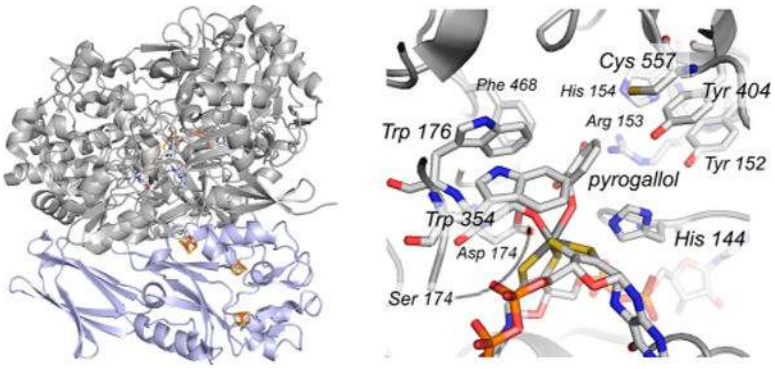

Figure 59.

The structure of pyrogallol:phloroglucinol transhydroxylase from *Pelobacter acidigallici* (PDB 1TI4). Left, the large molybdenum-containing subunit is in gray, and the smaller iron–sulfur containing subunit is in blue. Right, a close-up of the active site of reduced enzyme in complex with pyrogallol.